Shear Strength of Slab-Column Connections under Gravity and Cyclic Lateral Loading

Sunendro Aris Sutanto Himawan

School of Civil and Environmental Engineering

A thesis submitted to the Nanyang Technological University
in partial fulfillment of the requirement for the degree of
Doctor of Philosophy

2012

ACKNOWLEDGEMENTS

This thesis would not have been possible without the guidance and the help of several individuals who in one way or another contributed and extended their valuable assistance in the preparation and completion of this study.

First and foremost, I would like to offer my sincerest gratitude to my supervisor, Dr. Susanto Teng, who has been giving his great guidance, encouragement, and valuable advice throughout my PhD program.

I am also grateful to Prof. N. J. Gardner for his valuable comments and suggestions during his visit to Singapore.

The research grant from the Ministry of Education through Nanyang Technological University, Singapore is greatly appreciated.

The prestressing materials and equipment provided by VSL Singapore Pte Ltd are also much respected.

I am indebted to all laboratory technicians in the Protective Engineering Laboratory and Construction Technology Laboratory for their assistance during the experimental program.

Special thanks are also extended to Mervin and Grace for their help and contribution during the experimental works.

I would also like to thank my parents, elder sister, and younger brother. They always support me and encourage me with their best wishes.

Last but not least, I would like to express my sincere appreciation to my beloved wife, Lisa Carolina, for her continuous love, support and prayer. She always cheers me up and stands by me through the good and bad times.

TABLE OF CONTENTS

SUMMARY

The main objective of this research is to study the shear strengths of reinforced concrete and post-tensioned slab-column connections under gravity and cyclic lateral loading. This study covers interior, edge, and corner connections constructed using normalweight concrete. The effects of prestressing force, column rectangularity, unbalanced moment transfer, and cyclic loading are included. However, only slab-column connections without beams, drop panels, column capitals, openings, and any type of shear reinforcement are considered in this study.

Tests of three interior post-tensioned slab-column connections having rectangular columns with column aspect ratio of five were presented. The first specimen was tested under gravity load only. The second specimen was subjected to gravity and unidirectional cyclic lateral loading, whereas the last specimen was subjected to gravity and bidirectional cyclic lateral loading. It was confirmed that the strength and stiffness of the connections are much higher along the strong column direction than those along the weak column direction. The test results also indicate that bidirectional cyclic lateral loading significantly reduces the strength, drift capacity, ductility, and stiffness of the connections. The increase in shear strength due to prestressing for connections having rectangular columns tends to be lower compared with those having circular/square columns. Furthermore, a modification on the ACI shear strength equation is proposed to make the prediction conservative for connections having rectangular columns.

A method is presented for calculating the ultimate shear stresses at the critical section of interior and exterior slab-column connections due to combined gravity load and unbalanced moment transfer. The method is based on an interaction equation for shear and unbalanced moments, assuming that moment transfer capacity is limited solely by the available flexural reinforcement within an effective transfer width of c plus $1.5h$ on each side of the column. Column rectangularity and the influence of reinforcement ratios are taken into consideration. The proposed equation has been verified for accuracy by predicting the shear strengths of 556 slab-column connections including interior, edge, and corner connections, ranging

from symmetrically loaded connections to connections having rectangular columns transferring unbalanced moments. The proposed formula gives a very good agreement with experimental results and simplifies the design process.

Shear strength formula of reinforced concrete slabs is extended to consider the effect of prestressing by decompression method. It was shown that the proposed method is more accurate than ACI 318-11 and Eurocode 2 formulas. For post-tensioned slab-column connections transferring unbalanced moments, the ultimate shear stresses acting on the critical section are calculated based on an interaction equation of shear and unbalanced moments. The moment transfer capacity is assumed to be carried by nonprestressed reinforcement and prestressing steel within the effective transfer width of c plus $1.5h$ on each side of the column. In terms of accuracy and conservatism, the proposed method was shown to be much better compared with the eccentric shear stress model of ACI 318-11 and Eurocode 2 method.

The shear strengths of reinforced concrete and post-tensioned slab-column connections under cyclic loading were investigated. It was shown that the method proposed previously for slab-column connections under monotonic loading is also applicable for slab-column connections under cyclic loading, while maintaining its accuracy and safety margin. Thus, it is not necessary to introduce a strength degradation factor due to cyclic loading into the shear strength formula. For flat plate structures not designated as part of the seismic-force-resisting system, ACI 318-11 requirement on gravity shear ratio can be unconservative. Accordingly, a modification on the gravity-shear-ratio is proposed. The proposed modification leads to a more conservative result.

LIST OF TABLES

LIST OF FIGURES

LIST OF SYMBOLS

a_v = distance from loading point to column face

b = width of critical section

b_1, b_2 = widths of critical section measured parallel and perpendicular to moments considered, respectively

b_l, b_s = length of longer and shorter side of critical section, respectively

b_o = perimeter of critical section

b_t = effective transfer width (c + 1.5h on each side of the column)

c = column width

c_1, c_2 = column widths measured parallel and perpendicular to moments considered, respectively

A, B, C = constants

d = effective depth of nonprestressed reinforcement

d_p = effective depth of prestressing steel

DR_u = ultimate drift ratio at peak unbalanced moment

DR_{u80} = ultimate drift ratio at 80% of peak unbalanced moment

DR_y = yield drift ratio

e = eccentricity

f'_c = compressive strength of concrete cylinder

f_{ct} = tensile strength of concrete

f_{cu} = compressive strength of concrete cube

f_e = extreme fiber stress due to prestressing

f_{pc} = compressive stress in concrete due to prestressing

f_{ps} = stress in prestressing steel at flexural strength

f_{pu} = tensile strength of prestressing steel

f_{py} = yield strength of prestressing steel

f_{se} = effective stress in prestressing steel

f_y = yield strength of nonprestressed reinforcement

g = distance between centroid of column and centroid of critical section

h = slab thickness

J_c = properties of critical section analogous to polar moment of inertia

k = coefficient that depend on ratio of column dimensions (Eurocode 2)

K = parameter that relates shear and unbalanced moment ratio

k_d = depth factor (Eurocode 2) or size effect (proposed)

k_p = coefficient corresponding to increase in shear strength due to prestressing

ℓ = span length

m_d = decompression moment per unit width

M_f = flexural capacity of slab within effective transfer width

M_o = unbalanced moment capacity in the absence of shear force

M_s = ultimate unbalanced moment acting at centroid of critical section

M_u = ultimate unbalanced moment acting at centroid of column

M_v = unbalanced moment capacity based on shear failure

M_{yl} = slab flexural strength based on yield-line theory

s = distance from centroidal axis to extreme fibers of critical section

S = stiffness parameter

u = perimeter of critical section (Eurocode 2)

u^* = reduced critical section perimeter (Eurocode 2)

v = applied shear stress

V/m = ratio of shear force to moment per unit width

V_c = shear capacity

v_c = shear strength provided by concrete

v_n = shear strength

v_s = shear strength provided by shear reinforcement

v_u = ultimate shear stress

V_c = shear capacity provided by concrete

V_d = decompression load

V_o = shear capacity in the absence of unbalanced moment

V_p = vertical component of all effective prestress forces crossing critical section

V_{pd} = vertical component of all effective prestress forces crossing critical section (Eurocode 2)

V_u = ultimate shear force acting at the centroid of column

W = factor corresponding to shear stress distribution (Eurocode 2)

α_s = constant to compute v_c

β = ratio of long to short side of column

β_p = factor used to compute v_c in prestressed slabs

β_v = factor used to compute maximum ultimate shear stress (Eurocode 2)

ϕ = strength reduction factor

γ_f = fraction of unbalanced moment transferred by flexure

γ_v = fraction of unbalanced moment transferred by eccentric shear

λ = modification factor reflecting reduced mechanical properties of lightweight concrete

μ = connection ductility corresponding to DR_u

μ_{80} = connection ductility corresponding to DR_{u80}

ρ = nonprestressed tension reinforcement ratio within effective transfer width

ρ_l = nonprestressed tension reinforcement factor (Eurocode 2)

ρ_p = prestressing steel ratio within effective transfer width

ρ_t, ρ_b = respective top and bottom slab reinforcement ratios within effective transfer width

σ_1 = principal tensile stress

CHAPTER 1
INTRODUCTION

1.1 Background

One of the most common types of structural floor systems is the flat plat structure. This system consists of a slab supported directly on columns without column capitals, drop panels, or beams as shown in Figure 1.1. Flat plate structures offer many advantages compared with conventional beam-column systems, such as simpler formwork, faster construction speed, more flexible space arrangements, and better aesthetics.

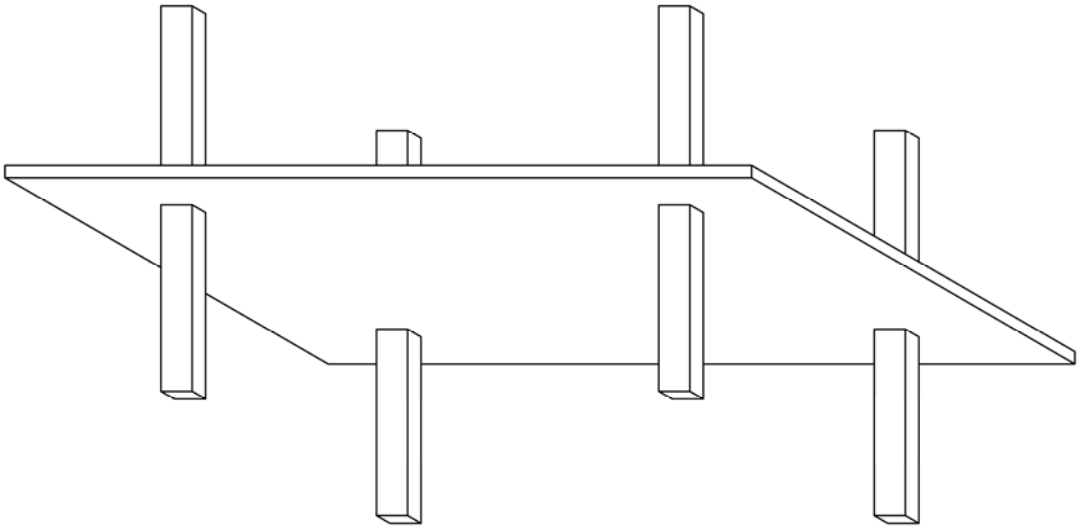

Figure 1.1 Flat plate structure

In a flat plate structure, the slab can be reinforced by ordinary reinforcing steel (i.e. reinforced concrete flat plate) or post-tensioned by prestressing steel (i.e. post-tensioned flat plate). The use of post-tensioning in flat plates makes them more efficient for longer spans. Prestressing also allows the designers to control cracks and deflection better. Compared with the reinforced concrete flat plate structure, the post-tensioned flat plate structure has more advantages:

- Longer spans and greater span-to-depth ratio. The greater span-to-depth ratio results in the reduction of dead load and floor-to-floor height. The reduced dead load has a beneficial effect upon the columns, walls, and foundations. In the seismic regions, this effect is important due to the smaller inertia forces generated by seismic accelerations. The saving in floor-to-floor height reduces the overall height of the building or enables additional floors to be incorporated in the building of a given height. Furthermore, this saving can also reduce the quantity of cladding and the energy used for air conditioner or heater.
- Very good behavior with respect to the cracks and deflections control.
- Higher punching shear strength due to the precompression.
- Less material to be handled and placed.
- Earlier stripping of the formwork, resulting in reduction of the overall construction time.

Post-tensioned slabs can be constructed using either bonded or unbonded tendons. Bonded tendons can be achieved by grouting the tendons after stressing so that there is a bond between concrete and strands. On the other hand, unbonded tendons have no bond between concrete and strands. The strands are greased prior inserting them into the plastic sheathing to prevent bond. In terms of ultimate capacity, bonded tendons are better than unbonded tendons. However, in terms of economy, unbonded tendons are preferable.

The major shortcoming of a flat plate structure is, however, its vulnerability to a brittle punching shear failure at its slab-column connections. A punching shear failure occurs along a truncated cone or pyramid caused by the critical diagonal tension crack around the concentrated load or column as shown in Figure 1.2. This kind of failure occurs without warning and may lead to progressive collapse of the structure. Hence, it is important to be able to predict accurately the shear strengths of slab-column connections.

Shear failure may occur at a slab-column connection due to transfer of shear forces and unbalanced moments between the slab and the column. The shear transfer usually comes from the gravity load whereas the unbalanced moment may come from different loading between the adjacent spans, or lateral loading, such as

strong wind or earthquake loading. For slab-column connections subjected to earthquake loading, the effect of cyclic loading may cause shear strength degradation that can lead to premature failure.

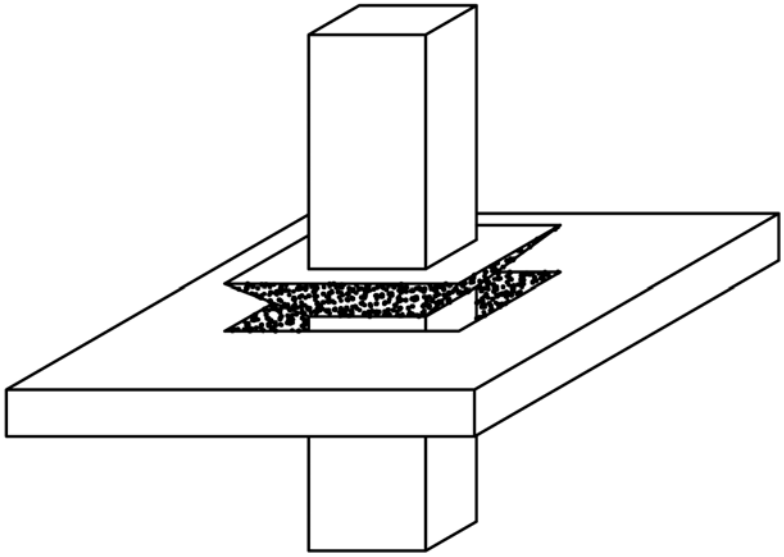

Figure 1.2 Punching shear failure

One of the main factors affecting shear strength is column rectangularity. For the same perimeter of critical section, rectangular geometry leads to lower shear strengths of slabs compared with square perimeter due to the stress concentration around the shorter side of the critical section. Unfortunately, past research on post-tensioned slab-column connections were limited to connections with square columns, and it seems no published data is available on post-tensioned slab-column connections with rectangular columns. The use of rectangular columns itself is very popular in high-rise apartment or residential buildings, due to architectural detailing that frequently require a column to be flush with the adjacent walls.

1.2 Objectives and scopes

The main objective of this research is to study the shear strengths of reinforced concrete and post-tensioned slab-column connections under gravity and cyclic lateral loading. This study covers interior, edge, and corner connections constructed using normalweight concrete. The effects of prestressing force, column rectangularity, unbalanced moment transfer, and cyclic loading are included. However, only slab-column connections without beams, drop panels, column capitals, openings, and any type of shear reinforcement are considered in this study.

1.3 Contributions

It seems that there is no published data available on post-tensioned slab-column connections with rectangular columns. The present experimental program involved testing of three interior post-tensioned slab-column connections with rectangular columns subjected to gravity and cyclic lateral loading. The author hopes this experimental data can be a significant contribution to the current knowledge.

The author extended further an equation previously developed by the author's supervisor to consider the effect of prestressing by decompression method. Note that the previous equation was developed to predict the shear strength of reinforced concrete slab-column connections under symmetrical punching, which includes the effects of openings and rectangular columns. The extended formula is now applicable for both reinforced concrete and post-tensioned slab-column connections. The effects of concrete strength, flexural reinforcement ratio, slab effective depth (size effect), column rectangularity, and prestressing force are taken into account. The extended equation had been verified against extensive experimental data on symmetrical punching and showed a very good agreement in terms of accuracy.

For slab column connections subjected to shear and unbalanced moment transfer, the author proposed a method to calculate the ultimate shear stresses acting at the critical section. The method is based on an interaction equation of shear and unbalanced moments. The accuracy of the proposed method had been verified against numerous experimental data, including interior, edge, and corner connections. The proposed method gives a very good agreement with experimental results and simplifies the computations.

The applicability of the proposed method for slab-column connections under cyclic loading had also been checked. It was found that the proposed method worked well for slab-column connection under cyclic loading, and it is not necessary to introduce any strength degradation factor due to cyclic loading. In addition, the author also collected 742 experimental data on reinforced concrete and post-tensioned slab-column connections from numerous literatures for verification purposes.

1.4 Organization of the report

This report consists of nine chapters. Chapter 1 provides background, objectives and scopes, contributions, and report layout for the present study. Chapter 2 reviews some theory on punching shear, including punching shear models, main factors affecting punching shear strength, prestressed concrete slabs, and slab-column connections under earthquake loading. Some code provisions on punching shear strength of slab-column connections are reviewed in Chapter 3. Chapter 4 describes the experimental program in this study, such as specimens, materials, test setup, instrumentation, and test procedures. Details of the experimental results are presented in Chapter 5. The proposed method to calculate punching shear strength is given in Chapters 6 and 7 for reinforced concrete and post-tensioned slab-column connections, respectively. Chapter 8 covers the strength of slab-column connections under cyclic loading. Last, the summary, conclusions, and recommendations of the present study are given in Chapter 9.

CHAPTER 2
REVIEW OF THEORY ON PUNCHING SHEAR

2.1 Introduction

This Chapter provides reviews of theory on punching shear strength. First, some theoretical models on punching shear strength of slab-column connections will be discussed. Subsequently, the main factors affecting the shear strength of slab-column connections will be reviewed. This section also discusses some methods to consider the effect of prestressing in calculating the shear capacity of slab-column connections. Finally, reviews on slab-column connections under earthquake loading will be presented in the last section.

2.2 Punching shear models

The punching behaviour of slab-column connections is very complex due to the combined flexural and diagonal tension cracks, and the three-dimensional nature of the problem. Hence, to analyze the punching shear strength, a number of theoretical models have been proposed before. Those theoretical models are discussed further below.

2.2.1 Linear stress variation model

Di Stasio and Van Buren (1960) proposed a method to calculate the punching shear strength of slab-column connections due to combined shear and unbalanced moments. The model assumes that the shear stress due to a portion of the unbalanced moment varies linearly on a critical section located at a specified distance away from the column face. Subsequently, the shear stress due to a fraction of the unbalanced moment can be added to the shear stress on the same section resulting from the direct shear force. Punching shear failure is deemed to occur when the maximum the shear stress reaches the punching shear strength.

In using this method, it is necessary to determine the portion of unbalanced moment transferred by shear. Moe (1961) conducted experimental work to determine the portion of unbalanced moment transferred by shear by assuming that the maximum shear stress at failure is equal to the shear stress at failure for the

slabs loaded concentrically. It was found that the ultimate shear strength of the slabs could be predicted with a standard deviation of 0.103 when the fraction of unbalanced moment transferred by shear was taken equal to 1/3.

2.2.2 Mechanical model

This model was initially proposed by Kinnunen and Nylander (1960). The model consists of a central truncated cone surrounded by tangential shear cracks and rigid slab segments, which are separated by radial cracks. Under load action, the segment turns around a centre of rotation located in the root of the shear crack. The internal forces are functions of the angle of rotation and the mechanical properties of the concrete and steel. The equation of equilibrium of the segmental parts and a criterion of failure determine the ultimate load. The failure criteria were expressed in terms of a limitation of the inclined radial compressive stress and a limitation of the tangential compressive strain at the shear crack. Reimann (1963) reviewed the mechanical model and accordingly proposed a similar failure mechanism. However, the compressed conical shell is replaced by a yield hinge around the column. Then, the circumferential concrete stress (rather than strain) is used as a critical design parameter at the column face.

Based on the observed crack patterns and linear deflection profiles of test specimens, Shehata and Regan (1989) developed a mechanical model similar to the model from Kinnunen and Nylander (1960). In the proposed model, the slab is divided into rigid radial segments that rotate around a center of rotation located at the column face and at the level of the neutral axis. This assumption is slightly different from Kinnunen and Nylander (1960) that assumed a centre of rotation located in the root of the shear crack. The failure criteria are defined into three critical conditions at the front part of the radial segment. First, if the angle of the compressive force reaches 20°, failure occurs by splitting of the concrete. Second, if the average radial strain reaches 0.0035 in the plastic length, failure occurs by radial crushing of the concrete. Third, if the tangential strain reaches 0.0035 at a distance x from the column face, failure occurs by tangential crushing of the concrete. A simplified version of the proposed model was presented by Shehata (1990).

Broms (1990) used the same analogy as Kinnunen and Nylander (1960). However, he postulated that punching occurs when the concrete in compression near the column is de-stressed either by a high tangential strain or by a high radial stress. Accordingly, Broms (1990) introduced two main modifications in his model. First, he utilized generally recognized values of concrete properties instead of calibrating his model against specific test results. Second, he calculated different heights of the compression zone in the radial and tangential directions instead of applying iteration procedure. In addition, the design method is extended to account for moment transfer and size effect.

Hallgren (1996) proposed a modification to the mechanical model by Kinnunen and Nylander (1960) based on previous test observations and numerical simulations. In the modified model, the failure criterion is taken as the ultimate tangential concrete strain and derived from a physical model based on non-linear fracture mechanics. It was found that the ultimate tangential concrete strain increases with increasing ductility of concrete and decreases with increasing depth of the tangential compression zone. Hence, the failure criterion reflects both the brittleness of concrete and the size effect. The upper load limit given by the flexural capacity of the slab is automatically included in the model as it is based on the equilibrium of internal forces from concrete in compression, reinforcing steel in tension (including yielding), and external forces from loads and supports reactions.

2.2.3 Model based on elastic plate theory

Mast (1970a) presented an analytical method to determine the torsional, flexural, and shear stresses around an interior slab-column connection. The method is based on the flexural theory of elastic plates. It was shown that, in transferring an unbalanced moment between the slab and the column, the contribution of torsional, flexural, and shear stresses was a variable, which depends on the shape and size of the column, as well as the dimensions and boundary conditions of the plate. Subsequently, the method was extended for the case of exterior slab-column connection by Mast (1970b).

2.2.4 Model based on flexural capacity

Gesund and Kaushik (1970) conducted a systematic study on the relationship between the flexural capacity (V_f) and the failure loads (V_u). They concluded that the ratios of V_f/V_u for 106 tests reported to fail in punching, have an average value of 1.015 and a standard deviation of 0.248. Consequently, Gesund and Dikshit (1971) proposed a punching shear formula based on the flexural yield line analysis. In the analysis, the material model for the concrete was assumed as a square yield locus. The flexural punching concept has been further developed by Gesund and Goli (1980), and Gesund (1981). Another flexural punching approach based on the lower bound solution was proposed by Clyde and Carmichael (1974). Furthermore, Yitzhaki (1966) and Herzog (1970) also derived relatively simple formulas to calculate the punching capacity, which give some recognition to the flexural capacity.

Long and Bond (1967) proposed a method to calculate the punching capacity of concrete slabs by considering the bending moments in the vicinity of the column as determined using elastic analysis. The punching failure is assumed to occur when the concrete stress state corresponds to a failure envelope of concrete under biaxial compression. To calibrate the predictions against the test results, numerous adjustment factors were introduced. Subsequently, Long (1975) proposed the simplified version of the method proposed earlier. The simplified method leads to a nominal shear stress value on a critical section at a distance $d/2$ from the column face, which a function of the reinforcement ratio and the shear span. The nominal shear stress is compared with the concrete tensile strength and assumed proportional to the square root of the concrete compressive strength. The method was extended for the case of unbonded post-tensioned slabs by Franklin et al. (1982). Furthermore, Rankin and Long (1987a, b) improved the method further by considering the spread of yielding in the flexural capacity.

Nölting (1984) proposed a method to calculate the punching capacity of concrete slabs using an inclined compression approach. Regardless of the reinforcement yielding, all failures at inclined cracks around the columns are considered as punching failure. The failure criterion is defined as a limiting strain in

the direction of the inclined compression around the column. The inclined compression strain is a function of the applied load and calculated using three relationships between: (1) the load and the critical moment at the column, (2) the critical moment and the horizontal strain of the concrete, and (3) the horizontal and inclined strains of the concrete.

2.2.5 Beam analogy model

Hawkins and Corley (1971) proposed a beam analogy model to calculate the strength of slab-column connections subjected to unbalanced moment and shear. This model assumes that the slab adjacent to the column are idealized as beams framing into column faces which can develop the ultimate bending moment, torque, or shear appropriate for the given loading. There are two possible modes of failure: moment-torsion and shear-torsion. Moment-torsion mode places a limit on the moment transferred to the column rather than limiting the shear, and significant rotations occur near the column prior to ultimate load. Shear-torsion mode is likely to occur when the shear transferred is significant and the rotation will be less than those for a moment-torsion failure.

Hawkins et al. (1974b) assumes that failure of an interior slab-column connection occurred when ultimate conditions of at least three beams framing into a column are reached. Thus, eight possible limiting combinations of bending, torsion, and shear need to be considered. These various combinations arise due to the possibility that deformations at failure are inadequate to allow simultaneous development of the ultimate capacities of all beam sections.

A modification of beam analogy model has been proposed by Park and Islam (1976). They calculate the strength of the connection by summing all flexural, torsional, and shear strength of all the beams framing into the column. It implies sufficient ductility in bending, torsion, and shear at the critical sections to allow simultaneous development of the ultimate capacities. This method also enables easier application for interior connections.

2.2.6 Model based on plasticity theory

A plastic solution for punching shear strength was initially developed by Bræstrup et al. (1976). A failure mechanism is assumed where the deformation is

concentrated in a rotationally symmetric surface, and the concrete body is punched out perpendicular to the slab while the remaining slab parts remain rigid.

Based on the failure mechanism, an upper bound solution is derived by equating the rate of external work done by the applied load with the rate of internal work dissipated in the failure surface. The lowest upper bound is found by minimizing the failure surface function, which yields a failure surface that consists of a catenary curve and a straight line. Another simplified upper bound value for the punching load was derived by Marti and Thürlimann (1977).

For the lower bound solution, the stresses at any point should satisfy the equilibrium equations as well as the boundary conditions. In addition, they should correspond to a yield line along the optimal failure surface and do not violate the yield condition. Pralong (1982) proposed an alternative lower bound approach involving the concrete tensile strength.

Using a modified Coulomb yield criterion for concrete, Bortolotti (1990) applied the plasticity theory to calculate the punching load. He introduced a procedure to consider the strain softening of concrete. Then, an upper bound solution is found by applying the virtual work equation. To obtain the failure surface, the lowest upper bound solution is solved using the Euler equation.

2.2.7 Truss analogy model

In this model, truss analogy is used to model the flow of forces at a slab-column connection. The model consists of a three-dimensional space truss composed of concrete compression struts, steel tension ties, and concrete ties. The concrete ties have to be introduced in slab-column connections without shear reinforcement to carry the tensile force in the vertical direction. The presence of cracks is not explicitly addressed but it can be considered in other failure criterion, like reducing the value of concrete compressive strength. Truss models with concrete ties to analyze punching shear were proposed by Pralong (1982) as well as by Andra (1982).

Alexander and Simmonds (1987) proposed a truss model for interior connections subjected to moment transfer. A similar model was also proposed by Simmonds and Alexander (1987) for edge connections. The model consists of a

three-dimensional space truss composed of concrete compression struts and steel tension ties. The vertical component of the concrete compression struts is responsible for transferring shear force. In the truss model, each compression strut is assumed straight and inclined at an angle α to the plane of the slab. The magnitude of α is assumed to be limited by conditions at the intersection of the strut and its attendant tension tie. In the analysis, the steel tension ties are always assumed to reach yield. Thus, a compression failure of the concrete strut will never govern.

The tests by Alexander and Simmonds (1992b) showed that the radial compression strut is curved (not straight). Accordingly, Alexander and Simmonds (1992a) proposed the bond model to account for the curved arch. The curved arch is a progression from the straight-line compression strut of the truss model. The curvature of the arch is governed by beam action shear perpendicular to the arch. If limited by bond, beam action shear can be represented as a critical shear stress. For brittle punching failure, bond strength of the reinforcement is seen as the significant factor limiting beam action shear. Based on this model, a simple lower bound estimate of the ultimate strength of a plate-column connection is derived.

2.2.8 Model based on concrete tensile strength

Georgopoulos (1988, 1989) developed a method to calculate the inclination of punching shear crack and the punching load of slab-column connections without shear reinforcement. First, the inclination of the punching shear crack is assumed a function of the mechanical reinforcement ratio. Subsequently, the punching load can be calculated by integrating the tensile stresses along the surface of punching shear crack. The model assumes that the stress distribution is a polynomial of third order.

Based on numerical simulation results by Menetrey et al. (1997), Menetrey (1996) proposed an analytical expression to compute the punching load. The model assumes that the punching failure corresponds to the failure of concrete tie. Hence, the punching load can be computed by integrating the vertical components of the concrete tensile stresses around the punching shear crack. The model is also generalized to include the dowel-effect from flexural reinforcement, shear

reinforcement contribution, and prestressing tendons contribution. In addition, Menetrey (1998) also proposed another analytical expression to relate flexural failure and punching failure.

2.3 Factors affecting punching shear strength

The shear strength of slab-column connections is influenced by several factors, such as concrete strength, flexural reinforcement, slab effective depth, column rectangularity, prestressing force, span-depth ratio, and ratio of column width to slab effective depth. These factors are discussed further in the following section.

2.3.1 Concrete strength

Mitchell et al. (2005) reviewed a series of tests by Elstner and Hognestad (1956), Ghannoum (1998), and McHarg et al. (2000) to investigate the influence of concrete strength on punching shear strength. Those series of tests used the concrete strength as the main variable. In general, the punching shear strength increases as the concrete strength increases. The increase in punching shear strength can be represented using the power of one-third or one-half. However, the cube root function is preferable for high strength concrete as it gives results that are more conservative. In addition, Marzouk and Hussein (1991), Gardner (1995), Sherif and Dilger (1996), and Teng et al. (2004) also proposed a punching shear equation that is proportional to the cube root of the concrete strength rather than the square root of the concrete strength.

2.3.2 Flexural reinforcement

Tests of slabs with the flexural reinforcement as a main variable, have been reported by Elstner and Hognestad (1956), Vanderbilt (1972), Marzouk and Hussein (1991), and Hallgren (1996). Based on those results, it can be concluded that the punching shear strength increases as the flexural reinforcement ratio increases. The influence of flexural reinforcement on punching shear strength is usually described using the reinforcement ratio to the power of certain value. Dilger et al. (2005) studied the series of tests by Richart (1948a, b) and showed that the influence of flexural reinforcement ratio on punching shear strength can be well described using both the power of one-fourth and one-third. Accordingly, Dilger et al. (2005) suggested using the power of one-third as it is also commonly used to reflect the

effect of concrete strength. The power of one-third is also recommended by other researchers, such as Regan and Bræstrup (1985), Takahashi et al. (1992), Gardner (1996), Sherif and Dilger (2000b), Dilger (2000), and Teng et al. (2004).

Based on series of tests by Moe (1961), and Bernaert and Puech (1966), no strong conclusion can be drawn with respect to the effect of yield strength of the flexural reinforcement on punching shear strength. However, it is obvious that if the yield strength of the flexural reinforcement is varied and flexural yielding does not occur, the punching shear strength will not be affected by the variation of the yield strength. The reason is that the stiffness of the flexural reinforcement is independent of its yield strength. Hence, only the stiffness of flexural reinforcement would affect the crack width and the shear capacity. The yield strength of the flexural reinforcement seems not to have any influence on punching shear capacity.

Moe (1961) also conducted two series of tests where the flexural reinforcement was concentrated in the vicinity of the column while the reinforcement ratio was kept constant. Based on those results, Moe (1961) concluded that the concentration of flexural reinforcement near the column does not increase the punching shear capacity. The same conclusion was also found by Elstner and Hognestad (1956), Regan (1986), and Hawkins et al. (1974a). In addition, Hawkins et al. (1974a) also concluded that concentrating the flexural reinforcement around the column increases the rigidity, the load corresponding to the initial yielding of the tension reinforcement, and leads to smaller crack width. However, the reasons behind it were not well understood. Alexander and Simmonds (1992b) stated that bond failure may be the reason why concentrating the flexural reinforcement in the vicinity of the column did not increase the punching capacity in the previous tests. McHarg et al. (2000) tested slabs with well-anchored flexural reinforcement to prevent any bond failures, and found that the punching capacity was increased by 14% when the flexural reinforcement is banded near the column. Hence, it can be concluded that the concentration of flexural reinforcement around the column leads to a small increase in the punching shear strength if there is no bond failure.

2.3.3 Slab effective depth (size effect)

Dilger et al. (2005) reviewed a series of tests by Lee et al. (1979), and Alexander and Simmonds (1992b) to study the effects of concrete cover on punching shear strength. They concluded that the slab effective depth should be used for calculating punching shear strength rather than the total slab thickness.

The series of tests conducted by Nylander and Sundquist (1972), Regan (1986), Li (2000), and Birkle (2004) used the slab effective depth as the main variable, whereas the other parameters were kept relatively unchanged. The results showed that the punching shear strength tends to decrease as the slab effective depth increases. This is known as the size effect.

Bažant and Cao (1987) stated that punching failure does not occur simultaneously along the failure surface (except for thin slabs), but it propagates across the slab with the energy dissipation localized into the cracking front. Hence, the punching capacity should be predicted using fracture mechanics instead of plastic limit analysis (based on energy and stability criteria instead of strength criteria). The main feature of this model is the size effect law as shown in Figure 2.1. For limit analysis, the punching shear strength will follow the yield criterion line, which is size independent. Conversely, according to fracture mechanics, the punching shear strength decreases as the size increases. However, the linear fracture mechanics usually overestimates the size effect of concrete slabs. Thus, the non-linear fracture mechanics must be used to represent the gradual transition from the failure criterion of limit analysis to the linear fracture mechanics.

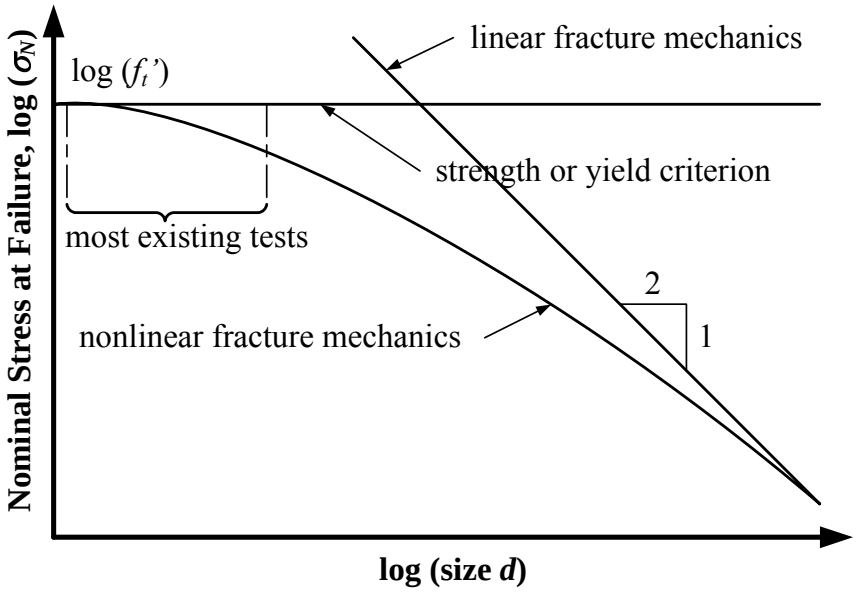

Figure 2.1 Size effect law (Bažant and Cao 1987)

2.3.4 Column rectangularity

The column rectangularity is usually defined as the ratio of longer to shorter sides of the column (column aspect ratio). If the column perimeter is held constant and the ratio of longer to shorter sides of the column is increased, the shear strength is decreased. This occurred due to the concentration of stress around the shorter side of the column. Therefore, the shear stresses are not uniformly distributed around the column or loaded area. The effect of column rectangularity on punching shear strength was initially studied by Hawkins et al. (1971). Other researchers who studied this issue are Lee (2004), Teng et al. (2004), and Oliveira et al. (2005).

2.3.5 Prestressing force

The prestressing force induces compressive stress in the concrete, hence increasing its shear strength. In addition, the vertical components of prestressing forces that pass through the critical section also provide some beneficial effects on punching shear strength. According to Regan and Bræstrup (1985), there are three approaches to consider the effect of prestressing into the punching shear calculation: (1) principal tensile stress approach, (2) equivalent reinforcement ratio approach, and (3) decompression approach. It was shown that, among the three methods, the

decompression approach gives the most accurate result. The details of each approach are discussed further below.

(1) Principal tensile stress approach

The principal tensile stress is based on the assumption that punching shear failure occurs when the principal tensile stress exceeds the tensile strength of concrete. Assuming a homogeneous, elastic, and uncracked section, the principal tensile stress (σ_1) of an element subjected to shear stress and horizontal compression stress can be computed as

$$\sigma_1 = \sqrt{v^2 + \left(\frac{f_{pc}}{2}\right)^2} - \frac{f_{pc}}{2} \tag{2.1}$$

where v is the applied shear stress; and f_{pc} is the horizontal compression stress (due to prestressing). To calculate the shear strength, the principal tensile stress σ_1 is set equal to the tensile strength of concrete and Eq. (2.1) is solved for the shear stress v. Hence, the shear strength (v_c) becomes

$$v_c = v = f_{ct}\sqrt{1 + \frac{f_{pc}}{f_{ct}}} \tag{2.2}$$

where f_{ct} is the tensile strength of concrete and f_{pc} is the compressive stress in concrete due to prestressing. For design purposes, the simplified form of Eq. (2.2) is usually used:

$$v_c = f_{ct} + k_p f_{pc} \tag{2.3}$$

where k_p is a coefficient corresponding to the increase in shear strength due to prestressing.

ACI 318-11 formula on shear strength of prestressed slabs [Eq. (3.4)] is based on the principal tensile strength approach [Eq. (2.3)]. The tensile strength of concrete f_{ct} is assumed $3.5\sqrt{f'_c}$ (psi) or $0.29\sqrt{f'_c}$ (MPa), and the coefficient k_p is set equal to 0.3. Furthermore, the effect of connection size ($\alpha_s d/b_o$) and the vertical component of prestressing force (V_p) are also included in the shear strength equation [Eq. (3.4)].

(2) Equivalent reinforcement ratio approach

The equivalent-reinforcement-ratio approach assumes that the effect of prestressing can be considered by increasing the slab reinforcement ratio to an equivalent value. Nylander et al. (1977) proposed the formulation of the equivalent reinforcement ratio ($\rho_{p,eq}$) as:

$$\rho_{p,eq} = \frac{f_{py}}{f_{py} - f_{se}} \rho_p \tag{2.4}$$

where f_{py} is the yield strength of the prestressing steel; f_{se} is the effective stress in the prestressing steel; and ρ_p is the reinforcement ratio of the prestressing steel. Accordingly, the calculation of punching shear strength can be performed as for reinforced concrete slabs by using the equivalent reinforcement ratio instead of the ordinary reinforcement ratio. If there is any ordinary bonded reinforcement, its ratio can be added to the equivalent reinforcement ratio.

(3) Decompression approach

The decompression approach assumes that after decompression stage, the behavior of prestressed slabs is similar to that of reinforced concrete slabs having the same amount of nonprestressed reinforcement. The decompression state itself is defined as a condition where the precompression effect from prestressing is canceled by the effect of external loading. Consequently, the shear strength of prestressed slabs can be expressed as:

$$v_{cp} = v_{cr}\left(1 + \frac{V_d}{V_{cr}}\right) \tag{2.5}$$

where v_{cr} and V_{cr} are the respective shear strength and shear capacity of reinforced concrete slabs having the same amount of nonprestressed reinforcement; and V_d is the decompression load (the load corresponding to zero stress at the extreme fiber tensioned by external loading). This method was initially introduced by Regan (1985).

The decompression load V_d in Eq. (2.5) can be calculated using the following expression:

$$V_d = \left(\frac{V}{m}\right) m_d \tag{2.6}$$

where V/m is the ratio of shear force to moment per unit width and m_d is the decompression moment per unit width (the moment corresponding to zero stress at the extreme fiber tensioned by external loading). The ratio of shear force to moment per unit width V/m depends on the column geometry and the loading arrangement, whereas the decompression moment per unit width m_d can be computed using the flexure formula:

$$m_d = \frac{h^2}{6} f_e \tag{2.7}$$

where h is the slab thickness; and f_e is the extreme fiber stress due to prestressing.

2.3.6 Span-depth ratio

The effect of span-depth ratio on punching shear strength was investigated by Lovrovich and McLean (1990). Ten axisymmetric slabs were tested until failure, in which five of them were slabs with shear reinforcement. In the experiment, the slab thickness was kept constant whereas the support diameter was varied to give different span-depth ratios. It was found that the punching shear strength significantly increases as the span-depth ratio decreases below six. For span-depth ratios greater than 6, the punching shear strength is relatively constant. The reason is probably due to the formation of compression struts (tied-arch mechanism) from the loading point to the support, as also observed in deep beams. In addition, in-plane compressive forces caused by restraining action at the supports may have also interacted with the arch mechanism. This interaction might contribute to the increased strength for specimens with small span-depth ratios. However, additional tests are needed to study in detail the failure mechanism associated with punching shear in thick slabs.

2.3.7 Ratio of column width to slab effective depth

In general, for the same c/d ratio (ratio of column width to slab effective depth), slabs supported on circular columns will fail at higher load compared with slabs supported on square columns. The reason is that stress concentrations occur

around the corner of square columns. However, results from different studies are inconsistent because relative effects are influenced by the *c*/*d* ratio. Vanderbilt (1972) found that the punching shear strength of slabs supported on circular columns was only 5% higher than those on square columns at *c*/*d* ratios of two and eight. The increased strength was greater at intermediate *c*/*d* ratios, with a maximum value of 35% for *c*/*d* ratio of four.

2.4 Slab-column connections under earthquake loading

Earthquake loading is an inertia force generated during a ground shaking due to the mass of the structure. The ground shaking resulting from an earthquake is a random and time-dependent motion. Hence, the earthquake load is considered a dynamic load. However, due to the complexity of analysis, dynamic loads are usually treated using statically equivalent loads for general design purposes. In an experimental program, earthquake loading is usually simulated using pseudo-dynamic cyclic loading to investigate the strength of slab-column connections.

Megally and Ghali (2000b) presented a punching shear design procedure for earthquake-resistant slab-column connections. To provide some ductility, the gravity load must be limited to a value, which is a function of the drift ratio. In addition, the maximum shear stress due to combined shear and unbalanced moment transfer must not exceed the nominal shear strength of the slab, otherwise shear reinforcement should be provided. The design procedure also suggested that the value of unbalanced moment is not necessary taken greater than a limit that depends on the probable flexural strength of the slab.

Hueste et al. (2007) reviewed past experimental data on interior slab-column connections subjected to earthquake-type loading and suggested performance-based seismic design criteria. The criteria are based on FEMA 356 (ASCE 2000) performance levels (immediate occupancy, life safety, and collapse prevention) and seismic design requirements for slab-column connections in ACI 318. Figure 2.2 is reproduced from Hueste et al. (2007), showing the proposed performance-based design criteria and the collected experimental data. The life-safety-performance level corresponds to the ACI 318 design limit.

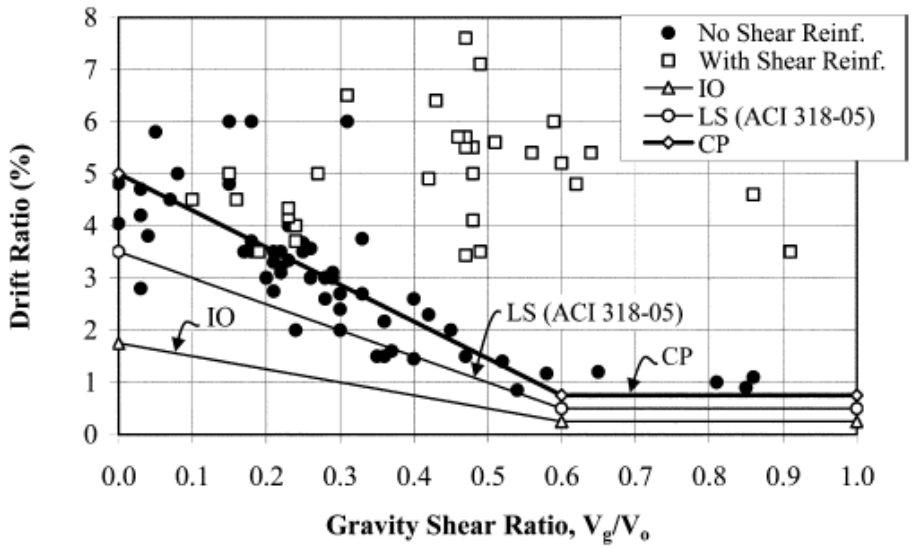

Figure 2.2 Performance-based design criteria (Hueste et al. 2007)

2.4.1 Drift ratio capacity

In low to moderate seismic regions, a slab-column frame may serve as a part of the seismic-force-resisting system. However, in high seismic regions, a flat plate structure is commonly used as a gravity-force-resisting system and combined with a seismic-force-resisting system, such as beam-column frame or shear wall, to resist the seismic force. Although the flat plate structure is assumed to carry gravity loads only, the slab-column connections should be able to undergo lateral deformations compatible to the attached seismic-force-resisting system without losing its function as gravity-force-resisting system. The lateral deformations imposed on the flat plate structure can establish significant unbalanced moments at a slab-column connection, hence increasing the potential of punching shear failures.

Sozen (1980) suggested that a seismic-force-resisting system must be provided to limit the interstory drift ratio of concrete structures to 1.5%. The interstory drift ratio is defined as the difference of lateral displacements between adjacent stories, divided by the story height. All the structural elements must be able to sustain the 1.5% drift ratio without failure. Pan and Moehle (1989) and ACI-ASCE Committee 352 (1997) also proposed the limit of 1.5% drift ratio for slab-column connections. Different limits of drift ratio are specified by UBC97 based on fundamental period of the structure. For structures having a fundamental period less than 0.7 s, the drift ratio is limited to 2.5%. Conversely, the limit of 2.0% drift ratio

applies to structures having a fundamental period greater than 0.7 s. The fundamental period is to be calculated in accordance with the UBC97 provisions.

2.4.2 Connection ductility

Ductility is an important parameter of structures that responds inelastically during severe earthquake loadings. The term ductility is defined as the ability of a structure or selected structural components to deform beyond the elastic range without excessive strength or stiffness degradation. The ductility factor can be quantified in many aspects, such as strain ductility, curvature ductility, and displacement ductility. However, for the particular case of slab-column connection, the displacement ductility is usually used.

Ductility of slab-column connections is defined as the ratio between the ultimate drift ratio and the yield drift ratio ($\mu = DR_u/DR_y$). However, the connection ductility cannot be defined uniquely as there is no distinct yield drift ratio on the unbalanced moment-drift ratio curve due to yield spreads gradually across the slab transverse width. Pan and Moehle (1989) proposed an arbitrary procedure to determine the connection ductility. In their method, the envelope of unbalanced moment-drift ratio curve is idealized as a bilinear elastoplastic behavior. The elastic portion intersects the actual curve at a value of unbalanced moment equal to two-thirds of the maximum unbalanced moment. The yield drift ratio is then taken as the intersection between the elastic and plastic portion, whereas the ultimate drift ratio is taken at the maximum unbalanced moment. Megally and Ghali (2000a) used the similar procedure as Pan and Moehle (1989) to determine the connection ductility; however, the ultimate drift ratio is taken at 80% of the maximum unbalanced moment instead of the maximum unbalanced moment.

The UBC91 code requires that the displacement ductility factor should be between three and four. Park and Paulay (1975) also stated that the typical values of the overall displacement ductility factor of frame structures in seismic zones are from three to five. To achieve a minimum drift ratio of 1.5%, Pan and Moehle (1989) suggested that shear walls and slab-column connections should have a minimum displacement ductility factor of 6 and 1.2, respectively.

2.4.3 Effect of gravity load

Tests by Kanoh and Yoshizaki (1975) showed that the level of gravity load acting on the slab is a main factor affecting the lateral displacement ductility. Subsequently, Pan and Moehle (1989) reviewed experimental data on reinforced concrete slab-column connections subjected to lateral loads. All the specimens were interior connections without shear reinforcement. Four of the specimens were tested by Pan and Moehle (1989), with two of them subjected to bidirectional cyclic lateral loading. It was also found that the gravity load mainly affects the lateral displacement capacity and ductility. Furthermore, bidirectional lateral loading reduces the lateral load stiffness, strength, and ductility. To achieve a minimum drift capacity of 1.5%, the gravity load is limited to 0.4 of the punching shear capacity. Similar conclusions were also obtained by Pan and Moehle (1992) and Moehle (1996).

Tan and Teng (2005) tested five interior slab-column connections subjected to gravity and cyclic lateral loading. The column shape was rectangular with the column aspect ratio of five. Two of them were reinforced with stud shear reinforcement. The main variables were the gravity shear ratio and the type of cyclic loadings (uniaxial or biaxial). It was found that biaxial unbalanced moments reduce the strength, ductility, drift capacity, and stiffness of the connection significantly. Furthermore, connections with rectangular columns having column aspect ratio of five and loaded biaxially may not be able to sustain a drift ratio of 1.5%, even if the gravity shear ratio is kept below 0.4. The gravity-shear-ratio limit was suggested to be 0.28. Subsequently, Anggadjaja and Teng (2008), and Widjaja and Teng (2006) conducted tests on edge and corner slab-column connections, respectively. The conclusions were similar as those in interior slab-column connections.

2.4.4 Effect of cyclic loading

Experiments on unconfined concrete (Popovics 1973) and confined concrete (Sinha et al. 1964) under cyclic loading showed that the stress-strain curve of monotonic loading form an envelope of the stress-strain response under cyclic loading. Consequently, no modification on the stress-strain curve is required when

calculating the flexural strength of concrete elements subjected to the stress reversals (Paulay and Priestley 1992).

The effect of cyclic loading on the punching shear strength of slab-column connections without shear reinforcement is still unclear. There is very limited data on tests of slab-column connections without shear reinforcement in which the nature of loading (monotonic or cyclic) was the only variable, whereas the other variables were kept relatively constant. Apparently, only specimens A1 and A2 tested by Hanson and Hanson (1968) and specimens 2 and 3C tested by Islam and Park (1976) belong to this category. It was found that there is no reduction in strength due to cyclic loading. In addition, Tian et al. (2008) concluded that the slab damage imposed by the previously applied cyclic loading has no detrimental effect on the connection gravity load-carrying capacity.

2.4.5 Effect of loading rate

Moe (1961) observed that there is no detrimental effect for a slab under a sustained load equal to three-quarters of its ultimate capacity for 3 months. On the other hand, Criswell (1970, 1974) concluded that rapid loadings might increase the strength of slabs compared with those loaded under static loadings. It was found that the shear and flexural strengths increased by 26% and 18%, respectively, when the maximum load was reached in 20 ms and 40 ms.

Ghali et al. (1976) conducted tests on six interior slab-column connections subjected to gravity and lateral loadings. The main variables were the type of the lateral load (static or dynamic) and the reinforcement ratio. It was shown that the specimens tested under dynamic loading failed at higher load compared with those tested under static loading. Hence, increasing the loading rate will also increase the material strengths (concrete and reinforcing steel). In addition, increasing the reinforcement ratio will lead to higher strength but reducing the rotation, ductility, and energy absorption.

2.5 Summary

- There are various models to calculate the punching shear strength of slab-column connections. Among them, only linear stress variation model, model based on elastic plate theory, beam analogy model, and truss analogy model can be used to

analyze the shear strength of slab-column connections transferring unbalanced moments. The other models are only suitable for slab-column connections under symmetrical punching.

- The punching shear strength of slab-column connections is influenced by several factors. However, the main parameters can be classified as concrete strength, flexural reinforcement ratio, slab effective depth, column rectangularity, and prestressing force.
- For prestressed slabs, there are three approaches to consider the effect of prestressing on the punching shear calculation: principal tensile stress approach, equivalent-reinforcement-ratio approach, and decompression approach.
- In addition to the strength requirement, slab-column connections under earthquake loading should have minimal drift ratio capacity and connection ductility. The connections ductility and drift ratio capacity depend mainly on the gravity shear ratio.

CHAPTER 3
CODE PROVISIONS ON PUNCHING SHEAR

3.1 Introduction

In most design codes, punching shear design is calculated at a critical section in the vicinity of the column, in such a way that the nominal shear strength should be greater than the applied shear stresses due to external loadings. The nominal shear strength is usually a function of several parameters, such as concrete tensile strength, flexural reinforcement ratio, prestressing force, slab thickness, and column dimensions. The methods used in design codes for punching shear design are mostly empirical and chosen mainly for the simplicity in practical applications.

Based on the similarity in treating punching shear of slab-column connections, design codes can be classified into two main groups. The first group consists of ACI 318-11 (ACI Committee 318 2011), CSA-A23.3-04 (CSA 2004), NZS 3101-2006 (NZS 2006), and AS 3600-2001 (AS 2001). The second group consists of Eurocode 2 (BSI 2004), BS 8110-1:1997 (BSI 1997), and CEB-FIP Model Code 1990 (CEB-FIP 1990). The same group of design codes were developed from the same model of punching shear calculation, but then underwent some modifications in the later development. In this study, only ACI 318-11 and Eurocode 2 will be discussed since they are the most widely used among them.

3.2 ACI 318-11

The critical section in ACI 318-11 is defined at a distance $d/2$ from the face of column so that its perimeter b_o is minimum. However, for square or rectangular columns, the critical section can be simplified into four straight sides.

3.2.1 Shear Strength

ACI 318-11 defines the punching shear strength of reinforced concrete slabs without shear reinforcement as the smallest of the following formulas:

$$v_c = \left(2 + \frac{4}{\beta}\right)\lambda\sqrt{f'_c} \text{ (psi) or } v_c = 0.17\left(1 + \frac{2}{\beta}\right)\lambda\sqrt{f'_c} \text{ (MPa)} \qquad (3.1)$$

$$v_c = \left(\frac{\alpha_s d}{b_o} + 2\right)\lambda\sqrt{f'_c} \text{ (psi) or } v_c = 0.083\left(\frac{\alpha_s d}{b_o} + 2\right)\lambda\sqrt{f'_c} \text{ (MPa)} \quad (3.2)$$

$$v_c = 4\lambda\sqrt{f'_c} \text{ (psi) or } v_c = 0.33\lambda\sqrt{f'_c} \text{ (MPa)} \quad (3.3)$$

where β is the ratio of longer side to shorter side of column; α_s is 40 for interior columns, 30 for edge columns, and 20 for corner columns; d is the average effective depth of slab; b_o is perimeter of critical section located at a distance $d/2$ from the column face; λ is the modification factor reflecting the reduced mechanical properties of lightweight concrete (λ = 1.0 for normalweight concrete, 0.85 for sand-lightweight concrete, and 0.75 for all-lightweight concrete); and f'_c is the compressive strength of concrete. For post-tensioned slabs without shear reinforcement, the punching shear strength can be calculated from

$$v_c = \beta_p\lambda\sqrt{f'_c} + 0.3f_{pc} + \frac{V_p}{b_o d} \quad (3.4)$$

where β_p is the smaller of 3.5 and ($\alpha_s d/b_o$+1.5) [for psi unit] or the smaller of 0.29 and 0.083($\alpha_s d/b_o$ +1.5) [for MPa unit]; f_{pc} is the average compressive stress in concrete in two orthogonal directions; and V_p is the vertical component of all effective prestress forces crossing the critical section.

ACI 318-11 requires that the use of Eq. (3.4) to be restricted to the following conditions:

- No portion of the column cross section shall be closer to a discontinuous edge than 4h;
- The value of $\sqrt{f'_c}$ shall not be taken greater than 70 psi (5.8 MPa);
- The value of f_{pc} in each direction shall be between 125 psi (0.9 MPa) and 500 psi (3.5 MPa).

If one of those conditions is not satisfied, the calculation of v_c shall be based on formula for reinforced concrete slabs [Eqs. (3.1) to (3.3)]. However, Foutch et al. (1990) and Silva et al. (2007) concluded that the limitations of concrete strength and compressive stress in ACI 318 are not necessary, as they do not improve the correlations with test results. Hence, in this study, the strength predictions of post-

tensioned slabs by ACI 318-11 were calculated using Eq. (3.4), ignoring the limitations of concrete strength and compressive stress. In addition, the value of λ is always taken to be unity as this study is limited only to slab-column connections cast with normalweight concrete.

3.2.2 Shear and Moment Transfer

For symmetrically loaded slab-column connections, the ultimate shear stress (v_u) acting on the critical section is assumed to be uniformly distributed. Thus, it can be calculated from

$$v_u = \frac{V_u}{b_o d} \tag{3.5}$$

where V_u is the applied shear force; b_o and d are as defined previously. If there is a transfer of unbalanced moment (M_u) between slab and column, ACI 318-11 presents a method known as the eccentric shear stress model to calculate the applied or load induced shear stresses due to both shear force and unbalanced moments. The model assumes that a fraction of the unbalanced moment ($\gamma_v M_u$) can be transferred to the slab critical section as eccentric shear stresses that can be added to the shear stresses on the same section resulting from the direct shear force [Eq. (3.5)]. The shear stresses due to a fraction of the unbalanced moment are distributed linearly about the centroid of the critical section. Punching shear failure occurs when the maximum sum of the shear stresses reaches the shear strength determined from Eqs. (3.1) to (3.4). Additional slab flexural steel is required within a width of c plus 1.5h on each side of the column to resist the portion of unbalanced moment not resisted by the slab shear stresses (transferred by flexure). When the portion of unbalanced moment transferred by flexure ($\gamma_f M_u$) reaches the limiting flexural strength (M_f) of slab reinforcement within the prescribed transfer width, flexural failure is deemed to have occurred at the connection.

Figure 3.1(a) shows the assumed critical section and the distribution of shear stresses for an interior connection subjected to unidirectional moment transfer. The maximum shear stress that occurs in the slab at the face AB is given by:

$$v_{uA} = v_{uB} = \frac{V_u}{b_o d} + \frac{\gamma_{vy} M_{uy} s_{AB}}{J_{cy}} \tag{3.6}$$

where V_u and M_u are the applied shear force and unbalanced moment acting at the centroid of the critical section, respectively; b_o and d are defined as in Eq. (3.2); γ_v is the fraction of unbalanced moment transferred by shear; s_{AB} is the distance from the centroidal axis of the critical section to the face AB; and J_c is the property of the critical section analogous to the polar moment of inertia. The subscript y represents the axis about which the unbalanced moment is transferred. When bidirectional unbalanced moments are transferred, the maximum shear stress occurs at one point on the critical section where the shear stresses due to the biaxial moments are additive [analogous to point B in Figure 3.1(c)]. It can be expressed by:

$$v_{uB} = \frac{V_u}{b_o d} + \frac{\gamma_{vy} M_{uy} s_{AB}}{J_{cy}} + \frac{\gamma_{vx} M_{ux} s_{BC}}{J_{cx}} \tag{3.7}$$

where s_{AB} and s_{BC} are the distances from the centroidal axes of the critical section to the faces AB and BC of the critical section, respectively [Figure 3.1(a)]. The subscripts x and y represent two perpendicular axes about which the unbalanced moments are transferred.

Figure 3.1(b) shows the distribution of shear stresses in the assumed critical section for an edge connection when moment is transferred about an axis parallel to the edge of the slab. The unbalanced moment acting at the centroid of the critical section M_s is calculated as ($M_u - V_u g$), where g is the distance between the centroidal axis of the critical section and the centroidal axis of the column. The maximum shear stress in the slab critical section occurs at either face AB, point C, or point D, and is given by:

$$v_{uA} = v_{uB} = \frac{V_u}{b_o d} + \frac{\gamma_{vy} (M_{uy} - V_u g_x) s_{AB}}{J_{cy}} \tag{3.8}$$

$$v_{uC} = v_{uD} = \frac{V_u}{b_o d} - \frac{\gamma_{vx} (M_{ux} - V_u g_y) s_{CD}}{J_{cx}} \tag{3.9}$$

where s_{AB} and s_{CD} are the distances from the centroidal axes of the critical section to tha faces AB and CD of the critical section, respectively [Figure 3.1(b)]. For an

unbalanced moment transferred about an axis perpendicular to the edge of the slab, the ultimate shear stresses are calculated as for the case of interior connections.

Figure 3.1(c) shows the distribution of shear stresses on the assumed critical section when bidirectional unbalanced moments are transferred in a corner connection. The parameters g_x and g_y are the distances between the centroidal axes of the critical section and the centroidal axes of the column. The maximum shear stress in the slab critical section occurs at either point A, B or C, and is given by:

$$v_{uA} = \frac{V_u}{b_o d} + \frac{\gamma_{vy}(M_{uy} - V_u g_x)s_{AB}}{J_{cy}} - \frac{\gamma_{vx}(M_{ux} - V_u g_y)s_{AD}}{J_{cx}} \tag{3.10}$$

$$v_{uB} = \frac{V_u}{b_o d} + \frac{\gamma_{vy}(M_{uy} - V_u g_x)s_{AB}}{J_{cy}} + \frac{\gamma_{vx}(M_{ux} - V_u g_y)s_{BC}}{J_{cx}} \tag{3.11}$$

$$v_{uC} = \frac{V_u}{b_o d} - \frac{\gamma_{vy}(M_{uy} - V_u g_x)s_{CD}}{J_{cy}} + \frac{\gamma_{vx}(M_{ux} - V_u g_y)s_{BC}}{J_{cx}} \tag{3.12}$$

where s_{AB}, s_{AD}, s_{BC}, and s_{CD} are the distances from the centroidal axes of the critical section to the faces AB, AD, BC, and CD of the critical section, respectively [Figure 3.1(c)].

The fraction of unbalanced moment transferred by shear (γ_v) used in Eqs. (3.6) to (3.12) is defined as

$$\gamma_v = 1 - \gamma_f \tag{3.13}$$

where γ_f is the fraction of unbalanced moment transferred by flexure, computed using the expression below

$$\gamma_f = \frac{1}{1 + (2/3)\sqrt{b_1 / b_2}} \tag{3.14}$$

where b_1 and b_2 are the respective widths of the critical section measured parallel and perpendicular to the directions of the span for which moments are determined. For connections of flat plates with rectangular columns, γ_v is bigger when b_1 exceeds b_2 [Eqs. (3.13) and (3.14)]. High shear stress results on the b_2 sides of the shear critical section due to the transfer of unbalanced moment about an axis parallel to the short side of the column. Shear strength of a connection, v_n is a

function of v_c and v_s (if shear reinforcement is provided), while the shear stress is induced by the internal forces at the slab-column connection: V_u, M_{ux} and M_{uy}.

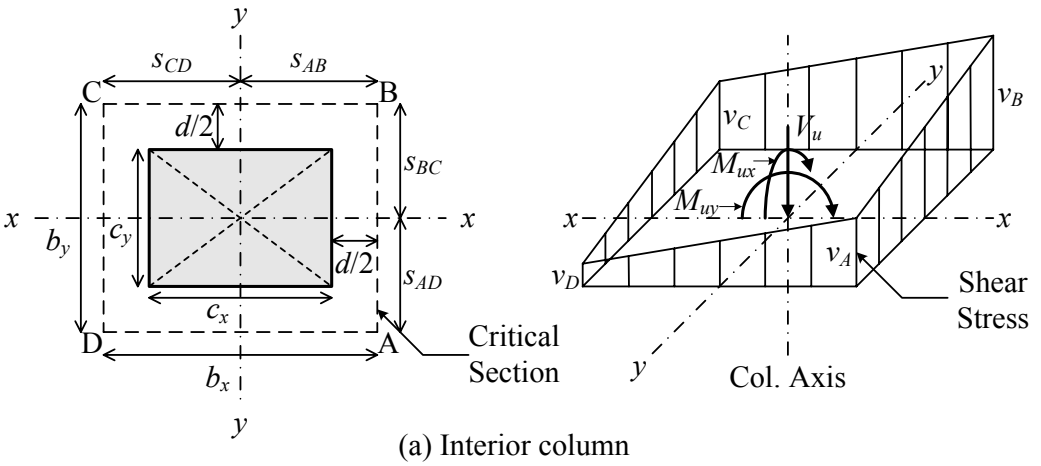

(a) Interior column

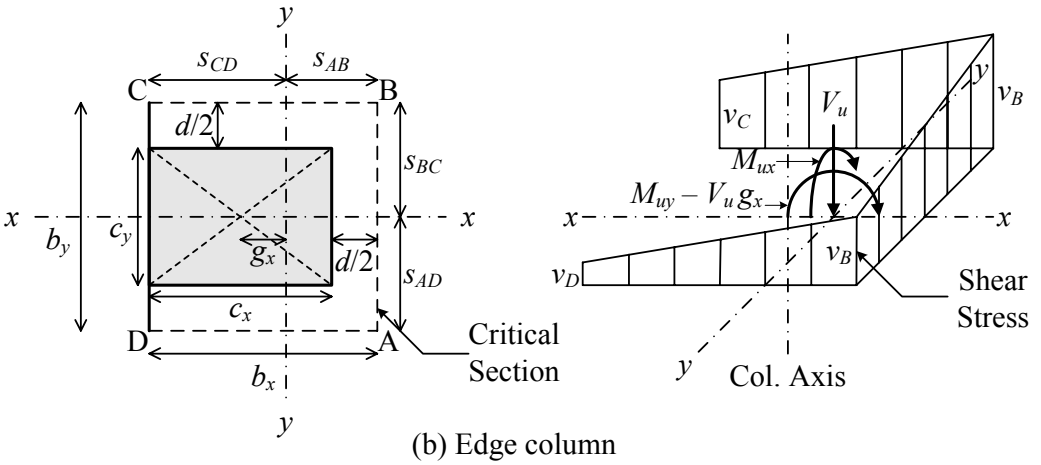

(b) Edge column

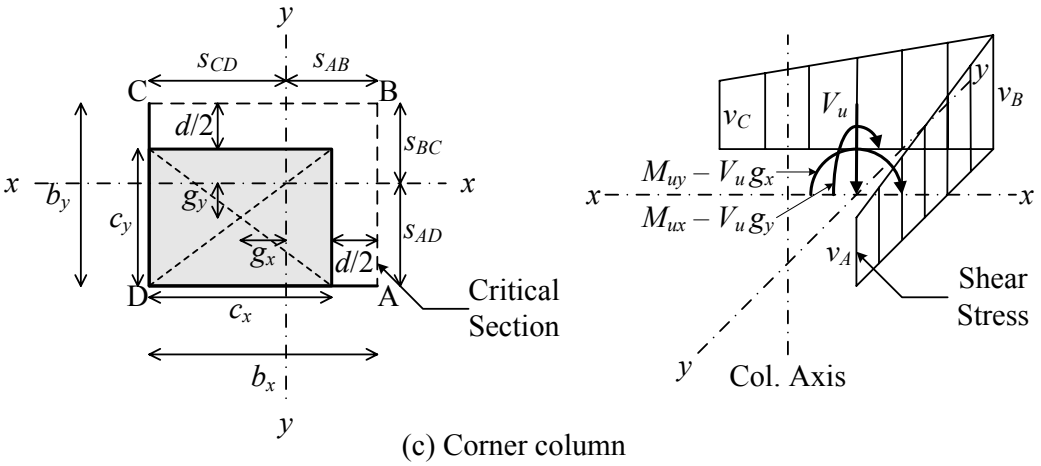

(c) Corner column

Figure 3.1 Critical sections and shear stress distribution according to ACI 318-11

The property of the critical section analogous to polar moment of inertia (J_c) is intended to consider torsions on the faces of the critical shear perimeter. To compute J_c, the critical sections is devided into two, three, four, or more individual sides. Then, the term J_c is the sum of the individual values computed for each side [Wight and Macgregor 2009]. For interior connections with moment transfer about y- and x-axes, the equations to compute J_c are given below:

$$J_{cy} = \frac{2(b_x d^3)}{12} + \frac{2(db_x^3)}{12} + 2(b_y d)\left(\frac{b_x}{2}\right)^2 \tag{3.15}$$

$$J_{cx} = \frac{2(b_y d^3)}{12} + \frac{2(db_y^3)}{12} + 2(b_x d)\left(\frac{b_y}{2}\right)^2 \tag{3.16}$$

where b_x and b_y are the widths of the critical shear perimeter along the x- and y-axes, respectively; and d is the average effective depth of slab. Similar equations may also be developed for edge and corner connections. The formulas to calculate J_c for edge connections with unbalanced moments about axes parallel (y-axis) and perpendicular (x-axis) to the slab edge are given below:

$$J_{cy} = \frac{2(b_x d^3)}{12} + \frac{2(db_x^3)}{12} + 2(b_x d)\left(\frac{b_x}{2} - s_{AB}\right)^2 + (b_y d)s_{AB}^2 \tag{3.17}$$

$$J_{cx} = \frac{b_y d^3}{12} + \frac{b_y^3 d}{12} + 2(b_x d)s_{BC}^2 \tag{3.18}$$

For corner connections with moment transfer about y- and x-axes, the formulas to compute J_c are provided below:

$$J_{cy} = \frac{b_x d^3}{12} + \frac{b_x^3 d}{12} + (b_x d)\left(\frac{b_x}{2} - s_{AB}\right)^2 + (b_y d)s_{AB}^2 \tag{3.19}$$

$$J_{cx} = \frac{b_y d^3}{12} + \frac{b_y^3 d}{12} + (b_y d)\left(\frac{b_y}{2} - s_{BC}\right)^2 + (b_x d)s_{BC}^2 \tag{3.20}$$

The definition of J_c is ambiguous as polar moment of inertia is known, in mechanics, as the second moment of a plane area about a point, not about an axis (x or y); but the assumed shear critical section is a spatial non-plane surface. The ambiguity of the definition of J_c can be a hurdle in accounting for the unbalanced

moment in punching shear design of connections having non-rectangular shapes. ACI 421.1R-08 gives a general equation that applies to any shear critical section having a polygonal shape.

3.2.3 Seismic Considerations

When a flat plate structure is assumed not to contribute to the seismic-force-resisting system, the slab-column connections shall be designed to resist the gravity shear force V_u and the induced moment transferred under the design displacement. Alternatively, the design story drift ratio should not exceed the larger of 0.005 and [0.035 – 0.05($V_u/\phi V_c$)]. The gravity shear ratio $V_u/\phi V_c$ is defined as the ratio of the gravity shear force V_u to the shear capacity V_c, given by:

$$V_c = v_c b_o d \tag{3.21}$$

where v_c is calculated using Eqs. (3.1) to (3.4), whichever is applicable. In this study, the strength reduction factor ϕ is taken equal to unity. If the design story drift ratio exceeds the limit given above, then slab shear reinforcement shall be provided. This requirement is based on recommendation from ACI 352.1R-89 that the gravity shear ratio should be kept below 0.4 to ensure some minimal ductility with the availability of approximately 1.5% drift capacity. The story drift requirement is depicted in Figure 3.2.

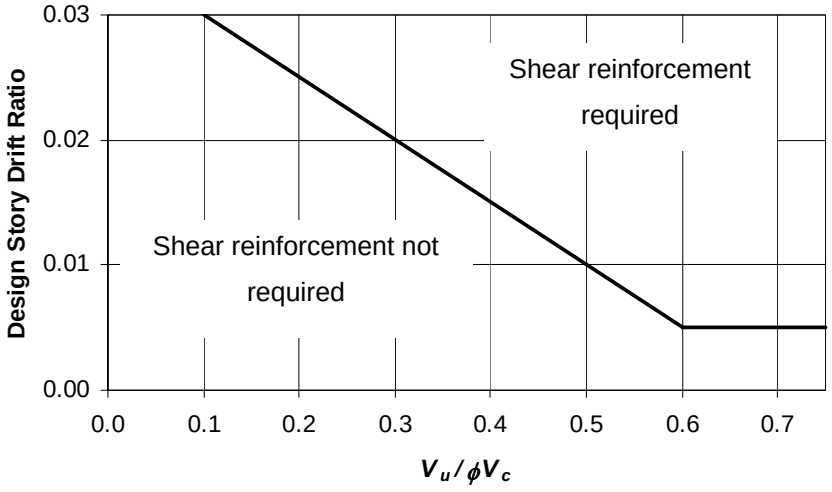

Figure 3.2 Story drift ratio requirements according to ACI 318-11

3.3 Eurocode 2

Eurocode 2 defines the critical section at a distance 2*d* from the face of column such that it gives a minimum length. Thus, the critical section at the corners of rectangular columns is a quadrant. Figure 3.3 shows the critical sections according to Eurocode 2.

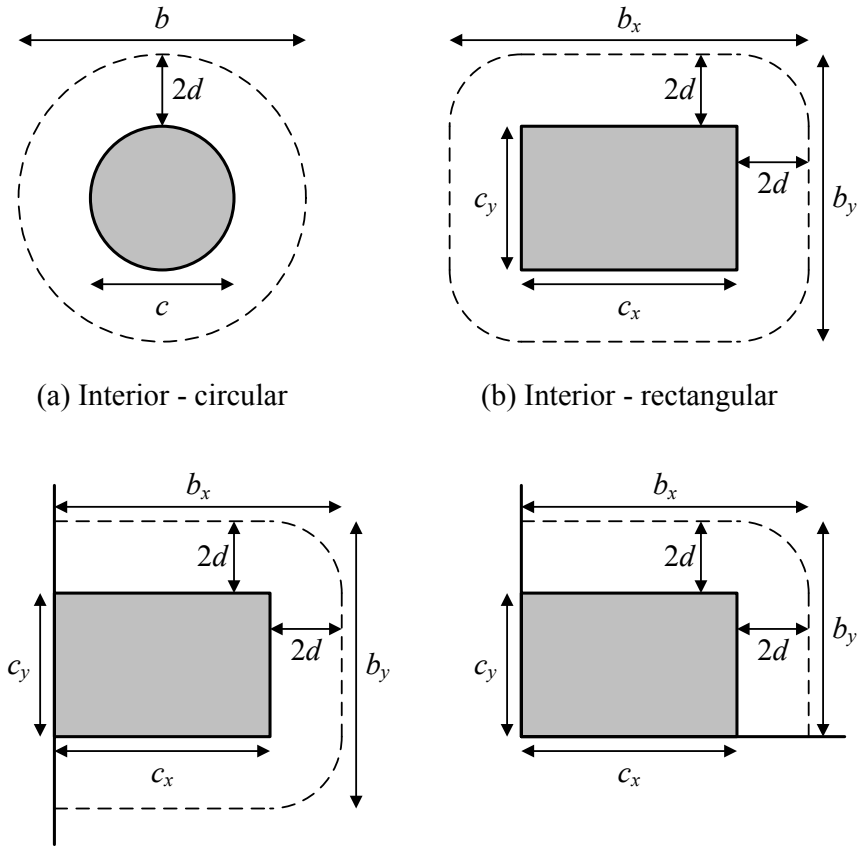

(a) Interior - circular (b) Interior - rectangular

(c) Edge - rectangular (d) Corner - rectangular

Figure 3.3 Critical sections according to Eurocode 2

3.3.1 Shear Strength

The punching shear resistance of slabs without shear reinforcement can be calculated using the following expression:

$$v_c = 0.18k_d(100\rho_l f'_c)^{1/3} + 0.1f_{pc} \geq 0.035k_d^{3/2}\sqrt{f'_c} \qquad (3.22)$$

where k_d is the depth factor; ρ_l is the tension reinforcement factor; f'_c is the compressive strength of concrete cylinder; and f_{pc} is the average compressive stress in concrete due to prestressing. The depth factor k_d is defined as

$$k_d = 1 + \sqrt{\frac{200}{d}} \leq 2.0 \tag{3.23}$$

where d is the average effective depth of reinforcing steel (in mm). The tension reinforcement factor ρ_l is given by:

$$\rho_l = \sqrt{\rho_{lx} \cdot \rho_{ly}} \leq 0.02 \tag{3.24}$$

where ρ_{lx} and ρ_{ly} are the flexural reinforcement ratios within a column width plus 3d on each side of the column in x- and y-directions, respectively.

3.3.2 Shear and Moment Transfer

When there is a transfer of moment between slab and column, Eurocode 2 introduces a factor β_v to calculate the maximum ultimate shear stress such that:

$$v_u = \beta_v \frac{V_u - V_{pd}}{ud} \tag{3.25}$$

where V_u is the applied shear force; V_{pd} is the vertical component of all effective prestressing force passing through the critical section; u is the perimeter of the critical section taken at a distance 2d from the column face; and d is the effective depth of bonded reinforcement. Figure 3.4 shows the shear stress distribution of an interior connection subjected to unidirectional moment transfer.

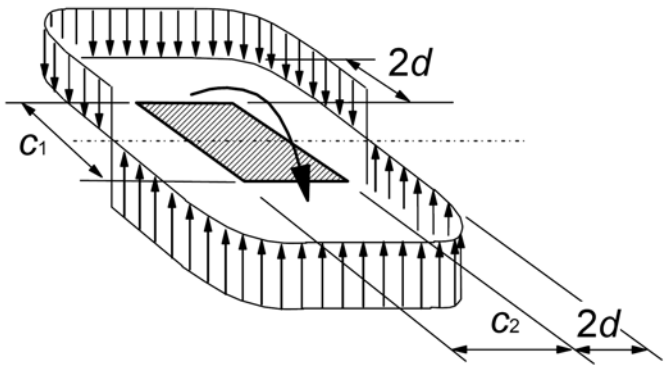

Figure 3.4 Shear stress distribution according to Eurocode 2

For interior connections transferring shear and unidirectional unbalanced moment, the factor β_v is given by:

$$\beta_v = 1 + k \frac{M_u}{V_u} \cdot \frac{u}{W} \tag{3.26}$$

where k is a coefficient that depends on the ratio of column dimensions c_1 and c_2; M_u is the applied unbalanced moment; and W is a factor corresponding to the shear stress distribution. Table 3.1 provides the values of k for rectangular columns. The general formula to calculate W is defined as:

$$W = \int_0^u |e_l| dl \tag{3.27}$$

where dl is the length increment of the critical section perimeter and e_l is the distance of dl from the axis about which the moment M_u acts. For interior connections with rectangular columns, the factor W can be computed using the following expression:

$$W = \frac{c_1^2}{2} + c_1 c_2 + 4c_2 d + 16d^2 + 2\pi d c_1 \tag{3.28}$$

where c_1 and c_2 are the respective column widths measured parallel and perpendicular to the directions of the span for which moments are determined. When bidirectional unbalanced moments are transferred between slabs and columns, the following formula may be used to estimate the β_v-value:

$$\beta_v = 1 + 1.8\sqrt{\left(\frac{e_x}{b_x}\right)^2 + \left(\frac{e_y}{b_y}\right)^2} \tag{3.29}$$

where e_x and e_y are the load eccentricities (calculated as M_u/V_u) along x- and y-axes, respectively; and b_x and b_y are the respective dimensions of the critical section along x- and y-axes. For interior connections with circular columns, the factor β_v can be calculated as:

$$\beta_v = 1 + 0.6\pi \frac{e}{c + 4d} \tag{3.30}$$

where c is the diameter of the circular column.

Table 3.1 Values of k for rectangular column (after Eurocode 2, 2004)

c_1/c_2	≤0.5	1.0	2.0	≥3.0
k	0.45	0.60	0.70	0.80

For edge connections where the eccentricity perpendicular to the slab edge (due to unbalanced moment about an axis parallel to the slab edge) is toward the interior and there is no eccentricity parallel to the slab edge, the punching shear stress may be considered to be uniformly distributed along the reduced critical section perimeter u^* as shown in Figure 3.5(a). Thus, the β_v-value is defined as:

$$\beta_v = \frac{u}{u^*} \tag{3.31}$$

When there are eccentricities in two orthogonal directions, β_v-value can be computed as:

$$\beta_v = \frac{u}{u^*} + k\frac{u}{W}e_y \tag{3.32}$$

where e_y is the eccentricity parallel to the slab edge (y-axis), calculated as (M_{ux}/V_u). The value of k can be obtained from Table 3.1 by using the ratio of $c_1/2c_2$ instead of c_1/c_2. The corresponding W-value for the reduced critical section is given as:

$$W = \frac{c_2^2}{4} + c_1c_2 + 4c_1d + 8d^2 + \pi dc_2 \tag{3.33}$$

If the eccentricity perpendicular to the slab edge is toward the exterior, the β_v-value is calculated using Eq. (3.26). Note that the distance e_l for calculating W should be measured from the centroid of the critical section.

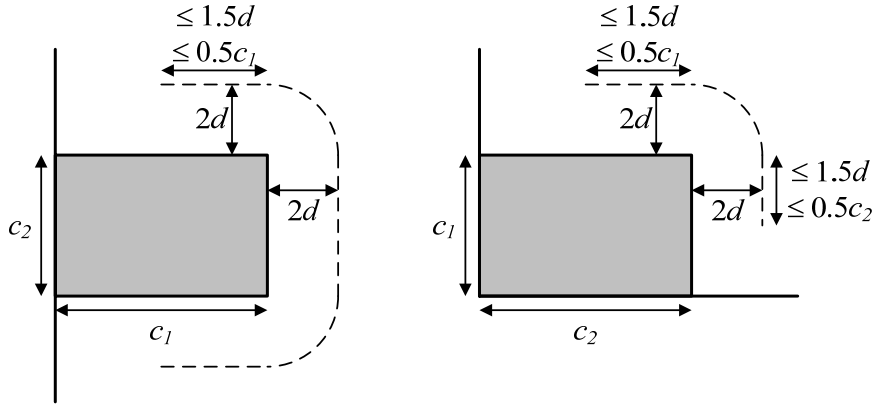

(a) Edge columns (b) Corner columns

Figure 3.5 Reduced critical section according to Eurocode 2

For corner connections, where the eccentricity is toward the interior, the punching shear stress is assumed to be uniformly distributed along the reduced critical section perimeter u^* as defined in Figure 3.5(b). Accordingly, the β_v-value is calculated using Eq. (3.31). If the eccentricity is toward the exterior, the β_v-value is calculated using Eq. (3.26).

For structures where the lateral stability does not depend on frame action between the slabs and columns, and where the adjacent spans do not differ by more than 25%, approximate values of β_v may be used. Recommended values of β_v are 1.15, 1.4, and 1.5 for interior, edge, and corner connections, respectively.

3.3.3 Seismic Considerations

Eurocode 2 does not give any specific consideration regarding the design of flat plate structures under seismic loading. However, it is common practice to design flat plate structures in seismic regions as secondary seismic members. Secondary seismic members are defined as members that are not considered as part of the seismic action resisting system of the building. Consequently, their strength and stiffness against seismic actions should be neglected in the analysis. Requirements on secondary seismic members are given in Eurocode 8 (BS EN 1998-1:2004). The code requires that the secondary seismic members should be designed and detailed to maintain their capacity to carry the gravity loads when subjected to maximum deformations under seismic loadings. To calculate the maximum deformations due to the seismic loadings, the contribution of secondary seismic members to the lateral stiffness is neglected, and the primary seismic members are modeled with their cracked flexural and shear stiffness. In addition, the analysis should include the P-Δ effects. Accordingly, the secondary seismic members are deemed to satisfy the requirements if the bending moments and shear forces calculated on the basis of the deformations and their cracked flexural and shear stiffness, do not exceed their design flexural and shear resistance, respectively, as given in Eurocode 2.

3.4 Summary

Based on reviews of the two design codes (ACI 318-11 and Eurocode 2) above, the following conclusions can be drawn:

- ACI 318-11 defines the critical section at a distance of 0.5*d* from the face of the column and assumes that the concrete tensile strength is proportional to the square root of the concrete compressive strength. In Eurocode 2, the critical section is defined at a distance of 2*d* from the face of the column and the concrete tensile strength is assumed proportional to the cube root of the concrete compressive strength. Thus, in general ACI 318-11 has a smaller critical section but higher shear strength compared with Eurocode 2.
- The nominal shear strength is governed by several factors, such as concrete tensile strength, flexural reinforcement ratio, prestressing force, slab thickness, and column dimension. ACI 318-11 does not consider the effect of flexural reinforcement ratio in the punching shear design calculation whereas Eurocode 2 takes into account all the factors above.
- For connections under symmetrical punching (without unbalanced moments), the factored shear stress is assumed to be uniform along the critical shear perimeter.
- For connections under unsymmetrical punching (with unbalanced moments), there are two different approaches. The first approach, adopted by ACI 318-11, assumes that the shear stress due to moment transfer is added or subtracted to the shear stress caused by direct shear force and the worse will govern. The second approach that is used by Eurocode 2 suggests increasing the shear stress to an effective value in order to take into account the effect of moment transfer.
- For connections under seismic loading, Eurocode 2 or Eurocode 8 has no special considerations, whereas ACI 318-11 requires that shear stress due to factored gravity load should not exceed 0.4 of the nominal shear strength in order to achieve sufficient lateral displacement ductility and a minimum story drift ratio of 1.5%.

CHAPTER 4
EXPERIMENTAL PROGRAM

4.1 Introduction

The main objective of this experimental program is to study the failure behavior of post-tensioned slab-column connections subjected to gravity and cyclic lateral loading. Thus, isolated slab-column connection specimen was chosen. This type of specimen may not be able to capture the overall behavior of the structure. However, the complexity of internal actions around the connections is confined to a localized area of the slab near the column. The stress concentrations in this region are very high but decrease rapidly with the distance from the column. Therefore, the strengths observed in this specimen are believed to estimate closely the strengths of connections in the actual structure. Compared with multi-panel specimen, isolated specimen is simpler and cheaper. Furthermore, isolated specimen is statically determinate so that moments and shears at the connection can be calculated directly.

The use of rectangular columns is very popular in high-rise apartment or residential buildings, due to architectural detailing that frequently require a column to be flush with the adjacent walls. However, it seems that there is no published data available on post-tensioned slab-column connections with rectangular columns. Hence, rectangular columns with aspect ratio of five were used in this experimental program. Unbonded tendons were chosen instead of bonded tendons as the former are more widely used in the slab systems and they have lower ultimate capacity than bonded tendons. For design purposes, having lower ultimate capacity is preferable as the results will be on the conservative side.

Three identical specimens representing a portion of interior slab-column connections were constructed and tested in the Protective Engineering Laboratory, School of Civil and Environmental Engineering, Nanyang Technological University, Singapore. The first specimen was tested under gravity load only to study the symmetrical punching capacity of post-tensioned slab-column connection with rectangular column. The second specimen was tested under gravity and unidirectional cyclic lateral loading to study the effect of cyclic moment transfer

about strong column axis. The last specimen was tested under gravity and bidirectional cyclic lateral loading to study the effect of cyclic moment transfer about two orthogonal axes.

4.2 Specimens

The specimen size was derived from an approximately ¾-scale model of a ten-story post-tensioned flat plate building as shown in Figure 4.1. The model structure has a typical column dimension of 180 mm × 900 mm (7.1 in × 35.4 in) and a story height of 2.25 m (7.38 ft). The slab thickness was 150 mm (5.9 in), the span lengths in two perpendicular directions were 5.25 m (17.22 ft) and 6.75 m (22.15 ft), resulting in span-to-depth ratios of 35 and 45, respectively in the short and long span directions, which are typical value for post-tensioned flat plate floors (Khan and Williams 1995).

The model structure was designed in accordance with ACI 318-11 as given in Appendix A. The slab was designed to support gravity loads only, which consist of self weight, superimposed dead load of 1.4 kPa (29.2 psf), and live load of 2.4 kPa (50.1 psf). Lateral wind or earthquake loading was assumed to be resisted by shear walls. About 90% of the dead load in the interior spans was assumed to be balanced by post-tensioning, resulting in 12 and 10 tendons in the longer-span and shorter-span directions, respectively. The tendons were banded in the longer-span direction and uniformly distributed in the shorter-span direction. Assuming an initial force per tendon of 130.2 kN (29.3 kip) [$\cong 0.7f_{pu}$], with the lump-sum losses of 20 kN (4.5 kip), the effective force per tendon becomes 110.2 kN (24.8 kip). Thus, the average compressive stresses in the slab due to prestress (f_{pc}) were 1.68 MPa (244 psi) and 1.09 MPa (158 psi) in the longer-span and shorter-span directions, respectively. At the connection regions, minimum top nonprestressed reinforcement was provided in accordance with Section 18.9.3 of ACI 318-11 [Eq. (18-8)]. Six bars of 13-mm diameter deformed bars (6ϕ13) were provided within a column width plus 1.5h on each side of the column, in each direction (x- and y-directions). The slab bottom reinforcement was provided based on the structural integrity requirement of ACI 352.1R-89. This recommendation leads to 4ϕ13 in each direction, however due to a space constraint, two bottom bars were provided in y-direction, and six bars were

provided in *x*-direction. The bottom bars were continuous through the column, satisfying the requirement from Section 13.3.8 of ACI 318-11.

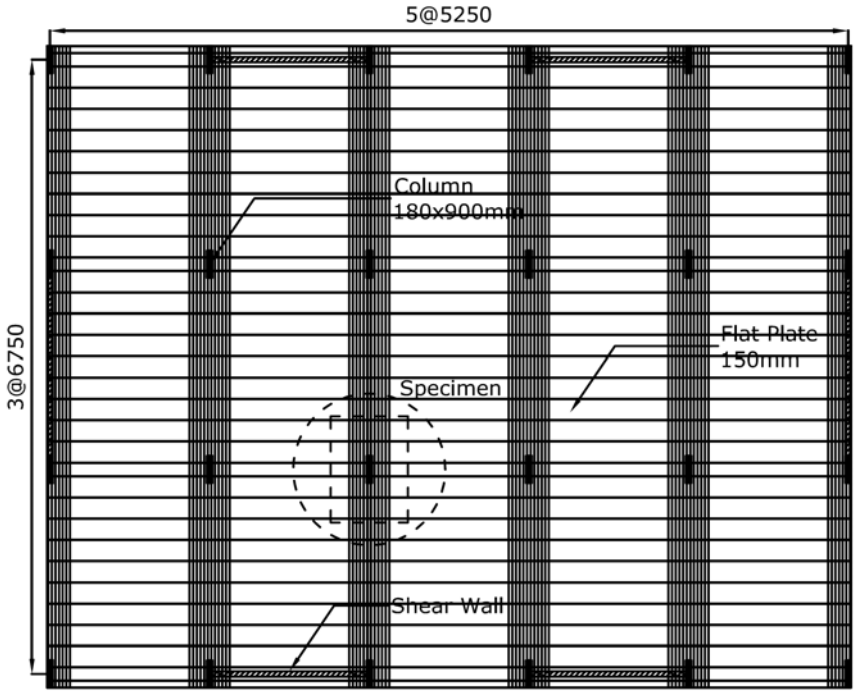

(a) Plan

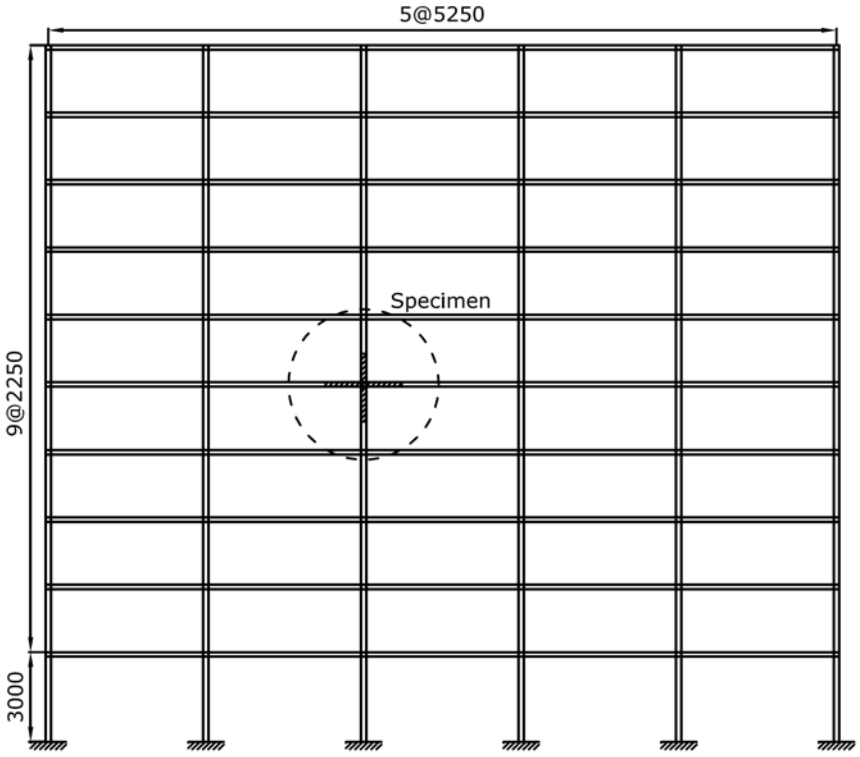

(b) Elevation (South)

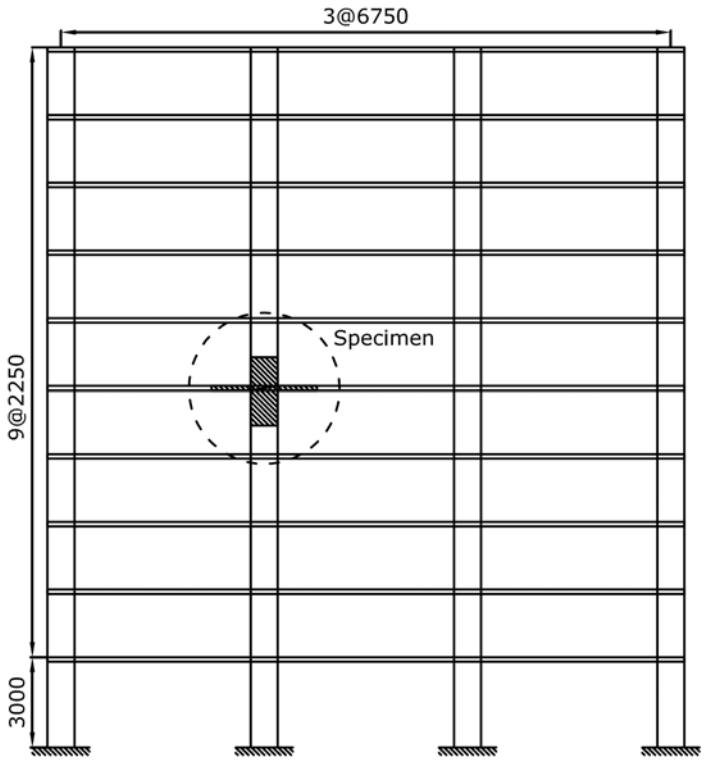

(c) Elevation (East)

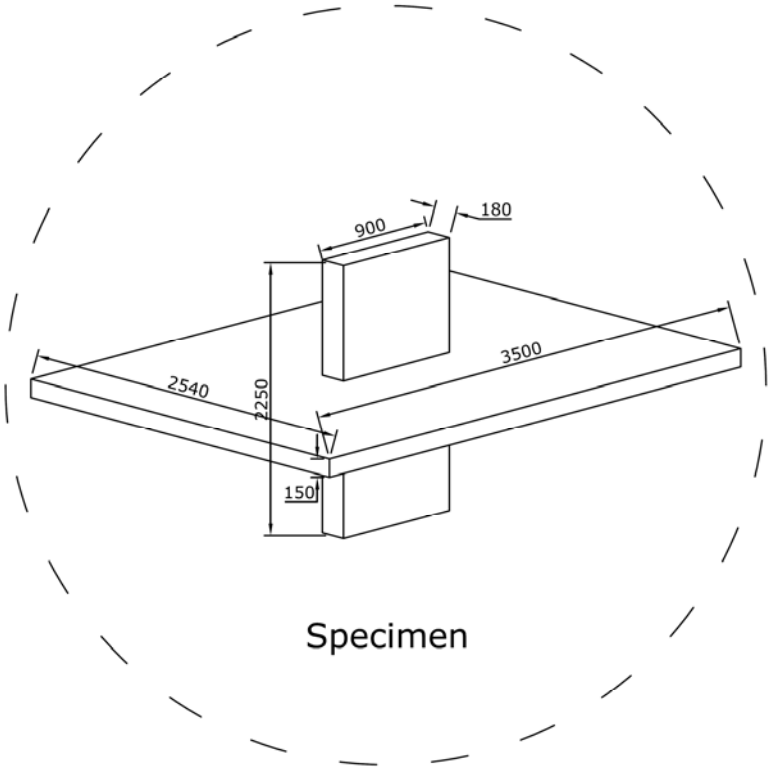

(d) Specimen

Figure 4.1 Model structure and specimen

The specimens represent interior slab-column connections, taken arbitrarily at the fifth story of the model structure. The slab was terminated around the lines of contraflexure under gravity loading, whereas the column was terminated at the middle of the story height. For slab-column connections under gravity loads combined with unbalanced moments, the contraflexure lines would move slightly away from the usual location, but it would not be at the midspan. The specimen dimensions were then adjusted to fit into the testing frame, resulting in a slab dimension of 2540 mm × 3500 mm (100.0 in × 137.8 in), and a column height of 950 mm (37.4 in) and 1150 mm (45.3 in) above and below the slab surface, respectively. The slab boundaries were assumed to be on rollers whereas the column bottom was supported on a pin as depicted in Figure 4.2.

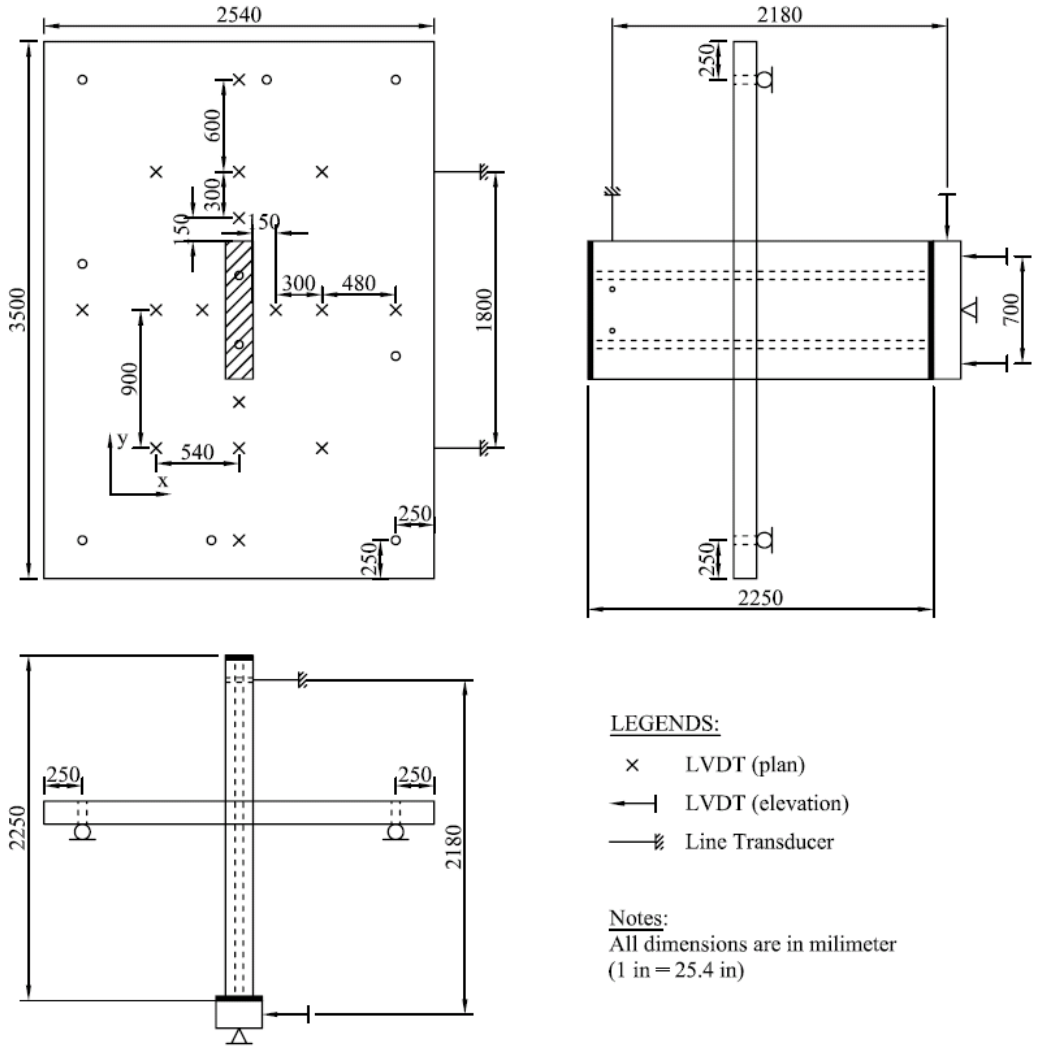

Figure 4.2 Boundary condition and transducer location

The specimen configuration leads to six (6) uniformly distributed tendons in *x*-direction (shorter direction) and 12 banded tendons in *y*-direction (longer direction). To obtain the same compressive stress as in the model structure, the effective forces per tendon of the specimen were then adjusted to 53.3 kN (12.0 kip) and 95.2 kN (21.4 kip) for tendons along *y*- and *x*-directions, respectively. At the slab edges, anchorage reinforcement (4ϕ10 and ϕ10@100 or 10-mm deformed bars at 100-mm center-to-center spacing) was provided to prevent splitting of concrete due to prestressing. This detail of reinforcement is similar to the requirement of ACI 423.3R-96. Figure 4.3 shows the layout and profile of the slab tendons. The top and bottom slab reinforcement were provided as in the model structure whereas the column reinforcement was designed such that the slab would fail first rather than the column. The details of the slab and column reinforcement are depicted in Figure 4.4 and Figure 4.5, respectively.

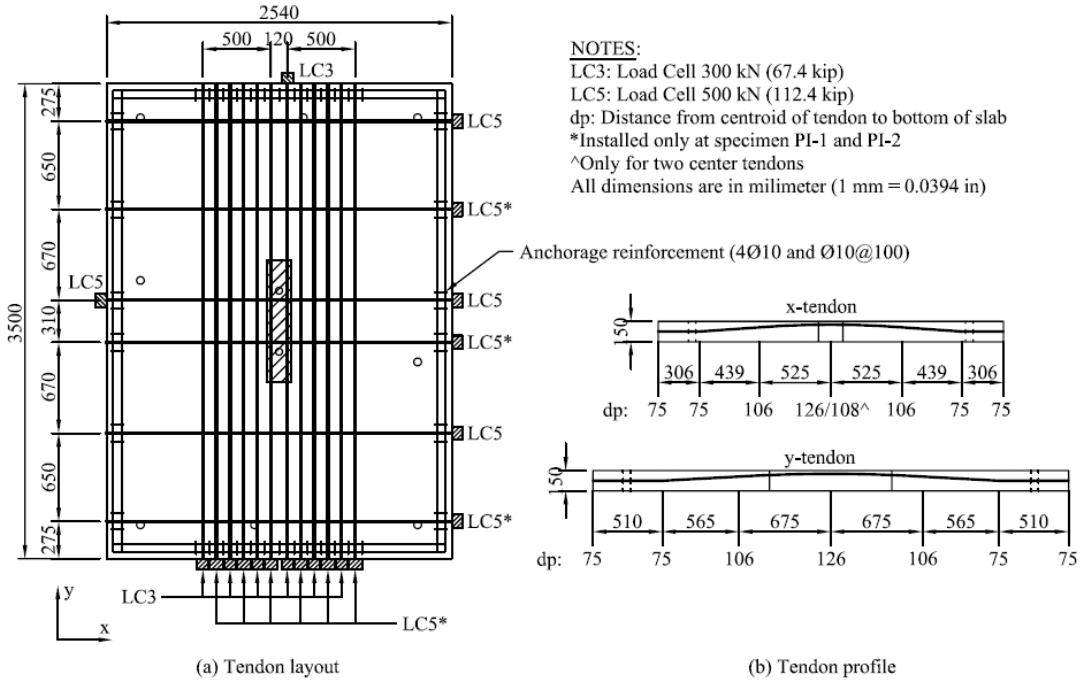

(a) Tendon layout (b) Tendon profile

Figure 4.3 Layout and profile of slab tendons

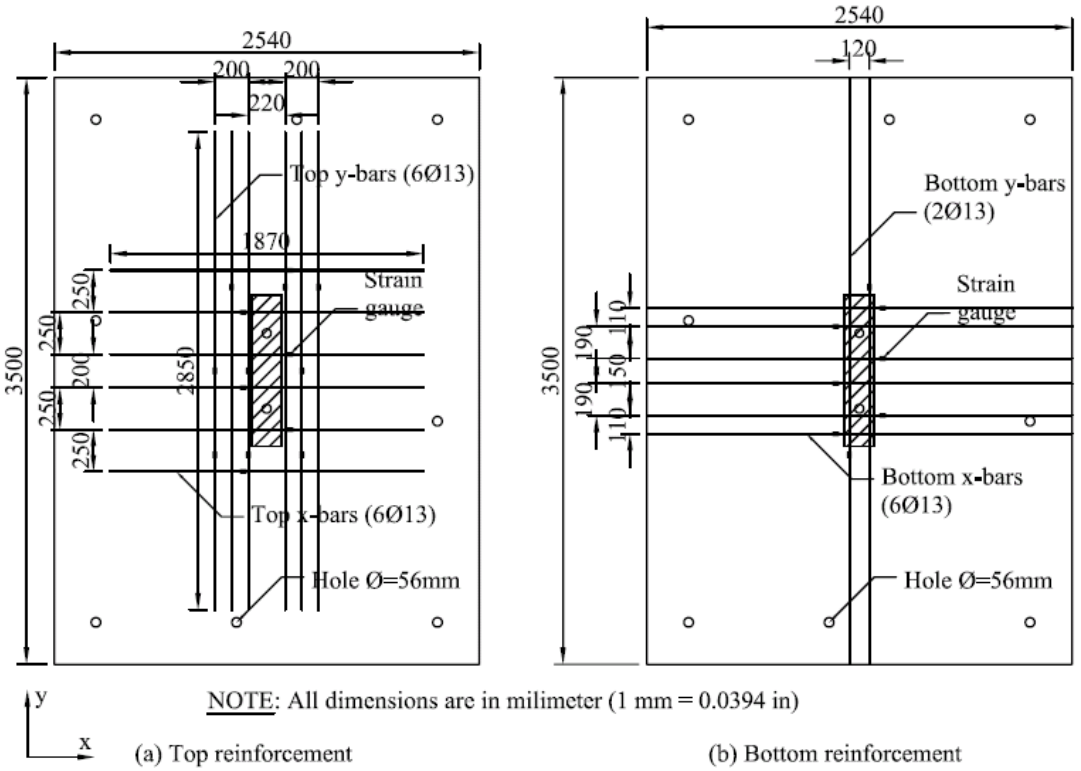

Figure 4.4 Slab reinforcement and strain gauges location

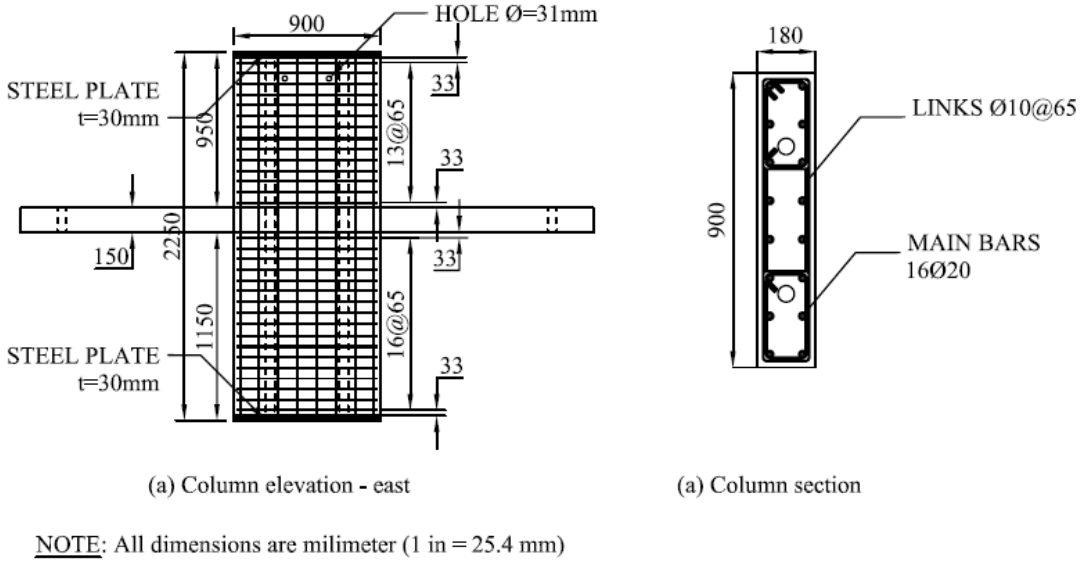

Figure 4.5 Column reinforcement

At a connection that is far from the slab edge (i.e. interior connection), the compressive stress in concrete due to prestressing is equal to the total effective force of the tendons across the full bay width divided by the cross sectional area of the slab. This compressive stress is the main factor that contributes to the punching shear strength of the connection. Therefore, it is important to maintain the same

compressive stress between the specimen and the model structure. For this reason, the effective force per tendon in the specimen was modified to 53.3 kN and 95.2 kN for tendons in *x*- and *y*-directions, respectively. These modifications in tendon force lead to a smaller vertical component of prestressing force that passes through the critical section. However, the error due to this effect was negligible since it was only about 1%.

Altogether, there were three specimen (PI-0, PI-1 and PI-2) tested in this experimental program. All the specimens were identical in shape and dimensions. The main variables in this study were the loading conditions. The specimens were labeled with "PI", followed by a hyphen and a number. Notation "PI" stand for "Prestressed Interior" while the number represents the type of loading, i.e. "0" refers to ultimate gravity load, "1" refers to unidirectional cyclic lateral loading, and "2" refers to bidirectional cyclic lateral loading.

4.3 Materials

4.3.1 Concrete

The specimens were cast using ready mixed concrete having a specified cube strength (f_{cu}) of 40 MPa (5800 psi) or specified cylinder strength (f'_c) of 32 MPa (4600 psi). The slump value was 125 ± 25 mm. The mix design was based on BS 8338 or SS 289 (Methods for Specifying Concrete, Including Ready Mixed Concrete). The proportion of materials for each m^3 of concrete is presented in Table 4.1.

Table 4.1 Mix design proportion

Materials	Type	Specific Gravity (SSD)	Mass (kg)
Cement	Ordinary Portland Cement	3.15	400
Water	Public Utility Board	1.00	170
Fine Aggregate	Natural/Crushed (max = 5mm)	2.61	780
Coarse Aggregate	Crushed (max = 20mm)	2.62	1000
Total			2350

Although all the three specimens were cast from the same batch of ready mixed concrete, the concrete cubes and cylinders were taken separately from each of specimen casting. The actual compressive strength of concrete were measured by testing of at least two cubes (150 mm × 150 mm × 150 mm) and two cylinders (150 mm × 300 mm) The concrete strength were monitored at 7, 14, 21, 28 days, and at the day of testing. At 28 days and at the day of testing, two concrete strain gauges were attached on each of the concrete cylinders to measure elastic modulus of the concrete. The average concrete compressive strength and the elastic modulus of each specimen are summarized in Table 4.2.

Table 4.2 Summary of concrete tests

Specimen	Cube Strength (MPa)	Cylinder Strength (MPa)	Elastic Modulus* (MPa)
PI-0	42.6	33.0	23189
PI-1	47.3	36.1	23643
PI-2	49.2	34.0	24573

Notes: * Secant modulus at stress 0.45 f'_c

4.3.2 Reinforcing bars

All the reinforcing bars used in this experimental program were from high strength deformed steel bars (T-bars) with a specified yield strength of 460 MPa (66.7 ksi). The top and bottom slab reinforcement were from T13 bars whereas the main column reinforcement was from T20 bars. T10 bars were used as links/stirrups in the columns and as anchorage reinforcement in the slab edges. To measure the actual properties of these reinforcing bars, tensile tests were conducted. For each size, three 600-mm-long reinforcing bars were taken from the same batch as the reinforcing bars used to construct the specimens. At the middle of each bar, two steel strain gauges were attached. The properties of the reinforcement were taken as the average value of the three samples and given in Table 4.3.

4.3.3 Prestressing tendons

Monostrand unbonded tendons were used as the slab main reinforcement. These tendons consist of strands coated with grease and extruded in plastic

sheathings to prevent bonding and corrosion. The plastic sheathings were made from polyethylene or polypropylene with approximately 1-mm (0.04-in) wall thickness and 18-mm (0.71-in) outside diameter. The strands were 13-mm (0.51-in) diameter seven-wire super strands having a nominal area of 100 mm^2 (0.155 in^2) and a specified yield strength of 1580 MPa (229 ksi) in accordance with BS 5896. Tensile tests were conducted to measure the actual properties of the strands. Three 600-mm-long strands were taken from the same batch of the strands used to construct the specimens. At the middle of each strand, three steel strain gauges were attached. The properties of the strands were taken as the average value of the three samples and given in Table 4.3.

Table 4.3 Properties of reinforcing bars and strand

Type	Diameter[1] (mm)	Area[2] (mm^2)	Yield Strength[3] (MPa)	Ultimate Strength[4] (MPa)	Elastic Modulus[5] (MPa)
T10	9.7	74.2	603	713	196918
T13	12.6	124.9	513	687	205631
T20	19.5	298.7	537	666	196837
Strand	13.1	101.3	1779	1881	208802

Notes:

[1] Measured across a diametrically opposite pair of outer bar/strand

[2] Nominal area (for T-bar) or calculated from the mass divided by the length and density (for strand)

[3] Determined from the stress corresponds to the top of knee of the stress-strain curve (for T-bar) or from the 0.1% offset method (for strand)

[4] Obtained from the breaking load divided by the area of T-bar/strand

[5] Tangent modulus at the initial part of the stress-strain curve

4.4 Fabrication and moving of specimen

Fabrication of the three specimens was done simultaneously outside the laboratory. First of all, the reinforcing bars, strands, plastic sheathings and formworks were cut according to the dimensions of specimens. Then, some steel strain gauges were attached on the slab reinforcement. The formworks were made from 10-mm thick plywood, reinforced with timber frames. Subsequently, the formworks of slab and lower column were assembled. The slab formworks were

supported on scaffoldings whereas the lower column formworks were sat on the bottom steel plate and stack of timbers. After these formworks had been set up, the column main reinforcement was placed and welded on to the bottom and top steel plate, followed by installing links/stirrups in the column. Afterward, the slab reinforcement and anchorage reinforcement were assembled and placed properly. For the slab tendons, the strands were greased and inserted into the plastic sheathing before placing them in the correct position. Four and two lifting hooks made from T16 bars were installed at the slab corner and upper column, respectively. Lastly, the upper column formworks were assembled and set up. These formworks did not cover the whole column height. Around 100-mm height at one of the column long side was left open for pouring concrete.

Before casting, all the reinforcement and tendons were checked properly and the actual measurements of depth and spacing were taken. The concrete for the three specimens was delivered in a ready mixed truck and poured directly from the truck outlet. First, the concrete was poured into the lower column through the slab-column joint. Then, the slab was cast by pouring directly the concrete into the slab. Subsequently, the concrete was poured into the upper column through the 100-mm gap at the formwork. During concreting, the concrete was compacted properly by vibrators to avoid honeycombing. Finally, the slab surface was leveled and finished. Some concrete cubes and cylinders were taken from each of the specimens.

After casting, some gunny sacks were put on the slab surface and the specimens were covered by plastic sheets. The specimens were kept wet for seven days by spraying with water. After seven days, the plastic sheets were removed and the top column formworks were stripped. The specimens were left outside the laboratory until they were ready for setup and testing.

Once the testing site was ready, the specimens were moved into the laboratory one by one. Prior to moving the specimen, steel hooks were installed at the top column and slab edge. The top column steel hooks were used for connecting the lateral jacks, whereas the slab edge steel hooks were used for connecting the torsion-restraining frame. To reduce stresses in the slab during movement, four

chains equipped with shackles and turnbuckles were installed from the lifting hooks at the corners of the slab to the top column, and then hand tightened.

The specimen was lifted by a lorry crane, using a chain attached to the top column hook. While the specimen was being lifted, the slab and bottom column formworks were stripped. During the shifting into the laboratory, the specimen was stabilized with a few scaffoldings. Once the lorry crane was inside the laboratory, the specimen was lifted and moved by the laboratory overhead crane.

4.5 Test setup

To simulate actual behavior of slab-column connections, the slab was supported on eight vertical struts equipped with universal pinned joints at both ends of the strut. The pinned condition at the column bottom was formed by a column support resting on a ball bearing and held by two steel arms in two perpendicular directions (Figure 4.6). Below the column support, a 2000-kN (449.6-kip) hydraulic jack was provided for applying gravity loads to the slab. At one of the slab edges, a torsion-restraining frame was attached to prevent any in plane, rigid-body rotations during the testing. This frame is free to move in the East-West direction; hence, it will not affect the moment about *y*-axis. The column top was held by two 500-kN (112.4-kip) lateral hydraulic jacks in two perpendicular directions to apply lateral loads simulating earthquake loading. To apply axial force in the column, two prestressing rods equipped with a 1000-kN (224.8-kip) hydraulic jack each were installed passing through the column center. The details of the test setup are shown in Figure 4.6. Once the setup was finished, the specimens were painted white so that cracks occurred during testing can be easily observed. After white washing, grid lines were drawn on the top and bottom slab surface to facilitate tracing of cracks. The grid lines were 180 mm × 180 mm square pattern.

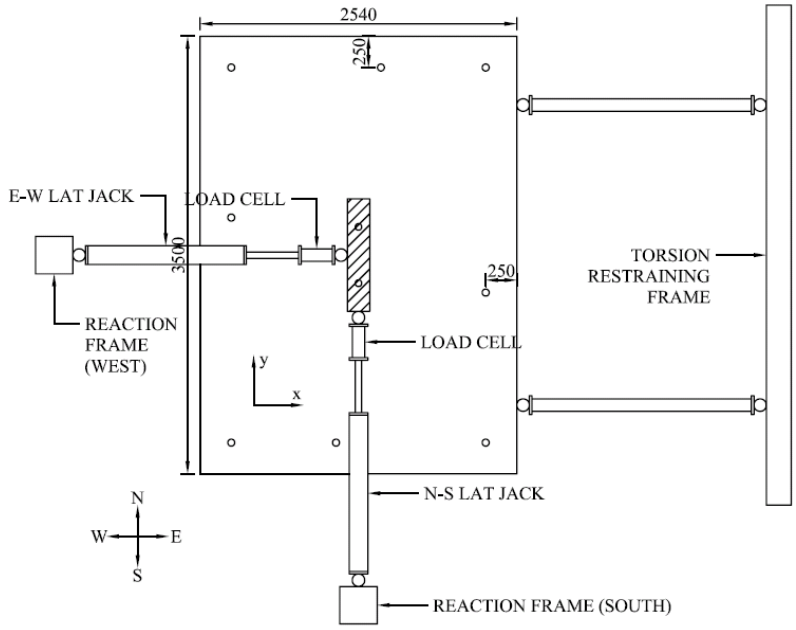

NOTE: All dimensions are in milimeter (1 mm = 0.0394 in)

(a) Plan view

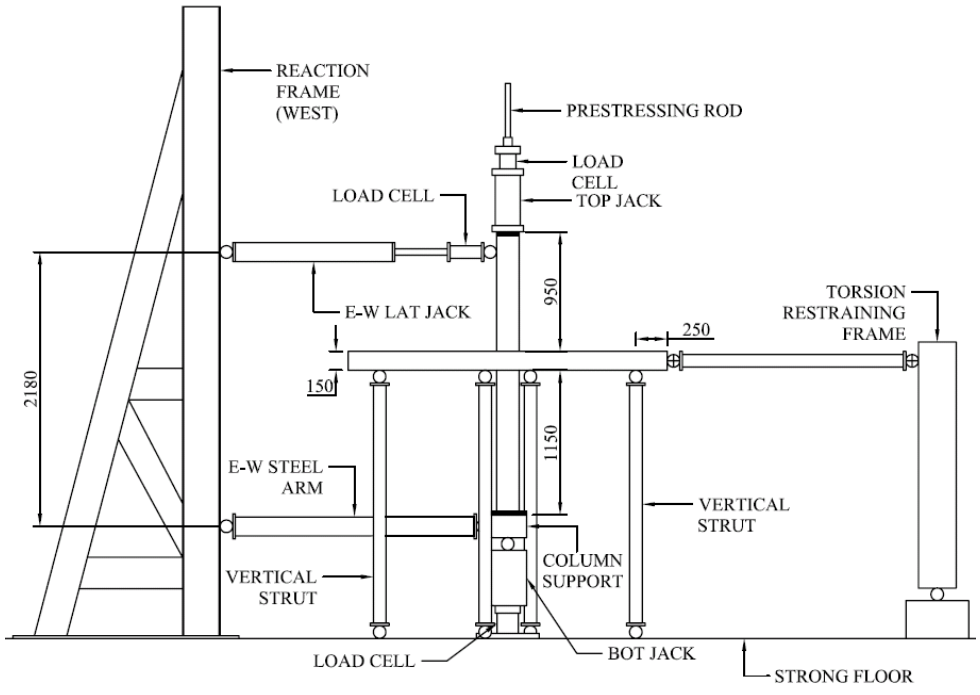

NOTE: All dimensions are in milimeter (1 mm = 0.0394 in)

(b) Elevation (South)

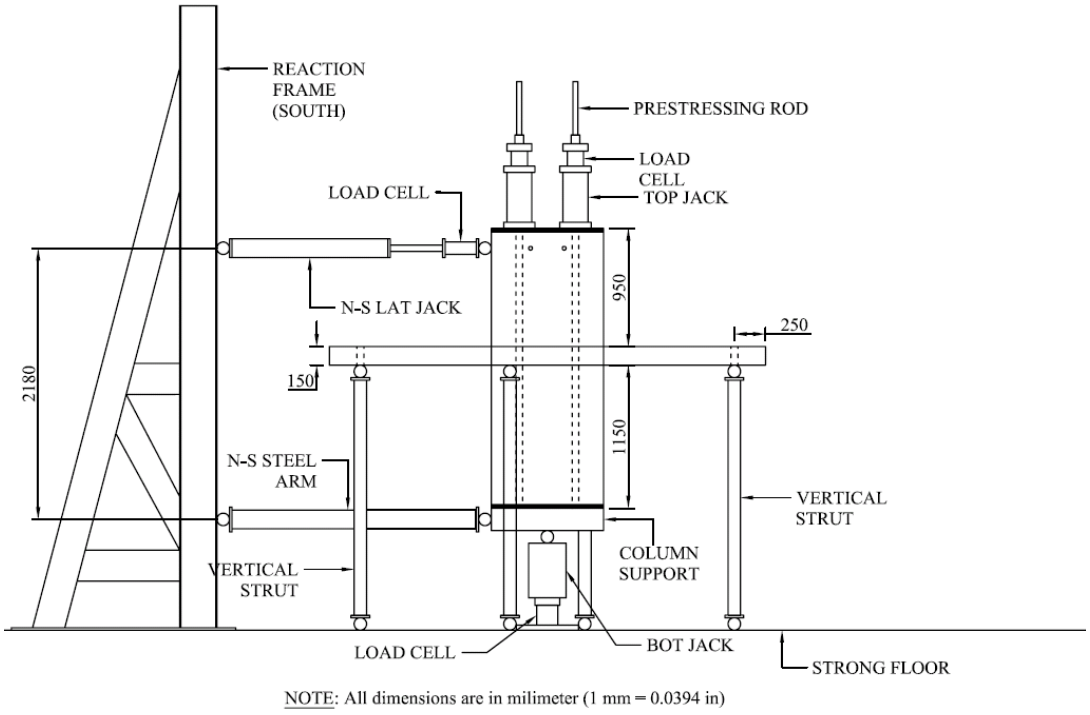

(c) Elevation (East)

Figure 4.6 Test setup

4.5.1 Column support

The column support consists of a ball bearing held by two steel arms in two perpendicular directions. The ball bearing allows free rotations, whereas the two steel arms restrain horizontal translations in two perpendicular directions. The two steel arms, equipped with universal pinned joints at both ends, were connected to the reaction frames. At the bottom of the column support, a 2000-kN (449.6-kip) hydraulic jack was provided for applying gravity loads in the slab. Detail of the column support is depicted in Figure 4.7.

Figure 4.7 Detail of column support

4.5.2 Torsion restraining frame

During the application of lateral displacements at the column top, the support condition of the specimen would result in significant in plane, rigid body rotations. To limit this rotation, a torsion-restraining frame was attached at one of the slab edges. This frame would allow the specimen to move horizontally in two perpendicular directions without any in plane, rigid body rotations. Figure 4.8 shows a picture of the torsion-restraining frame.

Figure 4.8 Torsion restraining frame

4.5.3 Lateral jacks

To apply lateral loads simulating earthquake loading, two 500-kN (112.4-kip) hydraulic jacks were attached to the column top and connected to the reaction frames. These hydraulic jacks were double-acting jacks so that the lateral displacements could be applied cyclically. Similar to the two steel arms at the bottom column, universal pinned joints were also provided at the both ends of these hydraulic jacks. The connections between column and lateral jacks are depicted in Figure 4.9.

Figure 4.9 Connections between column and lateral jacks

4.5.4 Vertical struts

Eight vertical struts, equipped with universal pinned joints at both ends, were provided along the slab edges. This type of connection would allow rotations and horizontal translations in two perpendicular directions without any vertical displacements. Figure 4.10 shows a universal pinned joint at one of the vertical struts.

Figure 4.10 Universal joint at vertical strut

4.5.5 Prestressing rods

To apply axial force in the column simulating loads from upper stories in the model structure, two 1000-kN (224.8-kip) hydraulic jacks were placed on top of the column. Then, two 40-mm (1.57-in) diameter of prestressing rods were installed passing through the hydraulic jacks and the column center. The prestressing rods were locked with nuts at both ends. This configuration is shown in Figure 4.11.

Figure 4.11 Prestressing rods with jacks

4.5.6 Prestressing anchorage

For the prestressing anchorage, reusable barrels and wedges were used at both ends of the tendons. At the dead end, 15-mm (0.59-in) thick steel plates with 16-

mm (0.63-in) diameter hole were provided as the end plates. A 40-mm (1.57-in) thick steel plate with 16-mm (0.63-in) wide slotted hole was provided at the live end to ease removal of load cells. Figure 4.12 shows the configuration of the prestressing anchorages at the dead and live ends.

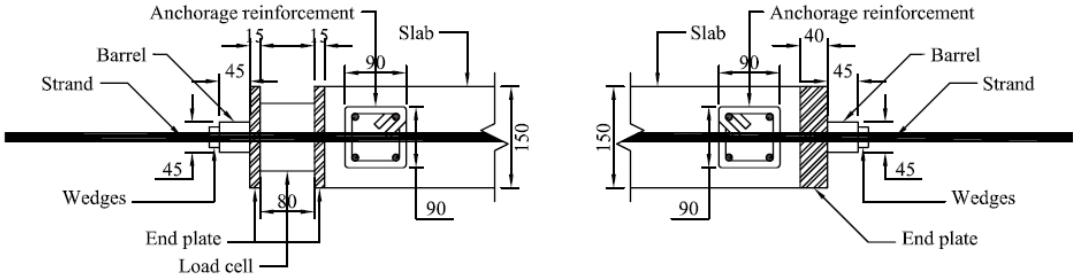

NOTE: All dimensions are in milimeter (1 mm = 0.0394 in)

(a) Dead end (b) Live end

Figure 4.12 Prestressing anchorage

4.6 Instrumentation

4.6.1 Strain gauges

Some steel strain gauges with 5-mm (0.20-in) gauge length were installed at the slab reinforcement, steel arms, vertical struts, and torsion-restraining frame. The strain gauges at the slab reinforcement are intended to measure strains induced during the testing. There were 23 steel strain gauges at the slab reinforcement, 15 strain gauges at the top reinforcement and 8 strain gauges at the bottom reinforcement. The layout of the strain gauges placed at the top and bottom slab reinforcement is shown in Figure 4.4. To monitor reactions in the steel arms, vertical struts, and torsion-restraining frame, two steel strain gauges were also installed at each of those elements.

4.6.2 Load cells

Five load cells were installed at each of the hydraulic jacks used in this testing. One load cell with the capacity of 2000 kN (449.6 kip) was put below the bottom hydraulic jack to measure the applied force from the jack. To measure the force in the column prestressing rods, two load cells with a capacity of 1000 kN (224.8 kip) each were placed above the jacks. At each of the lateral jacks, compression-tension load cells with a capacity of 500 kN (112.4 kip) were used. To measure the force at the slab tendons, load cells with the capacity of 300 kN (67.4 kip) and 500 kN

(112.4 kip) were used. For specimen PI-0, there were 11 load cells installed at the slab tendons whereas for specimen PI-1 and PI-2, 20 load cells were installed at the slab tendons. Location of the load cells at the slab tendons is shown in Figure 4.3.

4.6.3 Transducers

Any displacements occurred in the specimen during the testing were monitored by 20 Linear Variable Differential Transformer (LVDT) transducers and 4 line transducers. To measure slab vertical displacements, 16 LVDTs were installed below the slab. At the column bottom, two LVDTs were installed to measure vertical displacements whereas another two LVDTs were installed to measure lateral displacements. All LVDTs used in this experimental program have the capacity of 100 mm (3.94 in). Lateral displacements at the top column were measured by two line transducer with the capacity of 4000 mm (157.5 in). The slab rotations were monitored by two line transducers with the capacity of 2000 mm (78.7 in). Location of LVDTs and line transducers at the specimen is shown in Figure 4.2.

4.6.4 Data logging equipment

All the instrumentation (strain gauges, load cells, and transducers) was connected to a data logger through the switching boxes. For specimen PI-0, there were total 87 channels whereas for specimen PI-1 and PI-2, the total numbers of channels were 96. Therefore, one data logger and two switching boxes with the capacity of 50 channels each were used. A personal computer with software ProLog v1.1 was connected to the data logger to capture all the measured data throughout the testing.

4.7 Test procedures

4.7.1 Column axial load

The column axial load was applied by stressing the two prestressing rods (Figure 4.6) to 500 kN (112.4 kip) each, giving a total axial load of 1000 kN (224.8 kip) or 19% of the axial capacity of the column. This load was maintained throughout the test.

4.7.2 Stressing slab tendons

The slab tendons were stressed using VSL stressing jack type DKP-5. This type of jack has a stroke length of 200 mm (7.9 in), a piston area of 3103 mm^2 (4.81 in^2), and a capacity of 147 kN (33.05 kip). Since the tendons were very short, draw-in losses were very significant. To overcome this problem, the tendons were stressed several times. During the stressing, the forces were monitored by the load cells attached to the tendons and the pressure gauge at the pump. Actual elongations and draw-in were also measured and compared with the theoretical calculation. After stressing, the tendons were clamped with 6-mm (0.24-in) steel plates and tied with wire ropes for safety reason.

4.7.3 Gravity loads

Gravity loads in the slab were simulated by jacking up the bottom jack as well as by the slab self-weight. The gravity loads were introduced in load-controlled mode up to the desired level. For specimen PI-0, the gravity loads were applied until the specimen failed. For specimen PI-1 and PI-2, the gravity load was applied up to a level that represents 100% of dead load plus 25% of live load in the model structure [≅ 167 kN (37.5 kip)]. During earthquake loading, 25% of live load is assumed present. This load was kept constant during the application of the cyclic lateral displacements.

4.7.4 Cyclic lateral displacements

After the application of the gravity loading, cyclic lateral displacements were applied at the column top by means of two lateral jacks. These lateral displacements were introduced in displacement-controlled mode and followed displacement history shown in Figure 4.13. Two cycles were performed for each of target drift ratio. After 1.5% target drift ratio was reached, one cycle of 1% drift ratio was introduced at the end of second cycle target drift ratio. The purpose of this cycle was to study the behavior of the connection at service level after undergoing high drift ratio. Note that this displacement history was also used in all other testing programs on slab-column connections in NTU. The drift ratio expressed in percent is defined as the ratio of lateral displacements measured between two column ends to the column height. Since the bottom column was fixed against translations, held

by the two steel arms, the lateral displacements were measured at the top column (at the same level with lateral jacks). The column height was measured between the lateral jack level and the steel arms level.

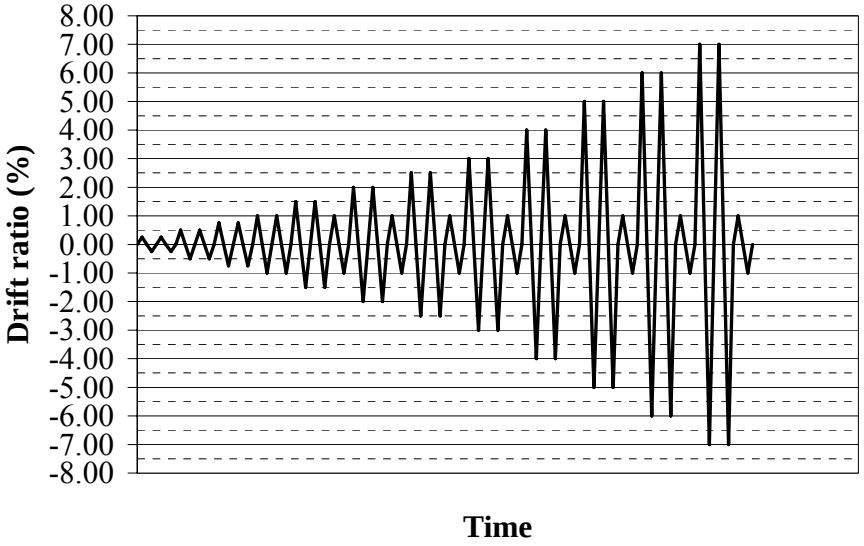

Figure 4.13 Cyclic displacement history

Specimen PI-1 was subjected to unidirectional cyclic displacements along (or parallel to) the strong column direction (*y*-direction), whereas specimen PI-2 was subjected to bidirectional cyclic displacements according to the pattern shown in Figure 4.14. This bidirectional pattern had the same displacement histories as shown in Figure 4.13 (i.e. bidirectional pattern applied at each of target drift ratio). The biaxial pattern followed sequential displacements stage from 0 to 16 to simulate severe wind or earthquake loading in every direction. Note that specimen PI-0 did not undergo cyclic lateral displacements since this specimen was subjected to gravity loading only.

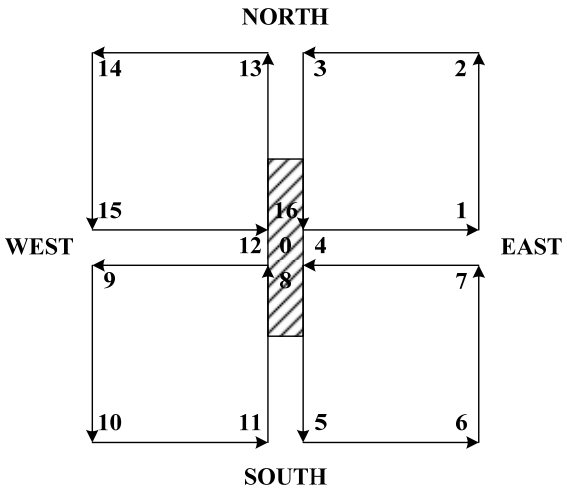

Figure 4.14 Bidirectional displacement pattern

4.7.5 Crack monitoring

Throughout the testing and before the specimen failed, formation of new cracks and development of existing cracks were marked and drawn on the slab surfaces. At some locations, crack widths were also measured and monitored. The purpose of crack monitoring was to study the serviceability of the slab at various loading stages.

4.7.6 Post testing

The test was terminated when the strength of the specimen had dropped to about 70% of the ultimate strength. Then, all the hydraulic jacks were retrieved back to zero forces due to the safety reasons. Photographs were taken and cracks at the slab surfaces were traced to a piece of paper. For de-stressing slab tendons, a specially designed steel chair was placed before the stressing jack and sat on the slab edge. Once the force in the tendon being de-stressed exceeds the locking force, the 40-mm (1.57-in) thick steel plate with 16-mm (0.63-in) slot could be easily taken out from the tendon. Subsequently, the tendons were cut and all the load cells, barrels, and wedges were removed. Finally, the tested specimen was dismantled from the testing frames and thrown away. Figure 4.15 shows one of the specimens after testing.

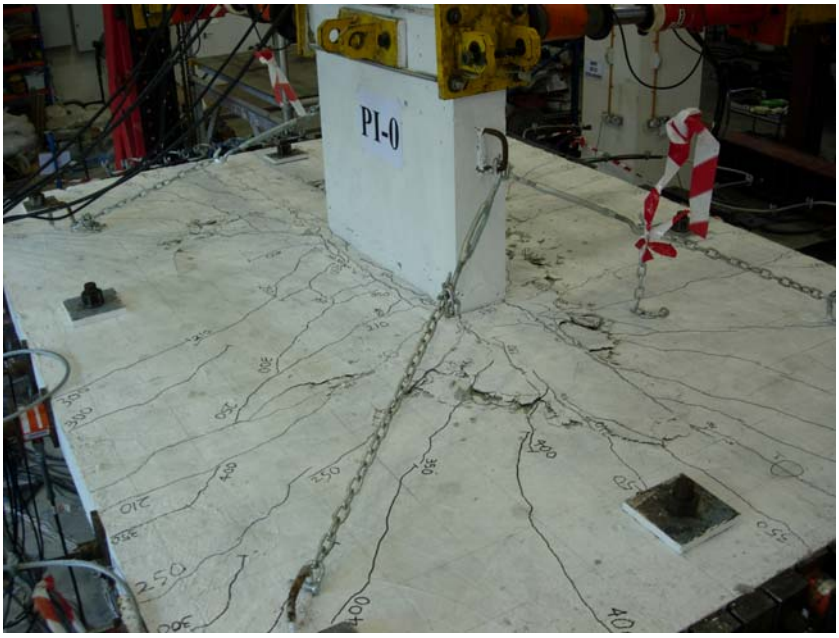

Figure 4.15 Specimen after testing

4.8 Summary

Three identical specimens representing a portion of interior slab-column connections were constructed and tested until failure for the present research program. The main variables were the types of loading. The first specimen (PI-0) was tested under gravity load only to study the symmetrical punching capacity of a connection with rectangular column. The second specimen (PI-1) was tested under gravity and unidirectional cyclic lateral loading to study the effects of cyclic moment transfer about the strong column axis. The last specimen (PI-2) was tested under gravity and bidirectional cyclic lateral loading to study the effects of cyclic moment transfer about two orthogonal axes. During the application of lateral loading, the gravity load was kept constant at a load equivalent to 100% of dead load and 25% of live load in the model structure. Some experimental photographs were presented in Appendix B.

It seems that there is no published data available on post-tensioned slab-column connections with rectangular columns. The present experimental program involved testing of three interior post-tensioned slab-column connections with rectangular columns subjected to gravity and cyclic lateral loading. The author hopes this experimental data can be a significant contribution to the current knowledge.

CHAPTER 5
EXPERIMENTAL RESULTS

5.1 Introduction

All the specimens failed in punching shear, indicated by the column punching through the slab. Figure 5.1 shows a punching shear failure of specimen PI-1. Specimen PI-0 that was tested under gravity load only failed at a shear force (V_u) of 511.8 kN (115.1 kip). Specimen PI-1 that was subjected to gravity and unidirectional cyclic lateral loading reached the maximum unbalanced moment about the strong column axis (M_{ux}) of 185.5 kN-m (136.8 kip-ft). The corresponding shear force (V_u) and drift ratio in the *y*-direction (DR_{uy}) were 164.0 kN (36.9 kip) and 2.50%, respectively. Specimen PI-2 that was subjected to gravity and bidirectional cyclic lateral loading reached the maximum unbalanced moments about the weak column axis (M_{uy}) and strong column axis (M_{ux}) of 79.8 kN-m (58.9 kip-ft) and 162.1 kN-m (119.6 kip-ft), respectively. The corresponding shear force (V_u) was 170.6 kN (38.4 kip), whereas the drift ratio capacities in *x*-direction (DR_{ux}) and *y*-direction (DR_{uy}) were 1.49%, and 1.52%, respectively. Table 5.1 presents the experimental results for each specimen.

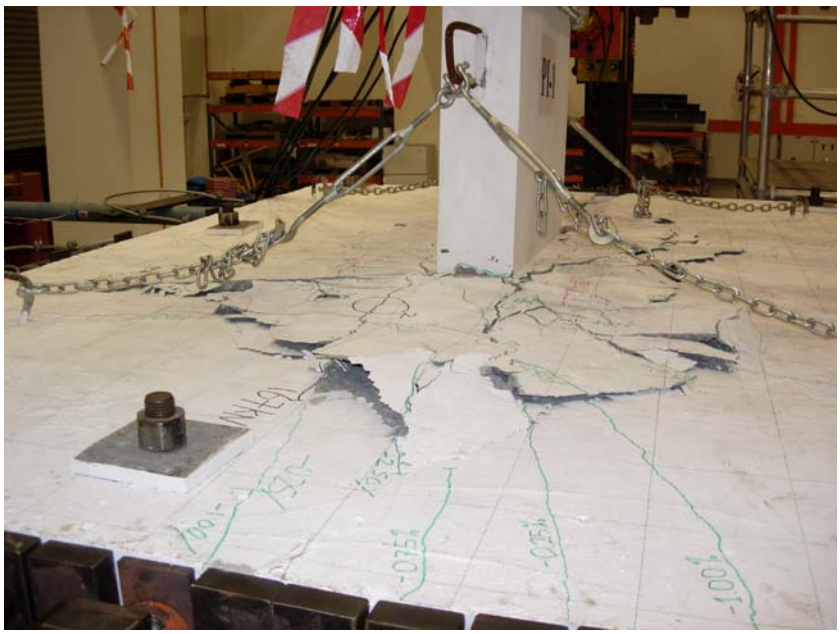

Figure 5.1 Punching shear failure (PI-1)

Table 5.1 Test results

Spec	V_u kN	M_{uy} kN-m	M_{ux} kN-m	DR_{ux} %	DR_{uy} %
PI-0	511.8	-	-	-	-
PI-1	164.0	-	185.5	-	2.50
PI-2	170.6	79.8	162.1	1.49	1.52

Notes: V_u = shear force at failure; M_{uy}, M_{ux} = peak unbalanced moment acting at centroid of column section about *y*- and *x*-axes, respectively; DR_{ux}, DR_{uy} = drift ratio at peak unbalanced moment in *x*- and *y*-directions, respectively (1 kN = 0.225 kip, 1 kN-m = 0.737 kip-ft)

5.2 Crack patterns

The first cracks were detected on top of the slab surface at a load of about 150 kN (33.7 kip). This load refers to the reaction at the bottom column and is equivalent to about 100% of dead load and 5% of live load in the prototype structure. These cracks were flexural cracks propagated radially from the corners of column toward the slab edges. Some cracks around the column perimeter were also detected at this level. Figure 5.2a, Figure 5.3a, and Figure 5.4a shows these cracks pattern for specimens PI-0, PI-1, and PI-2, respectively. The crack widths measured were around 0.1 mm (0.004 in).

For specimen PI-0, as the load increased, more radial cracks were observed while the existing cracks propagated further and became wider (see Figure 5.2b to Figure 5.2e). At a load of about 230 kN (51.7 kip), equivalent to full service load, the maximum radial and circumferential crack widths measured were around 0.7 mm (0.028 in). Diagonal shear cracks that passed through the top slab surface were observed at a load of about 450 kN (101.2 kip). These diagonal shear cracks propagated radially from the face of column at the bottom slab toward the top slab and caused spalling of concrete cover. The maximum radial and circumferential crack widths measured at this load level were more than 4 mm (0.157 in). The load was then increased and reached the maximum value of about 512 kN (115.1 kip). At this load level, the column punched through the slab, followed by a drastic drop in the load capacity, indicating that punching shear failure had occurred. The cracks

pattern of specimen PI-0 at failure can be seen in Figure 5.2f. There were no cracks observed on the bottom slab surfaces.

For specimens PI-1 and PI-2, before the application of cyclic lateral displacements, there were already a few cracks on the top slab surface (see Figure 5.3a and Figure 5.4a). As the lateral displacements were applied, more cracks were observed at the opposite side of the lateral displacement. The existing cracks were open and close depending on the direction of lateral displacements.

For specimen PI-1, when the top column was displaced to the North, cracks were observed at the South side and vice versa (see Figure 5.3b to Figure 5.3g). Note that the sign "+" for DR_y indicates the top column is displaced to the North. At a drift ratio of 1.0%, the maximum radial and circumferential cracks widths observed were around 1.3 mm (0.051 in). The bottom slab surface started to crack at a drift ratio of 1.5%. Diagonal shear cracks that passed through the top slab surface were obvious at a drift ratio of 3.0%. These diagonal shear cracks were followed by spalling of concrete cover. Figure 5.3h shows the cracks pattern of specimen PI-1 at failure. There were no cracks observed on the column surfaces.

For specimen PI-2, when the top column was displaced to the North-East, cracks were observed at the South-West side and vice versa. Similarly, when the top column was displaced to the South-East, cracks were observed at the North-West side and vice versa. Note that the signs "++" and "+-" for $DR_{x,y}$ indicate the top column is displaced to the North-East and South-East, respectively. These cracks pattern at various loading stages are depicted in Figure 5.4b to Figure 5.4i. At a drift ratio of 1.0%, the maximum radial and circumferential cracks widths observed were around 1.1 mm (0.043 in). The bottom slab surface started to crack at a drift ratio of 1.0%. Diagonal shear cracks that passed through the top slab surface were obvious at a drift ratio of 2.0%. These diagonal shear cracks were followed by spalling of concrete cover. The cracks pattern of specimen PI-2 at failure is shown Figure 5.4j. There were no cracks observed on the column surfaces.

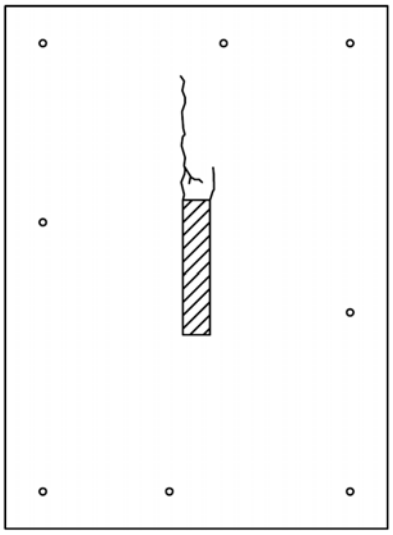

a) At V = 160 kN

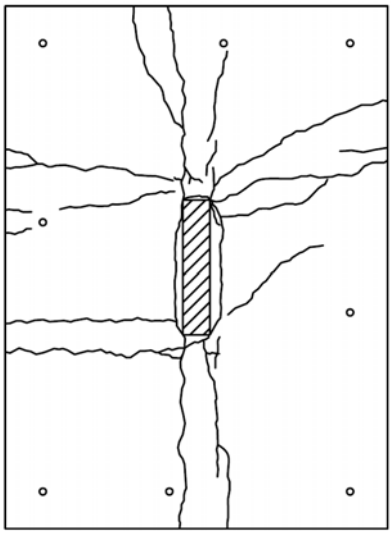

b) At V = 250 kN

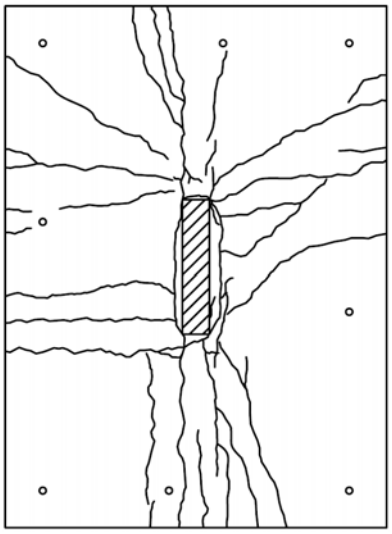

c) At V = 300 kN

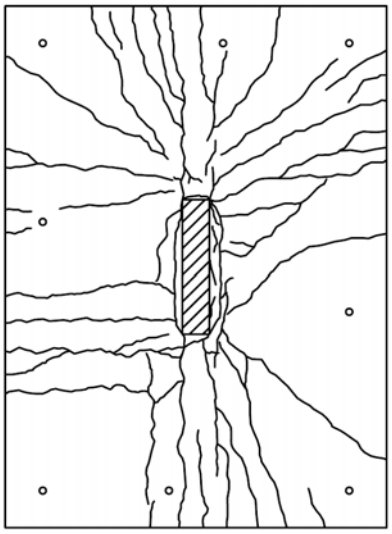

d) At V = 400 kN

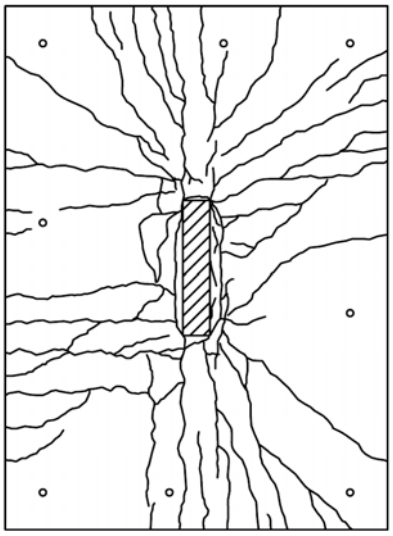

e) At V = 450 kN

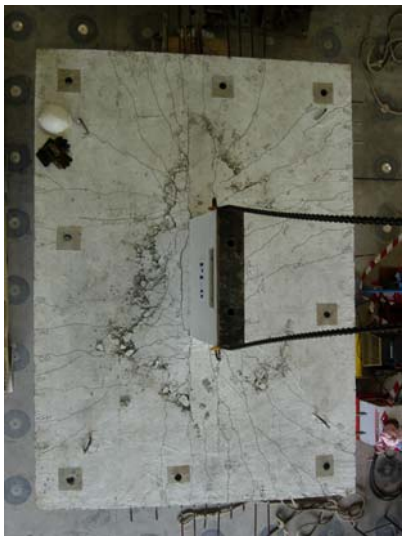

f) At failure

Figure 5.2 Cracks pattern of specimen PI-0

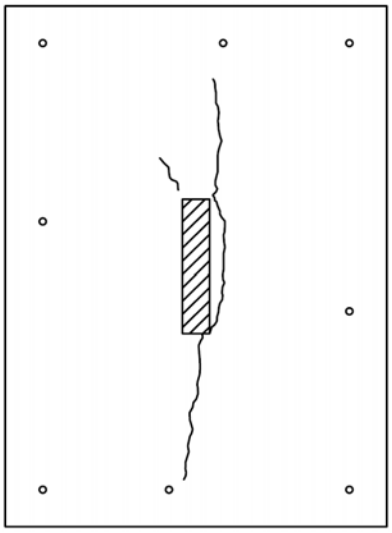

a) At V = 167 kN

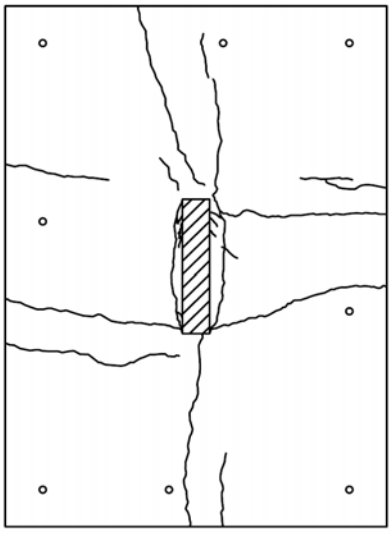

b) At DR_y = +0.50%

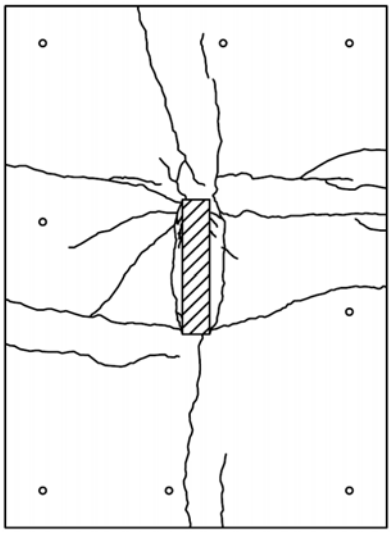

c) At DR_y = -0.50%

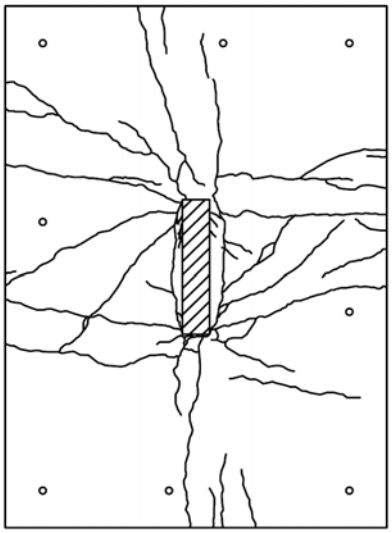

d) At DR_y = +1.00%

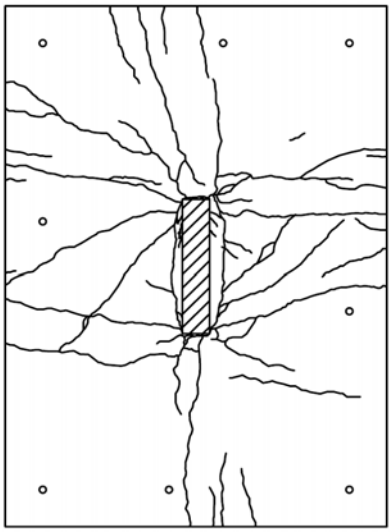

e) At DR_y = -1.00%

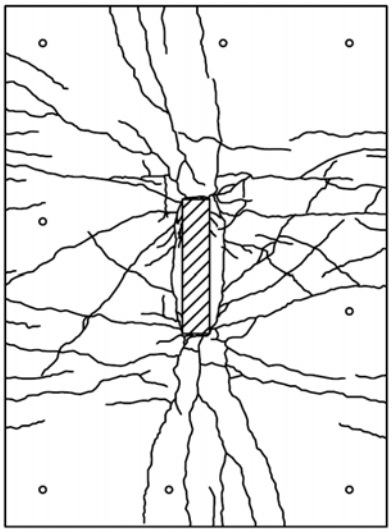

f) At DR_y = +2.50%

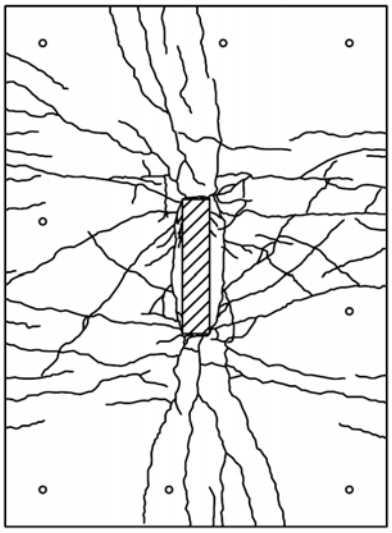

g) At DR_y = -2.50%

h) At failure

Figure 5.3 Cracks pattern of specimen PI-1

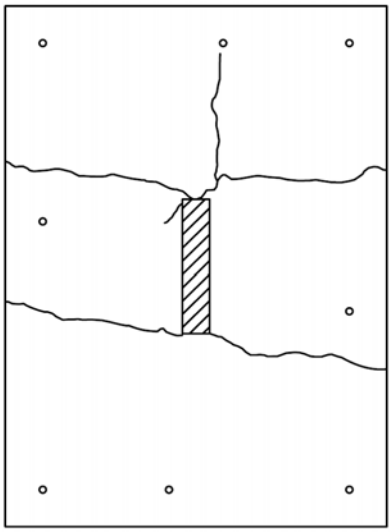

a) At V = 167 kN

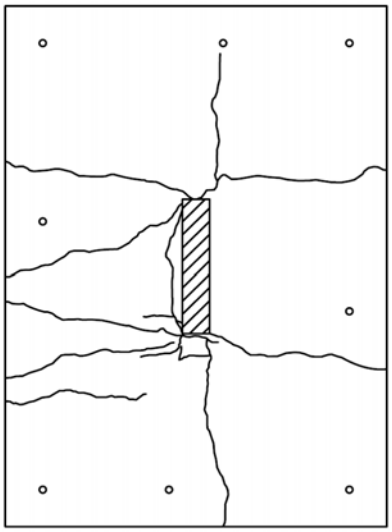

b) At $DR_{x,y}$ = ++0.50%

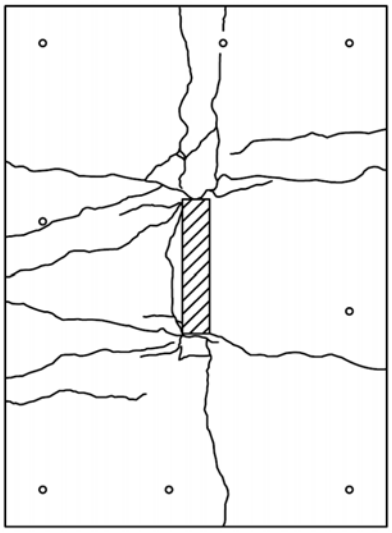

c) At $DR_{x,y}$ = +-0.50%

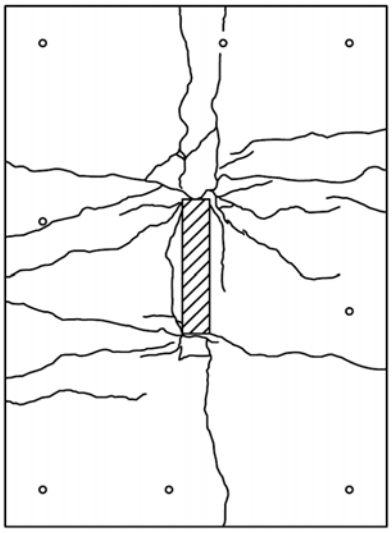

d) At $DR_{x,y}$ = --0.50%

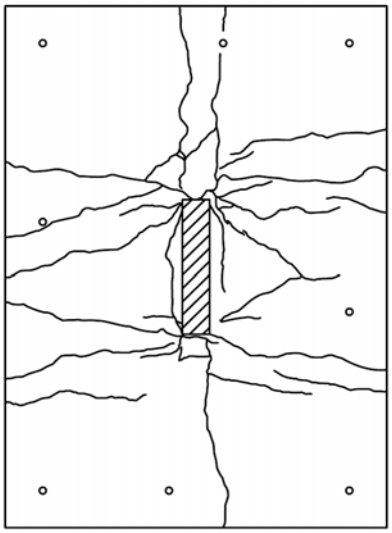

e) At $DR_{x,y}$ = -+0.50%

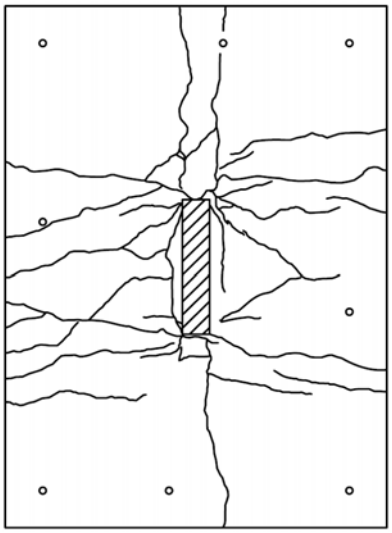

f) At $DR_{x,y}$ = ++1.00%

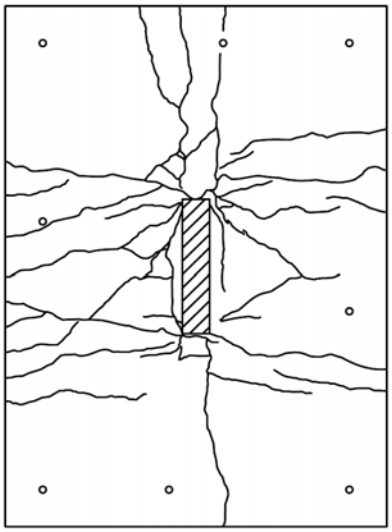

g) At $DR_{x,y}$ = +-1.00%

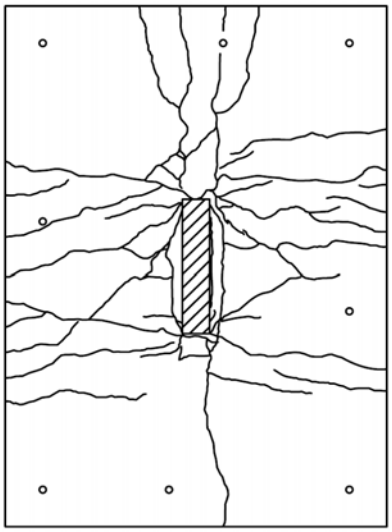

h) At $DR_{x,y}$ = --1.00%

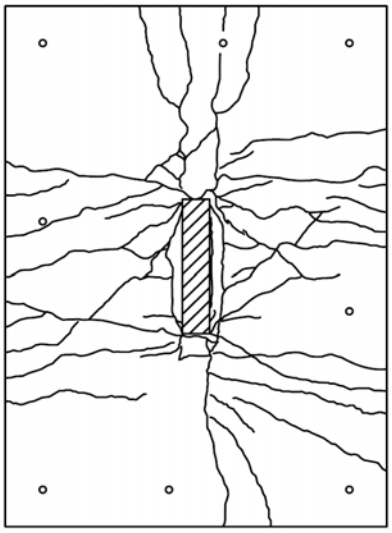

i) At $DR_{x,y}$ = -+1.00%

j) At failure

Figure 5.4 Cracks pattern of specimen PI-2

5.3 Vertical column displacements

The values of vertical column displacements recorded during the test are plotted against the drift ratios in Figure 5.5. Note that the vertical column displacements were taken at the end of the first cycle of each target drift ratio. It was shown that the vertical column displacements increased as the drift ratio increased, even though the gravity load was kept constant during the application of the cyclic lateral displacements. This occurred due to the deterioration of the connection stiffness caused by cyclic lateral displacements. Furthermore, for the same drift ratio, specimen PI-2 has higher vertical column displacement compared with specimen PI-1. This indicated that bidirectional loading caused more deterioration in stiffness than unidirectional loading.

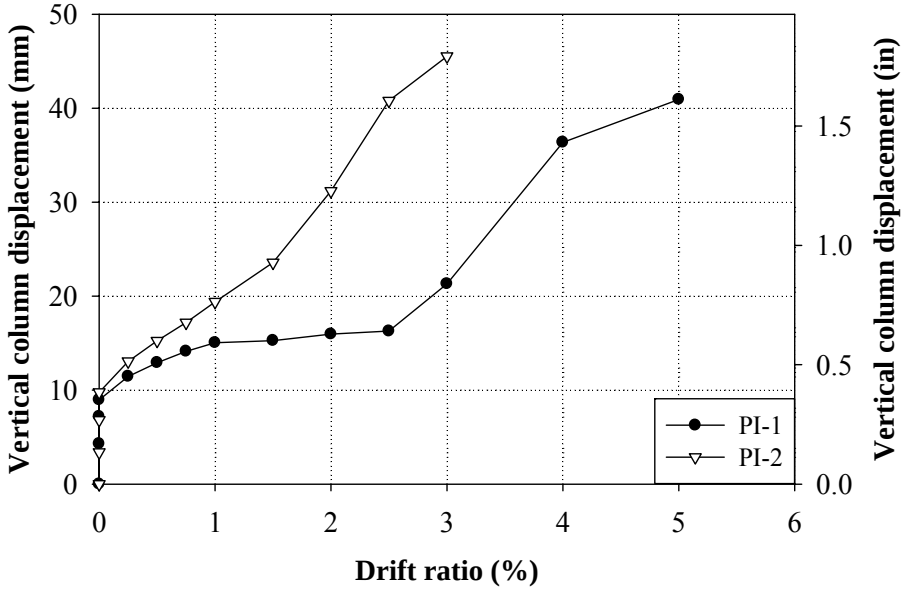

Figure 5.5 Vertical column displacement versus drift ratio

5.4 Strain in nonprestressed reinforcement

The strain in nonprestressed reinforcement for specimen PI-0 is plotted against gravity load in Figure 5.6. For specimen PI-1 and PI-2, the strain in nonprestressed reinforcement is plotted against drift ratio (Figure 5.7). For all specimens, except for specimen PI-2, the strain values plotted were taken from TX4-, TY4-, BX4-, and BY2-bars. The strain values for specimen PI-2 were taken from TY5-bar instead of TY4-bar as the strain gauge on TY4-bar was damaged. Note that T and B stand for Top and Bottom, respectively, whereas X and Y refer to the axis along which the reinforcement is placed. The bar numbers are counted from right to left (for TY- and BY-bars) or bottom to top (for TX- and BX-bars). It was shown that the strain increased as the gravity load and drift ratio increased. Some of the top bars in specimens PI-0 and PI-1 reached yield before the specimens reached the ultimate limit state. For specimen PI-0, the TX- and TY-bars started to yield at the gravity load of about 300 kN (67.4 kip) and 400 kN (89.9 kip), respectively. In addition, at the ultimate limit state, the bottom bars of specimen PI-0 also yielded. This is probably due to a transfer of forces from the top reinforcement and the concrete to the bottom reinforcement in a similar way as in a catenary action that cause the bottom bars to reach yield. For specimen PI-1, the TY- and TX-bars

began to yield at drift ratio of 1.00% and 3.00%, respectively. For specimen PI-2, none of the nonprestressed reinforcement yielded at the ultimate limit state.

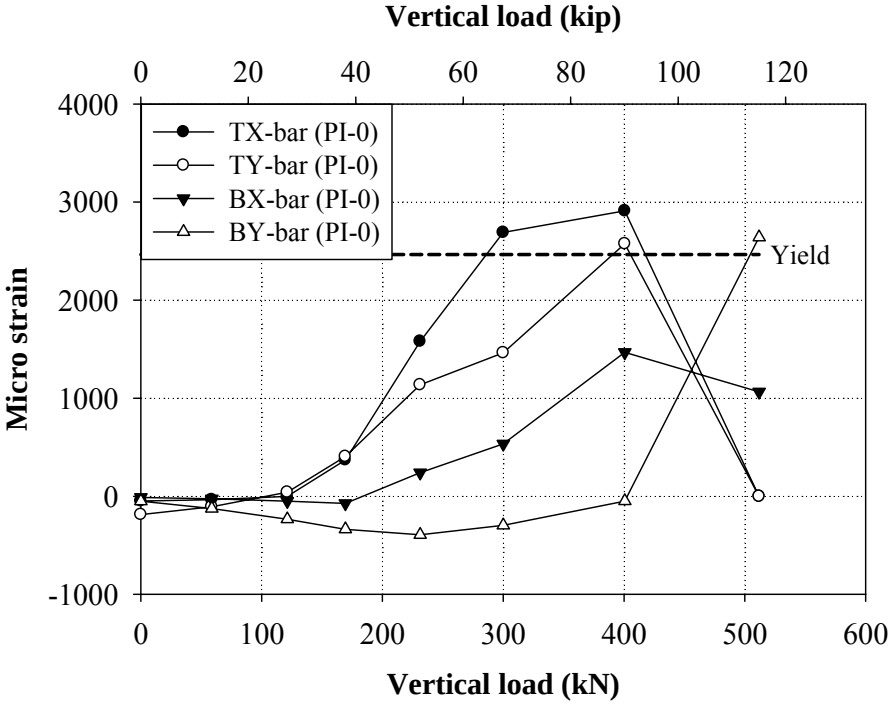

Figure 5.6 Strain in nonprestressed reinforcement versus gravity load

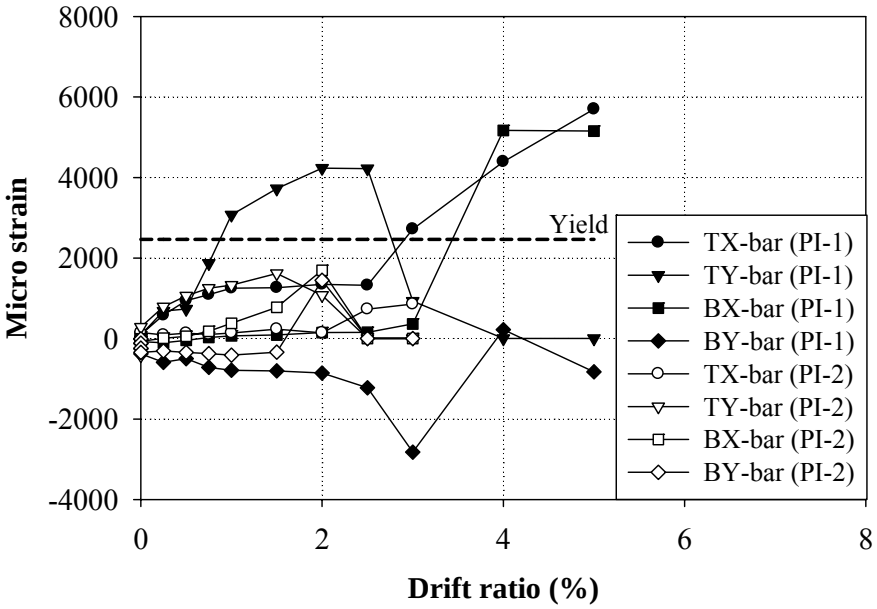

Figure 5.7 Strain in nonprestressed reinforcement versus drift ratio

5.5 Tendon forces

The average tendon forces for specimen PI-0 were plotted against gravity load in Figure 5.8. For specimens PI-1 and PI-2, the average tendon forces were plotted against drift ratio (Figure 5.9). It was shown that the tendon forces started to increase at a gravity load of about 150 kN (33.7 kip), this was the load where the slab started to crack. As the gravity load and drift ratio increased further, the tendon forces also increased. At the ultimate limit state, the tendon forces of specimen PI-0 were increased by 42.7 kN (9.6 kip) and 29.1 kN (6.5 kip) for *x*- and *y*-tendons, respectively. The increments of tendon forces in specimen PI-1 and PI-2 were smaller compared with those in specimen PI-0. The tendon forces of specimen PI-1 were increased by 10.2 kN (2.3 kip) and 11.5 kN (2.6 kip) for *x*- and *y*-tendons, respectively. For specimen PI-2, the tendon forces were increased by 10.6 kN (2.4 kip) and 13.4 kN (3.0 kip) for *x*- and *y*-tendons, respectively. Hence, at the ultimate limit state, specimens under pure shearing force have higher increments of tendon forces than specimens subjected to unbalanced moment transfer. Note that none of the tendons reached yield.

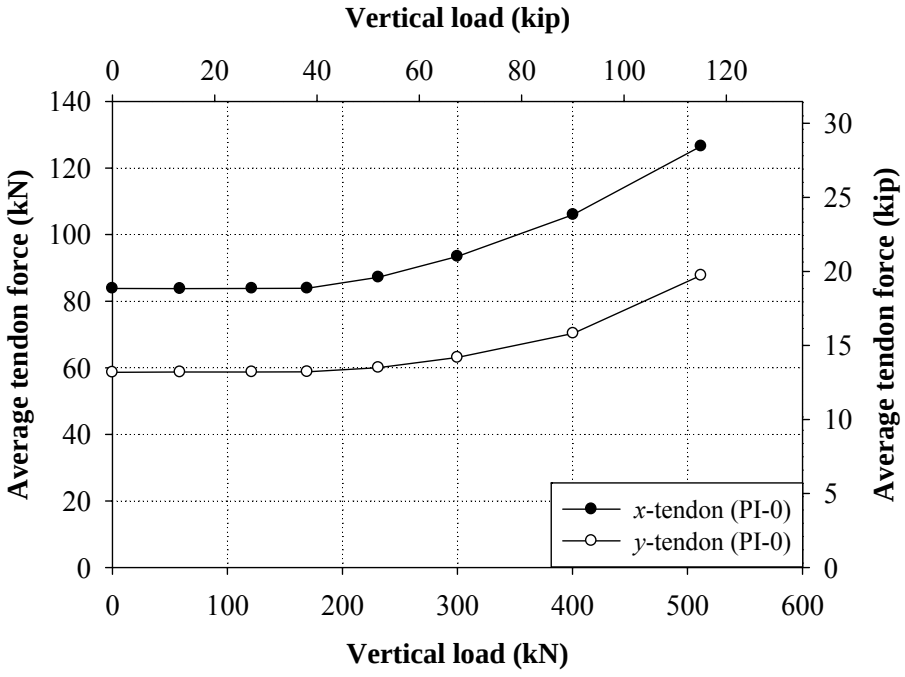

Figure 5.8 Average tendon forces versus gravity load

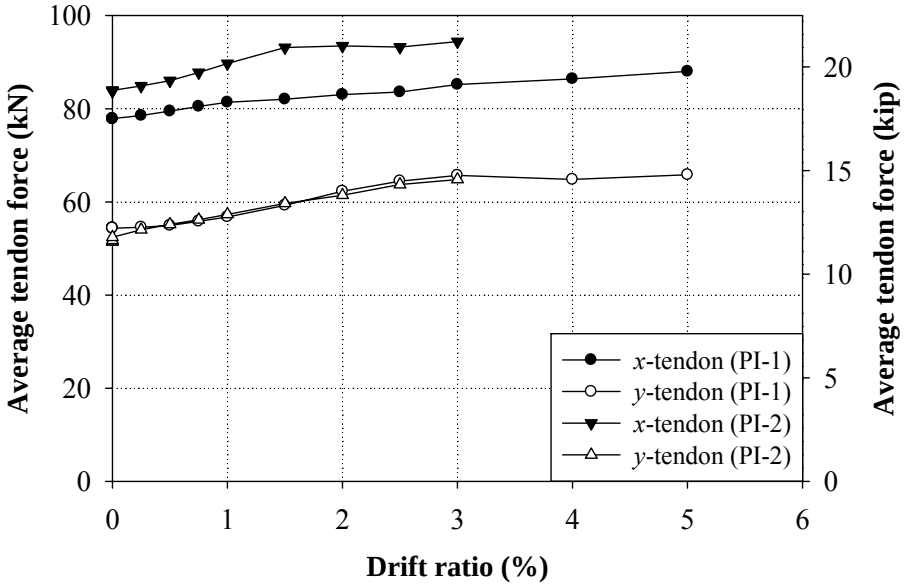

Figure 5.9 Average tendon forces versus drift ratio

The increments of tendon forces at the ultimate limit state according to Eq. (18-3) of ACI 318-11 were calculated to be about 15.1 kN (3.4 kip) and 8.5 kN (1.9 kip) for *x*- and *y*-tendons, respectively. These values are close to the values recorded in specimen PI-1 and PI-2, but different significantly from the values obtained in specimen PI-0. Note that Eq. (18-3) of ACI 318-11 was derived for tendons having f_{se} greater than $0.5f_{pu}$, whereas the values of f_{se} in this experiment are less than $0.5f_{pu}$. In addition, the tendons in these tests are very short compared with those in actual structures. Hence, Eq. (18-3) of ACI 318-11 is good for normal tendon length and it can be less accurate for short tendons.

5.6 Hysteretic response

The overall behavior of slab-column connections under cyclic lateral loading can be shown in hysteretic curves of unbalanced moments versus drift ratios. Figure 5.10 and Figure 5.11 present the hysteretic curves of unbalanced moments versus drift ratios for specimens PI-1 and PI-2. The unbalanced moment at a particular drift ratio was obtained by multiplying the applied lateral load with the effective column height. The effective column height is defined as the distance between the lateral jacks at the column top and the steel arms at the column bottom. The drift ratio was calculated as the ratio of the imposed lateral displacement at the column top to the effective column height. For interior connections, the positive and negative

unbalanced moments about an axis for the same drift ratio are expected to be about the same. However, due to the unsymmetrical formation of cracks, different distributions of prestress forces, etc, these unbalanced moments are not exactly equal. For analyses purposes, the values of unbalanced moments for the same drift ratio will be taken as the average of the positive and negative values.

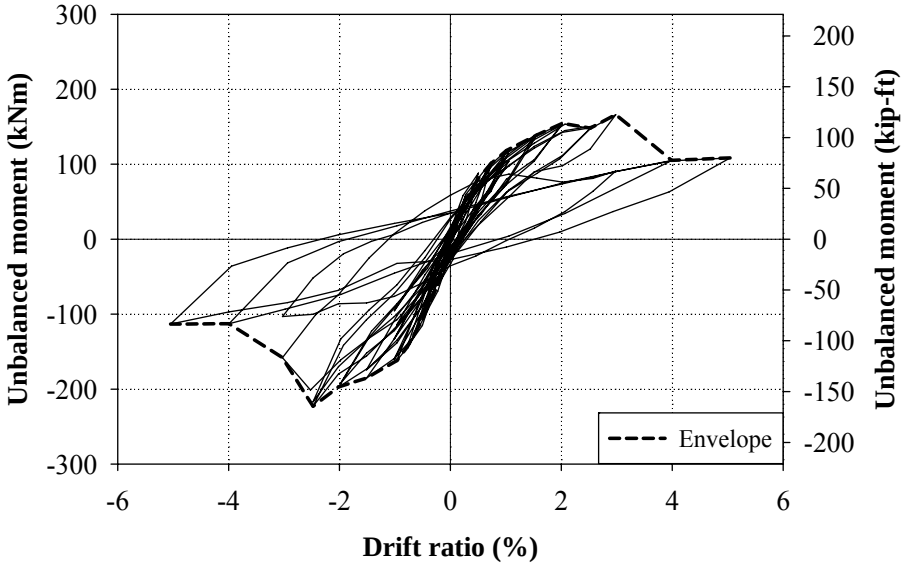

Figure 5.10 Hysteretic curve of unbalanced moment versus drift ratio (PI-1)

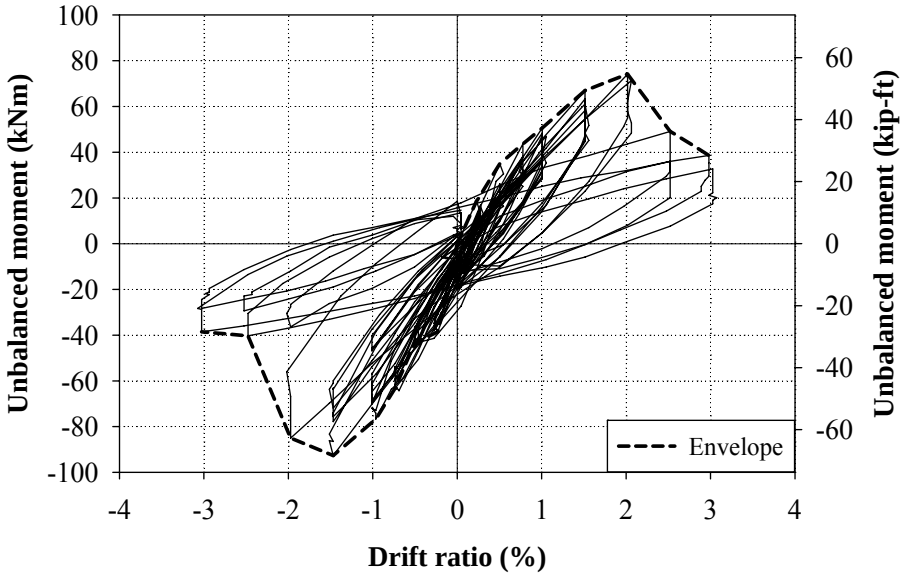

(a) In weak column direction (*x*-dir)

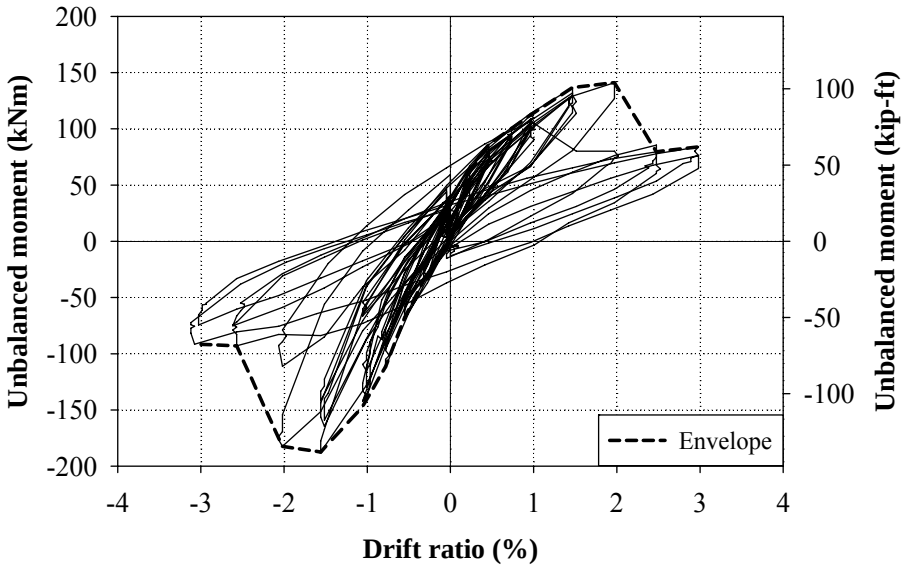

(b) In strong column direction (*y*-dir)

Figure 5.11 Hysteretic curve of unbalanced moment versus drift ratio (PI-2)

5.7 Effect of prestressing on shear strength

To investigate the effect of prestressing on shear strength, 47 slab-column connections were collected from literatures (Silva et al. 2007; Lee 2004; Oliveira et al. 2004; and Teng et al. 2004), including one specimen from the present study. The data collected consists of 41 connections having circular/square columns (Silva et al. 2007) and six connections having rectangular columns with a column aspect ratio of five (Lee 2004; Oliveira et al. 2004; and Teng et al. 2004). All the connections that have rectangular columns were reinforced concrete specimens, except one specimen from the present study (PI-0), which is a post-tensioned specimen. Figure 5.12 shows a plot of the normalized shear strength against the normalized compressive stress in concrete due to prestressing. The shear strength was calculated at a critical section located at a distance $d/2$ from the face of column, in the shape of a closed rectangle. To minimize the effects of different concrete strengths (f'_c), nonprestressed reinforcement ratios (ρ), and slab effective depths (d), the shear strength was normalized against $(f'_c.100\rho)^{1/3}(1+d/1000)^{-1/2}$. The selection of $(f'_c.100\rho)^{1/3}(1+d/1000)^{-1/2}$ as the normalizing quantity was based on the consideration that the shear strength of slabs is a function of $(f'_c.100\rho)^{1/3}(1+d/1000)^{-1/2}$ (Teng et al. 2004). The tension reinforcement ratio ρ was calculated over the

column width c plus 1.5h on each side of the column. The size effect factor $(1+d/1000)^{-1/2}$ was based on fracture mechanics as proposed by Bažant and Cao (1987). It can be seen from Figure 5.12 that connections having rectangular columns have lower shear strength compared with connections having circular/square columns. For $f_{pc} = 0$ (reinforced concrete slabs), the shear strength of slabs having rectangular columns with column aspect ratio of five is only about 75% than that of slabs having circular/square columns. As the compressive stress in concrete due to prestressing increases, the shear strength also increases. Apparently, the increase in shear strength due to prestressing for connections having rectangular columns with column aspect ratio of five tends to be lower (only 22%) than those having circular/square columns. It may also be influenced by the tendon arrangements (uniform or banded).

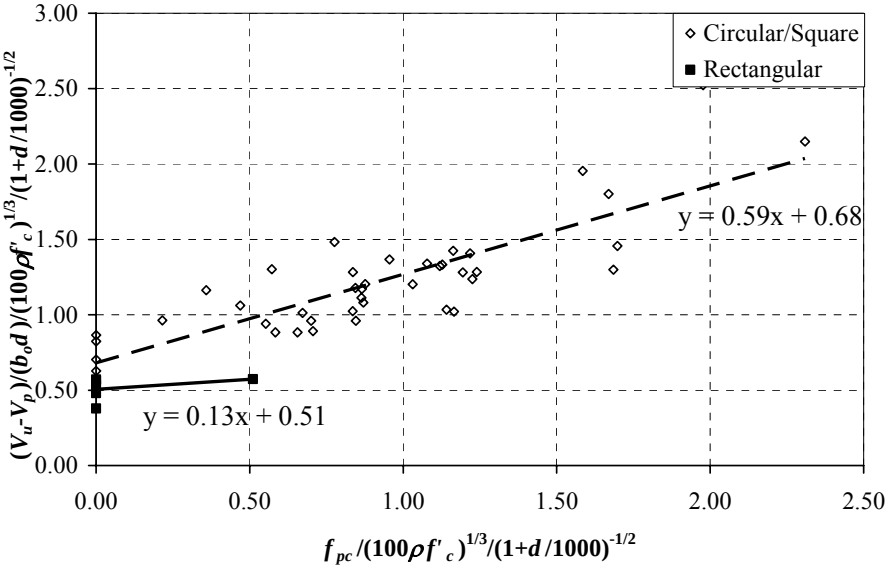

Figure 5.12 Normalized shear strength versus normalized precompression stress

5.8 Unbalanced moment capacity and drift capacity

The envelopes of the average unbalanced moments versus drift ratios are depicted in Figure 5.13. It is shown that a connection with a rectangular column can carry higher unbalanced moment about the strong column axis (M_x) than about the weak column axis (M_y). At the ultimate limit state, the unbalanced moment about the strong column axis (M_x) was about twice that about the weak column axis (M_y) [see specimen PI-2]. In addition, by comparing the values of unbalanced moment

about the strong column axis (M_x), we can see that the specimen under unidirectional loading (PI-1) has a higher unbalanced moment capacity compared with the specimen under bidirectional loading (PI-2). Hence, bidirectional loading reduces the unbalanced moment capacity considerably. Figure 5.13 also shows that specimen PI-1 failed at a drift ratio of 2.50%, whereas specimen PI-2 failed at a drift ratio of 1.50%. Both specimens have the same value of gravity shear ratio, $V_u/\phi V_c$. Thus, the specimen subjected to unidirectional loading has a higher drift capacity compared with the specimen subjected to bidirectional loading.

To study the effect of prestressing on the unbalanced moment capacity, specimen PI-2 will be compared with specimen YL-H2 tested by Tan and Teng (2005). Both specimens are almost identical in every aspect, except the nonprestressed reinforcement ratio and the presence of prestressing. The envelopes of the hysteretic curves of specimen YL-H2 are plotted in Figure 5.13. However, the unbalanced moment capacity cannot be compared directly as the flexural capacities of the two specimens are different. To minimize this effect, the unbalanced moment capacities (M_u) are normalized against the flexural capacity based on the yield-line theory (M_{yl}) [Gesund and Goli 1979]. Detail calculations of M_{yl} for specimens PI-2 and YL-H2 are presented in Appendix C. The ratios of the unbalanced moment capacity to the flexural capacity (M_u/M_{yl}) are also given in Figure 5.13. For moments about the strong column axis, the ratios M_u/M_{yl} for specimens PI-2 and YL-H2 are 0.28 and 0.22, respectively. This indicates that prestressing increases the unbalanced moment capacity. For moments about the weak column axis, the respective M_u/M_{yl} for specimens PI-2 and YL-H2 are 0.37 and 0.50. This indicates that prestressing does not increase, but reduces the unbalanced moment capacity. More data seems to be needed in order to draw a more definitive conclusion. In the tests by Gayed and Ghali (2006), the ratios of prestressed to non-prestressed reinforcement were changed but their flexural strengths were kept the same. Their post-tensioned connections were reinforced with the same amount of shear stud reinforcement. They concluded that prestressing increases the unbalanced moment strength.

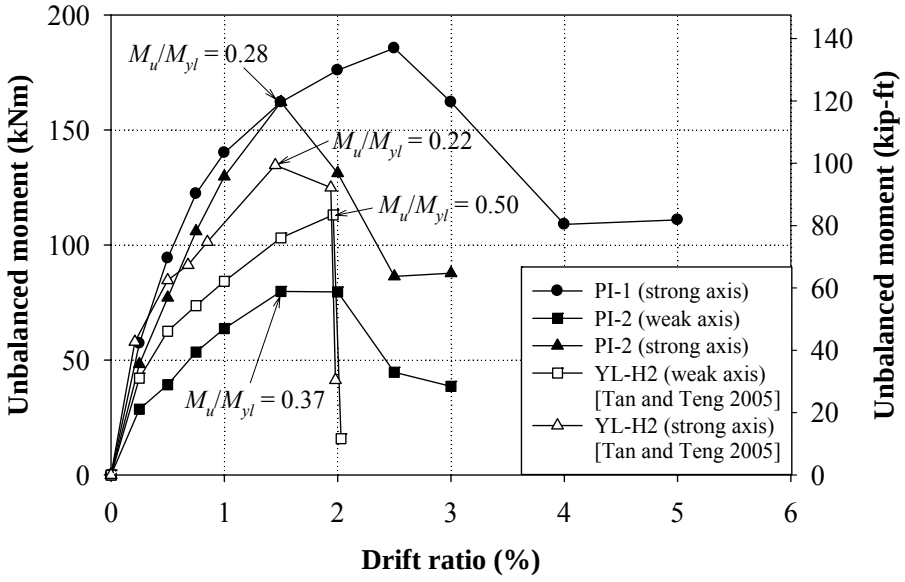

Figure 5.13 Envelope of unbalanced moment versus drift ratio

5.9 Connection ductility

Ductility of slab-column connections (μ) is usually defined as the ratio between the ultimate drift ratio and yield drift ratio ($\mu = DR_u/DR_y$). However, the connection ductility cannot be defined uniquely as there is no distinct yield drift ratio on the unbalanced moment-drift ratio envelope curve due to the gradual spreading of yield across the slab transverse width. Pan and Moehle (1989) proposed an arbitrary procedure to determine a representative yield drift ratio as illustrated in Figure 5.14. In their method, the envelope of unbalanced moment to drift ratio curve is idealized as a bilinear elastoplastic behavior. The elastic portion intersects the actual curve at a value of unbalanced moment equal to two-thirds of the maximum unbalanced moment. The yield drift ratio is then taken as the intersection between the elastic and plastic portion, whereas the ultimate drift ratio is taken at the maximum unbalanced moment. Megally and Ghali (2000a) used a similar procedure as Pan and Moehle (1989) to determine the connection ductility; however, the ultimate drift ratio is taken at 80% of the maximum unbalanced moment instead of at the maximum unbalanced moment. For comparison purposes, both values of connection ductility (μ and μ_{80}) are presented in Table 5.2.

It can be observed that bidirectional cyclic lateral loading significantly reduces the connection ductility. Comparing specimen PI-1 and PI-2, the connection

ductility in the *y*-direction (μ_{80y}) is reduced from 2.82 to 1.75 due to bidirectional cyclic lateral loading. The column rectangularity seems not to have any significant effect on the connection ductility as specimen PI-2 produces about the same values of connection ductility in *x*- and *y*-direction. This finding was also obtained in the tests by Tan and Teng (2005). The reason is probably due to the fact that once the connection fails in one direction; the strength in another direction also drops. Thus, the values of connection ductility in the two orthogonal directions become similar. If unidirectional cyclic lateral loading were applied independently in two orthogonal directions, the connection ductility in *x*- and *y*-directions would be significantly different as shown in the tests by Anggadjaja and Teng (2008). The connection ductility in *x*-direction (weak column direction) is expected to be higher compared with that in *y*-direction (strong column direction).

To observe the effect of prestressing on the connection ductility, specimen PI-2 will be compared with specimen YL-H2 tested by Tan and Teng (2005). The values of the connections ductility of specimen YL-H2 are also given in Table 5.2. The data shows that prestressing may increase or reduce the connection ductility. Thus, there is no clear effect of prestressing on the connection ductility. Gayed and Ghali (2006) also found that the level of prestressing did not consistently affect the connection ductility.

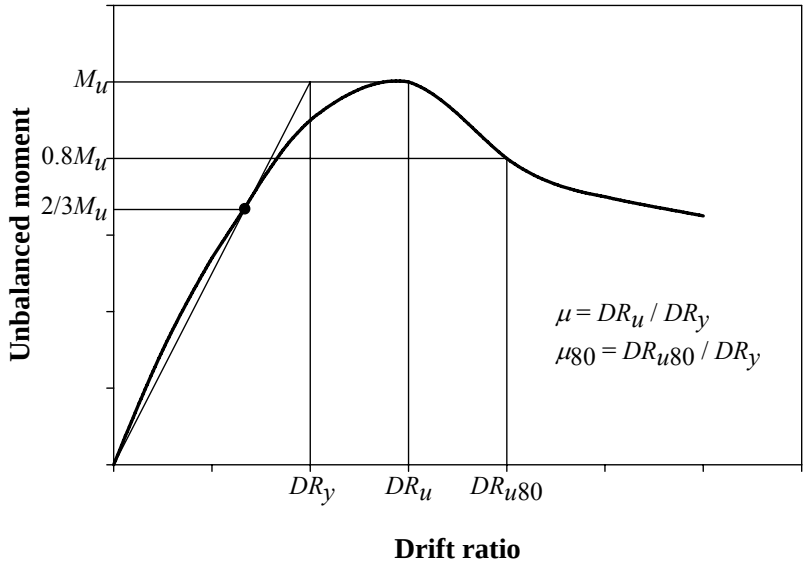

Figure 5.14 Definition of connection ductility

Table 5.2 Connection ductility

Spec	DR_{yx} %	DR_{yy} %	DR_{ux} %	DR_{uy} %	DR_{u80x} %	DR_{u80y} %	μ_x	μ_y	μ_{80x}	μ_{80y}
PI-0	-	-	-	-	-	-	-	-	-	-
PI-1	-	1.15	-	2.50	-	3.24	-	2.17	-	2.82
PI-2	1.14	1.16	1.49	1.52	2.24	2.03	1.31	1.31	1.96	1.75
YL-H2 (Tan and Teng 2005)	1.16	0.90	1.96	1.45	1.97	1.95	1.69	1.61	1.70	2.17

Notes: DR_{yx}, DR_{yy} = yield drift ratios in *x*- and *y*-directions, respectively; DR_{ux}, DR_{uy} = ultimate drift ratios at peak unbalanced moment in *x*- and *y*-directions, respectively; DR_{u80x}, DR_{u80y} = ultimate drift ratios at 80% peak unbalanced moment in *x*- and *y*-directions, respectively; μ_x, μ_y = ductility ratios corresponding to DR_u in *x*- and *y*-directions, respectively; μ_{80x}, μ_{80y} = ductility ratios corresponding to DR_{u80} in *x*- and *y*-directions, respectively

5.10 Connection stiffness

As the connection is loaded cyclically beyond its elastic range, the stiffness deteriorates. To measure the rate of stiffness deterioration, stiffness parameter *S* as illustrated in Figure 5.15 is adopted in this study. The stiffness parameter *S* is defined as the slope of the line joining peak-to-peak points of individual hysteretic curves. Figure 5.16 shows the plots of stiffness parameter *S* (taken at the first cycle of each target drift ratio) versus drift ratio. It was shown that the connection stiffness in the strong column direction (*y*-direction) is much higher than the stiffness in the weak column direction (*x*-direction). In addition, bidirectional cyclic lateral loading reduces the connection stiffness significantly.

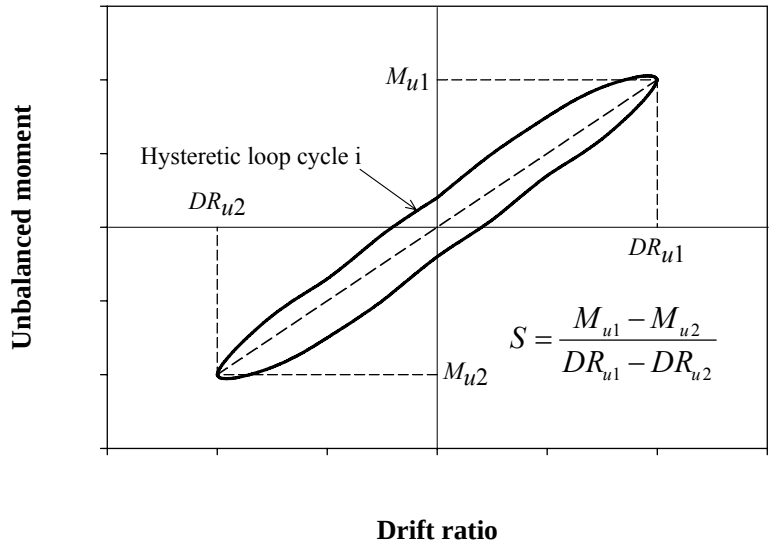

Figure 5.15 Definition of stiffness parameter *S*

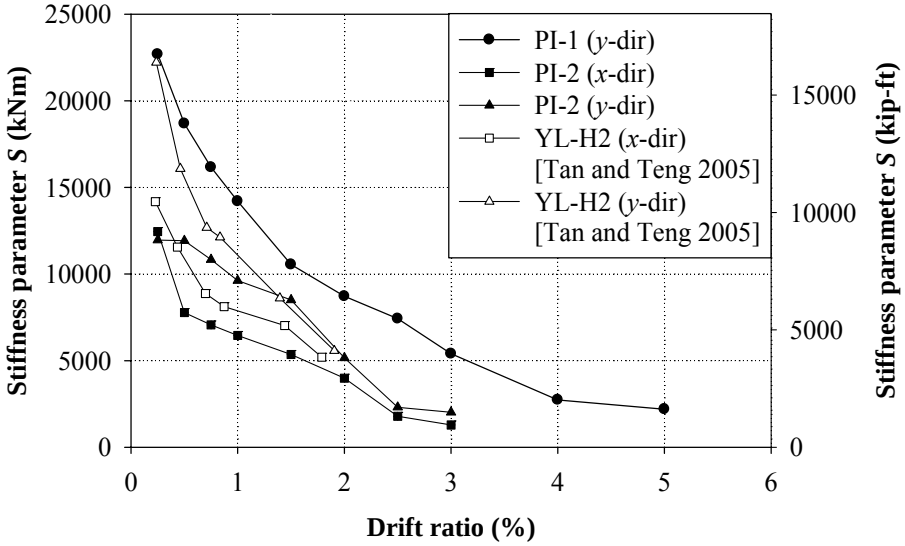

Figure 5.16 Stiffness parameter *S* versus drift ratio

To see the effect of prestressing on the connections stiffness, the stiffness parameter *S* of specimen YL-H2 tested by Tan and Teng (2005) is also plotted in Figure 5.16. It can be seen that the reinforced concrete specimen (YL-H2) has a higher stiffness compared with the post-tensioned specimen (PI-2). The reason may be due to the presence of ducts that reduces the effective area of the concrete, and consequently reduces the stiffness. In addition, stiffness degradation of post-tensioned flat plates subjected to cyclic reversed displacements depends on the amount and distribution of both the nonprestressed and prestressed reinforcement in

the column vicinity and in the direction of the cyclic reversed displacements. The tests by Gayed and Ghali (2006) also showed that the presence of prestressing had no consistent trend in the connection stiffness. Thus, no definitive conclusion can be drawn.

5.11 Comparison of ACI 318-11 predictions and experimental results

5.11.1 Strength Prediction

Table 5.3 presents the analysis results calculated using the ACI eccentric shear stress model. The ratios of the experimental strength to the predicted value based on shear failure, flexural failure about *y*-axis, and flexural failure about *x*-axis are shown in Columns (4), (7), and (10), respectively. The strength ratio in Column (11) of Table 5.3 is the maximum of the three ratios, namely v_u/v_c, $\gamma_{fy}M_{uy}/M_{fy}$, $\gamma_{fx}M_{ux}/M_{fx}$. Column (12) of Table 5.3 gives the predicted failure mode (shear or flexure) based on the governed values of Column (11). This analysis indicates that all the specimens failed in shear, which is in line with the experimental failure mode. In addition, the ACI 318-11 method is only conservative for specimen PI-2 and unconservative for the other two specimens (PI-0 and PI-1). Hence, ACI 318-11 method can be unconservative for post-tensioned slab-column connections having rectangular columns.

Table 5.3 Analysis results

Spec	v_c MPa	v_u MPa	v_u/v_c	M_{fy} kN-m	$\gamma_{fy}M_{uy}$ kN-m	$\gamma_{fy}M_{uy}/M_{fy}$	M_{fx} kN-m	$\gamma_{fx}M_{ux}$ kN-m	$\gamma_{fx}M_{ux}/M_{fx}$	Ratio	FM
(1)	(2)	(3)	(4)	(5)	(6)	(7)	(8)	(9)	(10)	(11)	(12)
PI-0	2.06	1.65	0.80	105.5	0.0	0.00	110.4	0.0	0.00	0.80	S
PI-1	2.10	1.86	0.88	105.5	0.0	0.00	109.3	83.1	0.76	0.88	S
PI-2	2.04	2.24	1.10	105.8	58.6	0.55	106.9	72.6	0.68	1.10	S

Notes: v_c = shear strength; v_u = ultimate shear stress; M_{fy}, M_{fx} = flexural capacities within c plus 1.5h on each side of column about *y*- and *x*-axes, respectively; γ_{fy}, γ_{fx} = fractions of unbalanced moments transferred by flexure about *y*- and *x*-axes, respectively; M_{uy}, M_{ux} = ultimate unbalanced moments acting at centroid of column section about *y*- and *x*-axes, respectively; Ratio = maximum value of columns (4), (7), and (10); FM = failure mode based on the ratio (S = Shear, F = Flexure) [1 MPa = 145 psi, 1 kN-m = 0.737 kip-ft]

5.11.2 Proposed modification to β_p

ACI 318-11 formula for shear capacity of prestressed slabs [Eq. (3.4)] does not take into account the effect of column rectangularity. Hence, it is likely to be the main reason why ACI 318-11 can be unsafe for post-tensioned connections having rectangular columns. A simple modification can be obtained by introducing the column rectangularity factor into β_p-coefficient in the formula for prestressed slabs [Eq. (3.4)] in the same way as the v_c formula for nonprestressed slabs. Hence, the shear strength formula for prestressed slabs becomes [Eq. (3.4) is rewritten for clarity]:

$$v_c = \beta_p \lambda \sqrt{f'_c} + 0.3 f_{pc} + \frac{V_p}{b_o d} \tag{3.4}$$

where β_p is now defined as

$$\beta_p = \min\begin{cases} 3.5 \\ (\alpha_s d / b_o + 1.5) \text{ (psi) or } \beta_p = \min \\ (1.5 + 4/\beta) \end{cases} \begin{cases} 0.29 \\ 0.083(\alpha_s d / b_o + 1.5) \text{ (MPa)} \\ 0.083(1.5 + 4/\beta) \end{cases} \tag{5.1}$$

All other terms are as previously defined. Note that the first two β_p were similar to Eqs. (3.3) and (3.2), except that ACI reduces the shear strength by $0.5\sqrt{f'_c}$ psi ($0.06\sqrt{f'_c}$ MPa). The author proposed to add the third β_p which is similar to Eq. (3.1) and reduce the strength by $0.5\sqrt{f'_c}$ psi ($0.06\sqrt{f'_c}$ MPa).

The shear strengths v_c calculated using the modified β_p-factor are 1.59 MPa, 1.60 MPa, and 1.56 MPa for specimen PI-0, PI-1, and PI-2, respectively. Consequently, the shear strength ratios (v_u/v_c) become 1.04, 1.16, and 1.43 for specimen PI-0, PI-1, and PI-2, respectively. As this modification leads to a more conservative result and it represents the failure modes correctly, Eq. (5.1) is therefore proposed to include the column rectangularity into the ACI 318-11 equation for prestressed slabs [Eq. (3.4)].

5.11.3 Gravity-shear-ratio requirement

To check the ACI 318-11 requirement on gravity shear ratio, 14 experimental data (including two data from the present study) were collected from literatures

(Trongtham and Hawkins 1977; Dilger and Shatila 1989; Martinez-Cruzado et al. 1994; and Han et al. 2006). All the specimens were interior post-tensioned slab-column connections without shear reinforcement and subjected to cyclic lateral loading. The term "interior" in this study refers to connections with four sides of critical section. Hence, one specimen of edge connection with overhanging slab (Dilger and Shatila 1989) was also included in this study. The specimens tested by the author were connections having rectangular columns with column aspect ratio of five, whereas the rest were connections having square columns. Figure 5.17 shows a plot of drift capacities at failure (DR_u) against gravity shear ratios ($V_u/\phi V_c$), with ϕ taken equal to 1.0. For the author's specimens, the gravity shear ratios were calculated using both the original and the modified β_p-factor. It can be seen that specimen PI-2 still falls below the bilinear line according to ACI 318-11 requirement, even though the modified β_p-factor was used. This indicates that the ACI 318-11 requirement on gravity-shear-ratio can still be unsafe for post-tensioned slab-column connection having rectangular columns with column aspect ratio of five and subjected to bidirectional cyclic lateral loading. More data are certainly needed.

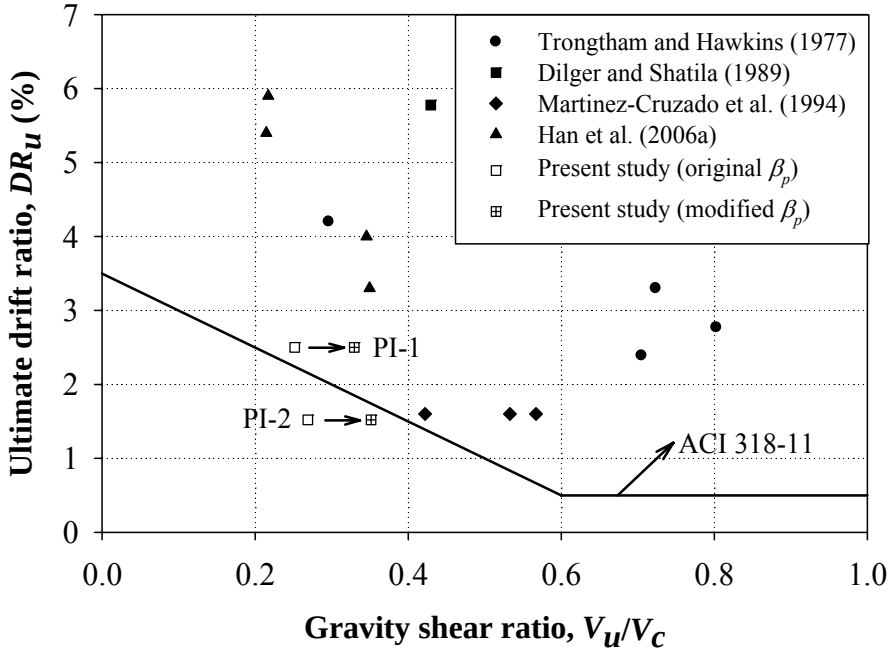

Figure 5.17 Ultimate drift ratio DR_u versus gravity shear ratio V_u/V_c

5.12 Summary

- The strength and stiffness of slab-column connections having rectangular columns with column aspect ratio of five are much higher along the strong column direction than those along the weak column direction.
- Cyclic lateral displacements cause deterioration of the connection stiffness, and the effect of bidirectional loading is more severe than unidirectional loading. It was shown that bidirectional cyclic lateral loading significantly reduces the unbalanced moment capacity, drift capacity, ductility, and stiffness of slab-column connections.
- Prestressing increases the shear strength of slab-column connections. The increase in shear strength due to prestressing for connections having rectangular columns tends to be lower compared with those having circular/square columns.
- ACI 318-11 equation on shear strength can be unconservative for post-tensioned connections having rectangular columns. Hence, a modification on the shear strength formula is proposed to make the strength prediction more conservative.
- The ACI 318-11 requirement on gravity shear ratio can be unsafe for post-tensioned slab-column connections having rectangular columns with column aspect ratio of five and subjected to bidirectional cyclic lateral loading.

CHAPTER 6
SHEAR STRENGTH OF REINFORCED CONCRETE SLAB-COLUMN CONNECTIONS

6.1 Introduction

The current ACI equations ignore the influence of slab flexural reinforcement; hence, they can lead to unconservative predictions for slabs with low reinforcement ratio and very conservative predictions for slabs with high reinforcement ratio. As shown in Figure 6.1, specimen IA30c-30 having ρ = 0.50% failed below the ACI 318-11 shear strength. It can also be seen from Figure 6.1 that shear strength actually increases as the reinforcement ratio increases. However, by adding ρ, it also increases the load that can be applied without causing bending failure. Consequently, the ductility of slab-column connections reduces as the slab reinforcement ratio increases.

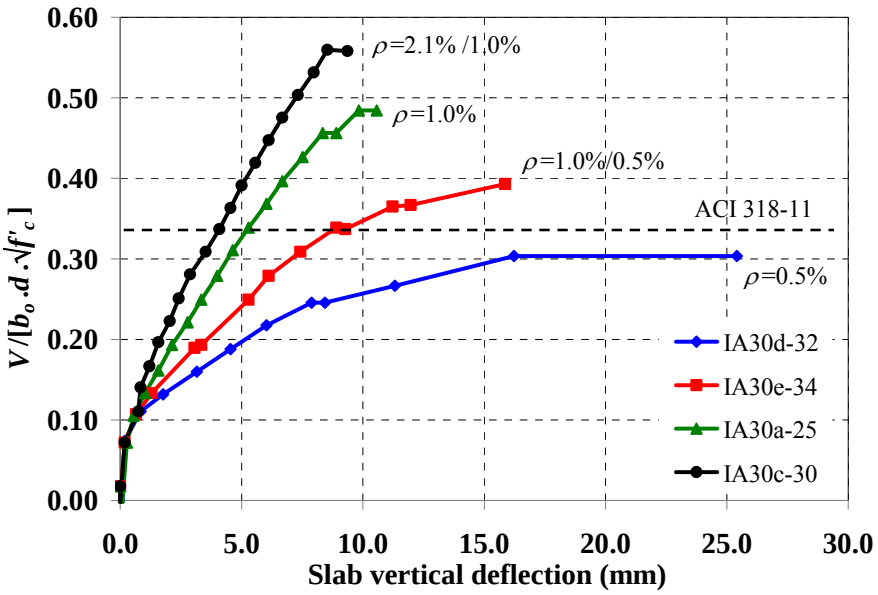

Figure 6.1Plots of load-deflection curves for tests by Kinnunen and Nylander (1960)

The shear strength of slabs v_c in the ACI 318-11 is expressed by three equations. Although these equations can give reasonable predictions, they can be improved further. The use of three equations for v_c can be simplified by using only one equation. In an attempt to improve the shear strength prediction for slabs, a

simple equation was introduced in a paper on symmetrical punching by Teng et al. (2004). This study extends the applicability of that proposed simple equation to predict the shear strength of slabs with unbalanced moment transfer. A new equation to calculate the slab ultimate shear stresses at the critical section is proposed and it has been verified by numerous experiments.

From Eqs. (3.1) to (3.3) above, it is clear that the ACI 318-11 method does not consider the possible advantage of having a higher percentage of slab flexural reinforcement on the shear capacity of the slabs v_c. The ultimate shear stress equations v_u shown in Eqs. (3.6) to (3.12) for slab-column connections with unbalanced moment transfer involved the calculation of the property of the critical section analogous to the polar moment of inertia J_c, in which the value is different for interior, edge, and corner connections. Ghali and Megally (1999) also pointed out that J_c is difficult to calculate for circular columns. Based on the above considerations, the author attempted to derive a new method to simplify calculations for both v_c and v_u, with improvement in accuracy.

This Chapter provides a summary of previous experimental data on reinforced concrete slab-column connections with and without moment transfer. The experimental data includes interior, edge, and corner connections. A simple equation is introduced for calculating the ultimate shear stresses at the critical section of slab-column connections under gravity load and unbalanced moment. The proposed model simplifies the design process and its accuracy and reliability has been checked against fairly extensive experimental data. The author hopes that this research will be useful to design engineers and researchers in this area.

6.2 Review of experimental data

A total of 556 experimental data on reinforced concrete slab-column connections subjected to combinations of shear and unbalanced moment were collected and reviewed (Elstner and Hognestad 1956; Kinnunen and Nylander 1960; Moe 1961; Taylor and Hayes 1965; Bernaert and Puech 1966; Manterola 1966; Yitzhaki 1966; Corley and Hawkins 1968; Hanson and Hanson 1968; Schaeidt et al. 1970; Zaghlool et al. 1970; Hawkins et al. 1971; Roll et al. 1971; Zaghlool 1971; Vanderbilt 1972; Ladner 1973; Zaghlool and Rawdon de Paiva 1973; Ingvarsson

1974; Stamenkovic and Chapman 1974; Ghali et al. 1976; Islam and Park 1976; Ladner et al. 1977; Marti et al. 1977; Hawkins et al. 1978; Kane 1978; Scavuzzo 1978; Pralong et al. 1979; Regan 1981; Swamy and Ali 1982; Hall and Rangan 1983; Kordina and Nölting 1984, 1986; Schaefers 1984; Regan 1986; Elgabry and Ghali 1987; Gilbert and Glass 1987; Rankin and Long 1987a; Walker and Regan 1987; Tolf 1988; Hawkins et al. 1989; Lovrovich and McLean 1990; Rangan 1990; Marzouk and Hussein 1991; Mortin and Ghali 1991; Chana and Desai 1992a, b; Falamaki and Loo 1992; Tomaszewicz 1993; Hammill and Ghali 1994; Lim and Rangan 1995; Luo and Durrani 1995a, b; Gardner and Shao 1996; Hallgren 1996; Marzouk et al. 1996; Ramdane 1996; Desayi and Seshadri 1997; Hassanzadeh 1998; Megally 1998; Marzouk et al. 1998; El-Salakawy et al. 1999; Broms 2000; McHarg et al. 2000; Melges 2000; Oliveira et al. 2000; Osman et al. 2000; Sherif and Dilger 2000a; Corrêa 2001; Khwaounjoo 2001; Suwita et al. 2001; Lee 2004; Oliveira et al. 2004; Teng et al. 2004; Papanikolaou et al. 2005; Widjaja and Teng 2006; Anggadjaja and Teng 2008; Birkle and Dilger 2008; Lee et al. 2008; Tian et al. 2008; Guandalini et al. 2009). All the specimens were reinforced concrete slab-column connections without beams, drop panels, column capitals, openings, and any type of shear reinforcement. Specimens that were cast with lightweight concrete and those that were tested under cyclic loadings were excluded. The data collected consists of 361 interior connections subjected to symmetrical punching, 77 interior connections with unbalanced moment transfer, 59 edge connections, and 59 corner connections. The data also includes 22 slab-column connections tested at Nanyang Technological University (NTU), Singapore. The NTU specimens were subjected to either gravity loading only (Teng et al. 2004; Lee 2004) or a combination of gravity and unbalanced moment transfer (Suwita et al. 2001; Widjaja and Teng 2006; Anggadjaja and Teng 2008).

The database is presented in Tables D.1 to D.8 of Appendix D. Tables D.1 and D.2 contain database on interior connections under symmetrical punching having circular/square columns (333 data) and rectangular columns (28 data), respectively. Database on interior connections with unbalanced moments transfer having square columns (61 data) and rectangular columns (16 data) are summarized in Tables D.3 and D.4, respectively. Tables D.5 and D.6 present database on edge

connections having square columns (42 data) and rectangular columns (17 data), respectively. Last, database on corner connections having square columns (55 data) and rectangular columns (4 data) are given in Tables D.7 and D.8, respectively. The notations of column dimensions and unbalanced moments for interior, edge, corner connections used in Tables D.1 to D.8 are illustrated in Figure 3.1.

The database covers a wide range of geometry, material properties, and reinforcement details. The slab thickness varies from 46 mm (1.81 in) to 500 mm (19.69 in), with the respective slab effective depth of 35 mm (1.38 in) and 456 mm (17.95 in). The column dimensions range from 51 mm (2.0 in) to 1250 mm (49.2 in), with the column aspect ratio (ratio of longer to shorter column side) varies from one to five. For the material properties, the concrete compressive strength varies from 9.3 MPa (1349 psi) to 119.0 MPa (17259 psi), whereas the reinforcement yield strength ranges from 255 MPa (37.0 ksi) to 749 MPa (108.6 ksi). The slab tension reinforcement ratio within c plus 1.5h on each side of the column varies from 0.18% to 8.50%.

6.3 Slab-column connections under symmetrical punching

6.3.1 Shear strength formula

Teng et al. (2004) proposed an equation to calculate the punching shear strength of slab-column connections under symmetrical punching that includes size effect term, $(1+d/B)^{-1/2}$, as proposed by Bažant and Cao (1987) in the form of:

$$v_c = A(100\rho)^{1/3} f'_c{}^{1/3} \left(1+\frac{d}{B}\right)^{-1/2} \left(\frac{b_l}{b_s}\right)^{-1/4} \tag{6.1}$$

where ρ is the ratio of tension reinforcement within c plus 1.5h on each side of the column; f'_c is the compressive strength of concrete; d is the slab effective depth; b_l and b_s are the lengths of longer and shorter sides of the critical section, respectively; and A and B are constants to fit the experimental data. The author found that a better strength prediction could be achieved when the constant A is taken equal to 0.55. Coefficient B depends on aggregate size (Bažant and Cao 1987) and here it has been found that it can be simplified to be 1000 mm. Hence, the complete equation can be written as:

$$v_c = 0.55(100\rho)^{1/3} f'_c{}^{1/3} \left(1 + \frac{d}{1000}\right)^{-1/2} \left(\frac{b_l}{b_s}\right)^{-1/4} \text{ (MPa)}$$

or

$$v_c = 15(100\rho)^{1/3} f'_c{}^{1/3} \left(1 + \frac{d}{40}\right)^{-1/2} \left(\frac{b_l}{b_s}\right)^{-1/4} \text{ (psi)} \qquad (6.2)$$

Note that the critical section for the proposed method is defined at a distance $d/2$ from the column face, in the shape of a closed rectangle. Eq. (6.2) is a single equation that is equivalent to ACI current three equations for v_c [Eqs. (3.1) to (3.3)]. The shear strength provided by concrete v_c calculated using the proposed formula (Eq. 6.2) is applicable for slabs without shear reinforcement. For slabs with shear reinforcement, the nominal shear strength contributed by the concrete, v_c, may drop slightly as indicated in the ACI 318-11.

6.3.2 Comparison with experimental data

Figure 6.2 shows the comparison of the predictions of the 361 slabs data calculated using the ACI equations for shear strength and the proposed simple design equation. In Figure 6.2(a), the horizontal axis is the punching shear strength calculated by using ACI Eqs. (3.1) to (3.3), whereas the proposed simple design formula shown in Eq. (6.2) is used in Figure 6.2(b). The vertical axis is the experimental shear stress on the critical section. It can be seen from Figure 6.2 that the proposed formula leads to a better prediction than the ACI equations.

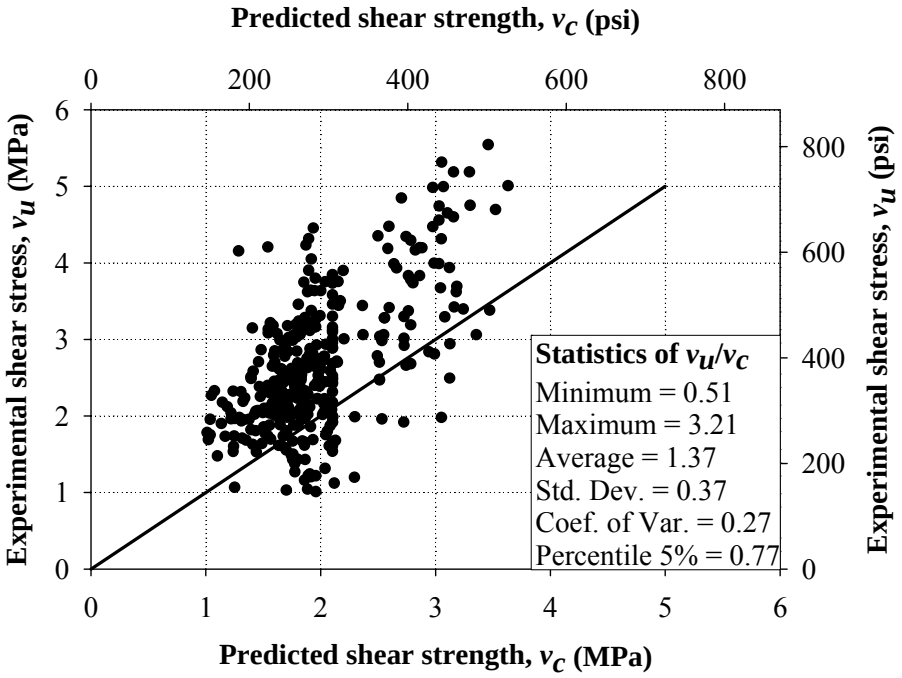

(a) ACI 318-11

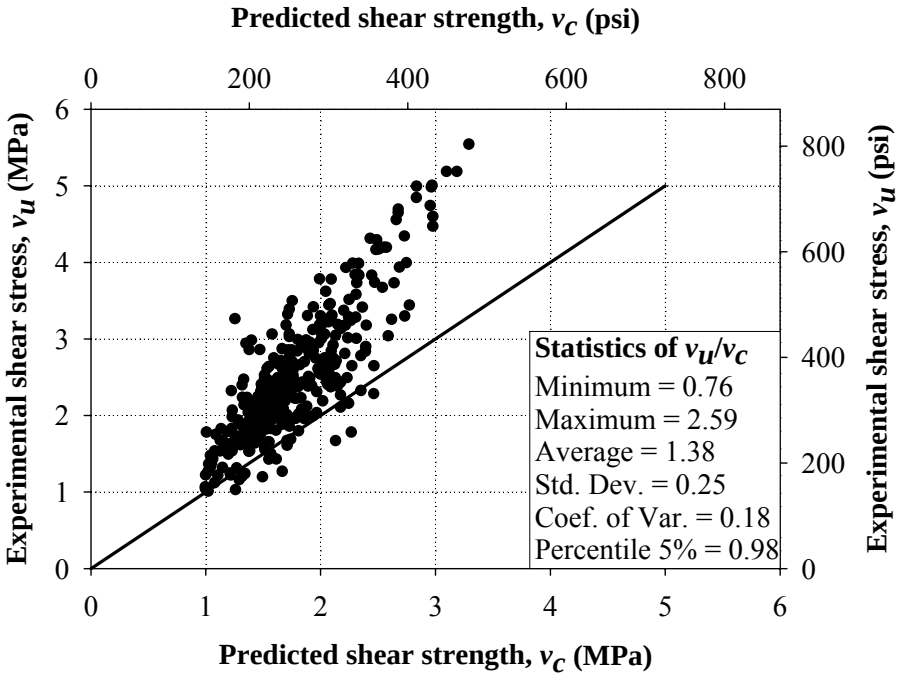

(b) Proposed

Figure 6.2 Strength predictions of reinforced concrete slab-column connections under symmetrical punching

Table 6.1 summarizes the performance of both the ACI and the proposed formulas in predicting the shear strength of reinforced concrete slab-column

connections under symmetrical punching having circular/square and rectangular columns. For connections with circular/square columns, the data are separated into two categories: (1) "*fib* Bulletin 12" data and (2) "Additional" data. The *fib* Bulletin 12 data category contains 140 data taken from the *fib* Bulletin 12 (2001), whereas the Additional data category contains 193 data collected from various literatures, including 60 data that were not included in the *fib* Bulletin 12 (2001). It can be seen from Table 6.1 that the prediction of the proposed formula is significantly better than those of the ACI 318-11 formulas for both categories. For the *fib* Bulletin 12 data category, the strength predictions using CEB-FIP Model Code 1990, British Standard 8110-97, and German Standard DIN 1045-1 (2000) equations produce coefficient of variations of 0.16, 0.16, and 0.17, respectively [taken from *fib* Bulletin 12 (2001)]. Hence, the proposed formula that gives a coefficient of variation of 0.15 is also better compared with those codes. For connections with rectangular columns, the proposed formula [Eq. (6.2)] also leads to a better prediction than the ACI formulas [Eqs. (3.1) to (3.3)], with the average shear strength ratio v_u/v_c of 1.32 and a coefficient of variation of 0.17.

Table 6.1 Summary of reinforced concrete slab-column connections under symmetrical punching

Case	**n**	**Method**	**Statistics of v_u/v_c**					
			Min	**Max**	**Avg**	**SD**	**CV**	**P5%**
Interior Circular/Square	333	ACI 318-11	0.51	3.21	1.38	0.37	0.27	0.78
		Proposed	**0.76**	**2.59**	**1.39**	**0.25**	**0.18**	**0.99**
Int. Circ/Sqre (*fib* Bulletin 12)	140	ACI 318-11	0.71	2.23	1.45	0.28	0.19	0.97
		Proposed	**0.76**	**1.89**	**1.42**	**0.21**	**0.15**	**1.06**
Int. Circ/Sqre (Additional)	193	ACI 318-11	0.51	3.21	1.33	0.42	0.31	0.64
		Proposed	**0.78**	**2.59**	**1.37**	**0.28**	**0.20**	**0.96**
Interior Rectangular	28	ACI 318-11	0.76	1.70	1.18	0.23	0.19	0.77
		Proposed	**0.88**	**1.93**	**1.32**	**0.22**	**0.17**	**0.92**

Notes: n = Number of data; Avg = Average; SD = Standard deviation; CV = Coefficient of variation; P5% = Percentile 5%

The consistency of size effect and column rectangularity factor used in the proposed formula (Eq. 6.2) is shown in Figure 6.3 and Figure 6.4, respectively. Figure 6.3 shows the plot of v_u/v_c against d for 333 data on reinforced concrete slab-

column connections having circular/square columns. Figure 6.4 shows the plot of v_u/v_c against b_l/b_s for 28 data on reinforced concrete slab-column connections having rectangular columns. It can be seen that v_u/v_c calculated using the proposed formula (Eq. 6.2) is essentially independent of d and b_l/b_s. Hence, the proposed size effect and column rectangularity factors successfully treat the effects of these parameters.

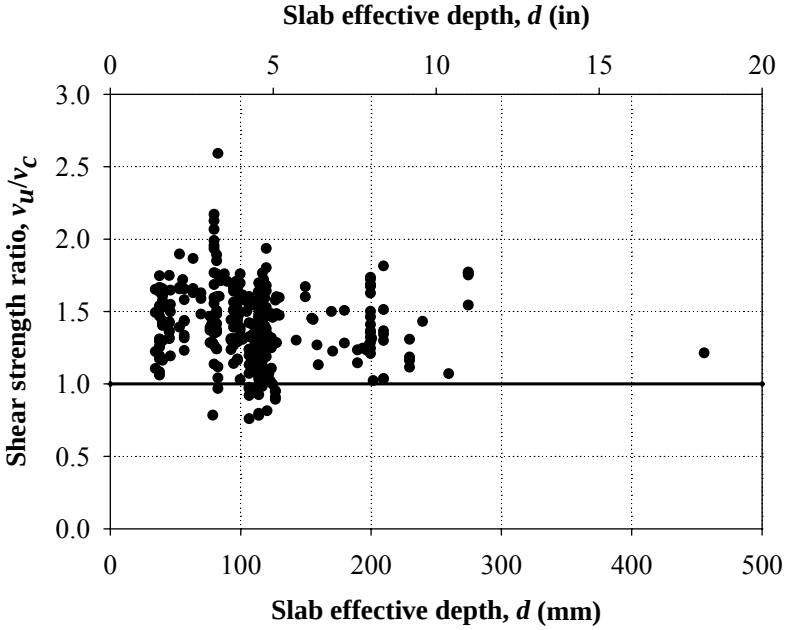

Figure 6.3 Shear strength ratio versus slab effective depth

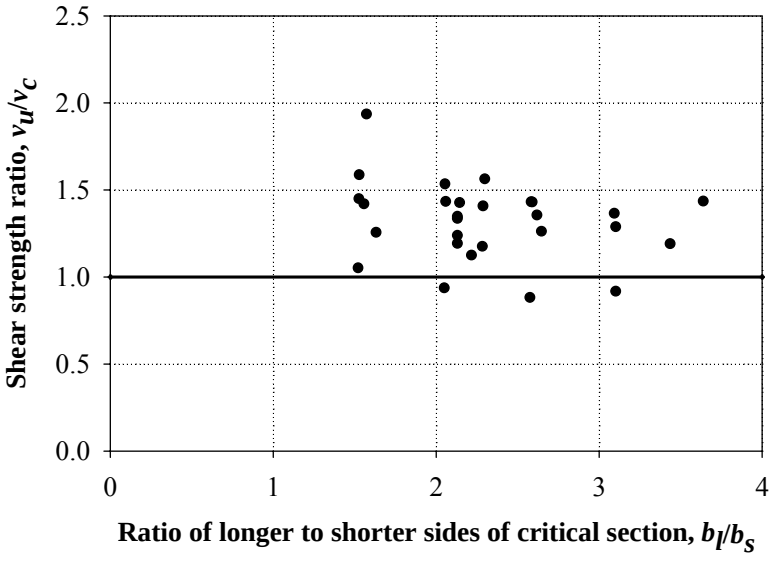

Figure 6.4 Shear strength ratio versus ratio of longer to shorter sides of critical section

6.4 Slab-column connections with unbalanced moment transfer

6.4.1 ACI unbalanced moment-and-shear interaction

The ACI 318-11 equation for slab-column connections with moment transfer given by Eq. (3.6) can also be written in a form of an interaction equation, as follows:

$$\frac{V_u}{V_o} + \frac{M_u}{M_o} = 1 \tag{6.3}$$

where V_u and M_u are the ultimate shear force and unbalanced moment at failure, respectively; V_o and M_o are the shear capacity in absence of unbalanced moment and unbalanced moment capacity in absence of shear force, respectively. They are expressed in Eqs. (6.4) and (6.5) below:

$$V_o = V_c = v_c b_o d \tag{6.4}$$

$$M_o = M_v = \frac{v_c J_c}{\gamma_v s} \tag{6.5}$$

where v_c is the ACI equations for shear strength determined from the lowest of Eqs. (3.1) to (3.3).

6.4.2 Proposed unbalanced moment-and-shear interaction

To study the interaction between unbalanced moment and shear for various type of connections (interior, edge, and corner connections), the series of tests by Hanson and Hanson (1968), Zaghlool (1971), Zaghlool and Rawdown de Paiva (1973), and Stamenković and Chapman (1974) are collected. Specimens from Hanson and Hanson (1968) [A Series], Zaghlool (1971) [Z-V Series], and Zaghlool and Rawdown de Paiva (1973) [Z-II Series] were interior, edge, and corner connections, respectively. Specimens from Stamenković and Chapman (1974) were interior connections with square columns (I Series), interior connections with rectangular columns (Ir Series), edge connections with unbalanced moments about an axis perpendicular to the slab edge (Et Series), edge connections with unbalanced moments about an axis parallel to the slab edge (En Series), and corner connections (C Series). In each test series, the connection geometry, reinforcement,

and material properties were kept nominally identical with slight variations in concrete strength. The main variable in each test series was the ratio between unbalanced moment and shear.

Figure 6.5 shows the interaction between unbalanced moment and shear at failure for these tests. The resisting unbalanced moment is normalized to the unbalanced moment strength M_o and the resisting shear is normalized to the shear strength V_o. It can be seen that for interior connections (A, I, and Ir series) and edge connections with unbalanced moments about an axis perpendicular to the slab edge (Et series), the interaction is close to linear. For edge connections with unbalanced moments about an axis parallel to the slab edge (Z-V and En series) and corner connections (Z-II and C series), the interaction is far from linear. Moehle (1988) suggested that for this type of connections (edge connections with unbalanced moments about an axis parallel to the slab edge and corner connections); the interaction is bilinear (rectangular shape).

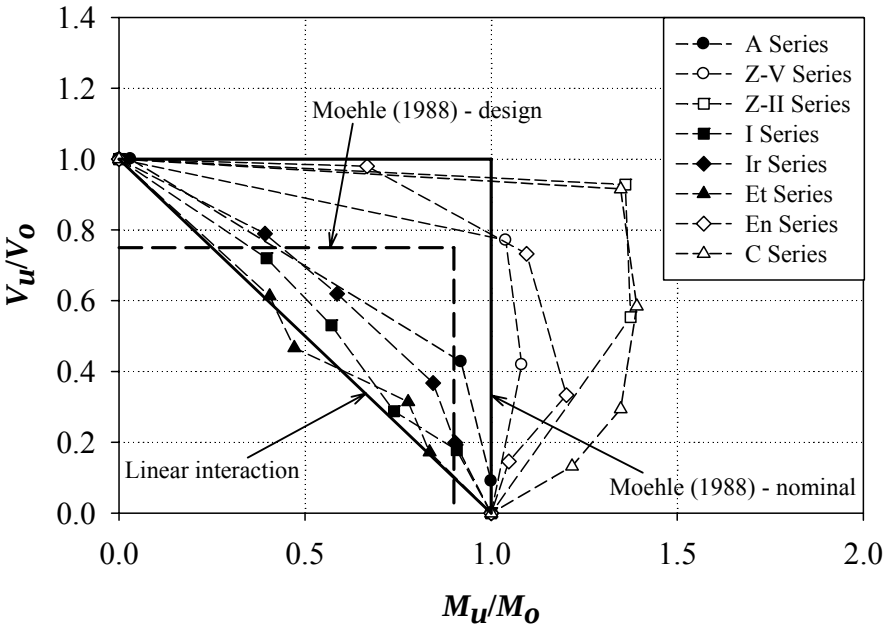

Figure 6.5 Interaction between shear and unbalanced moment

In this study, the author derived an interaction that is applicable to all types of connections (interior, edge, and corner connections). Thus, a non-linear interaction is proposed:

$$\frac{V_u}{V_o} + K\left(\frac{M_u}{M_o}\right)^n = 1 \tag{6.6}$$

where n is an empirical coefficient to fit the experimental data and K is a parameter that relates the shear and unbalanced moment ratios. In this study, n is taken equal to 1/4 with very little change in accuracy when n is taken between 1/3 and 1/5. The parameter K that relates the shear and unbalanced moment ratios is a function of gravity shear ratio V_u/V_o. Figure 6.6 shows the value of K as a function of gravity shear ratio V_u/V_o, where K is calculated using the proposed interaction equation [Eq. (6.6)] for n = 1/4. It can be seen that the parameter K can be approximated as a linear function of gravity shear ratio V_u/V_o:

$$K = 1 - \frac{V_u}{V_o} \tag{6.7}$$

Note that the linear regression analyses lead to R^2-values of 0.98, 0.99, and 0.99 for n equal to 1/3, 1/4, and 1.5, respectively. Figure 6.6 indicates that an increase in the gravity shear ratio would reduce the degree of interaction between the unbalanced moment and shear, or the parameter K. This suggests that for slab-column connections transferring high gravity shear, the allowable unbalanced moment ratio or the ratio of the ultimate unbalanced moment to the moment capacity will be lower.

The shear strength measured in the absence of unbalanced moment (V_o) is practically the punching capacity of slab-column connections under symmetrical punching (V_c). The unbalanced moment strength in the absence of shear (M_o) is assumed equal to flexural strength M_f within an effective transfer width of c plus 1.5h on each side of the column ($M_o = M_f$). Thus, the proposed interaction formula becomes:

$$\frac{V_u}{V_c} + \left(1 - \frac{V_u}{V_c}\right)\left(\frac{M_u}{M_f}\right)^{1/4} = 1 \tag{6.8}$$

where V_c is calculated using Eq. (6.4) with v_c taken from Eq. (6.2), and M_f is given by the following expression by assuming that all tension reinforcement within the effective transfer width reach yield:

$$M_f = \rho \cdot f_y \cdot b_t \cdot d^2 (1 - \frac{\rho \cdot f_y}{1.7 f'_c}) \tag{6.9}$$

where ρ is the ratio of tension slab reinforcement within the effective transfer width; f_y is the yield strength of slab reinforcement; b_t is the effective transfer width (c plus 1.5h on each side of the column); d is the slab effective depth; and f'_c is the compressive strength of concrete. For interior connections and edge connections with unbalanced moments about an axis perpendicular to the slab edge, the flexural strength M_f is provided by two faces. On one face, the flexural strength is contributed by the top reinforcement, and on the other face, the flexural strength is contributed by the bottom reinforcement. For edge connections with unbalanced moments about an axis parallel to the slab edge and corner connections, the flexural strength M_f is provided by single face only.

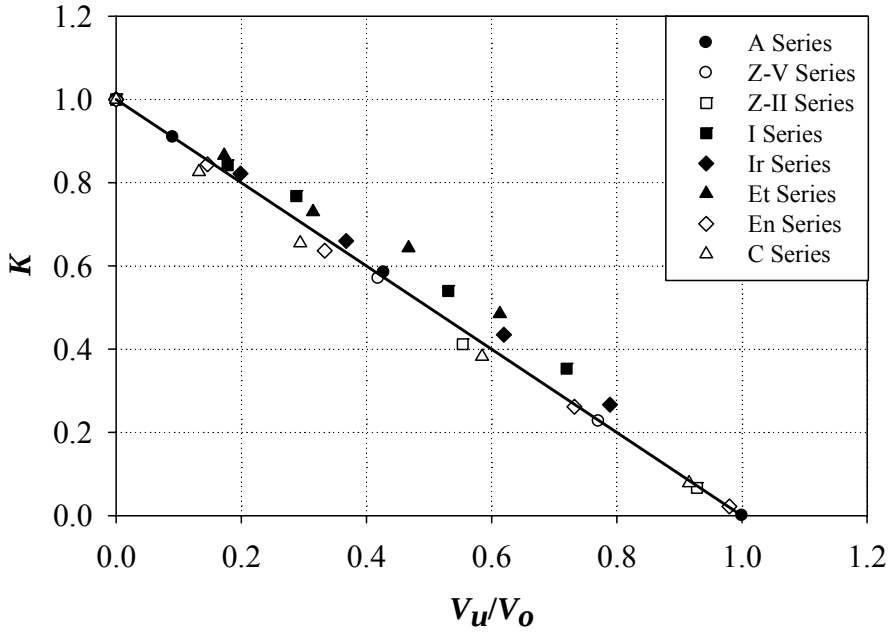

Figure 6.6 Relationship between parameter K and gravity shear ratio V_u/V_o

Figure 6.7 shows the comparison between the ACI 318-11 and proposed unbalanced moment-and-shear interaction for the data collected previously (Hanson and Hanson 1968; Zaghlool 1971, Zaghlool and Rawdown de Paiva 1973; Stamenković and Chapman 1974). The ACI 318-11 interaction was calculated according to Eq. (6.3), whereas the proposed interaction was calculated using Eq.

(6.8). The solid lines in Figure 6.7(a) and Figure 6.7(b) represent the theoretical interaction between shear and unbalanced moment according to Eqs. (6.3) and (6.8), respectively. It can be seen from Figure 6.7(a) and Figure 6.7(b) that a much improved relationship between shear and unbalanced moment were obtained using the proposed equations [Eq. (6.8)].

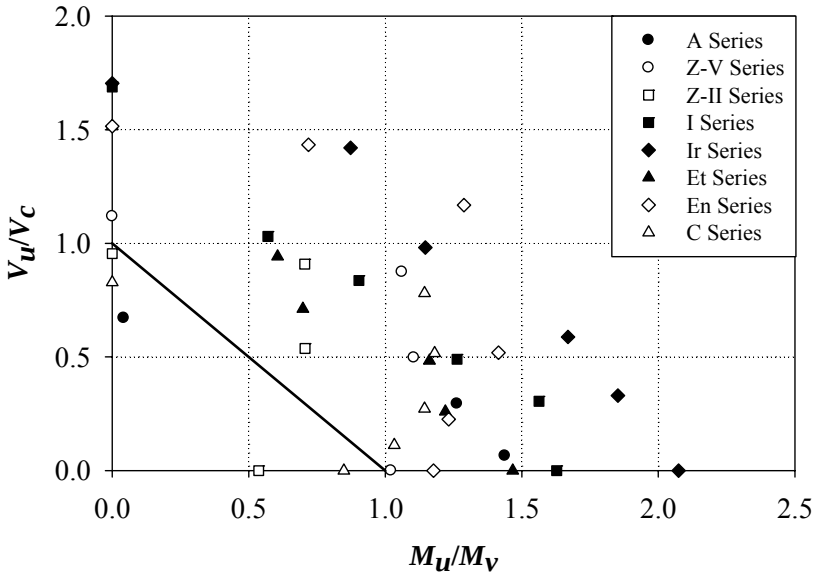

(a) ACI 318-11

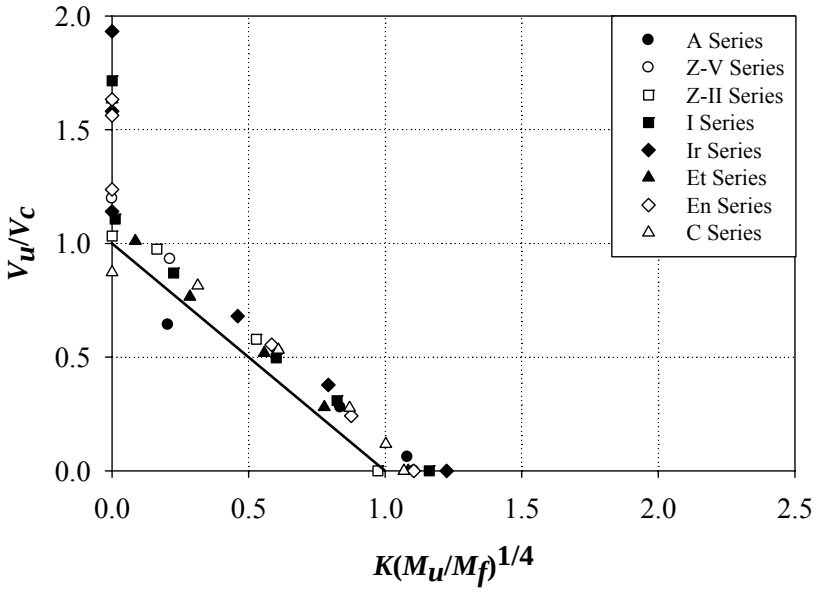

(b) Proposed Eq. (6.8)

Figure 6.7 Comparison of unbalanced moment-and-shear interaction

6.4.3 Ultimate shear stress equation

The proposed unbalanced moment-and-shear interaction equation as shown in Eq. (6.8) can also be written in a form of an equation to calculate the ultimate shear stress at the slab critical section. Assuming that shear failure occurs when the ultimate shear stress reaches the nominal shear strength, $v_u = v_c$, then Eq. (6.8) can be written as:

$$\frac{v_u}{v_c} = \frac{V_u}{V_c} + \left(1 - \frac{V_u}{V_c}\right)\left(\frac{M_u}{M_f}\right)^{1/4} \tag{6.10}$$

Multiplying Eq. (6.10) by v_c, resulted in an equation to calculate the slab ultimate shear stress based on the proposed unbalanced moment-and-shear interaction as shown below:

$$v_u = \frac{V_u}{b_o d} + \left(1 - \frac{V_u}{V_c}\right)\left(\frac{M_u}{M_f}\right)^{1/4} v_c \tag{6.11}$$

where V_u and M_u are the ultimate shear force and unbalanced moment, respectively; b_o is the perimeter of critical section in the shape of a closed rectangle at a distance $d/2$ from the column face; d is the average effective depth of slab; V_c is the shear capacity of slab under symmetrical loading calculated using Eq. (6.4) with v_c taken from Eq. (6.2); and M_f is the flexural strength of the slab within the effective transfer width given by Eq. (6.9).

The proposed equation to calculate the ultimate shear stress shown in Eq. (6.11) is a general equation applicable for interior, edge and corner slab-column connections. For connections with bidirectional moment transfer, a fully plastic behavior of the connection is assumed to occur. Thus, Eq. (6.11) should be applied independently for the shear and unbalanced moment about each principal axis of the column, and the worst case controls the design.

6.4.4 Comparison with experimental data

The accuracy of the proposed formula [Eq. (6.11)] to calculate the ultimate shear stress involving unbalanced moments transfer is shown in Figure 6.8. Comparing Figure 6.8(a) and Figure 6.8(b), we can see that the proposed equation

[Eq. (6.11)] as shown in Figure 6.8(b) is significantly better than the current ACI equation. Table 6.2 summarizes the performance of the proposed formula in predicting the strength of interior, edge, and corner reinforced concrete slab-column connections. Comparisons with the current ACI Code equations are also shown in Table 6.2. It can also be seen from Table 6.2 that the mean values of the measured over predicted strengths v_u/v_c, standard deviations and coefficients of variations from the proposed formula [Eq. (6.11)] are significantly better than those calculated using the ACI equation. In addition, all percentile-5% values of v_u/v_c from the proposed formula [Eq. (6.11)] are close to one, indicating that the proposed formula [Eq. (6.11)] is conservative enough for design purposes (95% of the data are safe).

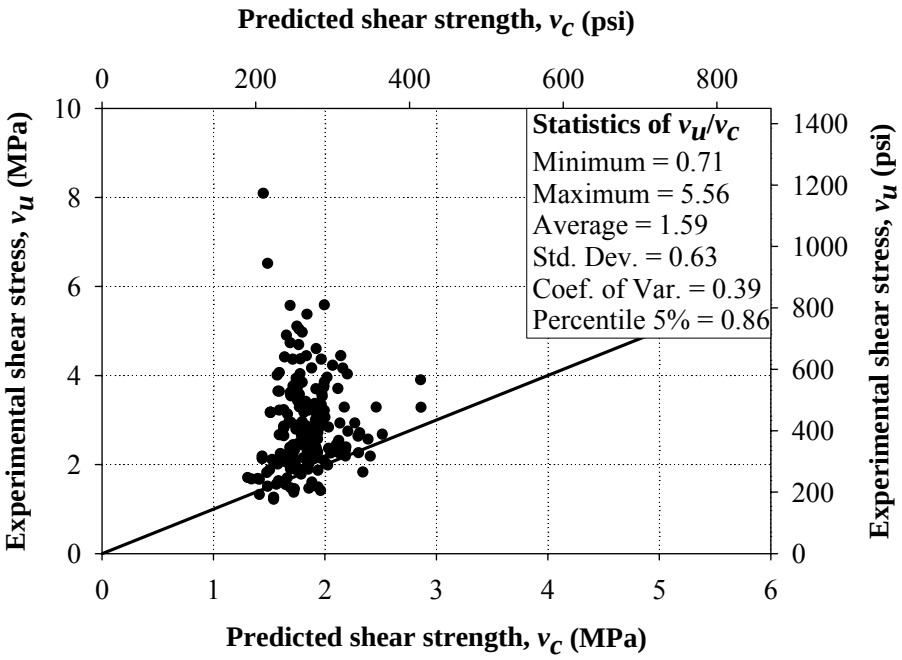

(a) ACI 318-11

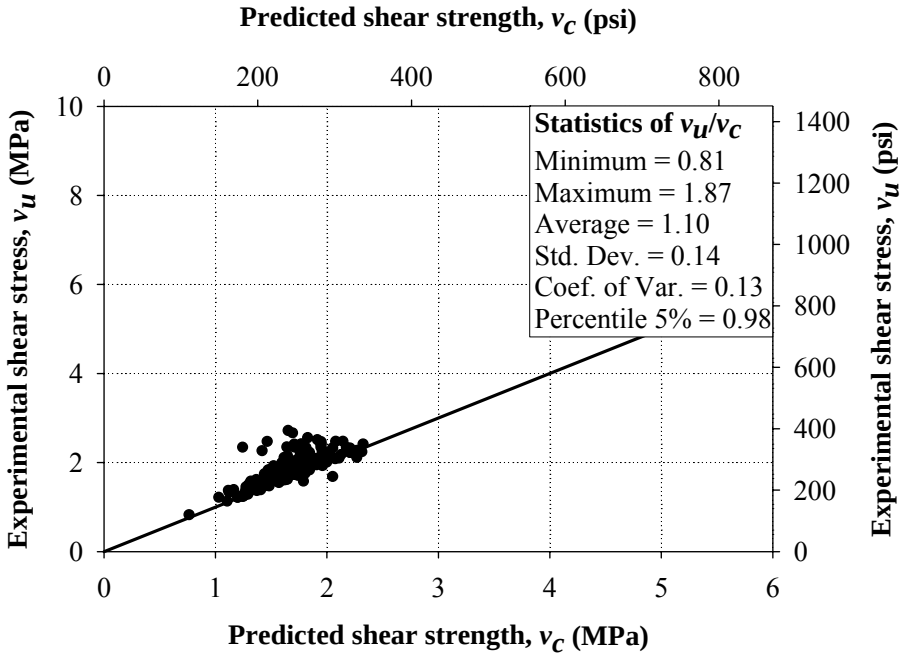

(b) Proposed

Figure 6.8 Strength predictions of reinforced concrete slab-column connections with unbalanced moment transfer

Table 6.2 Summary of reinforced concrete slab-column connections with unbalanced moment transfer

Case	n	Method	Statistics of v_u/v_c					
			Min	Max	Avg	SD	CV	P5%
Interior Square	61	ACI 318-11	0.71	2.10	1.28	0.29	0.23	0.86
		Proposed	**0.81**	**1.35**	**1.06**	**0.08**	**0.08**	**0.98**
Interior Rectangular	16	ACI 318-11	1.04	2.54	1.76	0.51	0.29	1.09
		Proposed	**0.98**	**1.58**	**1.12**	**0.15**	**0.13**	**0.99**
Edge Square	42	ACI 318-11	0.78	2.68	1.58	0.50	0.32	0.81
		Proposed	**0.98**	**1.63**	**1.09**	**0.13**	**0.12**	**1.00**
Edge Rectangular	17	ACI 318-11	0.96	1.56	1.28	0.18	0.14	1.00
		Proposed	**1.00**	**1.30**	**1.09**	**0.08**	**0.08**	**1.01**
Corner Square	55	ACI 318-11	0.78	4.36	1.94	0.67	0.34	1.04
		Proposed	**0.87**	**1.87**	**1.14**	**0.19**	**0.16**	**0.96**
Corner Rectangular	4	ACI 318-11	0.76	5.56	2.05	2.34	1.14	0.77
		Proposed	**1.06**	**1.21**	**1.14**	**0.06**	**0.06**	**1.07**

Notes: n = Number of data; Avg = Average; SD = Standard deviation; CV = Coefficient of variation; P5% = Percentile 5%

6.5 Summary

- The ACI 318-11 equations on shear strength of slabs [Eqs. (3.1) to (3.3)] do not consider the possible advantage of having higher percentage of slab flexural reinforcement. Teng et al. (2004) proposed a simple equation that takes into account the effects of slab flexural reinforcement, slab effective depth (size effect), and column rectangularity. The proposed single formula [Eq. (6.2)] has been shown to be more accurate than the ACI's three equations for v_c [Eqs. (3.1) to (3.3)]. It is also more accurate than the v_c equations from other codes (CEB-FIP Model Code 1990, British Standard 8110-97, and German Standard DIN 1045-1 (2000)).
- Experimental data indicates that the relationship between shear and unbalanced moment at interior connections and edge connections with moment transfer about axis perpendicular to the slab edge is close to linear, whereas the interaction at edge connections with moment transfer about an axis parallel to the slab edge and at corner connections are far from linear. Hence, a non-linear interaction that is applicable for all types of connections (interior, edge, and corner connections) is proposed. The proposed interaction [Eq. (6.8)] leads to a significant improvement over the performance of the current ACI formula. This is one of the author's main contributions.
- Based on the proposed interaction [Eq. (6.8)], a simple equation for calculating the ultimate shear stress at the critical section of slab-column connections under gravity and unbalanced moment transfer is derived [Eq. (6.11)]. The proposed method simplifies the design process and its accuracy and reliability has been checked against extensive experimental data. This is also one of the author's main contributions
- The performance of Eqs. (6.2), (6.8), and (6.11) have been shown to be very good against various experimental data, including interior, edge, and corner connections, ranging from symmetrical punching to connections having rectangular columns transferring unbalanced moments.

CHAPTER 7
SHEAR STRENGTH OF POST-TENSIONED SLAB-COLUMN CONNECTIONS

7.1 Introduction

In an attempt to improve the predictions of shear strength of reinforced concrete slabs under symmetrical punching, a simple equation was introduced by Teng et al. (2004). The proposed equation takes into account the effects of concrete strength, flexural reinforcement ratio, column rectangularity, and slab effective depth (size effect). In Chapter 6, the method was extended to predict the shear strength of reinforced concrete slab-column connections with unbalanced moment transfer. The proposed method is based on an interaction equation of shear and unbalanced moments, assuming that the moment transfer capacity is limited solely by the slab flexural reinforcement within the effective transfer width of c plus 1.5h on each side of the column. Accordingly, an equation to calculate the ultimate shear stress acting on the critical section was derived based on the proposed interaction. The method is applicable for all type of slab-column connections (interior, edge, and corner) and gives a very good agreement between the predicted and experimental values. Furthermore, the method also simplifies the design and analysis process.

This Chapter extends the method proposed previously for reinforced concrete slab-column connections to be used in post-tensioned slab-column connections. The shear strength formula of reinforced concrete slabs is extended to consider the effect of prestressing by decompression method. The ultimate shear stress is calculated based on an interaction equation of shear and unbalanced moments, assuming that the moment transfer capacity is carried by nonprestressed reinforcement and prestressing steel within the effective transfer width of c plus 1.5h on each side of the column. The proposed method is validated against experimental results and compared with ACI 318-11 and Eurocode 2 methods.

7.2 Review of experimental data

A total of 76 experimental data on prestressed slab-column connections subjected to combination of shear and unbalanced moment were collected and reviewed (Gerber and Burns 1971; Smith and Burns 1974; Burns and Hemakom 1977, 1985; Franklin & Long 1982; Shehata 1982; Kordina and Nölting 1984, 1986; Kosut et al. 1985; Foutch et al. 1990; Long and Cleland 1993; Hassanzadeh 1998; Melges 2000; Corrêa 2001; Khwaounjoo 2001; Silva 2004). All specimens were unbonded post-tensioned slab-column connections, with additional nonprestressed reinforcement, without beams, drop panels, column capitals, openings, and any types of shear reinforcement. Lift-slab specimens, lightweight concrete specimens, and specimens under cyclic loadings were not considered in this study. The database collected consists of 51 data on interior post-tensioned slab-column connections under symmetrical punching, and 25 data on post-tensioned slab-column connections subjected to shear and monotonic unbalanced moment, tabulated in Tables E.1 and E.2 of Appendix E, respectively.

Table E.1 contains specimen details for interior connections subjected to symmetrical punching. There are 51 data in Table E.1, comprises of 11 data on circular columns (Kordina and Nölting 1984, 1986; Hassanzadeh 1998), 39 data on square columns (Gerber and Burns 1971; Smith and Burns 1974; Burns and Hemakom 1977, 1985; Franklin and Long 1982; Shehata 1982; Melges 2000; Corrêa 2001; Silva 2004), and one data on rectangular columns with column aspect ratio five from the present study. Table E.2 presents details of specimens transferring shear and unbalanced moment. There are 25 data in Table E.2, consists of eight data on interior connections (Franklin and Long 1982; Burns and Hemakom 1985), 15 data on edge connections (Burns and Hemakom 1985; Kosut et al. 1985; Foutch et al. 1990; Long and Cleland 1993; Khwaounjoo 2001), and two data on corner connections (Kosut et al. 1985; Khwaounjoo 2001). All data in Table D.2 are slab-column connections with square columns. The notations of column dimensions and unbalanced moments for interior, edge, corner connections used in Tables E.1 and E.2 are illustrated in Figure 3.1.

The database covers a wide range of geometry, material properties, reinforcement content, and tendon details. The slab thickness (h) varies from 56 mm (2.20 in) to 220 mm (8.66 in) with the respective slab effective depths (d) of 44 mm (1.73 in) and 190 mm (7.48 in). The column width (c) is from 100 mm (3.9 in) to 900 mm (35.4 in) with the column aspect ratio (β) varies from one to five. The concrete strength (f'_c) ranges from 24.9 MPa (3611 psi) to 52.4 MPa (7600 psi). The yield strength of nonprestressed reinforcement (f_y) and prestressing steel (f_{py}) are from 379 MPa (55.0 ksi) to 675 MPa (97.9 ksi) and 1030 MPa (149.4 ksi) to 1729 MPa (250.8 ksi), respectively. The ratios of nonprestressed tension reinforcement (ρ) and prestressing steel (ρ_p) within c plus 1.5h on each side of the column vary from 0.18% to 1.43% and 0.06% to 1.64%, respectively. The effective stress in prestressing steel ranges from 587 MPa (85.1 ksi) to 1459 MPa (211.6 ksi), whereas the compressive stress in concrete due to prestressing (f_{pc}) varies from 0.70 MPa (102 psi) to 4.81 MPa (698 psi).

7.3 Slab-column connections under symmetrical punching

7.3.1 Proposed formula

The shear strength formula of reinforced concrete slabs [Eq. (6.2)] will be extended to consider the effect of prestressing by decompression method. Substituting Eq. (6.2) into Eq. (2.5) and taking into account the vertical component of prestress force, the shear strength of prestressed slabs can be expressed as:

$$v_c = 0.55(100\rho)^{1/3} f'_c{}^{1/3} \left(1+\frac{d}{1000}\right)^{-1/2} \left(\frac{b_l}{b_s}\right)^{-1/4} + \frac{V_d + V_p}{b_o d} \text{ (MPa)}$$

or

$$v_c = 15(100\rho)^{1/3} f'_c{}^{1/3} \left(1+\frac{d}{40}\right)^{-1/2} \left(\frac{b_l}{b_s}\right)^{-1/4} + \frac{V_d + V_p}{b_o d} \text{ (psi)} \qquad (7.1)$$

where ρ is the ratio of tension reinforcement within c plus 1.5h on each side of the column; f'_c is the compressive strength of concrete; d is the average effective depth of nonprestressed reinforcement; b_l and b_s are the lengths of longer and shorter sides of the critical section, respectively; b_o is the perimeter of critical section in the

shape of a closed rectangle at a distance $d/2$ from the face of column; V_p is the vertical component of prestress force crossing the critical section; and V_d is the decompression load given by Eq. (2.6) with m_d taken from Eq. (2.7).

The calculation of m_d in Eq. (2.7) involves the extreme fiber stress due to prestressing (f_e). For practical purposes, it is more convenient to use the stress value at the centroid of section (f_{pc}) rather than at the extreme fiber (f_e). Hence, the extreme fiber stress due to prestressing f_e can be replaced by the following expression:

$$f_e = f_{pc}\left[1 + \frac{6(d_p - h/2)}{h}\right] \tag{7.2}$$

where f_{pc} is the compressive stress in concrete due to prestressing at the centroid of section (input as positive value) and d_p is the effective depth of prestressing steel at the column centerline. It can be seen from Eq. (7.2) that f_e is equal to f_{pc} when the tendon is located at the mid height of slab ($d_p = h/2$).

The ratio of vertical shear force to the moment per unit width (V/m) depends on the column geometry and loading arrangement. Silva et al. (2005) showed that the redistribution of forces occurring after cracking makes it unnecessary to consider elastic concentration of stress. Hence, the moment can be averaged across the width of specimen or within the contraflexure lines. In this study, for simplicity, the value of V/m is estimated from the yield line theory by assuming a local yield line around the column as shown in Figure 7.1. Assuming a unit value of deflection at the column and applying the principle of virtual work, the V/m ratios of slab-column connections are worked out to be

$$\frac{V}{m} = 2\pi + \frac{\pi \cdot c}{a_v} \quad \text{for interior connections with circular columns} \tag{7.3}$$

$$\frac{V}{m} = 2\pi + \frac{2c_x}{a_{vy}} + \frac{2c_y}{a_{vx}} \quad \text{for interior connections with rectangular columns} \tag{7.4}$$

$$\frac{V}{m} = \pi + \frac{2c_x}{a_{vy}} + \frac{c_y}{a_{vx}} \quad \text{for edge connections with rectangular columns} \tag{7.5}$$

$$\frac{V}{m} = \frac{\pi}{2} + \frac{c_x}{a_{vy}} + \frac{c_y}{a_{vx}} \quad \text{for corner connections with rectangular columns} \qquad (7.6)$$

where c, c_x and c_y are the column dimensions; and a_v, a_{vx} and a_{vy} are the distances from the loading points to the column faces as illustrated in Figure 7.1. Detailed calculations of Eqs. (7.3) to (7.6) can be found in Appendix F. It can also be seen that Eqs. (7.4) to (7.6) are also valid for connections with square columns, provided that $c_x = c_y$ and $a_{vx} = a_{vy}$. In a continuous flat plate structure, the distance a_v can be measured from the column to the contraflexure line. This assumption is supported by the fact that flexural cracks could spread from the face of column to the contraflexure line as shown in the tests by Burns and Hemakom (1977, 1985), Kosut et al. (1985), and Gardner and Kallage (1998). According to linear-elastic analyses, the contraflexure line is approximately located at 0.2ℓ from the column centerline, where ℓ is the span length.

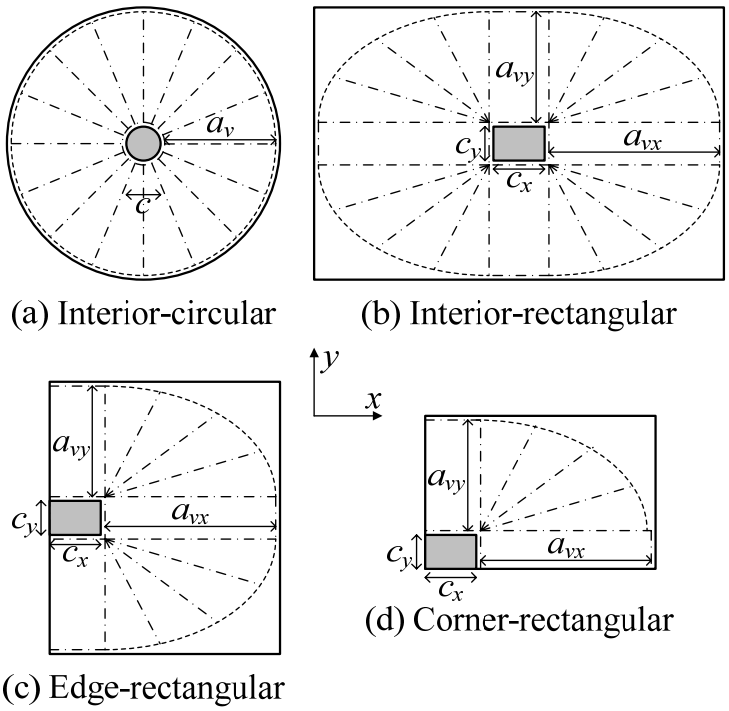

Figure 7.1 Yield line pattern of slab-column connections

Further investigation conducted by the author found that the accuracy of Eq. (7.1) is not sensitive to the changes of c/a_v in Eqs. (7.3) to (7.6). Typical values of c and a_v are from $1h$ to $5h$ and $6h$ to $10h$, respectively, where h is the slab thickness. Taking c equal to $3h$ and a_v equal to $8h$, the value of c/a_v is worked out to be 0.38.

Substituting c/a_v = 0.38 into Eqs. (7.3) to (7.6), the V/m ratios become 7.5, 7.8, 4.3, and 2.3 for Eqs. (7.3), (7.4), (7.5), and (7.6), respectively. For simplicity, the V/m values are proposed to be 7.5, 4, and 2 for interior, edge, and corner connections, respectively. Consequently, the computation of decompression load V_d simply becomes

$$V_d = \frac{f_{pc} h^2}{6}\left(\frac{V}{m}\right)\left[1+\frac{6(d_p - h/2)}{h}\right] \tag{7.7}$$

where f_{pc} is the average compressive stress in concrete due to prestressing; h is the slab thickness; V/m is the ratio of shear force to moment per unit width (V/m = 7.5 for interior connections, 4 for edge connections, and 2 for corner connections); and d_p is the average effective depth of prestressing steel at the column centerline.

7.3.2 Comparison with experimental data

Figure 7.2 shows the comparison of strength predictions among ACI 318-11, Eurocode 2, and the proposed methods for 51 interior connections under symmetrical punching listed in Table D.1. The vertical axis in Figure 7.2 corresponds to the experimental shear stress v_u computed using Eqs. (3.5) or (3.25), whereas the horizontal axis corresponds to the predicted shear strength v_c calculated using Eqs. (3.4), (3.22), and (7.1) for ACI 318-11, Eurocode 2, and the proposed methods, respectively. The statistical values of v_u/v_c (ratio of the experimental shear stress to the predicted shear strength) are also given in Figure 7.2. The analyses yield the coefficients of variation of 0.20, 0.19, and 0.18 for ACI 318-11, Eurocode 2, and the proposed methods, respectively. The respective standard deviations are 0.25, 0.24, and 0.23 for ACI 318-11, Eurocode 2, and the proposed methods. Hence, the proposed method gives slightly improvements on the accuracy compared with ACI 318-11 and Eurocode 2 methods.

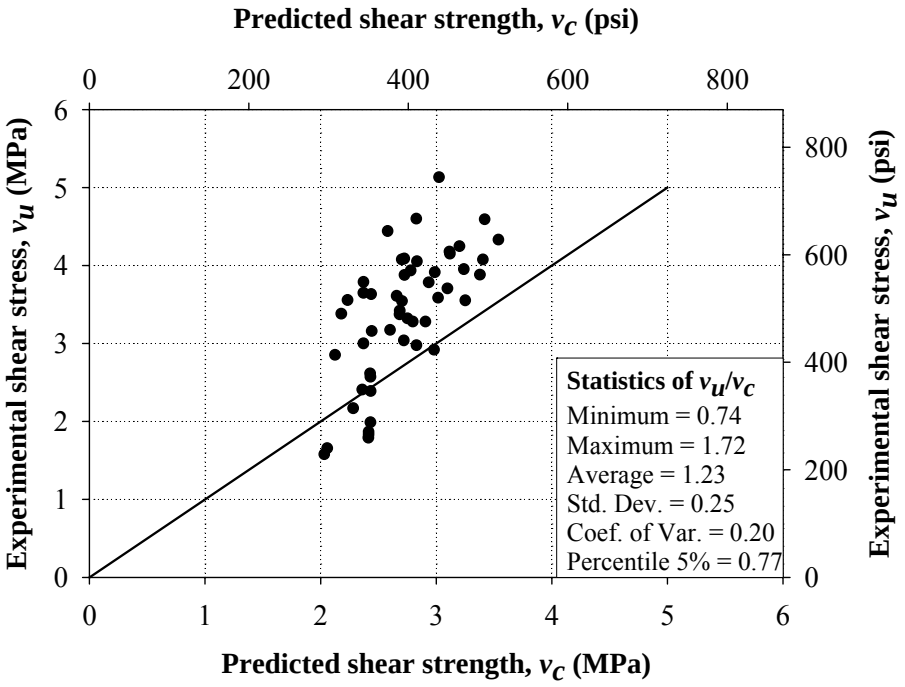

(a) ACI 318-11

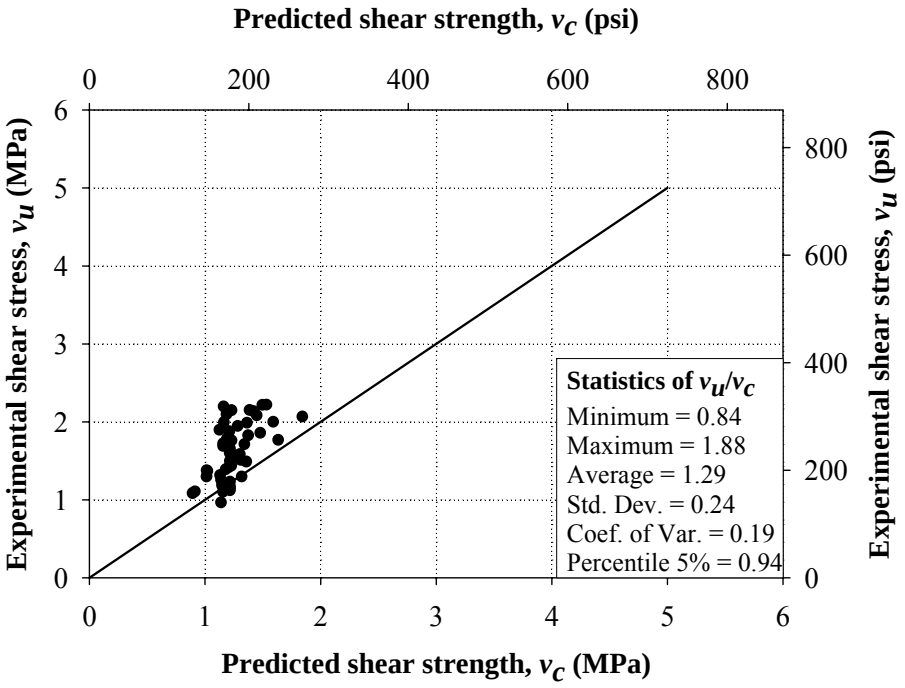

(b) Eurocode 2

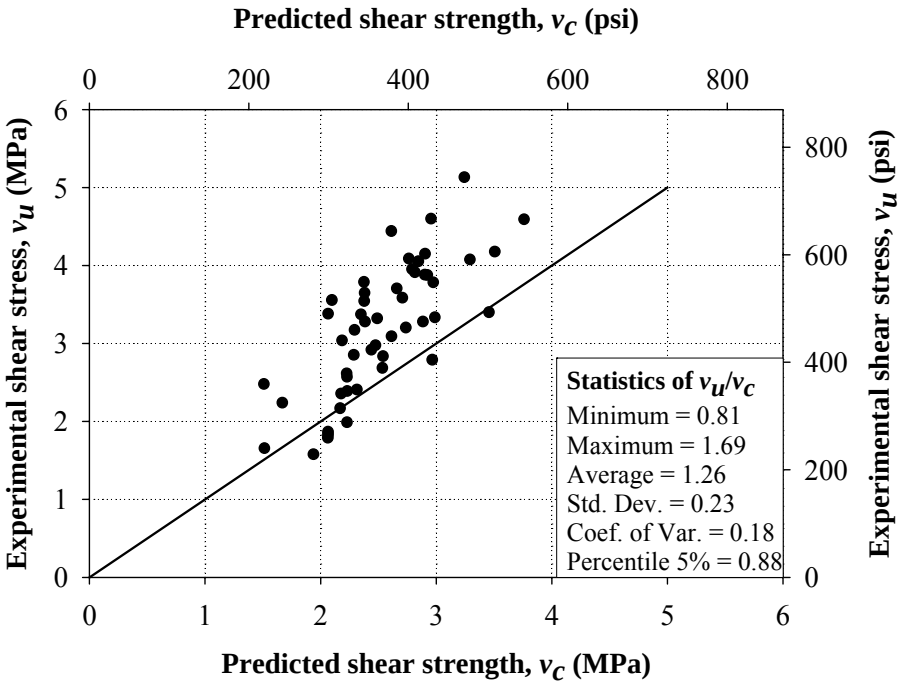

(c) Proposed

Figure 7.2 Strength predictions of post-tensioned slab-column connections under symmetrical punching

7.4 Slab-Column Connections with Unbalanced Moment Transfer

7.4.1 Unbalanced moment-and-shear interaction

As discussed in Chapter 6, the relationship between shear and unbalanced moment at interior connections and edge connections with moment transfer parallel to the slab edge is close to linear, whereas for edge connections with moment transfer perpendicular to the slab edge and corner connections, the relationship is far from linear. Accordingly, a non-linear interaction that is applicable for all types of connections (interior, edge, and corner) can be expressed in the form of

$$\frac{V_u}{V_c}+\left(1-\frac{V_u}{V_c}\right)\left(\frac{M_u}{M_f}\right)^{1/4}=1 \tag{7.8}$$

where V_u and M_u are the ultimate shear force and unbalanced moment, respectively; V_c is the shear capacity of slab-column connections under symmetrical punching; and M_f is the flexural strength within the effective transfer width. Eq. (7.8) was

derived based on the behavior of reinforced concrete slab-column connections with varying degree of unbalanced moment to shear force ratio.

In this study, the behavior of post-tensioned slab-column connections subjected to gravity load and unbalanced moment transfer is assumed similar to that of reinforced concrete slab-column connections. Thus, the relationship shown in Eq. (7.8) will also be used for post-tensioned concrete slab-column connections. The shear capacity of slab-column connections under symmetrical punching V_c is calculated using the following formula

$$V_c = v_c b_o d \tag{7.9}$$

were v_c is the punching resistance determined from Eq. (7.1); b_o is the perimeter of critical section in the shape of a closed rectangle at a distance $d/2$ from the face of column; and d is the average effective depth of nonprestressed reinforcement. The flexural strength M_f is assumed to be carried by nonprestressed reinforcement and prestressing steel within the effective transfer width of c plus $1.5h$ on each side of the column, given by

$$M_f = \rho \cdot b_t \cdot d \cdot f_y \left(d - \frac{a}{2} \right) + \rho_p \cdot b_t \cdot d_p \cdot f_{ps} \left(d_p - \frac{a}{2} \right) \tag{7.10}$$

where ρ is the ratio of nonprestressed tension reinforcement within the effective transfer width; d is the effective depth of nonprestressed reinforcement; f_y is the yield strength of nonprestressed reinforcement; ρ_p is the ratio of prestressing steel within the effective transfer width; d_p is the effective depth of prestressing steel at the column centerline; f_{ps} is the stress in prestressing steel at the flexural strength; b_t is the effective transfer width of c plus $1.5h$ on each side of the column; and a is the depth of compression block given by Eq. (7.11) below:

$$a = \frac{\rho \cdot d \cdot f_y + \rho_p \cdot d_p \cdot f_{ps}}{0.85 f'_c} \tag{7.11}$$

where f'_c is the compressive strength of concrete cylinder and all other terms are as previously defined. The stress in prestressing steel at the flexural strength f_{ps} can be estimated using Eq. (18-3) of ACI 318-11, given below:

$$f_{ps} = f_{se} + 10{,}000 + \frac{f'_c}{300\rho_p} \text{ (psi) or } f_{ps} = f_{se} + 70 + \frac{f'_c}{300\rho_p} \text{ (MPa)} \quad (7.12)$$

where f_{se} is the effective stress in prestressing steel (after allowance for all prestress losses); and all other terms are as previously defined. The value of f_{ps} in Eq. (7.12) shall not be taken greater than the lesser of f_{py} and (f_{se} + 30,000) [for psi unit] or (f_{se} + 210) [for MPa unit], where f_{py} is the yield strength of prestressing steel. For interior connections and edge connections with unbalanced moment about an axis perpendicular to the slab edge, the flexural strength M_f is provided by two faces (front and back faces). For edge connections with unbalanced moment about an axis parallel to the slab edge and corner connections, the flexural strength M_f is provided by single face only.

7.4.2 Ultimate shear stress equation

The proposed unbalanced moment-and-shear interaction equation as shown in Eq. (7.8) can also be written in a form of an equation to calculate the ultimate shear stress at the slab critical shear perimeter. Assuming that shear failure occurs when the ultimate shear stress reaches the nominal shear strength ($v_u = v_c$), then Eq. (7.8) can be rewritten as:

$$\frac{v_u}{v_c} = \frac{V_u}{V_c} + \left(1 - \frac{V_u}{V_c}\right)\left(\frac{M_u}{M_f}\right)^{1/4} \quad (7.13)$$

An equation to calculate the slab ultimate shear stress based on the proposed unbalanced moment-and-shear interaction can be obtained by multiplying Eq. (7.13) by v_c and shown below:

$$v_u = \frac{V_u}{b_o d} + \left(1 - \frac{V_u}{V_c}\right)\left(\frac{M_u}{M_f}\right)^{1/4} v_c \quad (7.14)$$

where V_u and M_u are the ultimate shear force and unbalanced moment, respectively; b_o is the perimeter of critical section in the shape of a closed rectangle at a distance $d/2$ from the face of column; d is the average effective depth of nonprestressed reinforcement; V_c is the shear capacity calculated using Eq. (7.9) with v_c taken from

Eq. (7.1); and M_f is the flexural strength within the effective transfer width given by Eq. (7.10).

The proposed equation for calculating the ultimate shear stress shown in Eq. (7.14) is a general equation applicable for interior, edge and corner slab-column connections. For connections with bidirectional moment transfer, a fully plastic condition is assumed to occur. Thus, Eq. (7.14) should be applied independently for the shear and unbalanced moment about each principal axis of the column, and the worst case will govern.

7.4.3 Comparison with experimental data

Figure 7.3 shows the comparison of strength predictions among ACI 318-11, Eurocode 2, and the proposed methods for 25 post-tensioned slab-column connections listed in Table D.2. The vertical axis in Figure 7.3 corresponds to the experimental shear stress v_u computed using Eqs. (3.6) to (3.12) for ACI 318-11 method, Eq. (3.25) for Eurocode 2 method, and Eq. (7.14) for the proposed method. The horizontal axis in Figure 7.3 corresponds to the predicted shear strength v_c calculated using Eqs. (3.4), (3.22), and (7.1) for ACI 318-11, Eurocode 2, and the proposed methods, respectively. The statistical values of v_u/v_c (ratio of the experimental shear stress to the predicted shear strength) are also given in Figure 7.3. The respective coefficients of variation are found to be 0.31, 0.39, and 0.07 for ACI 318-11, Eurocode 2, and the proposed methods. In addition, the analyses yield the percentile 5% values of 0.62, 0.52, and 0.93 for ACI 318-11, Eurocode 2, and the proposed methods, respectively. Thus, in terms of accuracy of conservatism, the proposed model is much better compared with the eccentric shear stress model of ACI 318-11 and Eurocode 2 method.

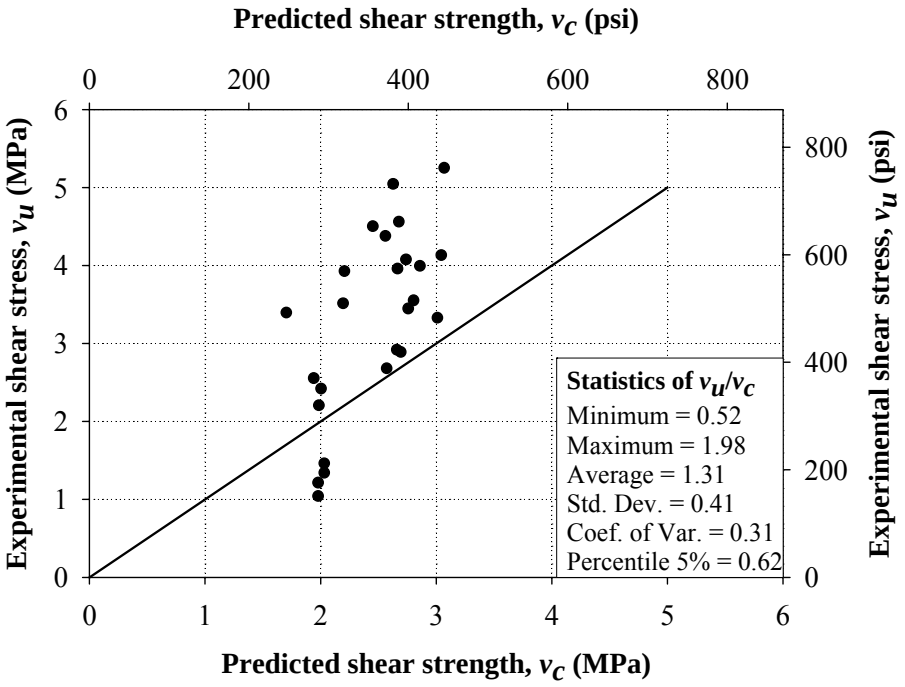

(a) ACI 318-11

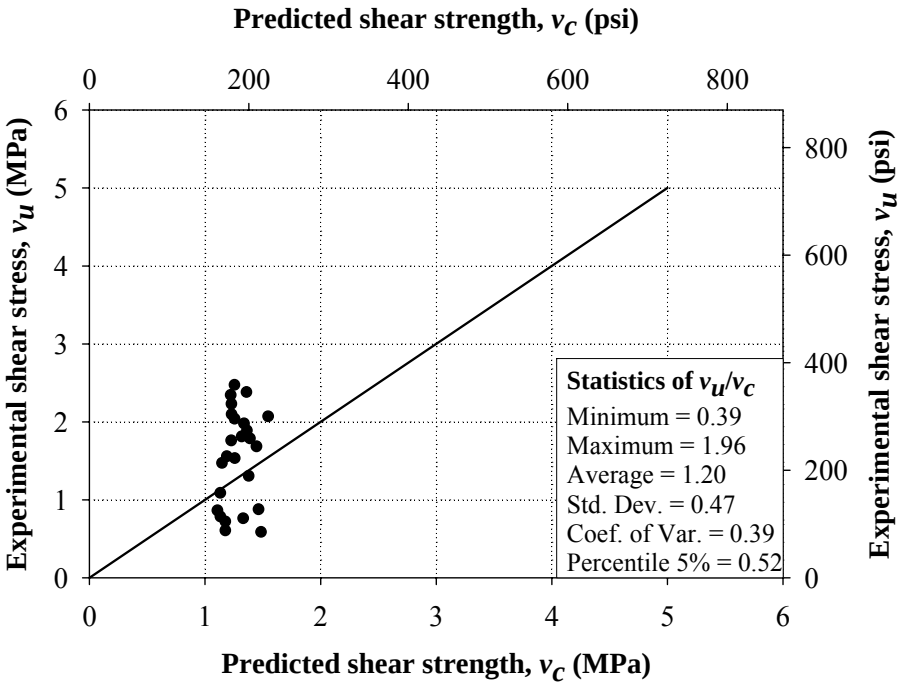

(b) Eurocode 2

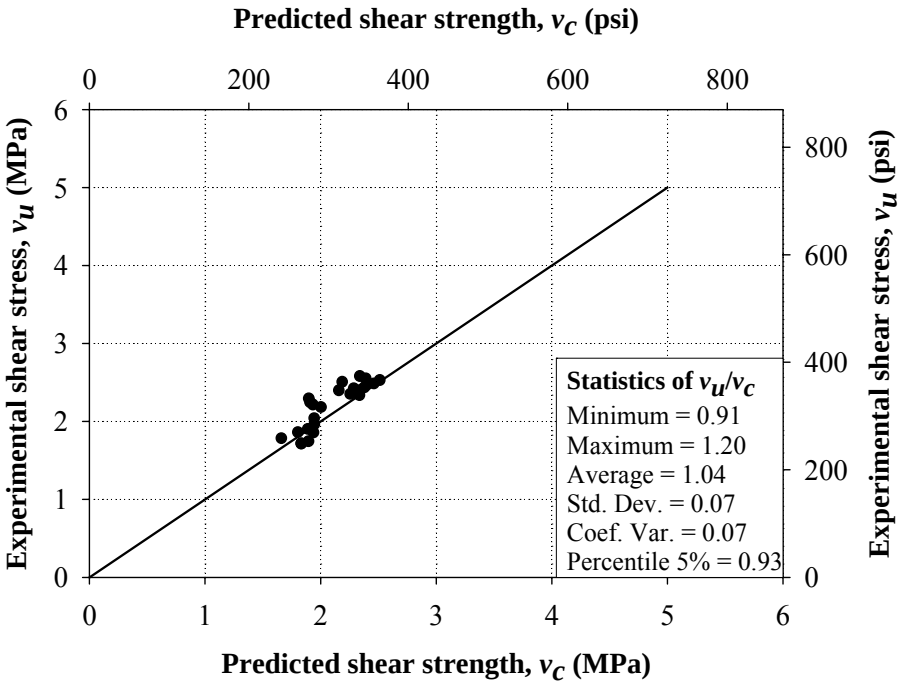

(c) Proposed

Figure 7.3 Strength predictions of post-tensioned slab-column connections with unbalanced moment transfer

7.5 Summary

- The shear strength formula for reinforced concrete slab-column connections [Eq. (6.4)] is extended to calculate the shear strength of post-tensioned slab-column connections using the decompression approach [Eq. (7.1)]. This is one of the author's main contributions.
- The proposed formula to estimate the shear strength of post-tensioned slabs [Eq. (7.1)] had been verified against 51 experimental data and compared with ACI 318-11 and Eurocode 2 equations. In terms of accuracy, the proposed formula [Eq. (7.1)] is better than ACI 318-11 and Eurocode 2 equations.
- The non-linear interaction equation of shear and unbalanced moment proposed previously for reinforced concrete slab-column connections [Eq. (7.8)] is used to derive a formula to calculate the ultimate shear stress of post-tensioned slab-column connections subjected to shear and moment transfer [Eq. (7.14)]. In the proposed formula [Eq. (7.14)], the moment transfer capacity is assumed to be

carried by nonprestressed reinforcement and prestressing steel within the effective transfer width of c plus 1.5h on each side of the column.

- The proposed formula to calculate the ultimate shear stress due to shear and unbalanced moment transfer [Eq. (7.14)] was shown to be more accurate and conservative than the eccentric shear stress model of ACI 318-11 and Eurocode 2 method in predicting 25 experimental results.

CHAPTER 8
SLAB-COLUMN CONNECTIONS UNDER CYCLIC LOADING

8.1 Introduction

Shear failure may occur at a slab-column connection due to transfer of shear forces and unbalanced moments between the slab and the column. The shear transfer usually comes from the gravity load whereas the unbalanced moment may come from different loading between the adjacent spans, or lateral loading, such as strong wind or earthquake loading. For slab-column connections subjected to earthquake loading, the effect of cyclic loading may cause shear strength degradation that can lead to premature failure. Furthermore, to provide some minimal ductility, the story drift ratio should be limited to a certain level that depends on the gravity shear ratio.

In an attempt to improve the predictions of shear strength of reinforced concrete slabs under symmetrical punching, a simple equation was introduced by Teng et al. (2004). The proposed equation takes into account the effects of concrete strength, flexural reinforcement ratio, column rectangularity, and slab effective depth (size effect). In Chapters 6 and 7, the method was extended to predict the shear strength of reinforced concrete and post-tensioned slab-column connections transferring monotonic unbalanced moments. In the proposed method, the effect of prestressing is taken into account by the decompression method, whereas the effect of moment transfer is assumed to follow an interaction equation of shear and unbalanced moments. Accordingly, an equation to calculate the ultimate shear stress acting on the critical section was derived based on the proposed interaction. The proposed method was shown to give a very good agreement between the predicted and experimental values. Furthermore, the proposed method also simplifies the design and analysis process.

This Chapter checks the applicability of the proposed method to calculate the shear strength of slab-column connections subjected to gravity and cyclic lateral loading. For comparison purposes, 110 experimental data on reinforced concrete and post-tensioned slab-column connections subjected to gravity and cyclic lateral

loading were collected and compared with the strength predictions using ACI 318-11. In addition, the plots of drift capacity against gravity shear ratio were also presented to provide a recommendation on slab-column connection subjected to seismic loading. Appendix H presents VBA programming to calculate the strength predictions of slab-column connections using ACI 318-11 as well as the proposed method.

8.2 Review of experimental data

A total of 110 experimental data on slab-column connections subjected to gravity and cyclic lateral loading were collected and reviewed (Hanson and Hanson 1968; Hawkins et al. 1974b; Islam and Park 1976; Symmonds et al. 1976; Trongtham and Hawkins 1977; Morrison et al. 1983; Zee and Moehle 1984; Shatila 1987; Pan and Moehle 1989; Robertson and Durrani 1990; Dilger and Cao 1991; Robertson and Durrani 1991; Pan and Moehle 1992; Robertson and; Durrani 1992; Wey and Durrani 1992; Farhey et al. 1993; Dilger and Brown 1994; Martinez-Cruzado et al. 1994; Durrani et al. 1995; Luo and Durrani 1995a, b; Emam et al. 1997; Megally 1998; Robertson et al. 2002; Tan and Teng 2005; Han et al. 2006a, b; Ritchie et al. 2006; Robertson and Johnson 2006; Widjaja and Teng 2006; Anggadjaja and Teng 2008; Kang and Wallace 2008; Tian et al. 2008). All the specimens were slab-column connections cast using normalweight concrete, without beams, drop panels, column capitals, openings, and any type of shear reinforcement. The database collected consists of 88 data on reinforced concrete slab-column connections and 22 data on post-tensioned slab-column connections, tabulated in Tables G.1 and G.2 of Appendix F, respectively. Lift-slab specimens and lightweight concrete specimens were not considered for this study.

Table G.1 contains specimen details of reinforced concrete slab-column connections subjected to gravity and cyclic lateral loading. There are 88 data in Table G.1, comprising 62 data on interior connections, 24 data on edge connections, and 2 data on corner connections. Table G.2 presents specimen details of post-tensioned slab-column connections subjected to gravity and cyclic lateral loading. There are 22 data in Table G.2, consisting of 14 data on interior connections, six data on edge connections, and 2 data on corner connections. All data in Table G.2

are connections with square columns, except two interior connections with rectangular columns having column aspect ratio of five. The notations of column dimensions and unbalanced moments for interior, edge, corner connections used in Tables G.1 and G.2 are illustrated in Figure 3.1.

8.3 Strength predictions

Figure 8.1 shows the comparison of strength predictions using ACI 318-11 and the proposed method for reinforced concrete slab-column connections. For ACI 318-11 method, the punching shear strengths (v_c) were calculated using Eqs. (3.1) to (3.3), whereas the ultimate shear stresses (v_u) were calculated using Eqs. (3.6) to (3.12). For the proposed method, the punching shear strengths (v_c) and the ultimate shear stresses (v_u) were calculated using Eqs. (6.2) and (6.11), respectively. It can be seen from Figure 8.1 that the accuracy of the proposed method is much better compared with ACI 318-11 method. The average shear strength ratio v_u/v_c (ratio of the experimental to the predicted shear strength) calculated using ACI 318-11 method is 1.19 with a coefficient of variation of 0.41, whereas the proposed method gives an average shear strength ratio v_u/v_c of 1.14 with a coefficient of variation of 0.09.

The comparison of strength predictions using ACI 318-11 and the proposed method for post-tensioned slab-column connections is shown in Figure 8.2. For ACI 318-11 method, the punching shear strengths (v_c) and the ultimate shear stresses (v_u) were calculated using Eqs. (3.4) and Eqs. (3.6) to (3.12), respectively. For the proposed method, the punching shear strengths (v_c) and the ultimate shear stresses (v_u) were calculated using Eq. (7.1) and (7.14), respectively. It can be seen from Figure 8.2 that the accuracy of the proposed method is much better compared with ACI 318-11 method. The average shear strength ratio v_u/v_c (ratio of the experimental to the predicted shear strength) calculated using ACI 318-11 method is 1.20 with a coefficient of variation of 0.21, whereas the proposed method gives an average shear strength ratio v_u/v_c of 1.04 with a coefficient of variation of 0.06.

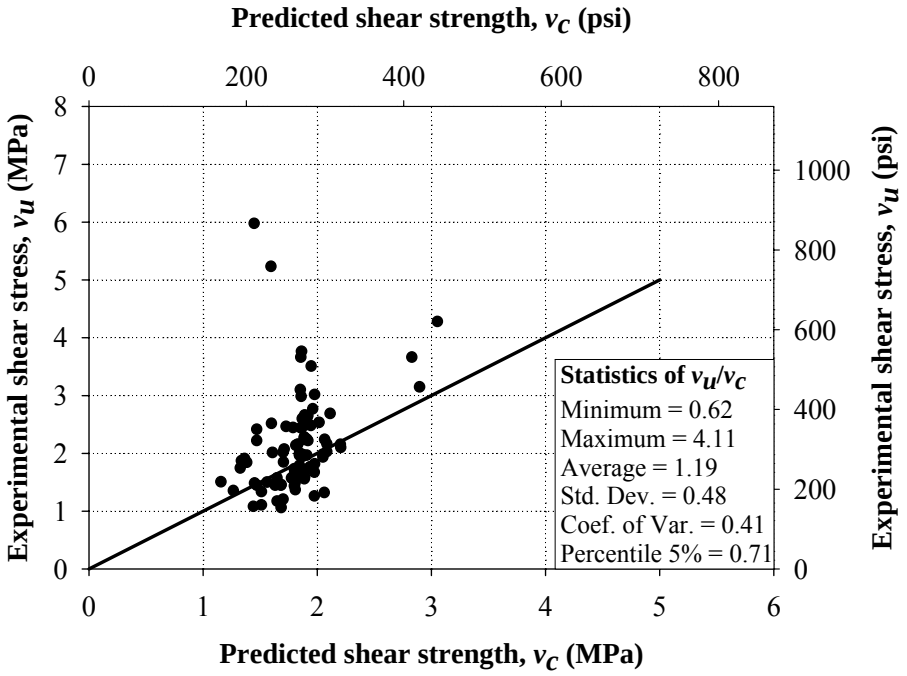

(a) ACI 318-11

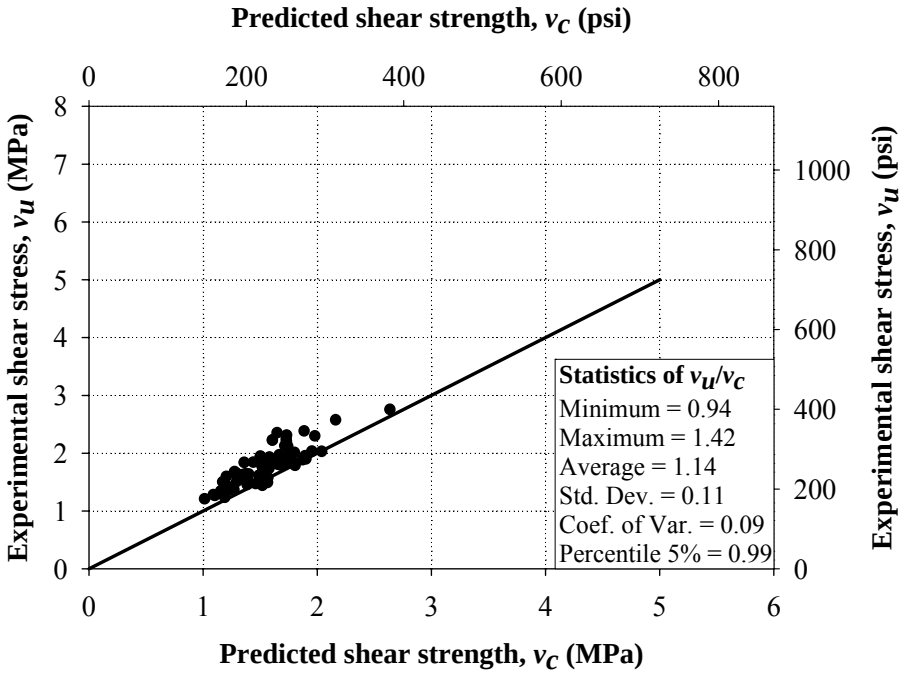

(b) Proposed

Figure 8.1 Strength predictions of reinforced concrete slab-column connections under cyclic loading

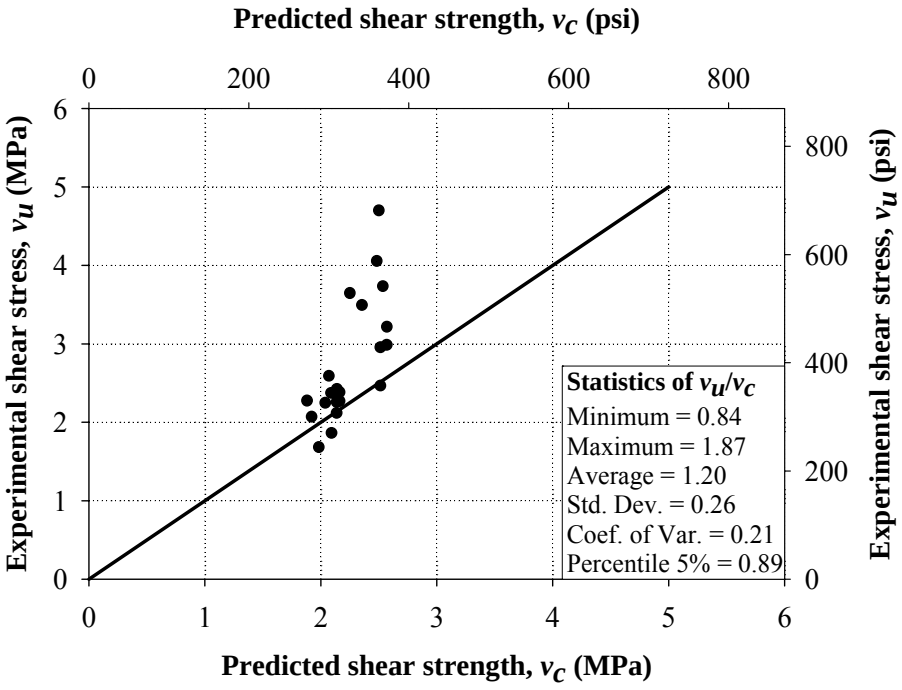

(a) ACI 318-11

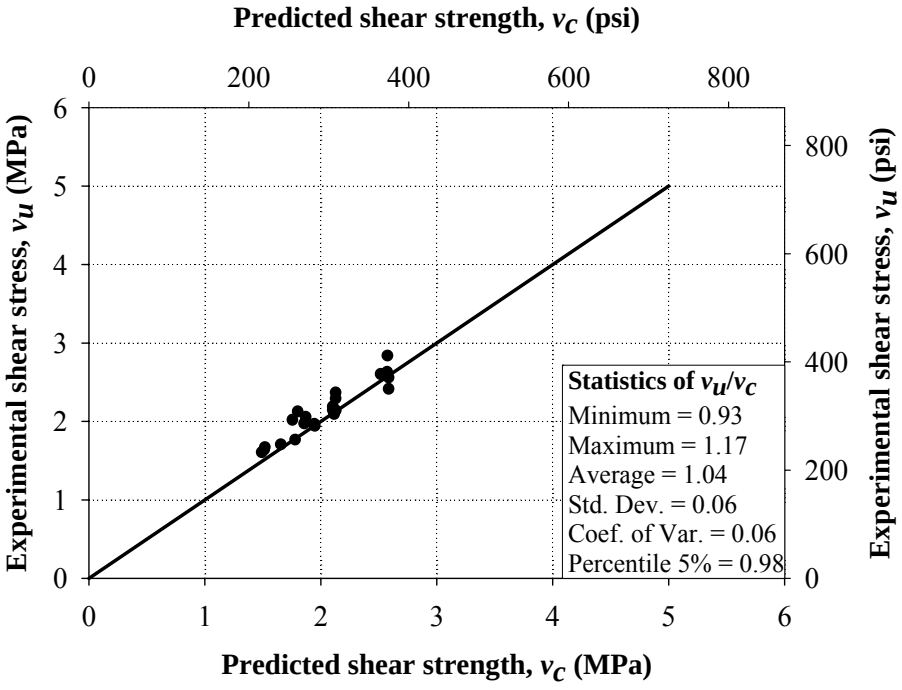

(b) Proposed

Figure 8.2 Strength predictions of post-tensioned slab-column connections under cyclic loading

8.4 Effect of cyclic loading

It was conventionally assumed that cyclic loading causes shear strength degradation, thus, a reduction factor needs to be introduced into the shear strength formula. The reduction factor due to cyclic loading is usually a function of ductility (μ) [Biskinis et al. 2004]. For slab-column connections, the ductility (μ) can be defined as the ratio between the ultimate drift ratio (DR_u) and the yield drift ratio (DR_y) [$\mu = DR_u/DR_y$]. However, the slab-column connection ductility cannot be defined uniquely as there is no distinct yield drift ratio due to yield spreads gradually across the slab transverse width (Pan and Moehle 1989). In this study, the possibility of shear strength degradation is assessed by comparing the analytical results of specimens subjected to monotonic loading and cyclic loading. The analytical results of reinforced concrete and post-tensioned slab-column connections under monotonic loading were obtained from Chapter 6 and Chapter 7, respectively.

Figure 8.3 presents the statistical values of v_u/v_c for reinforced concrete slab-column connections subjected to monotonic and cyclic moments transfer calculated using ACI 318-11 and the proposed method. Note that the analyses were based on 195 and 88 data on reinforced concrete specimens under monotonic and cyclic loading, respectively. Using ACI 318-11 method, the average v_u/v_c reduces from 1.59 to 1.19, whereas the percentile 5% value of v_u/v_c drops from 0.86 to 0.71. However, using the proposed method, the average and the percentile 5% values of v_u/v_c remain consistent. For post-tensioned slab-column connections under monotonic and cyclic moment transfer, the statistical values of v_u/v_c are given in Figure 8.4. The analyses were based on 25 and 22 data on post-tensioned slabs subjected to monotonic and cyclic loading, respectively. Again, the proposed method gives consistent results in terms of average as well as percentile 5% values of v_u/v_c, whereas ACI 318-11 method gives a drop in the average value and an increase in the percentile 5% value.

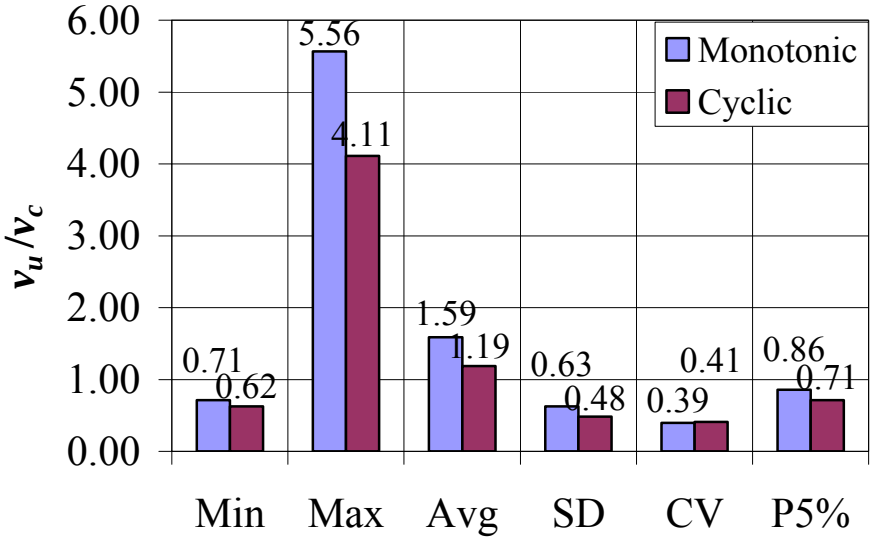

(a) ACI 318-11

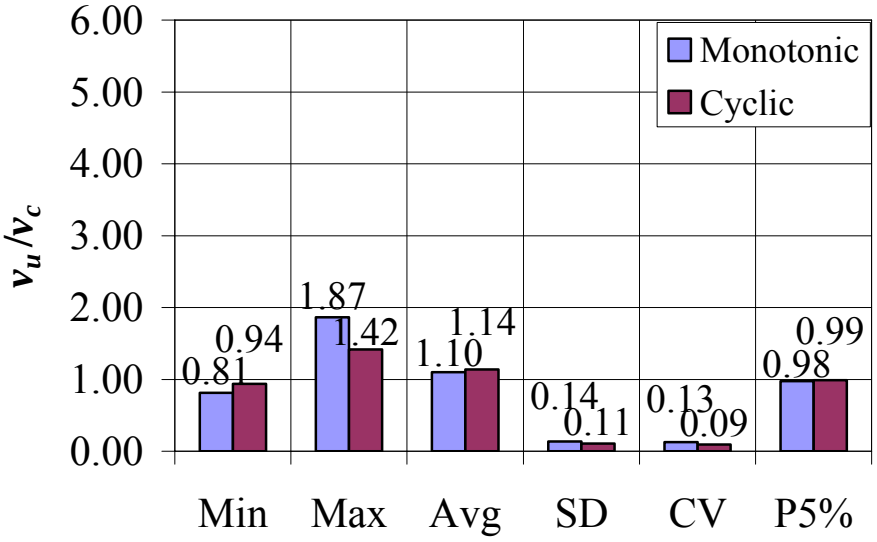

(b) Proposed

Figure 8.3 Statistical values of v_u/v_c for reinforced concrete slab-column connections under monotonic and cyclic loading

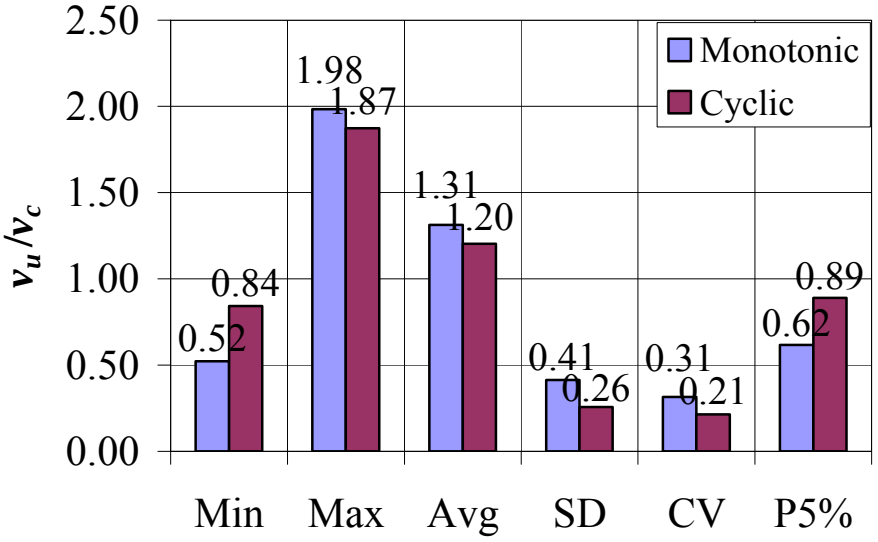

(a) ACI 318-11

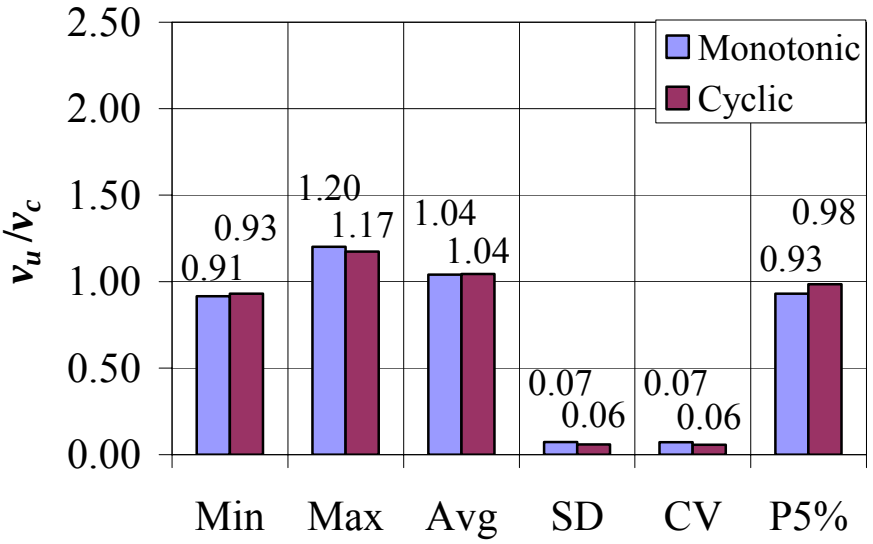

(b) Proposed

Figure 8.4 Statistical values of v_u/v_c for post-tensioned slab-column connections under monotonic and cyclic loading

Looking at the results using ACI 318-11, someone might think that cyclic loading causes deterioration of the shear strength. However, this could be due to inaccuracy of the ACI method. On the other hand, the proposed method gives consistent results between monotonic and cyclic loading case, without losing its accuracy and the safety margin.

There is very limited data on tests of slab-column connections without shear reinforcement in which the nature of loading (monotonic or cyclic) was the only variable, whereas the other variables were kept relatively constant. Apparently, only specimens A1 and A2 tested by Hanson and Hanson (1968) and specimens 2 and 3C tested by Islam and Park (1976) belong to this category. It was found that there is no reduction in strength due to cyclic loading. In addition, Tian et al. (2008) concluded that the slab damage imposed by the previously applied cyclic loading has no detrimental effect on the connection gravity load-carrying capacity.

To see more detail the effect of cyclic loading on the shear strength of slab-column connections, the shear strength ratios (v_u/v_c) were plotted against the ultimate drift ratios (DR_u) and against the number of cycles (n). The shear strength ratio v_u/v_c were calculated using the proposed method given by Eqs. (7.1) and (7.14). The ultimate drift ratio DR_u is the measured story drift ratio at the peak unbalanced moment. Note that the loading path of bidirectional cyclic loading is four times longer than that of unidirectional cyclic loading (see Figure 4.14). Therefore, to give an equivalent number of cycles as in the unidirectional cyclic loading, the number of cycles plotted for bidirectional cyclic loading were $2(n_x + n_y)$, where n_x and n_y are the number of cycles in x- and y-directions, respectively. The plots of v_u/v_c against DR_u and n are depicted in Figure 8.5 and Figure 8.6 for reinforced concrete slab-column connections, and Figure 8.7 and Figure 8.8 for post-tensioned slab-column connections. Note that 24 data (Hawkins et al. 1974b; Symmonds et al. 1976; Zee and Moehle 1984, Robertson and Durrani 1990; Dilger and Cao 1991; Dilger and Brown 1994, and Luo and Durrani 1995a,b) were ignored in Figure 8.6 as the author could not find the number-of-cycles data. The data shows that cyclic loading having ultimate drift ratio (DR_u) less than 6 % and number of cycles (n) less than 60 does not induce any strength degradation on slab-column connections. This behavior is somewhat similar to that of concrete under compression, where the monotonic loading stress-strain curve forms an envelope of the cyclic loading stress-strain response, resulting in no reduction of strength. The effect of cyclic loading having DR_u greater than 6 % and n greater than 60 is not known.

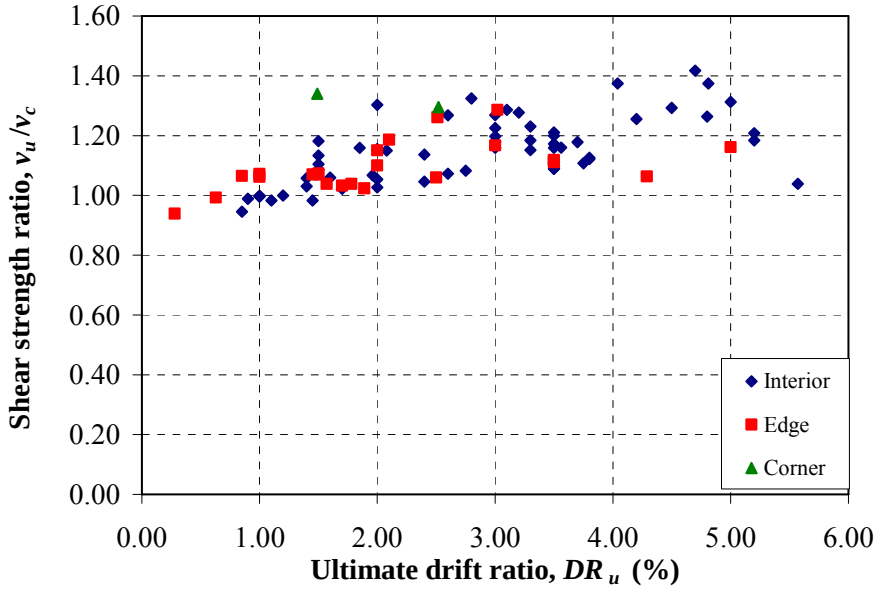

Figure 8.5 Shear strength ratio versus ultimate drift ratio for reinforced concrete slab-column connections

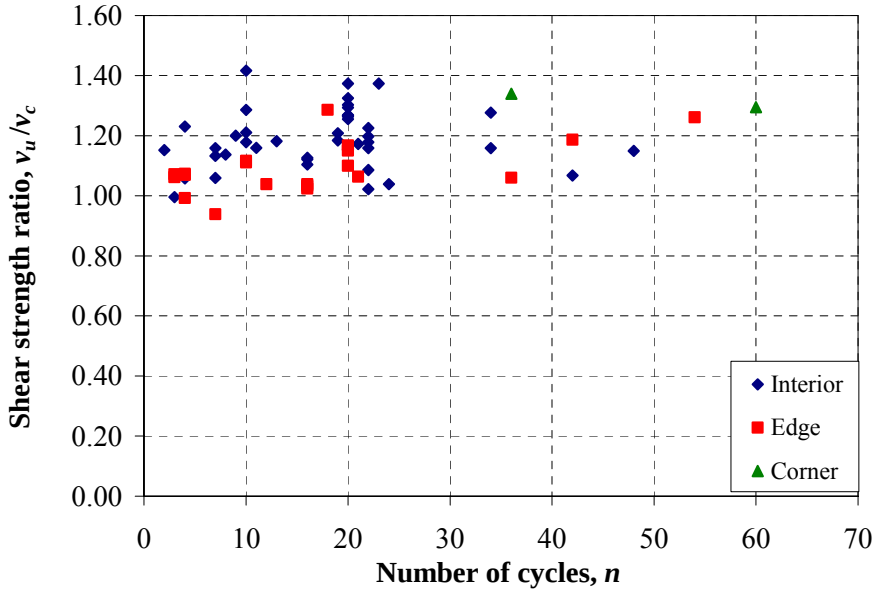

Figure 8.6 Shear strength ratio versus number of cycles for reinforced concrete slab-column connections

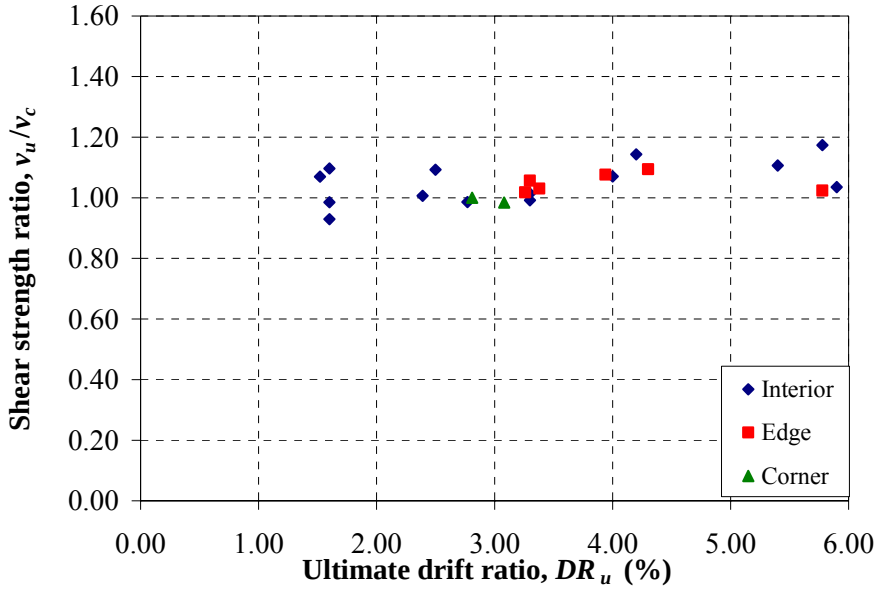

Figure 8.7 Shear strength ratio versus ultimate drift ratio for post-tensioned slab-column connections

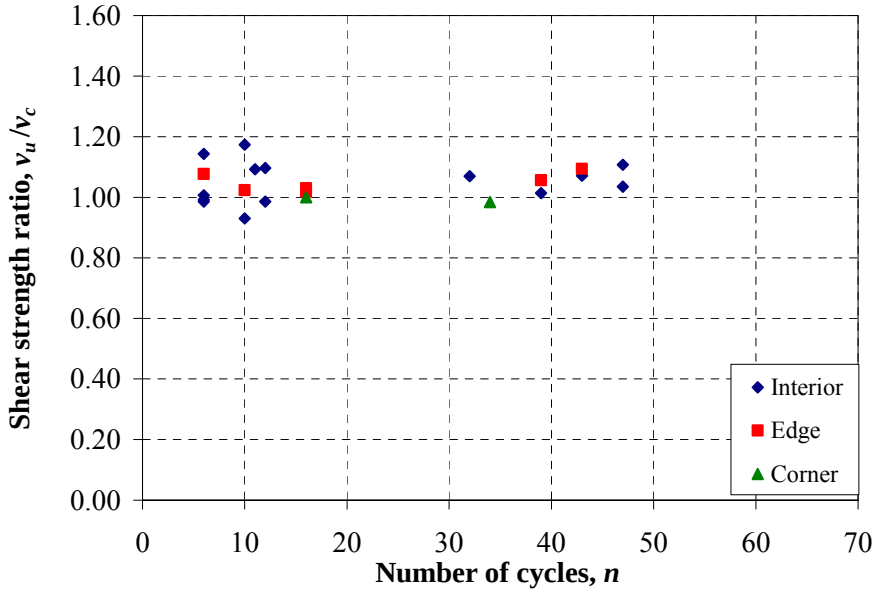

Figure 8.8 Shear strength ratio versus number of cycles for post-tensioned slab-column connections

8.5 Drift capacity versus gravity shear ratio

It is a common practice to limit the gravity shear ratio (V_u/V_c) for flat plate structures not designed as part of the seismic-force-resisting system. The limit on the gravity shear ratio is intended to provide a minimum ductility with the availability of approximately 1.5% drift capacity (ACI 352.1R-89). The validity of

ACI 318-11 requirement on gravity shear ratio is reviewed by plotting the ultimate drift capacities (DR_u) versus the gravity shear ratios (V_u/V_c) for the database collected previously.

Figure 8.9 and Figure 8.10 show the plots of ultimate drift capacities (DR_u) versus gravity shear ratios (V_u/V_c) for reinforced concrete and post-tensioned slab-column connections, respectively. The ultimate drift capacity DR_u is the measured story drift ratio at the peak unbalanced moment; whereas the gravity shear ratio V_u/V_c is the ratio of gravity shear V_u to shear capacity V_c. The shear capacity V_c is calculated using Eqs. (3.21) or (7.9), with the shear resistance v_c taken from Eqs. (3.1) to (3.4) and Eq. (7.1) for ACI 318-11 and the proposed method, respectively. For reinforced concrete slab-column connections (Figure 8.9), there is a clear trend of decreasing drift capacities as the gravity shear ratios increase. For post-tensioned slab-column connections (Figure 8.10), no obvious trend is observed.

The trend of decreasing drift capacities as the gravity shear ratio increases is in order with the ACI 318-11 requirement on gravity shear ratio. However, this requirement is not safe as several data (22 out of 88 and 1 out of 22 for reinforced concrete and post-tensioned slab-column connections, respectively) fall below the line of ACI requirement (Figure 8.9 and Figure 8.10). Thus, a modification on the gravity-shear-ratio requirement is required to make it more conservative. The present study and the past research (Tan and Teng 2005; Widjaja and Teng 2006; Anggadjaja and Teng 2008) indicated that for slab-column connections with rectangular columns, the gravity shear ratio should be kept below of about 0.3 to provide a minimum drift capacity of 1.5%. Accordingly, the limit of design story drift ratio is proposed to be

$$DR_u = \max\begin{cases} 0.005 \\ 0.03 - 0.05(V_u / V_c) \end{cases} \tag{8.1}$$

If the design story drift ratio exceeds the limit given above, then slab shear reinforcement shall be provided. This proposed recommendation leads to a more conservative result as shown in Figure 8.9 and Figure 8.10. Note that even though the trend of decreasing drift capacities against gravity shear ratios is not obvious for

post-tensioned slab-column connections, the proposed recommendation can still be applied. More data are certainly needed to support the current recommendation.

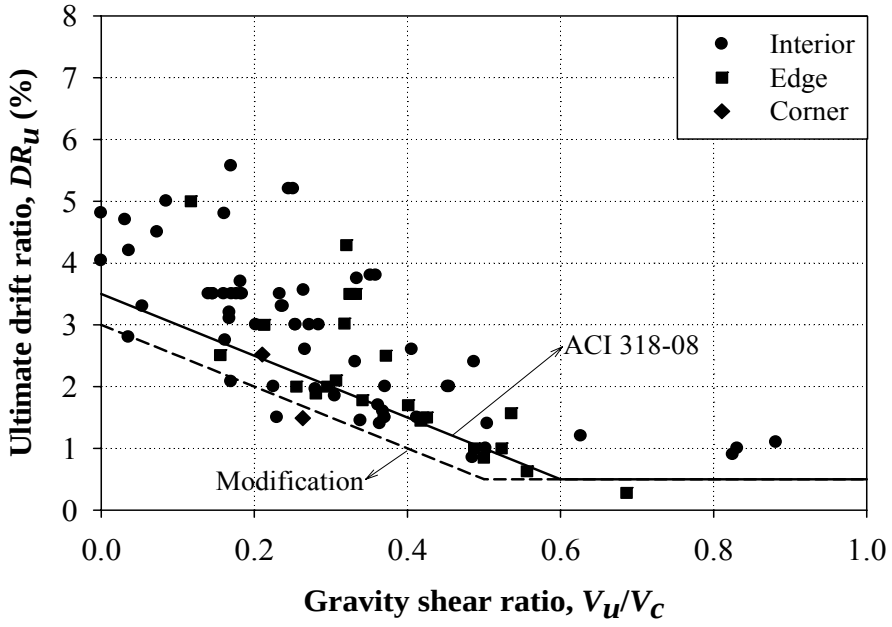

(a) ACI 318-11

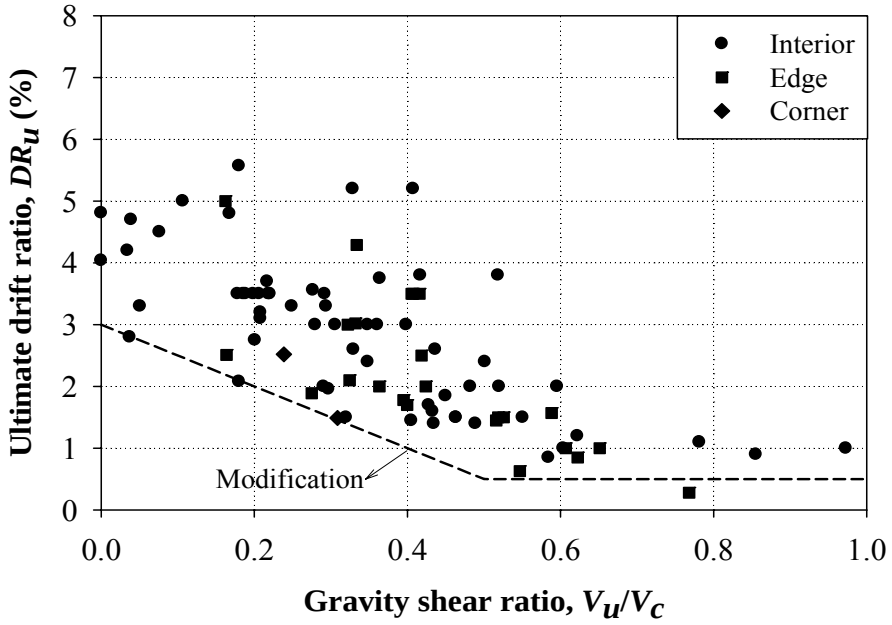

(b) Proposed

Figure 8.9 Drift capacity versus gravity shear ratio for reinforced concrete slab-column connections under cyclic loading

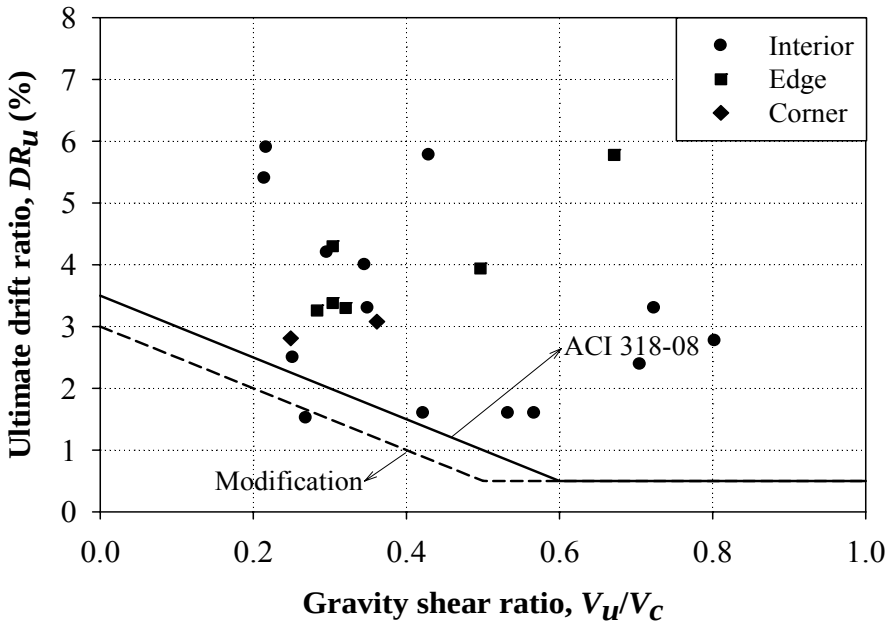

(a) ACI 318-11

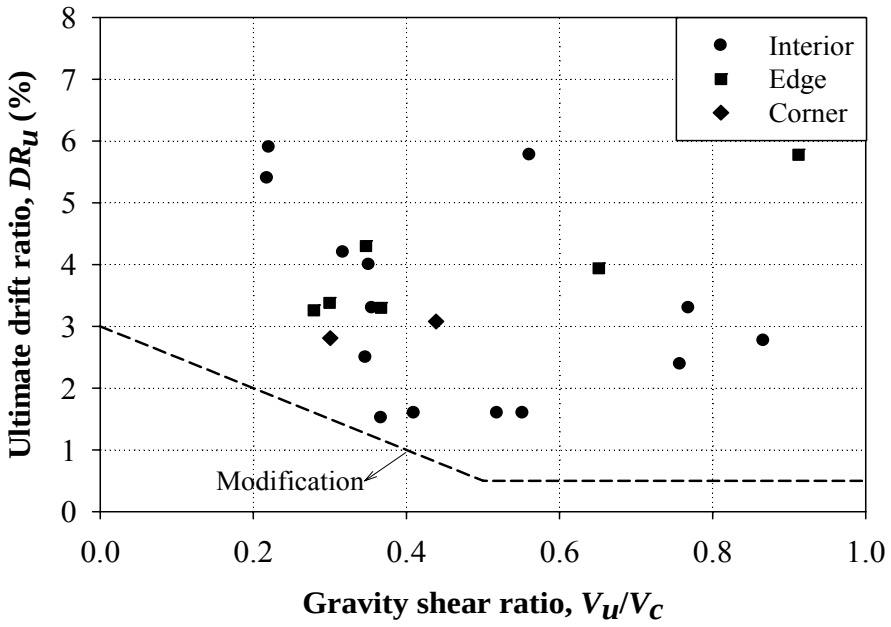

(b) Proposed

Figure 8.10 Drift capacity versus gravity shear ratio for post-tensioned slab-column connections under cyclic loading

8.6 Summary

- The method proposed previously for calculating the shear strength of slab-column connections under monotonic loading is also applicable for slab-column connections subjected to cyclic loading, while maintaining its accuracy and safety margin.
- The data shows that cyclic loading having ultimate drift ratio (DR_u) less than 6 % and number of cycles (n) less than 60 does not induce any strength degradation on slab-column connections. The effect of cyclic loading having DR_u greater than 6 % and n greater than 60 is not known.
- ACI 318-11 requirement on gravity shear ratio for members not designated as part of the seismic-force-resisting system can be unconservative. Accordingly, a modification on the gravity-shear-ratio requirement is proposed. The proposed modification leads to a more conservative result. This is one of the author' contributions.
- The proposed method is applicable to both reinforced concrete and post-tensioned slab-column connections subjected to combination of gravity and cyclic lateral loading. The procedure of designing slab-column connections by the proposed method can be summarized below:
  - Define the critical section at $d/2$ from the face of column in the shape of a closed rectangle.
  - Calculate the shear strength v_c using Eq. (7.1). For reinforced concrete slabs, the second term of Eq. (7.1) will theoretically be zero. Hence, Eq. (7.1) is transformed back to Eq. (6.2).
  - Calculate the shear capacity V_c using Eq. (7.9).
  - Calculate the flexural strength M_f using Eq. (7.10). The stress in prestressing steel at the flexural strength f_{ps} can be computed using Eq. (18-3) of ACI 318-11. For reinforced concrete slabs, the second term of Eq. (7.10) will theoretically be zero. Hence, Eq. (7.10) is transformed back to Eq. (6.9).
  - Calculate the ultimate shear stress v_u using Eq. (7.14).

- The design is satisfactory when the shear strength ϕv_c is greater than the ultimate shear stress v_u. For design purposes, the strength reduction factor ϕ can be taken equal to 0.75.
- For slab-column connections subjected to earthquake loading, the design story drift ratio DR_u shall not exceed the limit given in Eq. (8.1); otherwise, shear reinforcement is required. This requirement can be used as an alternative design to the strength requirement above.

CHAPTER 9
CONCLUSIONS AND RECOMMENDATIONS

9.1 Conclusions

Three interior post-tensioned slab-column connections having rectangular columns with column aspect ratio of five were tested. The first specimen was subjected to gravity load only. The second specimen was subjected to gravity and unidirectional cyclic lateral loading. The third specimen was subjected to gravity and bidirectional cyclic lateral loading. The conclusions related to this experimental study are listed below:

- The strength and stiffness of slab-column connections having rectangular columns with column aspect ratio of five are much higher along the strong column direction than those along the weak column direction.
- Cyclic lateral displacements cause deterioration of the connection stiffness, and the effect of bidirectional loading is more severe than unidirectional loading. It was shown that bidirectional cyclic lateral loading significantly reduces the unbalanced moment capacity, drift capacity, ductility, and stiffness of slab-column connections.
- The prestressing increases the shear strength of slab-column connections. The increase in shear strength due to prestressing for connections having rectangular columns tend to be lower compared with those having circular/square columns.
- ACI 318-11 equation on shear strength can be unconservative for post-tensioned connections having rectangular columns. Hence, a modification on the shear strength formula is proposed to make the strength prediction more conservative.
- The ACI 318-11 requirement on gravity shear ratio can be unsafe for post-tensioned slab-column connections having rectangular columns with column aspect ratio of five and subjected to bidirectional cyclic lateral loading.

The conclusions related to the analytical studies on shear strength of reinforced concrete slab-column connections are given below:

- The ACI 318-11 equations on shear strength of slabs [Eqs. (3.1) to (3.3)] do not consider the possible advantage of having higher percentage of slab flexural reinforcement. Teng et al. (2004) proposed a simple equation that takes into account the effects of slab flexural reinforcement, slab effective depth (size effect), and column rectangularity. The proposed single formula [Eq. (6.2)] has been shown to be more accurate than the ACI's three equations for v_c [Eqs. (3.1) to (3.3)]. It is also more accurate than the v_c equations from other codes (CEB-FIP Model Code 1990, British Standard 8110-97, and German Standard DIN 1045-1 (2000)).
- Experimental data indicates that the relationship between shear and unbalanced moment at interior connections and edge connections with moment transfer about axis perpendicular to the slab edge is close to linear, whereas the interaction at edge connections with moment transfer about an axis parallel to the slab edge and at corner connections are far from linear. Hence, a non-linear interaction that is applicable for all types of connections (interior, edge, and corner connections) is proposed. The proposed interaction [Eq. (6.8)] leads to a significant improvement over the performance of the current ACI formula.
- Based on the proposed interaction [Eq. (6.8)], a simple equation for calculating the ultimate shear stress at the critical section of slab-column connections under gravity and unbalanced moment transfer is derived [Eq. (6.11)]. The proposed method simplifies the design process and its accuracy and reliability has been checked against extensive experimental data.
- The performance of Eqs. (6.2), (6.8), and (6.11) have been shown to be very good against various experimental data, including interior, edge, and corner connections, ranging from symmetrical punching to connections having rectangular columns transferring unbalanced moments.

The conclusions related to the analytical studies on shear strength of post-tensioned slab-column connections are listed below:

- The shear strength formula proposed previously for reinforced concrete slab-column connections [Eq. (6.2)] is extended to calculate the shear strength of post-tensioned slab-column connections using the decompression approach [Eq. (7.1)].

- The proposed formula to estimate the shear strength of post-tensioned slabs [Eq. (7.1)] had been verified against 51 experimental data and compared with ACI 318-11 and Eurocode 2 equations. In terms of accuracy, the proposed formula [Eq. (7.1)] is better than ACI 318-11 and Eurocode 2 equations.
- The non-linear interaction equation of shear and unbalanced moment proposed previously for reinforced concrete slab-column connections [Eq. (6.8)] is used to derive a formula to calculate the ultimate shear stress of post-tensioned slab-column connections subjected to shear and moment transfer [Eq. (7.14)]. In the proposed formula [Eq. (7.14)], the moment transfer capacity is assumed to be carried by nonprestressed reinforcement and prestressing steel within the effective transfer width of c plus $1.5h$ on each side of the column.
- The proposed formula to calculate the ultimate shear stress due to shear and unbalanced moment transfer [Eq. (7.14)] was shown to be more accurate and conservative than the eccentric shear stress model of ACI 318-11 and Eurocode 2 method in predicting 25 experimental results.

The conclusions related to the analytical studies on slab-column connections under cyclic loading are given below:

- The method proposed previously for calculating the shear strength of slab-column connections under monotonic loading is also applicable for slab-column connections subjected to cyclic loading, while maintaining its accuracy and safety margin.
- The data shows that cyclic loading having ultimate drift ratio (DR_u) less than 6 % and number of cycles (n) less than 60 does not induce any strength degradation on slab-column connections. The effect of cyclic loading having DR_u greater than 6 % and n greater than 60 is not known.
- ACI 318-11 requirement on gravity shear ratio for members not designed as part of the seismic-force-resisting system can be unconservative. Accordingly, a modification on the gravity-shear-ratio requirement is proposed. The proposed modification leads to a more conservative result.

9.2 Recommendations

9.2.1 Further research

It was shown in Fig. 5.12 that the increase in shear strength due to prestressing for connections having rectangular columns tends to be lower than those having circular/square columns. This finding was based on one specimen having column aspect ratio of five (the author's specimen). Hence, more experimental data on post-tensioned slab-column connections with various column aspect ratios and prestressing force levels are needed to confirm this finding. In addition, shear strength of post-tensioned slab-column connections having rectangular columns may also be influenced by the tendon arrangements (uniform or banded). Thus, this variable is also recommended to investigate futher.

It is a common practice to limit the gravity shear ratio (V_u/V_c) for flat plate structures not designed as part of the seismic-force-resisting system. The limit on the gravity shear ratio is intended to provide a minimum ductility with the availability of approximately 1.5% drift capacity (ACI 352.1R-89). For reinforced concrete slab-column connections (Figure 8.9), there is a clear trend of decreasing drift capacities as the gravity shear ratios increase. For post-tensioned slab-column connections (Figure 8.10), no obvious trend is observed. Hence, more data on post-tensioned slab-column connections subjected to cyclic loading with various levels of gravity shear ratio are needed.

9.2.2 Changes for ACI 318-11

Based on the present study, the author would like to propose some changes for the code and commentary of ACI 318-11:

CODE	COMMENTARY
11.11.1.3 — For circular, square or rectangular columns, concentrated loads, or reaction areas, the critical sections with four straight sides shall be permitted.	
11.11.2.1 — For nonprestressed slabs and footings, V_c shall be $V_c = 0.55\rho^{1/3} f'_c{}^{1/3} k_d \beta^{-1/4} b_o d$ (SI) or	**R11.11.2.1** — Research (Teng et al. 2004; and present study) indicates that the shear strength of reinforced concrete slabs can be well predicted by Eq. (11-31). Mitchell et al. (2005) reviewed a series of tests by Elstner and Hognestad (1956), Ghannoum

$$V_c = 15\rho^{1/3} f'_c{}^{1/3} k_d \beta^{-1/4} b_o d \quad \text{(US)}$$

(11-31)

where ρ is the ratio of tension reinforcement within ***c*** plus **1.5*h*** on each side of the column (in percentage); f'_c is the compressive strength of concrete; β is the ratio of long side to short side of the column, concentrated load or reaction area; and k_d is the size effect factor defined in Eq. (11-32).

$$k_d = \left(1 + \frac{d}{1000}\right)^{-1/2} \quad \text{(SI)}$$

or

$$k_d = \left(1 + \frac{d}{40}\right)^{-1/2} \quad \text{(US)}$$

(11-32)

(1998), and McHarg et al. (2000) to investigate the influence of concrete strength on punching shear strength. Those series of tests used the concrete strength as the main variable. In general, the punching shear strength increases as the concrete strength increases. The increase in punching shear strength can be represented using the power of one-third or one-half. However, the cube root function is preferable for high strength concrete as it gives results that are more conservative.

Dilger et al. (2005) studied the series of tests by Richart (1948a, b) and showed that the influence of flexural reinforcement ratio on punching shear strength can be well described using both the power of one-fourth and one-third. Accordingly, Dilger et al. (2005) suggested using the power of one-third as it is also commonly used to reflect the effect of concrete strength. The power of one-third is also recommended by other researchers, such as Regan and Bræstrup (1985), Takahashi et al. (1992), Gardner (1996), Sherif and Dilger (2000b), Dilger (2000), and Teng et al. (2004).

The series of tests conducted by Nylander and Sundquist (1972), Regan (1986), Li (2000), and Birkle (2004) showed that the punching shear strength tends to decrease as the slab effective depth increases. This is known as the size effect. The size effect factor k_d is based on fracture mechanincs proposed by Bažant and Cao (1987). The coefficient 1000 or 40 are dependant on aggregate size. However, present study indicates that they can be conservatively simplified into Eq. (11-32).

If the column perimeter is held constant and the ratio of longer to shorter sides of the column is increased, the shear strength is decreased. This occurred due to the concentration of stress around the shorter side of the column. Teng et al. (2004) showed that this effect can be considered by introducing $\beta^{-1/4}$ into the shear strength formula.

For shapes other than rectangular, β is taken to be the ratio of the longest overall dimension of the effective loaded area to the largest overall perpendicular dimension of the effective loaded area, as illustrated for an L-shaped reaction area in Fig. R11.11.2. The effective loaded area is that area totally enclosing the actual loaded area, for which the perimeter is a minimum.

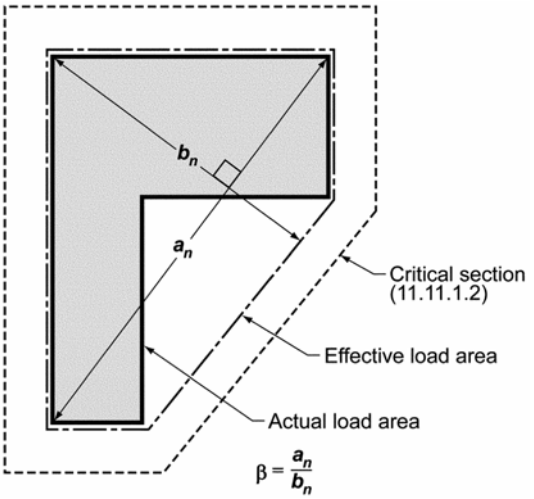

*Fig. R11.11.2—Value of **β** for a nonrectangular loaded area.*

11.11.2.2 — At columns of two-way prestressed slabs and footings that meet the requirements of 18.9.3

$$V_c = 0.55\rho^{1/3} f'_c{}^{1/3} k_d \beta^{-1/4} b_o d + V_d + V_p$$

(SI)

or

$$V_c = 15\rho^{1/3} f'_c{}^{1/3} k_d \beta^{-1/4} b_o d + V_d + V_p$$

(US)

(11.33)

where ρ is the ratio of tension reinforcement within ***c*** plus **1.5*h*** on each side of the column (in percentage); f'_c is the compressive strength of concrete; β is the ratio of long side to short side of the column, concentrated load or reaction area; k_d is the size effect factor defined in Eq. (11-32); V_p is the vertical component of prestress force crossing the critical section; and V_d is the decompression load given by Eq. (11-34).

$$V_d = \frac{f_{pc} h^2}{6}\left(\frac{V}{m}\right)\left[1 + \frac{6(d_p - h/2)}{h}\right] \quad (11\text{-}34)$$

where f_{pc} is the average compressive stress in concrete due to prestressing; ***h*** is the slab thickness; ***V/m*** is the ratio of shear force to moment per unit width (***V/m*** = 7.5 for interior connections, 4 for edge connections, and 2 for corner connections); and d_p is the average effective depth of prestressing steel at the column centerline.

R11.11.2.2 — Present study indicates that the shear strength of two-way prestressed slabs around interior columns is conservatively predicted by Eq. (11-33). V_c from Eq. (11-33) is extended from Eq. (11-31) by decompression method. The decompression approach assumes that after decompression stage, the behavior of prestressed slabs is similar to that of reinforced concrete slabs having the same amount of nonprestressed reinforcement. Studies by Foutch et al. (1990) and Silva et al. (2007) found that the limitations of concrete strength and compressive stress in the code are not necessary, as they do not improve the correlations with test results. When computing f_{pc}, loss of prestress due to restraint of the slab by shear walls and other structural elements should be taken into account.

In a prestressed slab with distributed tendons, the V_p term in Eq. (11-34) contributes only a small amount to the shear strength; therefore, it may be conservatively taken as zero. If V_p is to be included, the tendon profile assumed in the calculations should be noted.

For an exterior column support where the distance from the outside of the column to the edge of the slab is less than four times the slab thickness, the prestress is not fully effective around b_o, the total perimeter of the critical section. Shear strength in this case is therefore conservatively taken the same as for a nonprestressed slab.

The words “interior,” “edge,” and “corner columns” in 11.11.2.2 refer to critical sections with four, three, and two sides, respectively.

11.11.7.1 — Where gravity load, wind, earthquake, or other lateral forces cause transfer of unbalanced moment M_u between a slab and column, the shear stress resulting from moment transfer shall be computed using Eq. (11-37).

$$v_u = \frac{V_u}{b_o d} + \left(1 - \frac{V_u}{V_c}\right)\left(\frac{M_u}{M_f}\right)^{1/4} \frac{V_c}{b_o d} \quad \text{(11-37)}$$

where V_u and M_u are the ultimate shear force and unbalanced moment, respectively; V_c is the shear capacity of slab-column connections under symmetrical punching given by Eqs. (11-31) and (11-33); and M_f is the flexural strength within the effective transfer width of ***c*** plus **1.5*h*** on each side of the column.

R11.11.7.1 — Experimental data (Hanson and Hanson 1968; Zaghlool 1971, Zaghlool and Rawdown de Paiva 1973; Stamenković and Chapman 1974) indicates that the relationship between shear and unbalanced moment at interior connections and edge connections with moment transfer about axis perpendicular to the slab edge is close to linear, whereas the interaction at edge connections with moment transfer about an axis parallel to the slab edge and at corner connections are far from linear. Present study found that a non-linear interaction that is applicable for all types of connections (interior, edge, and corner connections) can be represented by the following relationship:

$$\frac{V_u}{V_c} + \left(1 - \frac{V_u}{V_c}\right)\left(\frac{M_u}{M_f}\right)^{1/4} = 1$$

The unbalanced moment-and-shear interaction equation above can also be written in a form of an equation to calculate the ultimate shear stress at the slab critical section. The equation to calculate the ultimate shear stress shown in Eq. (11-37) is a general equation applicable for interior, edge and corner slab-column connections. For interior connections and edge connections with unbalanced moments about an axis perpendicular to the slab edge, the flexural strength M_f is provided by two faces. On one face, the flexural strength is contributed by the top reinforcement, and on the other face, the flexural strength is contributed by the bottom reinforcement. For edge connections with unbalanced moments about an axis parallel to the slab edge and corner connections, the flexural strength M_f is provided by single face only.

For connections with bidirectional moment transfer, a fully plastic behavior of the connection is assumed to occur. Thus, Eq. (11-37) should be applied independently for the shear and unbalanced moment about each principal axis of the column, and the worst case controls the design.

Present study also indicates that the moment transfer strength of a prestressed slab-to-column connection can be calculated using the procedures of 11.11.7.1. For prestressed slabs, the flexural strength M_f is assumed to be carried by nonprestressed reinforcement and prestressing steel within the effective transfer width of ***c*** plus ***1.5h*** on each side of the column.

13.5.3 — (removed)

R13.5.3 — (removed)

21.13.6 — For slab-column connections of two-way slabs without beams, slab shear reinforcement satisfying the requirements of 11.11.3 and 11.11.5 and providing V_s not less than **3.5** $b_o d$ shall extend at least four times the slab thickness from the face of the support, unless either (a) or (b) is satisfied:

(a) The requirements of 11.11.7 using the design shear V_{ug} and the induced moment transferred between the slab and column under the design displacement;

(b) The design story drift ratio does not exceed the larger of 0.005 and **[0.03 – 0.05(**$V_{ug}/\phi V_c$**)]**.

Design story drift ratio shall be taken as the larger of the design story drift ratios of the adjacent stories above and below the slab-column connection. V_c is defined in 11.11.2. V_{ug} is the factored shear force on the slab critical section for two-way action, calculated for the load combination **1.2***D* **+ 1.0***L* **+ 0.2***S*.

The load factor on the live load, ***L***, shall be permitted to be reduced to 0.5 except for garages, areas occupied as places of public assembly, and all areas where ***L*** is greater than 4.8 kN/m^2 (100 lb/ft^2).

R21.13.6 — Provisions for shear reinforcement at slabcolumn connections were added in 2005 to reduce the likelihood of slab punching shear failure. The shear reinforcement is required unless either 21.13.6(a) or (b) is satisfied.

Section 21.13.6(a) requires calculation of shear stress due to the factored shear force and induced moment according to 11.11.7.1. The induced moment is the moment that is calculated to occur at the slab-column connection when subjected to the design displacement. Section 13.5.1.2 and the accompanying Commentary provide guidance on selection of the stiffness of the slab-column connection for the purpose of this calculation.

Section 21.13.6(b) does not require the calculation of induced moments, and is based on research (Megally and Ghali 2002; Moehle 1996; and present study) that identifies the likelihood of punching shear failure considering the story drift ratio and shear due to gravity loads. Figure R21.13.6 illustrates the requirement. The requirement can be satisfied by adding slab shear reinforcement, increasing slab thickness, changing the design to reduce the design story drift ratio, or a combination of these.

If column capitals, drop panels, shear caps, or other changes in slab thickness are used, the requirements of 21.13.6 are evaluated at all potential critical sections, as required by 11.11.1.2.

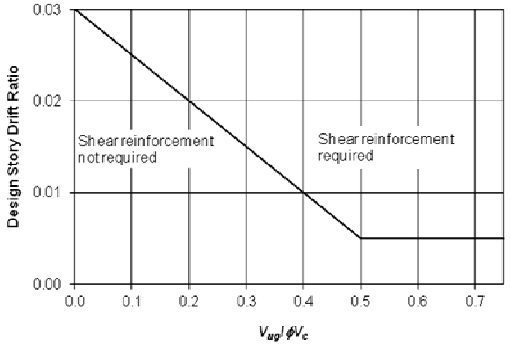

Fig. R21.13.6—Illustration of the criterion of 21.13.6(b).

REFERENCES

ACI Committee 318, 2011, "Building Code Requirements for Structural Concrete (ACI 318-11) and Commentary," American Concrete Institute, Farmington Hills, MI., 503 pp.

ACI Committee 423, 1996, "Recommendations for Concrete Members Prestressed with Unbonded Tendons (ACI 423.3R-96)," American Concrete Institute, Farmington Hills, MI, 19 pp.

Alexander, S. D. B., and Simmonds, S. H., 1987, "Ultimate Strength of Slab-Column Connections," *ACI Structural Journal*, V. 84, No. 3, May-June, pp. 255-261.

Alexander, S. D. B., and Simmonds, S. H., 1992a, "Bond Model for Concentric Punching Shear," *ACI Structural Journal*, V. 89, No. 3, May-June, pp. 325-334.

Alexander, S. D. B., and Simmonds, S. H., 1992b, "Test of Column-Flat Plate Connections," *ACI Structural Journal*, V. 89, No. 5, Sept.-Oct., pp. 495-502.

American Society of Civil Engineers (ASCE), 2000, "Prestandard and Commentary for the Seismic Rehabilitation of Buildings (FEMA Publication 356)," Federal Emergency Management Agency, Washington, D.C., 528 pp.

Andrä, H. -P., 1982, "Zum Tragverhalten des Auflagerbereichs von Flachdecken," Dissertation, Universität Stuttgart, Germany.

Anggadjaja, E, and Teng, S., 2008, "Edge-Column Slab Connections under Gravity and Lateral Loading," *ACI Structural Journal*, V. 105, No. 5, Sept.-Oct., pp. 541-551.

AS, 2001, "Concrete Structures (AS 3600-2001)," Standards Australia International, Sydney, New South Wales, 176 pp.

Bažant, Z. P., and Cao, Z., 1987, "Size Effect in Punching Shear Failure of Slabs," *ACI Structural Journal*, V. 84, No. 1, Jan.-Feb., pp. 44-53.

Bernaert, M., and Puech, M., 1966, "Compte Rendu des Travaux du Groupe de Travail Poinçonnement," *CEB-Bull. d'Information* No. 57, Comité Européen du Béton (Hrsg.), Dalles, Structures Planes, Paris, France.

Birkle, G., 2004, "Punching of Flat Slabs: Influence of Slab Thickness and Stud Layout," PhD thesis, University of Calgary, Calgary, Alberta, Canada, 152 pp.

Birkle, G., and Dilger, W. H., 2008, "Influence of Slab Thickness on Punching Shear Strength," *ACI Structural Journal*, V. 105, No. 2, Mar.-Apr., pp. 180-188.

Biskinis, D. E.; Roupakias, G. K.; and Fardis, M. N., "Degradation of Shear Strength of Reinforced Concrete Members with Inelastic Cyclic Displacements," *ACI Structural Journal*, V. 101, No. 6, Nov.-Dec. 2004, pp. 773-783.

Bortolotti, L., "Punching Shear Strength in Concrete Slabs," *ACI Structural Journal*, V. 84, No. 2, Mar.-Apr. 1990, pp. 208-219.

Bræstrup, M. W.; Nielsen, M. P.; Jensen, B. C.; and Bach, F., "Axisymmetric Punching of Plain and Reinforced Concrete," *Report* R75, Structural Research Laboratory, Technical University of Denmark, Copenhagen, Denmark, 1976.

Broms, C. E., 1990, "Punching of Flat Plates – A Question of Concrete Properties in Biaxial Compression and Size Effect," *ACI Structural Journal*, V. 87, No. 3, May-June, pp. 292-304.

Broms, C. E., 2000, "Elimination of Flat Plate Punching Failure Mode," *ACI Structural Journal*, V. 97, No. 1, Jan.-Feb., pp. 94-101.

BSI, 1997, "Structural Use of Concrete (BS 8110-1:1997)," British Standards Institution, London, UK, 168 pp.

BSI, 2004, "Eurocode 2: Design of Concrete Structures (BS EN 1992-1-1:2004)," British Standards Institution, London, UK, 230 pp.

BSI, 2004, "Eurocode 8: Design of Structures for Earthquake Resistance (BS EN 1998-1:2004)," British Standards Institution, London, UK, 232 pp.

Burns, N. H., and Hemakom, R., 1977, "Test of Scale Model Post-Tensioned Flat Plate, *Journal of the Structural Division*, ASCE, V. 103, No. ST6, June, pp. 1237-1255.

Burns, N. H., and Hemakom, R., 1985, "Test of Post-Tensioned Flat Plate with Banded Tendons, *Journal of the Structural Division*, ASCE, V. 111, No. 9, Sept., pp. 1899-1915.

CEB-FIP, 1990, "CEB-FIP Model Code 1990: Design Code," Comite Euro-International du Beton and Federation International de la Precontrainte, Paris, France, 437 pp.

Chana, P. S., and Desai, S. B., 1992a, "Design of Shear Reinforcement Against Punching," *The Structural Engineer*, V. 70, No. 9, May, pp. 159-164.

Chana, P. S., and Desai, S. B., 1992b, "Membrane Action, and Design Against Punching Shear," *The Structural Engineer*, V. 70, No. 19, Oct., pp. 339-343.

Clyde, D. H., and Carmichael, D., 1974, "Lower Bound Flexural Fields and Slab Shear, *Shear in Reinforced Concrete*, V. 2, SP-42, American Concrete Institute, Farmington Hills, MI, pp. 769-784.

Corley, W. G., and Hawkins, N. M., 1968, "Shearhead Reinforcement for Slabs," ACI Journal, *Proceedings* V. 65, No. 10, Oct., pp. 811-824.

Corrêa, G. S., 2001, "Puncionamento em Lajes Cogumelo Protendidas com Cabos Não Aderentes," MSc dissertation, Department of Civil and Environmental Engineering, University of Brasília, Brasília, Brasil, 153 pp.

Criswell, M. E., 1970, "Strength and Behavior of Reinforced Concrete Slab-Column Connections Subjected to Static and Dynamic Loadings," *Technical Report* No. N-70-1, U. S. Army Engineer Waterways Experiment Station, Vicksburg, Dec., 170 pp.

Criswell, M. E., 1974, "Static and Dynamic Response of Reinforced Concrete Slab-Column Connections," *Shear in Reinforced Concrete*, V. 2, SP-42, American Concrete Institute, Detroit, pp. 721-746.

CSA, 2004, "Design of Concrete Structures (CSA-A23.3-04)," Canadian Standards Association, Mississauga, Ontario, Canada, 214 pp.

Desayi, P., and Seshadri, H. K., 1997, "Punching Shear Strength of Flat Slab Corner Column Connections. Part 1. Reinforced Concrete Connections," *Proceedings of the Institution of Civil Engineers*, Structures and Buildings, V. 122, No. 1, Feb., pp. 10-20.

Di Stasio, J., Sr., and Van Buren, M. P., 1960, "Transfer of Bending Moment Between Flat Plate Floor and Column," ACI Journal, *Proceedings* V. 57, No. 9, Sept., pp. 299-314.

Dilger, W. H., 2000, "Flat Slab-Column Connections," *Progress in Structural Engineering and Materials*, V. 2, No. 3, July-Sept., pp. 386-399.

Dilger, W. H., and Brown, S. J., 1994, "Earthquake Resistance of Slab Column Connections," Proceedings of Canadian Society of Civil Engineering, V. 2, Winnipeg, Canada.

Dilger, W. H., and Shatila, M., 1989, "Shear Strength of Prestressed Concrete Edge Slab-Column Connections with and without Shear Stud Reinforcement," *Canadian Journal of Civil Engineering*, V. 16, No. 6, Dec., pp. 807-819.

Dilger, W., and Cao, H., 1991, "Behaviour of Slab-Column Connections under Reversed Cyclic Loading," Proceedings, 2nd International Conference of High Rise Buildings, China.

Dilger, W.; Birkle, G.; and Mitchell, D., 2005, "Effect of Flexural Reinforcement on Punching Shear Resistance," *Punching Shear in Reinforced Concrete Slabs*, SP-232, M. A. Polak, ed., American Concrete Institute, Farmington Hills, MI, pp. 57-73.

Durrani, A. J.; Du, Y.; and Luo, Y. H., 1995, "Seismic Resistance of Nonductile Slab-Column Connections in Existing Flat-Slab Buildings," *ACI Structural Journal*, V. 92, No. 4, July-Aug., pp. 479-487.

Elgabry, A. A., and Ghali, A., 1987, "Tests on Concrete Slab-Column Connections with Stud-Shear Reinforcement Subjected to Shear-Moment Transfer," *ACI Structural Journal*, V. 84, No.5, Sept.-Oct., pp. 433-442.

El-Salakawy, E. F.; Polak, M. A.; and Soliman, M. H., 1999, "Reinforced Concrete Slab-Column Edge Connections with Openings," *ACI Structural Journal*, V. 96, No. 1, Jan.-Feb., pp. 79-87.

Elstner, R. C., and Hognestad, E., 1956, "Shearing Strength of Reinforced Concrete Slabs," ACI Journal, *Proceedings* V. 53, No. 1, July, pp. 29-58.

Emam, M.; Marzouk, H.; and Hilal, M. S., 1997, "Seismic Response of Slab-Column Connections Constructed with High-Strength Concrete," *ACI Structural Journal*, V. 94, No. 2, Mar.-Apr., pp. 197-205.

Falamaki, M., and Loo, Y.-C., 1992, "Punching Shear Tests of Half-Scale Reinforced Concrete Flat-Plate Models with Spandrel Beams," *ACI Structural Journal*, V. 89, No. 3, May-June, pp. 263-271.

Farhey, D. N.; Adin, M. A.; and Yankelevsky, D. Z., 1993, "RC Flat Slab-Column Subassemblages under Lateral Loading," *Journal of Structural Engineering*, ASCE, V. 119, No. 6, June, pp. 1903-1916.

fib Task Group 4.3, 2001, "Punching of Structural Concrete Slabs," *Bulletin* 12, International Federation for Structural Concrete, Lausanne, Switzerland, 307 pp.

Foutch, D. A.; Gamble, W. L.; and Sunidja, H., 1990, "Tests of Post-Tensioned Concrete Slab-Edge Column Connections," *ACI Structural Journal*, V. 87, No. 2, Mar.-Apr., pp. 167-179.

Franklin, S. O., and Long, A. E., 1982, "The Punching Behaviour of Unbonded Post-Tensioned Flat Plates," *Proceedings of the Institution of Civil Engineers*, Part 2, V. 73, No. 3, Sept., pp. 609-631.

Franklin, S. O.; Cleland, D. F.; and Long, A. E., 1982, "A Flexural Method for the Prediction of the Punching Capacity of Unbonded Post-Tensioned Flat Slabs at Internal Columns," *Proceedings of the Institution of Civil Engineers*, Part 2, V. 73, No. 2, June, pp. 277-298.

Gardner, N. J., 1995, "Discussion on Punching Shear Provisions for Reinforced and Prestressed Concrete Flat Slabs," Proceedings of the Canadian Society for Civil Engineering Annual Conference, Ottawa, Ontario, Canada, June, pp. 247-256.

Gardner, N. J., 1996, "Punching Shear Provisions for Reinforced and Prestressed Concrete Flat Slabs," *Canadian Journal of Civil Engineering*, V. 23, pp. 502-510.

Gardner, N. J., and Kallage, M. R., 1998, "Punching Shear Strength of Continuous Post-Tensioned Concrete Flat Plates," *ACI Materials Journal*, V. 95, No. 3, May-June, pp. 272-283.

Gardner, N. J., and Shao, X.-Y., 1996, "Punching Shear of Continuous Flat Reinforced Concrete Slabs," *ACI Structural Journal*, V. 93, No. 2, Mar.-Apr., pp. 218-228.

Gayed, R. B., and Ghali, A., 2006, "Seismic-Resistant Joints of Interior Columns with Prestressed Slabs," *ACI Structural Journal*, V. 103, No. 5, Sept.-Oct., pp. 710-719.

Georgopoulos, T., 1988, "Einfaches Verfahren zur Bemessung des Stützbereichs punktförmig gestützter Stahlbetonplatten," *BuStb*, Vol. 83, No. H7, pp. 190-192.

Georgopoulos, T., 1989, "Durchstanzlast und Durchstanzwinkel punktförmig gestützter Stahlbetonplatten ohne Schubbewehrung and ohne Schubbewehrung," *Bauingenieur*, Vol. 64, pp. 187-191.

Gerber, L. L., and Burns, N. H., 1971, "Ultimate Strength Tests of Post-Tensioned Flat Plates," *PCI Journal*, V. 16, No. 6, Nov.-Dec., pp. 40-58.

Gesund, H., 1981, "Limit Design of Slabs for Concentrated Loads, *Journal of the Structural Division*, ASCE, V. 107, No. ST9, Sept., pp. 1839-1856.

Gesund, H., and Dikshit, O. P., 1971, "Yield Line Analysis of the Punching Problem at Slab/Column Intersections, *Cracking, Deflection, and Ultimate Load of Concrete Slab Systems*, SP-30, American Concrete Institute, Farmington Hills, MI, pp. 177-201.

Gesund, H., and Goli, H. B., 1979, "Limit Analysis of Flat-Slab Buildings for Lateral Loads," Journal of the Structural Division, ASCE, V. 105, No. ST11, Nov., pp. 2187-2202.

Gesund, H., and Goli, H. B., 1980, "Local Flexural Strength of Slabs at Interior Columns, *Journal of the Structural Division*, ASCE, V. 106, No. ST5, May, pp. 1063-1078.

Gesund, H., and Kaushik, Y. P., 1970, "Yield Line Analysis of Punching Failures in Slabs," *IABSE Proceedings*, V. 30, No. 1, pp. 41-60.

Ghali, A., and Megally, S., 1999, "Design for Punching Shear Strength with ACI 318-95," *ACI Structural Journal*, V. 96, No. 4, July-Aug., pp. 539-549.

Ghali, A.; Elmasri, M. Z.; and Dilger, W., 1976, "Punching of Flat Plates under Static and Dynamic Horizontal Forces," ACI Journal, *Proceedings* V. 73, No. 10, Oct., pp. 566-572.

Ghannoum, C. M., 1988, "Effect of High-Strength Concrete on the Performance of Slab-Column Specimens," MEng thesis, Department of Civil Engineering and Applied Mechanics, McGill University, Montreal, Québec, Canada, 91 pp.

Gilbert, S. G., and Glass, C., 1987, "Punching Failure of Reinforced Concrete Flat Slabs at Edge Columns," *The Structural Engineer*, V. 65B, No. 1, Mar., pp. 16-21.

Guandalini, S.; Burdet, O. L.; and Muttoni, A., 2009, "Punching Tests of Slabs with Low Reinforcement Ratios," *ACI Structural Journal*, V. 16, No. 1, Jan.-Feb., pp. 87-95.

Hall, A. S., and Rangan, B. V., 1983, "Forces in the Vicinity of Edge Columns in Flat-Slab Floors," *Magazine of Concrete Research*, V. 35, No. 122, Mar., pp. 19-26.

Hallgren, M., 1996, "Punching Shear Capacity of Reinforced High Strength Concrete Slabs," Doctoral thesis, Department of Structural Engineering, Royal Institute of Technology, Stockholm, Sweden, 206 pp.

Hammill, N., and Ghali, A., 1994, "Punching Shear Resistance of Corner Slab-Column Connections," *ACI Structural Journal*, V. 91, No. 6, Nov.-Dec., pp. 697-707.

Han, S. W.; Kee, S. H.; Kang, T. H. K.; Ha, S. S.; Wallace, J. W.; and Lee, L. H., 2006a, "Cyclic Behaviour of Interior Post-Tensioned Flat Plate Connections," *Magazine of Concrete Research*, V. 58, No. 10, Dec., pp. 699-711.

Han, S. W.; Kee, S.-H.; Park, Y.-M.; Lee, L.-H.; and Kang, T. H.-K, 2006b, "Hysteretic Behavior of Exterior Post-Tensioned Flat Plate Connections," *Engineering Structures*, V. 28, No. 4, Dec., pp. 1983-1996.

Hanson, N. W., and Hanson, J. M., 1968, "Shear and Moment Transfer between Concrete Slabs and Columns," *Journal of the Portland Cement Association*, Research and Development Laboratories, V. 10, No. 1, Jan., pp. 2-16.

Hassanzadeh, G., 1998, "Betongplattor pa Pelare, Dimensionerings Metoder för Plattor Med Icke Vidhäftande Spännarmering," *TRITA-BKN Bulletin* 43, Institutionen för Byggkonstruktion, Kungl-Tekniska Högskolan, Stockholm, Sweden, pp. 110-130.

Hawkins, N. M., and Corley, W. G., 1971, "Transfer of Unbalanced Moment and Shear from Flat Plates to Columns," *Cracking, Deflection, and Ultimate Load of Concrete Slab Systems*, SP-30, American Concrete Institute, Farmington Hills, MI, pp. 147-176.

Hawkins, N. M.; Bao, A.; and Yamazaki, J., 1989, "Moment Transfer from Concrete Slabs to Columns," *ACI Structural Journal*, V. 86, No. 6, Nov.-Dec., pp. 705-716.

Hawkins, N. M.; Criswell, M. E.; and Roll, F., 1974a, "Shear Strength of Slabs without Shear Reinforcement," *Shear in Reinforced Concrete*, V. 2, SP-42, American Concrete Institute, Farmington Hills, MI, pp. 677-720.

Hawkins, N. M.; Fallsen, H. B.; and Hinojosa, R. C., 1971, "Influence of Column Rectangularity on the Behaviour of Flat Plate Structures," *Cracking, Deflection, and Ultimate Load of Concrete Slab Systems*, SP-30, American Concrete Institute, Farmington Hills, MI, pp. 127-146.

Hawkins, N. M.; Mitchell, D.; and Sheu, M. S., 1974b, "Cyclic Behavior of Six Reinforced Concrete Slab-Column Specimens Transferring Moment and

Shear," *Progress Report 1973-74* on NSF Project GI-38717, Department of Civil Engineering, University of Washington, Seattle, WA.

Hawkins, N. M.; Wong, C. F.; and Yang, C. H., 1978, "Slab-Edge Column Connections Transferring High Intensity Reversing Moments Normal to the Edge of the Slab," *Structures and Mechanics Report* No. SM78-1, Department of Civil Engineering, University of Washington, Seattle, WA, May.

Herzog, M., 1970, "A New Evaluation of Earlier Punching Shear Tests," *Concrete* (London), V. 4, No. 12, Dec., pp. 448-450.

Hueste, M. D.; Browning, J.; Lepage, A.; and Wallace, J. W., 2007, "Seismic Design Criteria for Slab-Column Connections," *ACI Structural Journal*, V. 104, No. 4, July-Aug., pp. 448-458.

Ingvarsson, H., 1974, "Experimentellt Studium av Betongplattor Understödda av Hörnpelare, (Experimental Study of Concrete Slabs Supported by Corner Columns)" *Meddelande* Nr.111, Institutionen för Byggnadsstatik, Kungliga Tekniska Högskolon, Stockholm, Sweden.

Islam, S., and Park, R., 1976, "Test on Slab-Column Connections with Shear and Unbalanced Flexure," *Journal of the Structural Division*, ASCE, V. 102, No. ST3, Mar., pp. 549-568.

Joint ACI-ASCE Committee 352, 1997, "Recommendations for Design of Slab-Column Connections in Monolithic Reinforced Concrete Structures (ACI 352.1R-89) (Reapproved 1997)," American Concrete Institute, Farmington Hills, MI, 22 pp.

Joint ACI-ASCE Committee 421, 2008, "Guide to Shear Reinforcement for Slabs (ACI 421.1R-08)," American Concrete Institute, Farmington Hills, MI, 23 pp.

Kane, K. A., 1978, "Some Model Tests on the Punching Action of Reinforced Concrete Slabs at Edge Columns," Honours Project, Queen's University Belfast, Northern Ireland.

Kang, T. H.-K., and Wallace, J. W., 2008, "Seismic Performance of Reinforced Concrete Slab-Column Connections with Thin Plate Stirrups," *ACI Structural Journal*, V. 105, No. 5, Sept.-Oct., pp. 617-625.

Kanoh, Y., and Yoshizaki, S., 1975, "Experiments on Slab-Column and Slab-Wall Connections of Flat Plate Structures," *Concrete Journal* (Tokyo), V. 13, June, pp. 7-19.

Khan, S., and Williams, M., 1995, "Post-Tensioned Concrete Floors," Butterworth-Heinemann Ltd, Oxford, 312 pp.

Khwaounjoo, Y. R., 2001, "Behaviour of Prestressed Concrete Slab-Column Connections," PhD thesis, School of Civil and Environmental Engineering, University of New South Wales, Sydney, Australia, Feb., 488 pp.

Kinnunen, S., and Nylander, H., 1960, "Punching of Concrete Slabs without Shear Reinforcement," *Transaction* No. 158, Royal Institute of Technology, Stockholm, Sweden, 112 pp.

Kordina, K., and Nölting, D., 1984, "Versuche zum Durchstanzen ohne Verbund Vorgespannter Flachdecken," Lehrstuhl für Massivbau, Technische Universität, Braunschweig, Germany, 59 pp.

Kordina, K., and Nölting, D., 1986, "Tragfähigkeit durchstanzgefährdeter stahlbetonplatten," Deutscher Ausschuss für Stahlbeton, Berlin, Germany, 60 pp.

Kosut, G. M.; Burns, N. H.; and Winter, C. V., 1985, "Test of Four-Panel Post-Tensioned Flat Plate," *Journal of the Structural Division*, ASCE, V. 111, No. 9, Sept., pp. 1916-1929.

Ladner, M., 1973, "Einfluß der Maßstabgröße bei Durchstanzversuchen – Ableitung eines begründeten Übertragunggesetzes," Material und Technik, pp. 60-68.

Ladner, M.; Schaeidt, W.; and Gut, S., 1977 "Experimentelle Untersuchungen an Stahlbeton-Flachdecken," Eidgenössische Materialprüfungs- und Versuchsanstalt, *Bericht* Nr. 205, Dübendorf, Switzerland.

Lee, J.-H.; Yoon, Y.-S.; Lee, S.-H.; Cook, W. D.; and Mitchell, D., 2008, "Enhancing Performance of Slab-Column Connections," *Journal of Structural Engineering*, ASCE, V. 134, No. 3, Mar., pp. 448-457.

Lee, S. C., 2004, "Shear Strength of Reinforced Concrete Slabs under Symmetric Punching," PhD thesis, School of Civil and Environmental Engineering, Nanyang Technological University, Singapore, 202 pp.

Lee, Y. M., Mitchell, D., and Harris, P. J., 1979, "Lessons from Structural Performance – Slabs Containing Improperly Placed Reinforcing," *Concrete International*, Design and Construction, American Concrete Institute, V. 1, No. 6, June, pp. 45-53.

Li, K. K. L., 2000, "Influence of Size on Punching Shear Strength of Concrete Slabs," MEng thesis, Department of Civil Engineering and Applied Mechanics, McGill University, Montreal, Québec, Canada, 78 pp.

Lim, F. K., and Rangan, B. V., 1995, "Studies on Concrete Slabs with Stud Shear Reinforcement in Vicinity of Edge and Corner Columns," *ACI Structural Journal*, V. 92, No. 5, Sept.-Oct., pp. 515-525.

Long, A. E., 1975, "A Two-Phase Approach to the Prediction of Punching Strength," ACI Journal, *Proceedings* V. 72, No. 2, Feb., pp. 37-45.

Long, A. E., and Bond, D., 1967, "Punching Failure of Reinforced Concrete Slabs," *Proceedings of the Institution of Civil Engineers*, V. 37, No. 1, May, pp. 109-135.

Long, A. E., and Cleland, D. J., 1993, "Post-Tensioned Concrete Flat Slabs at Edge Columns," *ACI Materials Journal*, V. 90, No. 3, May-June, pp. 207- 213.

Lovrovich, J. S., and McLean, D. I., 1990, "Punching Shear Behavior of Slabs with Varying Span-Depth Ratios," *ACI Structural Journal*, V. 87, No. 5, Sept.-Oct., pp. 507-511.

Luo, Y. H., and Durrani, A. J., 1995a, "Equivalent Beam Model for Flat-Slab Buildings–Part I: Interior Connections," *ACI Structural Journal*, V. 92, No. 1, Jan.-Feb., pp. 115-124.

Luo, Y. H., and Durrani, A. J., 1995b, "Equivalent Beam Model for Flat-Slab Buildings–Part II: Exterior Connections," *ACI Structural Journal*, V. 92, No. 2, Mar.-Apr., pp. 250-257.

Manterola, M., 1966, "Poinçonnement de Dalles Sans Armature d'effort Trenchant," *CEB-Bull. d'Information* No. 58, Comité Européen du Béton (Hrsg.), Dalles, Structures Planes, Paris, France.

Marti, P., and Thürlimann, B., 1977, "Fliessbedingung für Stahlbeton mit Berücksichtigung der Betonzugfestigkeit," *BuStb* 72, H. 1, pp. 7-12.

Marti, P.; Pralong, J.; and Thürlimann, B., 1977, "Schubversuche an Stahlbeton-Platten," *IBKonstruktion Bericht* Nr. 7305-2, ETH Zürich, Birkhäuser, Basel, Switzerland.

Martinez-Cruzado, J. A.; Qaisrani, A. N.; and Moehle, J. P., 1994, "Post-Tensioned Flat Plate Slab-Column Connections Subjected to Earthquake Loading," *Proceedings of 5th National Conference on Earthquake Engineering*, EERI, Chicago, IL, 10-14 July.

Marzouk, H., and Hussein, A., 1991, "Punching Shear Analysis of Reinforced High-Strength Concrete Slabs," *Canadian Journal of Civil Engineering*, V. 18, No. 6, Dec., pp. 954-963.

Marzouk, H.; Emam, M.; and Hilal, M. S., 1996, "Effect of High-Strength Concrete Columns on the Behavior of Slab-Column Connections," *ACI Structural Journal*, V. 93, No. 5, Sept.-Oct., pp. 1-8.

Marzouk, H.; Emam, M.; and Hilal, M. S., 1998, "Effect of High-Strength Concrete Slab on the Behavior of Slab-Column Connections," *ACI Structural Journal*, V. 95, No. 3, May-June, pp. 227-237.

Mast, P. E., 1970a, "Stresses in Flat Plates near Columns," ACI Journal, *Proceedings* V. 67, No. 10, Oct., pp. 761-768.

Mast, P. E., 1970b, "Plate Stresses at Columns near the Free Edge," ACI Journal, *Proceedings* V. 67, No. 11, Nov., pp. 898-902.

McHarg, P. J.; Cook, W. D.; Mitchell, D.; and Yoon, Y.-S., 2000, "Benefits of Concentrated Slab Reinforcement and Steel Fibers on Performance of Slab-Column Connections," *ACI Structural Journal*, V. 97, No. 2, Mar.-Apr., pp. 225-234.

Megally, S. H., 1998, "Punching Shear Resistance of Concrete Slabs to Gravity and Earthquake," PhD dissertation, Department of Civil Engineering, University of Calgary, Alberta, Canada, June, 468 pp.

Megally, S., and Ghali, A., 2000a, "Seismic Behavior of Edge Column-Slab Connections with Stud Shear Reinforcement," *ACI Structural Journal*, V. 97, No. 1, Jan.-Feb., pp. 53-60.

Megally, S., and Ghali, A., 2000b, "Punching Shear Design of Earthquake-Resistant Slab-Column Connections," *ACI Structural Journal*, V. 97, No. 5, Sept.-Oct., pp. 720-730.

Melges, J. L. P., 2000, "Análise Experimental da Punção em Lajes de Concreto Armado e Protendido," PhDEng thesis, Escola de Engenharia de São Carlos, Universidade de São Paulo, São Carlos, Brasil, 350 pp.

Menétrey, P., 1996, "Analytical Computation of the Punching Strength of Reinforced Concrete," *ACI Structural Journal*, V. 93, No. 5, Sept.-Oct., pp. 503-511.

Menétrey, P., 1998, "Relationships between Flexural and Punching Failure," *ACI Structural Journal*, V. 95, No. 4, July-Aug., pp. 412-419.

Menétrey, P.; Walther, R.; Zimmermann, T.; Willam, K. J.; and Regan, P. E., 1997, "Simulation of Punching Failure in Reinforced-Concrete Structures," *Journal of Structural Engineering*, ASCE, V. 123, No. 5, May, pp. 652-659.

Mitchell, D.; Cook, W. D.; and Dilger, W., 2005, "Effects of Size, Geometry and Material Properties on Punching Shear Resistance," *Punching Shear in Reinforced Concrete Slabs*, SP-232, M. A. Polak, ed., American Concrete Institute, Farmington Hills, MI, pp. 39-55.

Moe, J., 1961, "Shearing Strength of Reinforced Concrete Slabs and Footings Under Concentrated Loads," *Bulletin D47*, Portland Cement Association, Research and Development Laboratories, Skokie, IL, Apr., 130 pp.

Moehle, J. P., 1988, "Strength of Slab-Column Edge Connections," *ACI Structural Journal*, V. 85, No. 1, Jan.-Feb., pp. 89-98.

Moehle, J. P., 1996, "Seismic Design Considerations for Flat Plate Construction," *Mete A. Sozen Symposium: A Tribute from his Students*, SP-162, J. K. Wight and M. E. Kreger, eds., American Concrete Institute, Farmington Hills, MI, Aug., pp. 1-35.

Morrison, D. G.; Hirasawa, I.; and Sozen, M. A., 1983, "Lateral-Load Tests of R/C Slab-Column Connections," *Journal of Structural Engineering*, ASCE, V. 109, No. 11, Nov., pp. 2698-2714.

Mortin, J. D., and Ghali, A., 1991, "Connection of Flat Plates to Edge Columns," *ACI Structural Journal*, V. 88, No. 2, Mar.-Apr., pp. 191-198.

Nölting, D., 1984, "Des Durchstanzen von Platten aus Stahlbeton-Tragverhalten, Berechnung, Bemessung," *Heft* 62, Institut für Baustoffe Massivbau und Brandschutz, Technischen Universität Braunschweig, Germany.

Nylander, H., and Sundquist, H., 1972, "Genomstansning av Pelarunderstödd Plattbro av Betong med Ospänd Armering," *Meddelande* Nr.104, Institutionen för Byggnadsstatik, Kungliga Tekniska Högskolan, Stockholm, Sweden.

Nylander, H.; Kinnunen, S.; and Ingvarsson, H., 1977, "Genomstansning av Pelar-Understödd Plattbro av Betong med Spänd och Ospänd Armering," *Meddelande* Nr.123, Institutionen för Byggnadsstatik, Kungliga Tekniska Högskolan, Stockholm, Sweden,.

NZS, 2006, "Concrete Structures Standard (NZS 3101-2006)," Standards New Zealand, Wellington, New Zealand.

Oliveira, D. R. C.; Regan, P. E.; and Melo, G. S. S. A, 2004, "Punching Resistance of RC Slabs with Rectangular Columns," *Magazine of Concrete Research*, V. 56, No. 3, Apr., pp. 123-138.

Oliveira, D. R.; Melo, G. S.; and Regan, P. E., 2000, "Punching Strengths of Flat Plates with Vertical or Inclined Stirrups," *ACI Structural Journal*, V. 97, No. 3, May-June, pp. 485-491.

Osman, M.; Marzouk, H.; and Helmy, S., "Behavior of High-Strength Lightweight Concrete Slabs under Punching Loads," *ACI Structural Journal*, V. 97, No. 3, May-June 2000, pp. 492-498.

Pan, A. D., and Moehle, J. P., 1992, "An Experimental Study of Slab-Column Connections," *ACI Structural Journal*, V. 89, No. 6, Nov.-Dec., pp. 626-638.

Pan, A., and Moehle, J. P., 1989, "Lateral Displacement Ductility of Reinforced Concrete Flat Plates," *ACI Structural Journal*, V. 86, No. 3, May-June, pp. 250-258.

Papanikolaou, K. V.; Tegos, I. A.; and Kappos, A. J., 2005, "Punching Shear Testing of Reinforced Concrete Slabs, and Design Implications," *Magazine of Concrete Research*, V. 57, No. 3, Apr., pp. 167-177.

Park, R., and Islam, S., 1976, "Strength of Slab-Column Connections with Shear and Unbalanced Flexure," *Journal of the Structural Division*, ASCE, V. 102, No. ST9, Sept., pp. 1879-1901.

Park, R., and Paulay, T., 1975, "Reinforced Concrete Structures," John Wiley & Sons, Inc., New York, 769 pp.

Paulay, T., and Priestley, M. J. N., 1992, "Seismic Design of Reinforced Concrete and Masonry Buildings," John Wiley & Sons, Inc., New York, 744 pp.

Popovics, S., 1973, "A Numerical Approach to the Complete Stress-Strain Curves for Concrete," *Cement and Concrete Research*, V. 3, No. 5, Sept., pp. 583-599.

Pralong, J., 1982, "Poinçonnement Symétrique des Planchers-Dalles," *IBK-Bericht* Nr. 131, Institut für Baustatik und Konstruktion, ETH Zürich, Switzerland, June.

Pralong, J.; Brändli, W.; and Thürlimann, B., 1979, "Durchstanzversuche an Stahlbeton- und Spannbetonplatten," *IBK-Bericht* Nr. 7305-3, ETH Zürich, Birkhäuser, Basel, Switzerland.

Ramdane, K.-E., 1996, "Punching Shear of High Performance Concrete Slabs," *Utilization of High Strength/*High *Performance Concrete*, Proc. V. 3, Laboratoire Central des Ponts et Chausées, Paris, France, pp. 1015-1026.

Rangan, B. V., 1990, "Tests on Slabs in the Vicinity of Edge Columns," *ACI Structural Journal*, V. 87, No. 6, Nov.-Dec., pp. 623-629.

Rankin, G. I. B., and Long, A. E., 1987a, "Predicting the Punching Strength of Conventional Slab-Column Specimens," *Proceedings of the Institution of Civil Engineers*, Part 1, V. 82, No. 2, Apr., pp. 327-346.

Rankin, G. I. B., and Long, A. E., 1987b, "Predicting the Enhanced Punching Strength of Interior Slab-Column Specimens," *Proceedings of the Institution of Civil Engineers*, Part 1, V. 82, No. 4, Dec., pp. 1165-1186.

Regan, P. E., 1981, "Behavior of Reinforced Concrete Flat Slabs," *CIRIA Report* No. 89, Construction Industry Research and Information Association, London, England.

Regan, P. E., 1985, "The Punching Resistance of Prestressed Concrete Slabs," *Proceedings of the Institution of Civil Engineers*, Part 2, V. 79, No. 4, Dec., pp. 657-680.

Regan, P. E., 1986, "Symmetrical Punching of Reinforced Concrete Slabs," *Magazine of Concrete Research*, V. 38, No. 136, Sept., pp. 115-128.

Regan, P. E., and Braestrup, M. W., 1985, "Punching Shear in Reinforced Concrete: A State of the Art Report," *Bulletin D'Information*, No. 168, Comité Euro-International du Béton, Lausanne, Switzerland, Jan., 232 pp.

Reimann, H., 1963, "Method for Calculating the Punching Loads of Flat Slabs Supported by Columns without Capitals (Zur Bemessung von dünnen Plattendecken auf Stützen ohne Kopf gegen Durchstanzen)," Dr.-Ing. thesis, Technischen Hochschule, Stuttgart, Germany, Jan., 157 pp.

Richart, F. E., 1948a, "Reinforced Concrete Wall and Column Footings, Part 1," ACI Journal, *Proceedings* V. 45, No. 2, Oct., pp. 97-127.

Richart, F. E., 1948b, "Reinforced Concrete Wall and Column Footings, Part 2," ACI Journal, *Proceedings* V. 45, No. 3, Nov., pp. 237-260.

Ritchie, M.; Ghali, A.; Dilger, W.; and Gayed, R. B., 2006, "Unbalanced Moment Resistance by Shear in Slab-Column Connections: Experimental Assessment," *ACI Structural Journal*, V. 103. No. 1, Jan.-Feb., pp. 74-82.

Robertson, I. N., and Durrani, A. J., 1990, "Seismic Response of Connections in Indeterminate Flat-Slab Subassemblies," Structural Research at Rice, *Report* No. 41, Department of Civil Engineering, Rice University, Houston, TX, July, 266 pp.

Robertson, I. N., and Durrani, A. J., 1991, "Gravity Load Effect on Seismic Behavior of Exterior Slab-Column Connections," *ACI Structural Journal*, V. 88, No. 3, May-June, pp. 255-267.

Robertson, I. N., and Durrani, A. J., 1992, "Gravity Load Effect on Seismic Behavior of Interior Slab-Column Connections," *ACI Structural Journal*, V. 89, No. 1, Jan.-Feb., pp. 37-45.

Robertson, I. N.; Kawai, T.; Lee, J.; and Enomoto, B., 2002, "Cyclic Testing of Slab-Column Connections with Shear Reinforcement," *ACI Structural Journal*, V. 99, No. 5, Sept.-Oct., pp. 605-613.

Robertson, I., and Johnson, G., 2006, "Cyclic Lateral Loading of Nonductile Slab-Column Connections," *ACI Structural Journal*, V. 103, No. 3, May-June, pp. 356-364.

Roll, F.; Zaidi, S. T. H.; Sabnis, G.; and Chuang, K., 1971, "Shear Resistance of Perforated Reinforced Concrete Slabs," *Crack, Deflection and Ultimate Load of Concrete Slab System*, SP-30, American Concrete Institute, Farmington Hills, MI, pp. 77-101.

Scavuzzo, L., 1978, "Shear Reinforcement at Slab-Column Connections in a Reinforced Concrete Flat Plate Structure," Royal Military College, Kingston, Ontario, Canada.

Schaefers, U., 1984, "Konstruktion, Bemessung und Sicherheit gegen Durchstanzen von balkenlosen Stalbetondecken im Bereich der Innenstützen," *DafStb Heft* 357, Beuth-Verlag, Berlin, Germany.

Schaeidt, W.; Ladner, M.; and Rösli, A., 1970, "Berechnung von Flachdecken auf Durchstanzen," Eidgenössische Materialprüfugs- und Versuchsanstalt, Dübendorf, Switzerland.

Shehata, I. A. E. M., 1990, "Simplified Model for Estimating The Punching Resistance of Reinforced Concrete Slabs," *Materials and Structures*, V. 23, No. 5, Sept., pp. 364-371.

Shehata, I. A. E. M., and Regan, P. E., 1989, "Punching in R.C. Slabs," *Journal of the Structural Engineering*, ASCE, V. 115, No. 7, July, pp. 1726-1740.

Shehata, I. A., 1982, "Punching of Prestressed and Non-Prestressed Reinforced Concrete Flat Slabs," MPhil thesis, Polytechnic of Central London, London, 336 pp.

Sherif, A. G., and Dilger, W. H., 2000a, "Tests of Full-Scale Continuous Reinforced Concrete Flat Slabs," *ACI Structural Journal*, V. 97, No. 3, May-June, pp. 455-467.

Sherif, A. G., and Dilger, W. H., 2000b, "Punching Failure of a Full Scale High Strength Concrete Flat Slab," *International Workshop on Punching Shear Capacity on RC Slabs*, Proc., Stockholm, Sweden, pp 235-243.

Sherif, G., and Dilger, W. H., 1996, "Critical Review of the CSA A23.3-94 Punching Shear Provisions for Interior Columns," *Canadian Journal of Civil Engineering*, V. 23, No. 5, Oct., pp. 998-1011.

Silva, R. J. C., 2004, "Punção em Lajes Cogumelo Protendida," PhD thesis, Department of Civil and Environmental Engineering, University of Brasília, Brasília, Brasil, 223 pp.

Silva, R. J. C.; Regan, P. E.; and Melo, G. S. S. A., 2005, "Punching Resistances of Unbonded Post-Tensioned Slabs by Decompression Methods," *Structural Concrete*, Journal of the fib, V. 6, No. 1, Mar., pp. 9-21.

Silva, R. J. C.; Regan, P. E.; and Melo, G. S. S. A., 2007, "Punching of Post-Tensioned Slabs - Tests and Codes," *ACI Structural Journal*, V. 104, No. 2, Mar.-Apr., pp. 123-132.

Simmonds, S. H., and Alexander, S. D. B., 1987, "Truss Model for Edge Column-Slab Connections," *ACI Structural Journal*, V. 84, No. 4, July-Aug., pp. 296-303.

Sinha, B. P.; Gerstle, K. H.; and Tulin, L. G., 1964, "Stress-Strain Relations for Concrete under Cyclic Loading," ACI Journal, *Proceedings* V. 61, No. 2, Feb., pp. 195-211.

Smith, S. W., and Burns, N. H., 1974, "Post-Tensioned Flat Plate to Column Connection Behavior, *PCI Journal*, V. 19, No. 3, May-June, pp. 74-91.

Sozen, M. A., 1980, "Review of Earthquake Response of Reinforced Concrete Buildings with a View to Drift Control, State-of-the-Art in Earthquake Engineering," *7th World Conference on Earthquake Engineering*, Istanbul, Turkey, pp. 119-174.

Stamenković, A., and Chapman, J. C., 1974, "Local Strength at Column Heads in Flat Slabs Subjected to a Combined Vertical and Horizontal Loading," *Proceedings of the Institution of Civil Engineers*, Part 2, V. 57, No. 2, June, pp. 205-232.

Suwita, M. G.; Irawan, P.; Teng, S., 2001, "Strength of Slab-Column Connections with Biaxial Unbalanced Moments," *Final Report*, A BCA-NTU Joint Research on Flat-Plate Structures, Phase-1B, School of Civil and Structural Engineering, Nanyang Technological University, Singapore, Jan., 158 pp.

Swamy, R. N., and Ali, S. A. R., 1982, "Punching Shear Behavior of Reinforced Slab-Column Connections Made with Steel Fiber Concrete," ACI Journal, *Proceedings* V. 79, No. 5, Sept.-Oct., pp. 392-406.

Symmonds, D. W.; Mitchell, D.; and Hawkins, N. M., 1976, "Slab-Column Connections Subjected to High Intensity Shear and Transferring Reversed Moments," *Progress Report* on NSF Project GI-38717, Department of Civil Engineering, University of Washington, Seattle, WA.

Takahashi, Y.; Kakuta, Y.; and Sato, Y., 1992, "Experimental Study on Shear Failure of Concrete Slabs Reinforced with Grid-Shaped FRP Bars," Japan Concrete Institute, *Transactions* V. 14, pp. 267-272.

Tan, Y., and Teng, S., 2005, "Interior Slab-Rectangular Column Connections under Biaxial Lateral Loadings," *Punching Shear in Reinforced Concrete Slabs*, SP-

232, M. A. Polak, ed., American Concrete Institute, Farmington Hills, MI, pp. 147-174.

Taylor, R., and Hayes, B., 1965, "Some Tests on the Effect of Edge Restraint on Punching Shear in Reinforced Concrete Slab," *Magazine of Concrete Research*, V. 17, No. 50, Mar., pp. 39-44.

Teng, S.; Cheong, H. K.; Kuang, K. L.; and Geng J. Z., 2004, "Punching Shear Strength of Slabs with Openings and Supported on Rectangular Columns," *ACI Structural Journal*, V. 101, No. 5, Sept.-Oct., pp. 678-687.

Tian, Y.; Jirsa, J. O.; Bayrak, O.; Widianto; and Argudo, J. F., 2008, "Behavior of Slab-Column Connections of Existing Flat-Plate Structures," *ACI Structural Journal*, V. 105, No. 5, Sept.-Oct., pp. 561-569.

Tolf, P., 1988, "Plattjocklelens Inverkan På Betongplattors Hållfasthet vid Genomstansning," Försök med cikulära platter, *TRITA-BST Bull. 146*, Institutionen för Byggnadsstatik, KTH, Stockholm, Sweden, 64 pp.

Tomaszewicz, A., 1993, "High Strength Concrete: SP2 – Plates and Shells Report 2.3 Punching Shear Capacity of Reinforced Concrete Slabs," *Report* No. STF70 A93082, SINTEF Structures and Concrete, Trondheim, Norway, July, 36 pp.

Trongtham, N., and Hawkins, N. M., 1977, "Moment Transfer to Column in Unbonded Post-Tensioned Prestressed Concrete Slabs," *Report* SM 77-3, Department of Civil Engineering, University of Washington, Seattle, WA, Oct., 186 pp.

Vanderbilt, M. D., 1972, "Shear Strength of Continuous Plates," *Journal of Structural Division*, ASCE, V. 98, No. ST5, May, pp. 961-973.

Walker, P. R., and Regan, P. E., 1987, "Corner Column-Slab Connections in Concrete Flat Plates," *Journal of Structural Engineering*, ASCE, V. 113, No. 4, Apr., pp. 704-720.

Wey, E. H., and Durrani, A. J., 1992, "Seismic Response of Interior Slab-Column Connections with Shear Capitals," *ACI Structural Journal*, V. 89, No. 6, Nov.-Dec., pp. 682-691.

Widjaja, S., and Teng, S., 2006, "Corner Slab-Rectangular Column Connections under Biaxial Cyclic Lateral Loading," *Final Report,* A BCA-NTU Joint Research on Flat Plate Structures, Phase IIIB, School of Civil and Environmental Engineering, Nanyang Technological University, Singapore, 250 pp.

Wight, J. K., and MacGregor, J. G., 2009, "Reinforced Concrete: Mechanics and Design," 5th Ed., Pearson Prentice Hall, Upper Saddle River, New Jersey, 1128 pp.

Yitzhaki, D., 1966, "Punching Strength of Reinforced Concrete Slabs," ACI Journal, *Proceedings* V. 63, No. 5, May, pp. 527-542.

Zaghlool, E. R. F., 1971, "Strength and Behavior of Corner and Edge Column-Slab Connections in Reinforced Concrete Flat Plates," PhD thesis, Department of Civil Engineering, University of Calgary, Alberta, Canada, 366 pp.

Zaghlool, E. R. F., and Rawdon de Paiva, H. A., 1973, "Tests of Flat-Plate Corner Column-Slab Connections," *Journal of the Structural Division*, ASCE, V. 99, No. ST3, Mar., pp. 551-572.

Zaghlool, E. R. F.; Rawdon de Paiva, H. A.; and Glockner, P. G., 1970, "Tests of Reinforced Concrete Flat Plate Floors," *Journal of the Structural Division*, ASCE, V. 96, No. ST3, Mar., pp. 487-507.

Zee, H. L., and Moehle, J. P., 1984, "Behavior of Interior and Exterior Flat Plate Connections Subjected to Inelastic Load Reversals," *Report* No. UCB/EERC-84/07, College of Engineering, University of California, Berkeley, CA, Aug., 130 pp.

APPENDIX A

DESIGN OF MODEL STRUCTURE

A.1 Prototype Model

The prototype structure was a ten-story building with five and three bays in *x*- and *y*-directions, respectively as shown in Fig. A.1.

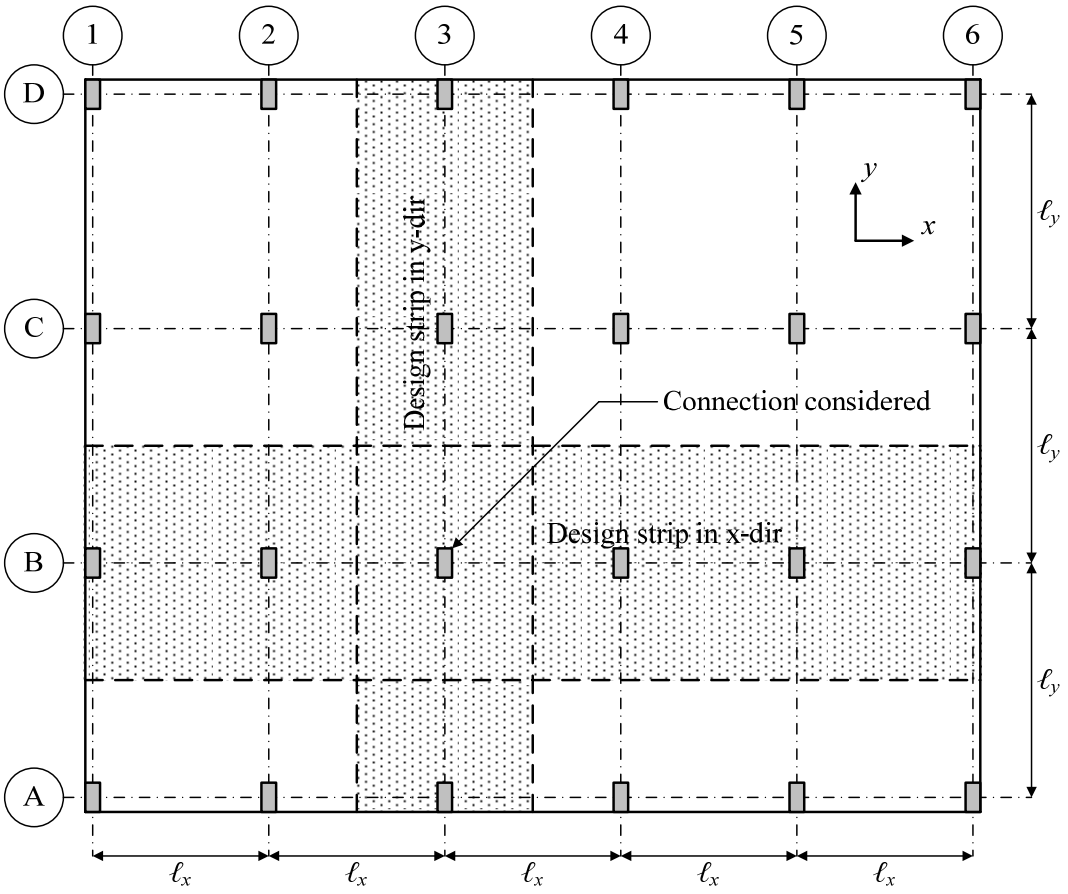

Fig. A.1 Prototype structure

Span lengths in *x*- and *y*-directions:

ℓ_x = 5250 mm

ℓ_y = 6750 mm

Story height:

H = 2250 mm

Column widths in *x*-and *y*-directions:

c_x = 180 mm

c_y = 900 mm

Slab thickness:

h = 150 mm

A.2 Material Properties

A.2.1 Concrete

The concrete was assumed using Grade 40 of normal weight concrete, having the compressive strength of concrete cube (f_{cu}) of 40.0 MPa.

Compressive strength of concrete cylinder:

$f'_c = 0.80\, f_{cu} = 32.0$ MPa

Concrete strength at transfer:

$f'_{ci} = 0.75 \times f'_c = 24.0$ MPa

Elastic modulus of concrete:

$E_c = 4700 \sqrt{f'_c} = 26{,}587$ MPa

Density of concrete:

$\gamma_c = 24$ kN/m^3

For f'_c = 32 MPa, the factor relating depth of equivalent rectangular compressive stress block to neutral axis depth:

$$\beta_1 = 0.85 - 0.05\left(\frac{f'_c - 28}{7}\right) = 0.82$$

For normal weight of concrete, the modification factor reflecting the reduced mechanical properties of lightweight concrete:

$\lambda = 1.00$

A.2.2 Reinforcing Steel

The reinforcing steels were assumed using Grade 460 of high-strength deformed steel bars (T-bars).

Yield strength of reinforcing steel:

$f_y = 460$ MPa

A.2.3 Prestressing Steel

The prestressing steels were assumed using 0.5" diameter seven-wire super strands in accordance with BS 5896. The strand has a nominal diameter of 12.9 mm and a nominal area of 100 mm^2.

Yield strength of strand:

f_{py} = 1580 MPa

Ultimate strength of strand:

f_{pu} = 1860 MPa

Initial stress in strand:

$f_{si} = 0.70\, f_{pu}$ = 1302 MPa

Initial force of strand:

$F_i = f_{si} \times 100\ mm^2$ = 130.2 kN

Lump-sum losses:

η = 200 MPa

Effective stress in strand:

$f_{se} = f_{si} - \eta$ = 1102 MPa

Effective force of strand:

$F_e = f_{se} \times 100\ mm^2$ = 110.2 kN

A.3 Loading

The flat-plate structure was assumed to carry gravity loads only, whereas the lateral loads were assumed to be carried by lateral-force-resisting systems, e.g. shear walls.

Self-weight of slab:

$w_{SW} = \gamma_c \times h$ = 3.60 kPa

Superimposed dead load:

w_{SD} = 1.40 kPa

Dead load:

$w_D = w_{SW} + w_{SD} = 5.00$ kPa

Live load:

$w_L = 2.40$ kPa

Service load:

$w_S = w_D + w_L = 7.40$ kPa

Factored/ultimate load:

$w_U = 1.2D + 1.6L = 9.84$ kPa

A.4 Tendon Profiles

The tendon profiles were assumed a series of parabolic curves. Assuming a tendon diameter of 18 mm with the clear concrete cover of 15 mm, the distance from the slab surface to the centroid of the tendon was worked out to be 24 mm. Maximum effective depth of prestressing steel:

$d_p = h - 24 = 126$ mm

Maximum eccentricity of tendon:

$e = h/2 - 24 = 51$ mm

Fig. A.2 shows the typical tendon profiles for the exterior and interior spans. Note that the tendon eccentricity is measured positive (+) when it is below the neutral axis, and vice versa.

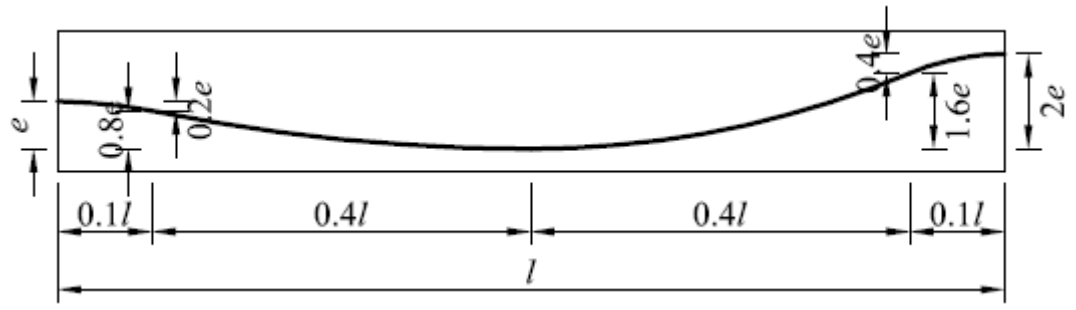

(a) Exterior spans

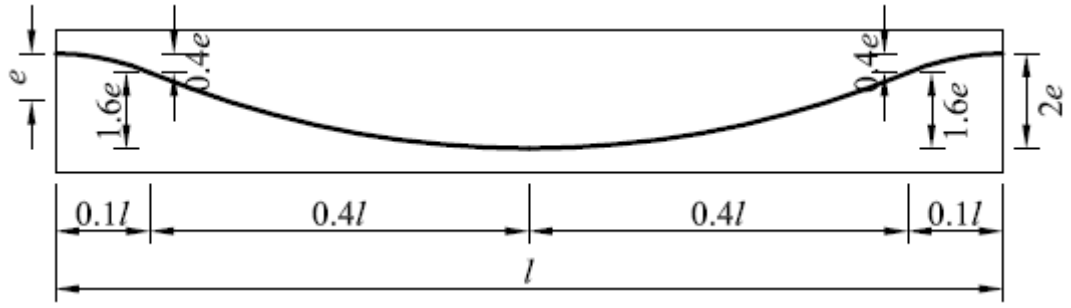

(b) Interior spans

Fig. A.2 Typical tendon profiles

A.5 Equivalent Frame Analysis

A.5.1 Gravity Loading

Self-weight of slab for frame in *x*- and *y*-directions:

$SW_x = w_{SW} \times \ell_y = 24.30$ kN/m

$SW_y = w_{SW} \times \ell_x = 18.90$ kN/m

Superimposed dead loads for frame in *x*- and *y*-directions:

$SD_x = w_{SD} \times \ell_y = 9.45$ kN/m

$SD_y = w_{SD} \times \ell_x = 7.35$ kN/m

Dead loads for frame in *x*- and *y*-directions:

$D_x = SW_x + SD_x = 33.75$ kN/m

$D_y = SW_y + SD_y = 26.25$ kN/m

Live loads for frame in *x*- and *y*-directions:

$L_x = w_L \times \ell_y = 16.20$ kN/m

$L_y = w_L \times \ell_x = 12.60$ kN/m

Service loads for frame in *x*- and *y*-directions:

$S_x = D_x + L_x = 49.95$ kN/m

$S_y = D_y + L_y = 38.85$ kN/m

Factored/ultimate loads for frame in *x*- and *y*-directions:

$U_x = 1.2D_x + 1.6L_x = 66.42$ kN/m

$U_y = 1.2D_y + 1.6L_y = 51.66$ kN/m

As the live load is less than 0.75 of the dead load, the live load is assumed to act simultaneously in all spans. Fig. A.3 shows the gravity loads for frame in *x*- and *y*-directions.

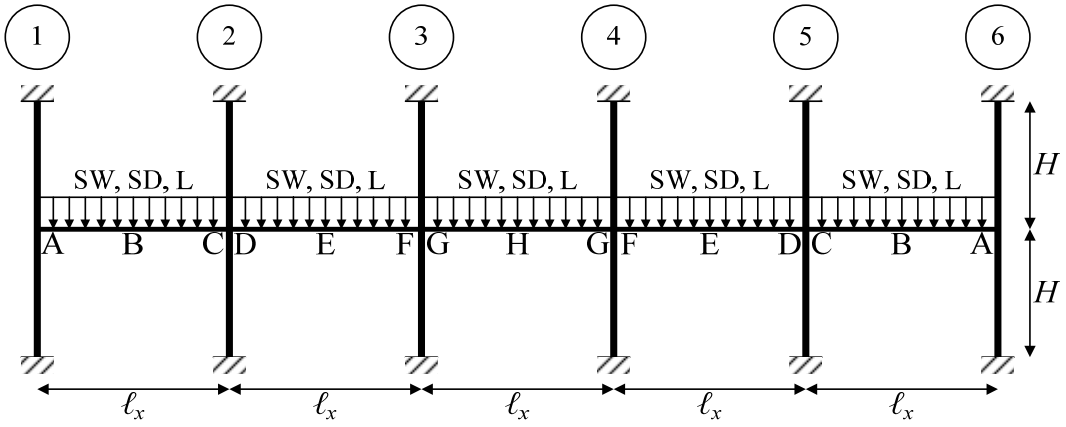

(a) Frame in *x*-direction

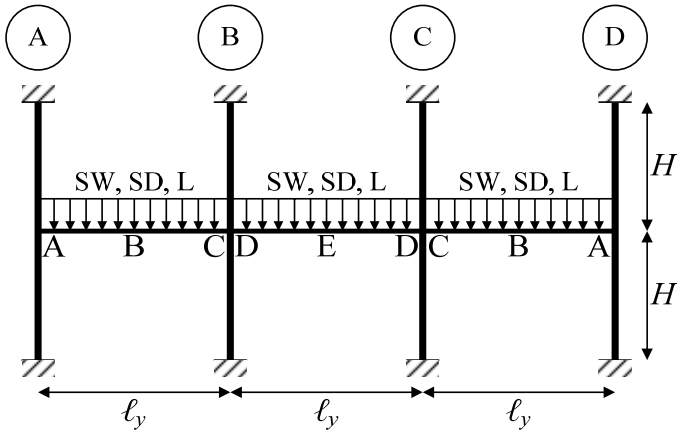

(b) Frame in *y*-direction

Fig. A.3 Gravity loads

A.5.2 Load Balancing (*B*)

To calculate the number of tendons, 90% of dead load in the interior span was assumed to be balanced by the prestressing force.

Total prestressing forces required in *x*- and *y*-directions:

$P_{ex,req} = 0.9D_x \times \ell_x^2 / (8 \times 2e) = 1026$ kN

$$P_{ey,req} = 0.9D_y \times \ell_y^2 \ / (8 \times 2e) = 1319 \text{ kN}$$

Total number of tendons required in *x*- and *y*-directions:

$$n_{px,req} = 1026 / F_e = 9.31 \text{ nos} \rightarrow \text{use 10 nos}$$

$$n_{py,req} = 1319 / F_e = 11.97 \text{ nos} \rightarrow \text{use 12 nos}$$

Tendons in *x*-direction were uniformly distributed with a spacing of 675 mm, whereas tendons in *y*-directions were banded with a spacing of 100 mm.

Total prestressing forces in *x*- and *y*-directions:

$$P_{ex} = 10 \times F_e = 1102.0 \text{ kN}$$

$$P_{ey} = 12 \times F_e = 1322.4 \text{ kN}$$

Compressive stresses in concrete in *x*- and *y*-directions:

$$f_{pcx} = P_e / \ell_y / h = 1.09 \text{ MPa}$$

$$f_{pcy} = P_e / \ell_x / h = 1.68 \text{ MPa}$$

Knowing the tendon profile and the total prestressing force, the balancing loads along the spans can be computed.

Balancing loads at exterior support for frame in *x*- and *y*-directions:

$$w_{1x} = 8 P_{ex} (0.2e) / (2 \times 0.1\ell_x)^2 = 81.56 \text{ kN/m}$$

$$w_{1y} = 8 P_{ey} (0.2e) / (2 \times 0.1\ell_y)^2 = 59.21 \text{ kN/m}$$

Balancing loads at exterior span for frame in *x*- and *y*-directions:

$$w_{2x} = 8 P_{ex} (0.8e) / (2 \times 0.4\ell_x)^2 = 20.29 \text{ kN/m}$$

$$w_{2y} = 8 P_{ey} (0.8e) / (2 \times 0.4\ell_y)^2 = 14.80 \text{ kN/m}$$

Balancing loads at interior span for frame in *x*- and *y*-directions:

$$w_{3x} = 8 P_{ex} (1.6e) / (2 \times 0.4\ell_x)^2 = 40.78 \text{ kN/m}$$

$$w_{3y} = 8 P_{ey} (1.6e) / (2 \times 0.4\ell_y)^2 = 29.60 \text{ kN/m}$$

Balancing loads at interior support for frame in *x*- and *y*-directions:

$$w_{4x} = 8 P_{ex} (0.4e) / (2 \times 0.1\ell_x)^2 = 163.13 \text{ kN/m}$$

$w_{4y} = 8\ P_{ey}\ (0.4e) / (2 \times 0.1\ell_y)^2 = 118.42$ kN/m

Balancing loads for the initial phase (at transfer) can also be computed by replacing P_e with P_i. Fig. A.4 shows the balancing loads for frame in *x*- and *y*-directions.

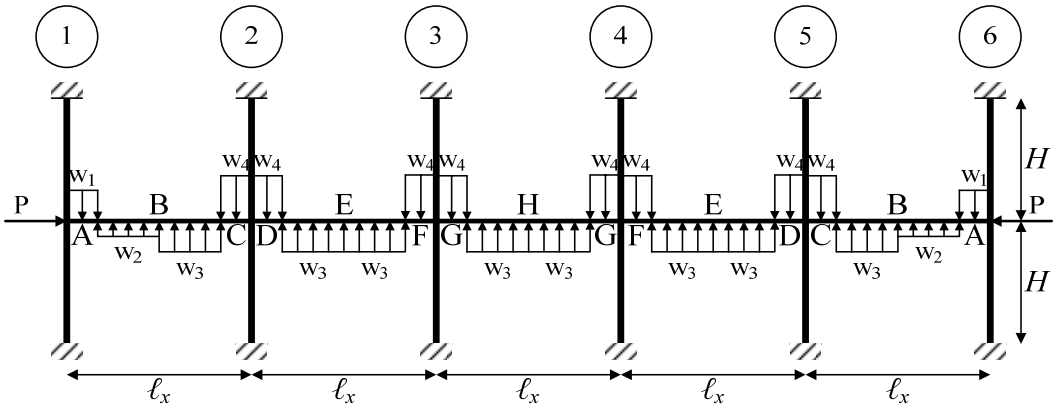

(a) Frame in *x*-direction

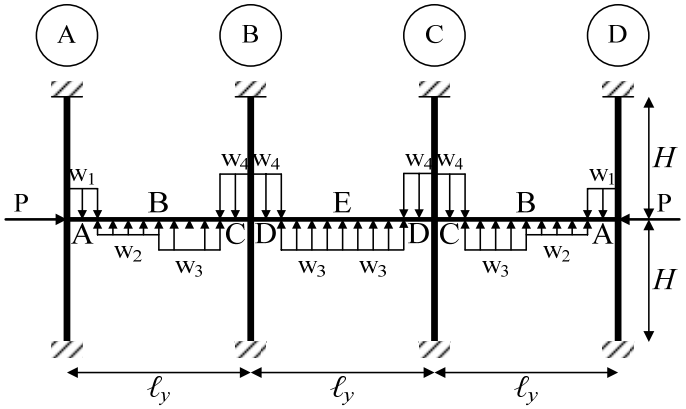

(b) Frame in *y*-direction

Fig. A.4 Balancing loads

A.5.3 Structural Analysis

The structural analysis was conducted using SAP2000 program by modifying the member properties at joints.

Second moments of area of slab for frame in *x*- and *y*-directions:

$$I_{sy} = \frac{\ell_y h^3}{12} = 1.90 \times 10^9 \text{ mm}^4$$

$$I_{sx} = \frac{\ell_x h^3}{12} = 1.48 \times 10^9 \text{ mm}^4$$

Second moments of area of slab at joint for frame in *x*- and *y*-directions:

$$I_{sjy} = \frac{I_{sy}}{(1 - c_y / \ell_y)^2} = 2.53 \times 10^9 \text{ mm}^4$$

$$I_{sjx} = \frac{I_{sx}}{(1 - c_x / \ell_x)^2} = 1.58 \times 10^9 \text{ mm}^4$$

Second moments of area of column for frame in *x*- and *y*-directions:

$$I_{cy} = \frac{c_y c_x^3}{12} = 4.37 \times 10^8 \text{ mm}^4$$

$$I_{cx} = \frac{c_x c_y^3}{12} = 1.09 \times 10^{10} \text{ mm}^4$$

Column stiffness (Rice et al. 1985[1]) for frame in *x*- and *y*-directions:

$$K_{cy} = \frac{4E_c I_{cy}}{H - 2h} = 2.39 \times 10^{10} \text{ MPa}$$

$$K_{cx} = \frac{4E_c I_{cx}}{H - 2h} = 5.96 \times 10^{11} \text{ MPa}$$

Constant *C* for frame in *x*- and *y*-directions:

$$C_y = \sum \left(1 - 0.63 \frac{h}{c_x}\right) \frac{h^3 c_x}{3} = 9.62 \times 10^7 \text{ mm}^4$$

$$C_x = \sum \left(1 - 0.63 \frac{h}{c_y}\right) \frac{h^3 c_y}{3} = 9.06 \times 10^8 \text{ mm}^4$$

Torsional member stiffness for frame in *x*- and *y*-directions:

$$K_{ty} = \sum \frac{9E_c C_y}{\ell_y (1 - c_y / \ell_y)^3} = 1.05 \times 10^{10} \text{ MPa}$$

$$K_{tx} = \sum \frac{9E_c C_x}{\ell_x (1 - c_x / \ell_x)^3} = 9.17 \times 10^{10} \text{ MPa}$$

[1] Rice, P. F.; Hoffman, E. S.; Gustafson, D. P.; and Gouwens, A. J., 1985, "Structural Design Guide to the ACI Building Code", 3rd Ed., Van Nostrand Reinhold, New York.

Equivalent column stiffness for frame in *x*- and *y*-directions:

$$K_{ecy} = \frac{\Sigma K_{cy} \times K_{ty}}{\Sigma K_{cy} + K_{ty}} = 8.59 \times 10^{9} \text{ MPa}$$

$$K_{ecx} = \frac{\Sigma K_{cx} \times K_{tx}}{\Sigma K_{cx} + K_{tx}} = 8.52 \times 10^{10} \text{ MPa}$$

Equivalent column stiffness per column for frame in *x*- and *y*-directions:

$$K^{*}_{ecy} = K_{ecy} \frac{K_{cy}}{\Sigma K_{cy}} = 4.29 \times 10^{9} \text{ MPa}$$

$$K^{*}_{ecx} = K_{ecx} \frac{K_{cx}}{\Sigma K_{cx}} = 4.26 \times 10^{10} \text{ MPa}$$

Second moments of area of column at joint for frame in *x*- and *y*-directions:

$$I_{cjy} = I_{cy} \frac{K^{*}_{ecy}}{K_{cy}} = 7.88 \times 10^{7} \text{ mm}^4$$

$$I_{cjx} = I_{cx} \frac{K^{*}_{ecx}}{K_{cx}} = 7.81 \times 10^{8} \text{ mm}^4$$

From the structural analysis, the critical values of bending moments and shear forces can be obtained. Tables A.1 and A.2 present the values of bending moments and shear forces at the column faces and mid-spans for frame in *x*- and *y*-directions, respectively.

Table A.1 Moment and shear values for frame in *x*-direction

Section		A	B	C	D	E	F	G	H
Moment (kN-m)	M_{SW}	-6.5	42.4	-63.6	-61.7	22.3	-48.6	-49.2	28.3
	M_{SD}	-2.5	16.5	-24.7	-24.0	8.7	-18.9	-19.1	11.0
	M_L	-4.3	28.2	-42.4	-41.1	14.9	-32.4	-32.8	18.9
	M_S	-13.4	87.1	-130.8	-126.8	45.9	-99.8	-101.0	58.1
	M_U	-17.8	115.8	-173.9	-168.5	61.0	-132.8	-134.4	77.3
	M_{Bi}	10.1	-50.8	84.4	83.6	-49.2	79.5	79.6	-51.1
	M_{Be}	8.6	-43.0	71.5	70.8	-41.6	67.2	67.4	-43.2
Shear (kN)	V_{SW}	-50.3	11.3	72.9	-64.2	-2.6	59.0	-61.6	0.0
	V_{SD}	-19.6	4.4	28.3	-25.0	-1.0	23.0	-24.0	0.0
	V_L	-33.6	7.5	48.6	-42.8	-1.7	39.3	-41.1	0.0
	V_S	-103.5	23.2	149.8	-131.9	-5.3	121.3	-126.6	0.0
	V_U	-137.6	30.8	199.2	-175.4	-7.1	161.3	-168.4	0.0
	V_{Bi}	7.0	-4.4	-19.0	18.2	0.8	-16.5	17.3	0.0
	V_{Be}	6.0	-3.7	-16.1	15.4	0.7	-14.0	14.7	0.0

Table A.2 Moment and shear values for frame in *y*-direction

Section		A	B	C	D	E
Moment (kN-m)	M_{SW}	-31.5	39.6	-50.9	-46.6	34.2
	M_{SD}	-12.3	15.4	-19.8	-18.1	13.3
	M_L	-21.0	26.4	-34.0	-31.1	22.8
	M_S	-64.8	81.4	-104.7	-95.8	70.4
	M_U	-86.2	108.3	-139.3	-127.4	93.6
	M_{Bi}	41.7	-49.9	76.2	81.6	-63.6
	M_{Be}	35.3	-42.3	64.5	69.1	-53.8
Shear (kN)	V_{SW}	-52.0	3.3	58.6	-55.3	0.0
	V_{SD}	-20.2	1.3	22.8	-21.5	0.0
	V_L	-34.6	2.2	39.1	-36.9	0.0
	V_S	-106.8	6.8	120.5	-113.6	0.0
	V_U	-142.0	9.1	160.2	-151.1	0.0
	V_{Bi}	38.0	6.5	-56.4	62.9	0.0
	V_{Be}	32.1	5.5	-47.8	53.3	0.0

A.6 Flexural Stress Checks

The flexural stress checks for frame in *x*- and *y*-directions are tabulated in Tables A.3 and A.4, respectively.

Table A.3 Flexural stress checks for frame in *x*-direction

Section		A	B	C	D	E	F	G	H
e (mm)		0.3	51.0	-50.4	-50.4	51.0	-50.4	-50.4	51.0
Transfer	M_{1i} (kN-m)	-0.4	-66.4	65.6	65.6	-66.4	65.6	65.6	-66.4
	M_{2i} (kN-m)	10.5	15.6	18.8	18.0	17.2	13.8	14.0	15.3
	f_{ti} (MPa)	1.84	1.57	2.85	2.87	0.90	3.05	3.04	0.99
	f_{bi} (MPa)	0.73	1.00	-0.28	-0.29	1.67	-0.48	-0.47	1.58
	Check	OK	OK	OK	OK	OK	OK	OK	OK
Service	M_{1i} (kN-m)	-0.3	-56.2	55.5	55.5	-56.2	55.5	55.5	-56.2
	M_{2i} (kN-m)	8.9	13.2	15.9	15.2	14.6	11.7	11.9	13.0
	f_{ti} (MPa)	1.57	3.34	0.20	0.29	1.83	1.03	0.99	2.17
	f_{bi} (MPa)	1.00	-0.77	2.37	2.28	0.74	1.54	1.58	0.40
	Check	OK	OK	OK	OK	OK	OK	OK	OK

Table A.4 Flexural stress checks for frame in *y*-direction

Section		A	B	C	D	E
e (mm)		4.5	51.0	-41.9	-41.9	51.0
Transfer	M_{1i} (kN-m)	-7.1	-79.7	65.5	65.5	-79.7
	M_{2i} (kN-m)	48.8	29.8	10.7	16.1	16.1
	f_{ti} (MPa)	4.98	2.97	3.81	4.58	1.31
	f_{bi} (MPa)	-1.01	1.00	0.16	-0.61	2.66
	Check	OK	OK	OK	OK	OK
Service	M_{1i} (kN-m)	-6.0	-67.4	55.5	55.5	-67.4
	M_{2i} (kN-m)	41.3	25.2	9.1	13.6	13.6
	f_{ti} (MPa)	3.28	5.09	1.08	2.08	3.15
	f_{bi} (MPa)	0.68	-1.13	2.89	1.89	0.82
	Check	OK	OK	OK	OK	OK

Given a tendon profile, the tendon eccentricity (*e*) at a particular section can be determined. Accordingly, the flexural stresses at top and bottom fibers can be calculated.

A.6.1 At Transfer (Initial)

Primary moment at transfer:

$$M_{1i} = P_i \times e$$

Secondary moment at transfer:

$$M_{2i} = M_{Bi} - M_{1i}$$

Top fiber stress at transfer:

$$f_{ti} = -\frac{P_i}{\ell_y h} - \frac{6(M_{SW} + M_{Bi} + M_{2i})h}{\ell_y h^3}$$

Bottom fiber stress at transfer:

$$f_{bi} = -\frac{P_i}{\ell_y h} + \frac{6(M_{SW} + M_{Bi} + M_{2i})h}{\ell_y h^3}$$

Note that the top and bottom fiber stresses at transfer should fall within the allowable compressive and tensile stresses at transfer.

Allowable compressive stress at transfer:

$$f_{ci,all} = -0.60\, f'_{ci} = -14.4 \text{ MPa}$$

Allowable tensile stress at transfer:

$$f_{ti,all} = 0.25\, \sqrt{f'_{ci}} = 1.22 \text{ MPa}$$

A.6.2 At Service (Effective)

Primary moment at transfer:

$$M_{1e} = P_e \times e$$

Secondary moment at transfer:

$$M_{2e} = M_{Be} - M_{1e}$$

Top fiber stress at service:

$$f_{te} = -\frac{P_e}{\ell_y h} - \frac{6(M_S + M_{Be} + M_{2e})h}{\ell_y h^3}$$

Bottom fiber stress at service:

$$f_{be} = -\frac{P_e}{\ell_y h} + \frac{6(M_S + M_{Be} + M_{2e})h}{\ell_y h^3}$$

Note that the top and bottom fiber stresses at service should fall within the allowable compressive and tensile stresses at service.

Allowable compressive stress at service:

$f_{ce,all} = -0.45 f'_c = -14.4$ MPa

Allowable tensile stress at service:

$f_{te,all} = 0.50 \sqrt{f'_c} = 2.83$ MPa

A.7 Nonprestressed Reinforcement

A.7.1 Top Reinforcement

Top reinforcement in negative moment areas at column supports was provided based on minimum reinforcement requirement:

$A_{st} = 0.00075 \times \max(\ell_x, \ell_y) \times h = 759$ mm^2

Using 13-mm diameter of reinforcing bars with the area of one bar of 133 mm^2, the number of reinforcement:

$n_t = 759 / 133 = 5.7$ nos → use 6 nos

This reinforcement was provided within a transfer width of c plus 1.5h on each side of the column in each direction.

A.7.2 Bottom Reinforcement

It can be seen that all effective tensile stresses in positive moment areas are less than $0.17\sqrt{f'_c}$, except the stress in the exterior span along y-direction. Thus, bottom reinforcement will only be provided in this area:

$$f_t = \frac{6M_S}{\ell_x h^2} = 4.13 \text{ MPa}$$

$$N_c = \frac{3M_S}{\ell_x h} = 0.31 \text{ N}$$

$$A_{sb} = \frac{N_c}{0.5 f_y} = 1.35 \text{ mm}^2$$

Using 13-mm diameter of reinforcing bars with the area of one bar of 133 mm^2, the number of reinforcement:

n_b = 1.35 / 133 = 0.01 nos → use 1 nos

To increase the resistance of the structural system to progressive collapse, structural integrity reinforcement in the form of continuous bottom bars will be provided. According to Joint ACI-ASCE Committee 352 (1997), at interior connections, the minimum area of continuous bottom reinforcement in each principal direction:

$$A_{sb} = \frac{0.5 \max(w_u, 2w_D) \ell_x \ell_y}{0.9 f_y} = 428 \text{ mm}^2$$

Using 13-mm diameter of reinforcing bars with the area of one bar of 133 mm^2, the number of reinforcement:

n_b = 428 / 133 = 3.2 nos → use 4 nos

This reinforcement shall be provided within the column cage in each principal direction. However, due to a space constraint, two bottom bars were provided in *y*-direction, and six bars were provided in *x*-direction.

A.8 Ultimate Flexural Strength

Nonprestressed reinforcement and the prestressing steels are to be placed at the same level. Thus, the effective depth of slab becomes:

$d = d_p$ = 126 mm

The ultimate flexural strength will be checked at the sections where the maximum negative and positive bending moments occur.

A.8.1 Negative Moment

From the structural analysis, maximum negative bending moments occur at sections C for both frame in *x*- and *y*-directions. Thus, taking into account the effect of secondary moments, the ultimate bending moments about *y*- and *x*-axes:

M_{uy} = -173.9 + 15.9 = -158.0 kN-m

M_{ux} = -139.3 + 9.1 = -130.2 kN-m

Effective depths of prestressing steel in *x*- and *y*-directions:

d_{px} = 125 mm

d_{py} = 117 mm

Areas of nonprestressed tension reinforcement in *x*- and *y*-directions:

$A_{sx} = 6 \times 133 = 798$ mm^2

$A_{sy} = 6 \times 133 = 798$ mm^2

Areas of nonprestressed compression reinforcement in *x*- and *y*-directions:

$A'_{sx} = 6 \times 133 = 798$ mm^2

$A'_{sy} = 2 \times 133 = 266$ mm^2

Areas of prestressing steel in *x*- and *y*-directions:

$A_{psx} = 10 \times 100 = 1000$ mm^2

$A_{psy} = 12 \times 100 = 1200$ mm^2

Ratios of prestressing steel in *x*- and *y*-directions:

$$\rho_{px} = \frac{A_{psx}}{\ell_y d_p} = 0.0012$$

$$\rho_{py} = \frac{A_{psy}}{\ell_x d_p} = 0.0020$$

Stresses in prestressing steel at nominal flexural strength in *x*- and *y*-directions:

$$f_{psx} = f_{se} + 70 + \frac{f'_c}{300\rho_{px}} = 1262 \text{ MPa}$$

$$f_{psy} = f_{se} + 70 + \frac{f'_c}{300\rho_{py}} = 1227 \text{ MPa}$$

Depths of equivalent rectangular stress block in *x*- and *y*-directions:

$$a_x = \frac{A_{psx} f_{psx} + A_{sx} f_y - A'_{sx} f_y}{0.85 f'_c \ell_y} = 6.9 \text{ mm}$$

$$a_y = \frac{A_{psy} f_{psy} + A_{sy} f_y - A'_{sy} f_y}{0.85 f'_c \ell_x} = 12.0 \text{ mm}$$

Distances from extreme compression fiber to neutral axis in *x*- and *y*-directions:

$$c_x = \frac{a_x}{\beta_1} = 8.4 \text{ mm}$$

$$c_y = \frac{a_y}{\beta_1} = 14.6 \text{ mm}$$

Net tensile strains in extreme tension steel in *x*- and *y*-directions:

$$\varepsilon_{tx} = 0.003\left(\frac{d - c_x}{c_x}\right) = 0.042 > 0.005 \rightarrow \text{tension-controlled}$$

$$\varepsilon_{ty} = 0.003\left(\frac{d - c_y}{c_y}\right) = 0.023 > 0.005 \rightarrow \text{tension-controlled}$$

Strength reduction factors for flexure about *y*- and *x*-axes:

$\phi_y = 0.90$

$\phi_x = 0.90$

Nominal flexural strengths about *y*- and *x*-axes:

$$M_{ny} = A_{psx} f_{psx} (d_{px} - a_x/2) + A_{sx} f_y (d - a_x/2) - A'_{sx} f_y (d' - a_x/2) = 191.3 \text{ kN-m}$$

$$M_{nx} = A_{psy} f_{psy} (d_{py} - a_y/2) + A_{sy} f_y (d - a_y/2) - A'_{sy} f_y (d' - a_y/2) = 205.0 \text{ kN-m}$$

Design values of flexural strength about *y*- and *x*-axes:

$\phi_y M_{ny} = 0.90 \times 191.3 = 172.2$ kN-m $> M_{uy} = 158.0$ kN-m (OK)

$\phi_x M_{nx} = 0.90 \times 205.0 = 184.5$ kN-m $> M_{ux} = 130.2$ kN-m (OK)

A.8.2 Positive Moment

From the structural analysis, maximum positive bending moments occur at sections B for both frame in *x*- and *y*-directions. Thus, taking into account the effect of secondary moments, the ultimate bending moments about *y*- and *x*-axes:

$M_{uy} = 115.8 + 13.2 = 129.0$ kN-m

M_{ux} = 108.3 + 25.2 = 133.5 kN-m

Effective depths of prestressing steel in *x*- and *y*-directions:

d_{px} = 126 mm

d_{py} = 126 mm

Areas of nonprestressed tension reinforcement in *x*- and *y*-directions:

$A_{sx} = 6 \times 133 = 798$ mm^2

$A_{sy} = 2 \times 133 = 266$ mm^2

Areas of nonprestressed compression reinforcement in *x*- and *y*-directions:

$A'_{sx} = 0$

$A'_{sy} = 0$

Areas of prestressing steel in *x*- and *y*-directions:

$A_{psx} = 10 \times 100 = 1000$ mm^2

$A_{psy} = 12 \times 100 = 1200$ mm^2

Ratios of prestressing steel in *x*- and *y*-directions:

$$\rho_{px} = \frac{A_{psx}}{\ell_y d_p} = 0.0012$$

$$\rho_{py} = \frac{A_{psy}}{\ell_x d_p} = 0.0018$$

Stresses in prestressing steel at nominal flexural strength in *x*- and *y*-directions:

$$f_{psx} = f_{se} + 70 + \frac{f'_c}{300\rho_{px}} = 1262 \text{ MPa}$$

$$f_{psy} = f_{se} + 70 + \frac{f'_c}{300\rho_{py}} = 1231 \text{ MPa}$$

Depths of equivalent rectangular stress block in *x*- and *y*-directions:

$$a_x = \frac{A_{psx} f_{psx} + A_{sx} f_y - A'_{sx} f_y}{0.85 f'_c \ell_y} = 8.9 \text{ mm}$$

$$a_y = \frac{A_{psy} f_{psy} + A_{sy} f_y - A'_{sy} f_y}{0.85 f'_c \ell_x} = 11.2 \text{ mm}$$

Distances from extreme compression fiber to neutral axis in *x*- and *y*-directions:

$$c_x = \frac{a_x}{\beta_1} = 10.8 \text{ mm}$$

$$c_y = \frac{a_y}{\beta_1} = 13.6 \text{ mm}$$

Net tensile strains in extreme tension steel in *x*- and *y*-directions:

$$\varepsilon_{tx} = 0.003\left(\frac{d - c_x}{c_x}\right) = 0.032 > 0.005 \rightarrow \text{tension-controlled}$$

$$\varepsilon_{ty} = 0.003\left(\frac{d - c_y}{c_y}\right) = 0.025 > 0.005 \rightarrow \text{tension-controlled}$$

Strength reduction factors for flexure about *y*- and *x*-axes:

$\phi_y = 0.90$

$\phi_x = 0.90$

Nominal flexural strengths about *y*- and *x*-axes:

$$M_{ny} = A_{psx} f_{psx}(d_{px} - a_x/2) + A_{sx} f_y(d - a_x/2) - A'_{sx} f_y(d' - a_x/2) = 198.0 \text{ kN-m}$$

$$M_{nx} = A_{psy} f_{psy}(d_{py} - a_y/2) + A_{sy} f_y(d - a_y/2) - A'_{sy} f_y(d' - a_y/2) = 192.5 \text{ kN-m}$$

Design values of flexural strength about *y*- and *x*-axes:

$\phi_y M_{ny} = 0.90 \times 198.0 = 178.2 \text{ kN-m} > M_{uy} = 129.0 \text{ kN-m}$ (OK)

$\phi_x M_{nx} = 0.90 \times 192.5 = 173.3 \text{ kN-m} > M_{ux} = 133.5 \text{ kN-m}$ (OK)

A.9 One-Way Shear

From the structural analysis, maximum ultimate shear forces occur at sections C for both frame in *x*- and *y*-directions. Thus, one-way shear will be investigated at these locations.

Ultimate shear forces in *x*- and *y*-directions:

V_{ux} = 199.2 kN

V_{uy} = 160.2 kN

Effective depths of prestressing steel in *x*- and *y*-directions:

d_{px} = 125 mm

d_{py} = 117 mm

Ultimate bending moments about *y*- and *x*-axes:

M_{uy} = 173.9 kN-m

M_{ux} = 139.3 kN-m

Nominal shear strengths in *x*- and *y*-directions:

$$V_{cx} = \left(0.05\lambda\sqrt{f'_c} + 4.8\frac{V_{ux}d_{px}}{M_{uy}} \right)\ell_y d = 826.9 \text{ kN}$$

$$V_{cy} = \left(0.05\lambda\sqrt{f'_c} + 4.8\frac{V_{uy}d_{py}}{M_{ux}} \right)\ell_x d = 636.1 \text{ kN}$$

For shear, the strength reduction factor ϕ is taken equal to 0.75. Thus, the design value of shear strengths:

$\phi V_{cx} = 0.75 \times 826.9 = 620.2 \text{ kN} > V_{ux} = 199.2 \text{ kN}$ (OK)

$\phi V_{cy} = 0.75 \times 636.1 = 477.1 \text{ kN} > V_{uy} = 160.2 \text{ kN}$ (OK)

A.10 Two-Way Shear (Punching)

A.10.1 Shear Strength

Widths of critical section in *x*- and *y*-directions:

$b_x = c_x + d$ = 306 mm

$b_y = c_y + d$ = 1026 mm

Perimeter of critical section:

$b_o = 2\ (b_x + b_y)$ = 2664 mm

Average compressive stress in concrete:

$f_{pc} = (f_{pcx} + f_{pcy}) / 2$ = 1.38 MPa

Tendon inclinations in *x*- and *y*-directions:

$$\sin \alpha_x = \frac{2e}{\sqrt{(2e)^2 + (0.5\ell_x)^2}} = 0.0388$$

$$\sin \alpha_y = \frac{2e}{\sqrt{(2e)^2 + (0.5\ell_y)^2}} = 0.0302$$

There are two tendons in each direction that pass through the critical section. Thus, the vertical component of all prestress force crossing the critical section:

$$V_p = 4\, F_{ex} \sin \alpha_x + 4\, F_{ey} \sin \alpha_y = 30.4 \text{ kN}$$

Taking α_s equal to 40 for interior columns, the factor β_p:

$$\beta_p = \min [0.29, 0.083(\alpha_s d/b_o + 1.5)] = 0.28$$

Nominal shear strength of slab:

$$v_c = \beta_p \lambda \sqrt{f'_c} + 0.3 f_{pc} + \frac{V_p}{b_o d} = 2.10 \text{ MPa}$$

For shear, the strength reduction factor ϕ is taken equal to 0.75. Thus, the design value of shear strength:

$$\phi v_c = 0.75 \times 2.10 = 1.57 \text{ MPa}$$

A.10.2 Moment Transferred by Shear

Tributary area of interior column:

$$A_t = (\ell_x \ell_y) - (b_x b_y) = 35{,}123{,}544 \text{ mm}^2$$

Ultimate shear force:

$$V_u = w_U \times A_t = 345.6 \text{ kN}$$

Moment transfer at a connection is the difference between bending moments in the two adjacent spans. Hence, the values of moment transfer about *y*- and *x*-axes:

$$M_{uy} = 149.8 - 147.5 = 2.3 \text{ kN-m}$$

$$M_{ux} = 214.9 - 200.6 = 14.3 \text{ kN-m}$$

Fractions of unbalanced moment transferred by flexure about *y*- and *x*-axes:

$$\gamma_{fy} = \frac{1}{1+(2/3)\sqrt{b_1/b_2}} = 0.7$$

$$\gamma_{fx} = \frac{1}{1+(2/3)\sqrt{b_1/b_2}} = 0.5$$

Fractions of unbalanced moment transferred by shear about *y*- and *x*-axes:

$\gamma_{vy} = 1 - \gamma_{fy} = 0.3$

$\gamma_{vx} = 1 - \gamma_{fx} = 0.5$

Properties of critical section analogous to polar moment of inertia about *y*- and *x*-axes:

$$J_{cy} = \frac{2(b_x d^3)}{12} + \frac{2(db_x^3)}{12} + 2(b_y d)\left(\frac{b_x}{2}\right)^2 = 6.76 \times 10^9 \text{ mm}^4$$

$$J_{cx} = \frac{2(b_y d^3)}{12} + \frac{2(db_y^3)}{12} + 2(b_x d)\left(\frac{b_y}{2}\right)^2 = 4.33 \times 10^{10} \text{ mm}^4$$

Ultimate shear stress due to combined shear and unbalanced moment transfer:

$$v_u = \frac{V_u}{b_o d} + \frac{\gamma_{vy} M_{uy} b_x / 2}{J_{cy}} + \frac{\gamma_{vx} M_{ux} b_y / 2}{J_{cx}} = 1.14 \text{ MPa} < \phi v_c = 1.57 \text{ MPa (OK)}$$

A.10.3 Moment Transferred by Flexure:

The fraction of unbalanced moments transferred by flexure will be checked against the moment resistances within the width of *c* plus 1.5*h* on each side of the column.

Unbalanced moments transferred by flexure about *y*- and *x*-axes:

$\gamma_{fy} M_{uy} = 0.7 \times 2.3 = 1.7$ kN-m

$\gamma_{fx} M_{ux} = 0.5 \times 14.3 = 6.4$ kN-m

Effective depths of tendons in *x*- and *y*-directions:

$d_{px} = 126$ mm

$d_{py} = 126$ mm

Areas of nonprestressed tension reinforcement in *x*- and *y*-directions:

$A_{sx} = 6 \times 133 = 798 \text{ mm}^2$

$A_{sy} = 6 \times 133 = 798 \text{ mm}^2$

Areas of nonprestressed compression reinforcement in *x*- and *y*-directions:

$A'_{sx} = 6 \times 133 = 798 \text{ mm}^2$

$A'_{sy} = 2 \times 133 = 266 \text{ mm}^2$

Areas of prestressing steel in *x*- and *y*-directions:

$A_{psx} = 2 \times 100 = 200 \text{ mm}^2$

$A_{psy} = 6 \times 100 = 600 \text{ mm}^2$

Ratios of prestressing steel in *x*- and *y*-directions:

$$\rho_{px} = \frac{A_{psx}}{(c_y + 3h)d_p} = 0.0012$$

$$\rho_{py} = \frac{A_{psy}}{(c_x + 3h)d_p} = 0.0076$$

Stresses in prestressing steel at nominal flexural strength in *x*- and *y*-directions:

$$f_{psx} = f_{se} + 70 + \frac{f'_c}{300\rho_{px}} = 1263 \text{ MPa}$$

$$f_{psy} = f_{se} + 70 + \frac{f'_c}{300\rho_{py}} = 1186 \text{ MPa}$$

Depths of equivalent rectangular stress block in *x*- and *y*-directions:

$$a_x = \frac{A_{psx} f_{psx} + A_{sx} f_y - A'_{sx} f_y}{0.85 f'_c \ell_y} = 6.9 \text{ mm}$$

$$a_y = \frac{A_{psy} f_{psy} + A_{sy} f_y - A'_{sy} f_y}{0.85 f'_c \ell_x} = 55.8 \text{ mm}$$

Distances from extreme compression fiber to neutral axis in *x*- and *y*-directions:

$$c_x = \frac{a_x}{\beta_1} = 8.4 \text{ mm}$$

$$c_y = \frac{a_y}{\beta_1} = 67.9 \text{ mm}$$

Net tensile strains in extreme tension steel in *x*- and *y*-directions:

$$\varepsilon_{tx} = 0.003\left(\frac{d - c_x}{c_x}\right) = 0.042 > 0.005 \rightarrow \text{tension-controlled}$$

$$\varepsilon_{ty} = 0.003\left(\frac{d - c_y}{c_y}\right) = 0.003,\ 0.002 < \varepsilon_{ty} < 0.005 \rightarrow \text{transition}$$

Strength reduction factors for flexure about *y*- and *x*-axes:

$\phi_y = 0.90$

$\phi_x = 0.65 + (\varepsilon_{tx} - 0.002)(250/3) = 0.70$

Nominal flexural strengths about *y*- and *x*-axes:

$M_{ny} = A_{psx}f_{psx}(d_{px} - a_x/2) + A_{sx}f_y(d - a_x/2) - A'_{sx}f_y(d' - a_x/2) = 68.3$ kN-m

$M_{nx} = A_{psy}f_{psy}(d_{py} - a_y/2) + A_{sy}f_y(d - a_y/2) - A'_{sy}f_y(d' - a_y/2) = 106.2$ kN-m

Design values of flexural strength about *y*- and *x*-axes:

$\phi_y M_{ny} = 0.90 \times 68.3 = 61.5$ kN-m $> \gamma_{fy}M_{uy} = 1.7$ kN-m (OK)

$\phi_x M_{nx} = 0.70 \times 106.2 = 74.1$ kN-m $> \gamma_{fx}M_{ux} = 6.4$ kN-m (OK)

A.11 Deflection

A.11.1 Immediate Deflection

It was assumed that 90% of dead load balanced by the prestressing force. Thus, the loading considered to calculate the slab deflection:

$w_d = 0.1\ w_D + w_L = 2.9$ kPa

Coefficient *k*:

$$k = 0.11(1.5 - 0.5\frac{\ell_y}{\ell_x}) = 0.09$$

Slab immediate deflection:

$$\Delta_i = k\frac{w_d \ell_y^4}{E_c h^3} = 6.3 \text{ mm} < \Delta_{i,all} = \ell_y / 360 = 18.8 \text{ mm (OK)}$$

A.11.2 Long-Term Deflection

The time-dependent factor (ξ) is assumed equal to 2. Thus, the slab long-term deflection:

$$\Delta_l = \xi \times \Delta_i = 12.6 \text{ mm} < \Delta_{l,all} = \ell_y / 480 = 14.1 \text{ mm (OK)}$$

APPENDIX B

EXPERIMENTAL PHOTOGRAPHS

Fig. B.1 Construction of specimen

Fig. B.2 Casting of specimen

Fig. B.3 Curing of concrete

Fig. B.4 Compression test of concrete cubes

Fig. B.5 Compression test of concrete cylinders

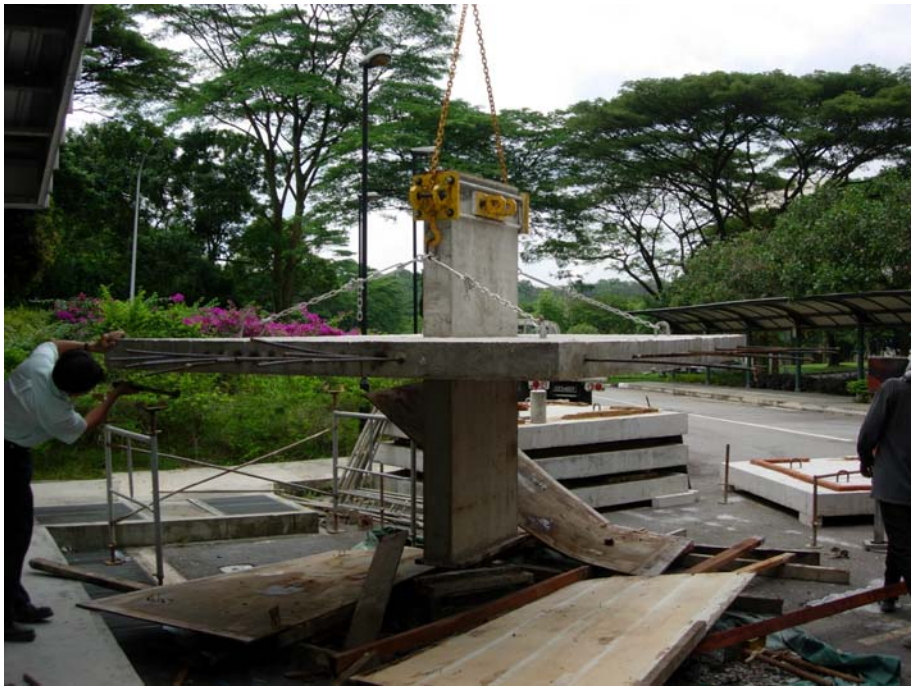

Fig. B.6 Lifting of specimen before test

Fig. B.7 Specimen setup

Fig. B.8 Stressing of tendon

Fig. B.9 Safety precaution

Fig. B.10 De-stressing of tendons

Fig. B.11 Tensile test of reinforcing bars

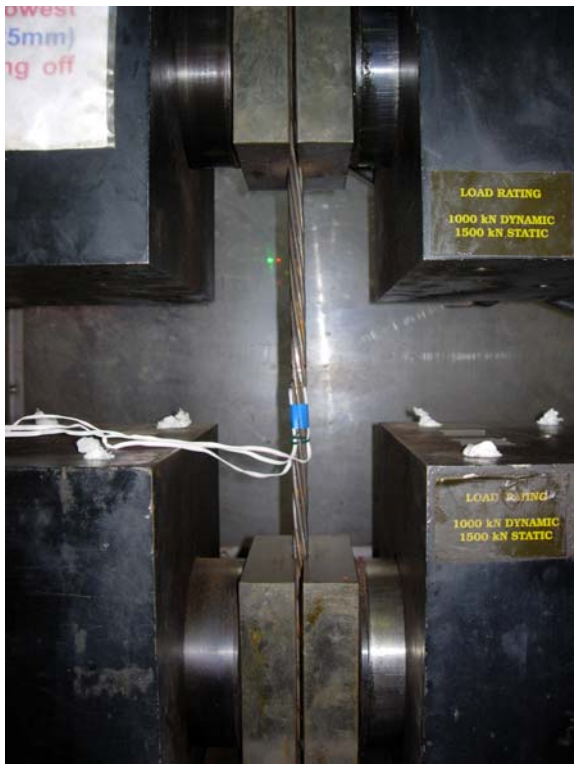

Fig. B.12 Tensile test of strands

APPENDIX C
FLEXURAL CAPACITY BASED ON YIELD-LINE THEORY

Gesund and Goli (1979) presented yield-line patterns that produce flexural failure mechanisms due to combined shear force and unbalanced moment. For interior slab-column connections having rectangular columns, the flexural capacity based on yield-line theory (M_{yl}) is given by:

$$M_{yl} = K \cdot c \cdot \left(m_x + m'_x + m_y + m'_y\right) - \frac{V \cdot c}{2} \tag{C.1}$$

where K is a factor that depend on the column shape and orthotropy of the slab reinforcement; c is the column width perpendicular to the axis of unbalanced moment; V is the applied shear force; and m and m' are the negative and positive yield moments per unit width, respectively. The subscripts x and y denote the direction of reinforcement corresponding to the acting unbalanced moment.

Assuming that the reinforcement is yielded, the yield moment per unit width can be computed:

$$m = \rho \cdot d \cdot f_y \left(d - \frac{a}{2}\right) + \rho_p \cdot d_p \cdot f_{ps} \left(d_p - \frac{a}{2}\right) \tag{C.2}$$

where ρ is the ratio of nonprestressed tension reinforcement within the effective transfer width of c plus 1.5h on each side of the column; d is the effective depth of nonprestressed reinforcement; f_y is the yield strength of nonprestressed reinforcement; ρ_p is the ratio of prestressing steel within the effective transfer width of c plus 1.5h on each side of the column; d_p is the effective depth of prestressing steel at the column centerline; f_{ps} is the stress in prestressing steel at the flexural strength; and a is the depth of compression block given by Eq. (C.3) below:

$$a = \frac{\rho \cdot d \cdot f_y + \rho_p \cdot d_p \cdot f_{ps}}{0.85 f'_c} \tag{C.3}$$

where f'_c is the compressive strength of concrete cylinder and all other terms are as previously defined. The stress in prestressing steel at the flexural strength f_{ps} can be estimated using Eq. (18-3) of ACI 318-11, given below:

$$f_{ps} = f_{se} + 10{,}000 + \frac{f'_c}{300\rho_p} \text{ (psi) or } f_{ps} = f_{se} + 70 + \frac{f'_c}{300\rho_p} \text{ (MPa)} \tag{C.4}$$

where f_{se} is the effective stress in prestressing steel (after allowance for all prestress losses); and all other terms are as previously defined. The value of f_{ps} in Eq. (C.4) shall not be taken greater than the lesser of f_{py} and (f_{se} + 30,000) [for psi unit] or (f_{se} + 210) [for MPa unit], where f_{py} is the yield strength of prestressing steel.

The factor K can be obtained from Fig. C.1 which depends on two factors λ and μ. The factor λ is defined as the ratio of column sides parallel to perpendicular to the axis of unbalanced moment. The coefficients of orthotropy (μ) for unbalanced moments about y- and x-axis are defined as:

$$\mu_y = \frac{m_x + m'_x}{m_y + m'_y} \tag{C.5a}$$

$$\mu_x = \frac{m_y + m'_y}{m_x + m'_x} \tag{C.5b}$$

where all the terms are as previously defined.

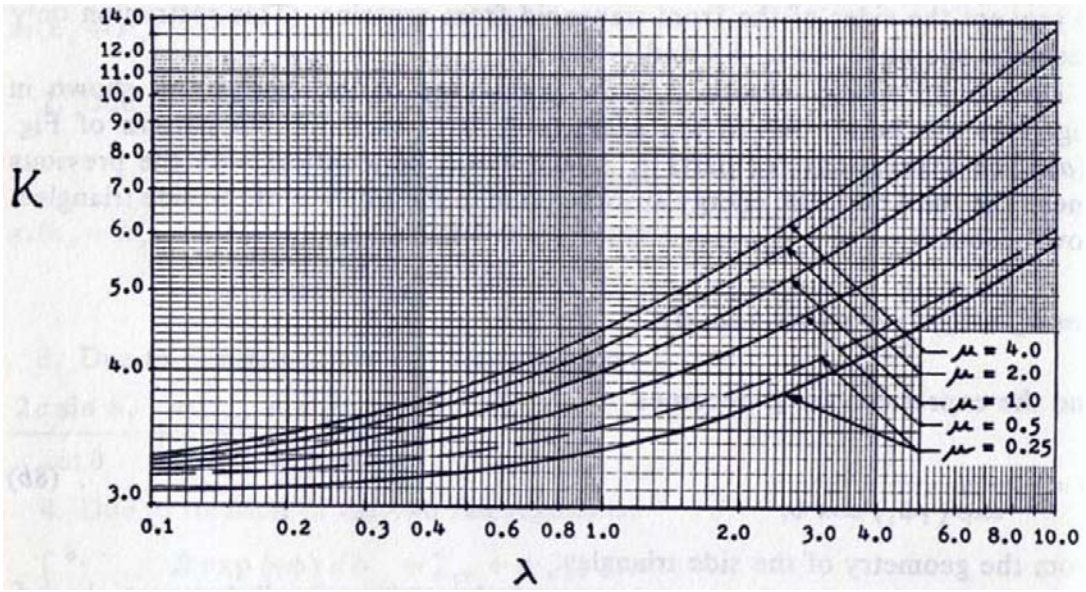

Fig. C.1 Values of K for rectangular columns (Gesund and Goli 1979)

Specimen YL-H2 (Tan and Teng 2005)

The depth of compression block:

$$a_x = \frac{\rho_{tx} \cdot d \cdot f_y}{0.85 f'_c} = 23 \text{ mm}$$

$$a'_x = \frac{\rho_{bx} \cdot d \cdot f_y}{0.85 f'_c} = 8 \text{ mm}$$

$$a_y = \frac{\rho_{ty} \cdot d \cdot f_y}{0.85 f'_c} = 23 \text{ mm}$$

$$a'_y = \frac{\rho_{by} \cdot d \cdot f_y}{0.85 f'_c} = 8 \text{ mm}$$

The yield moment per unit width:

$$m_x = \rho_{tx} \cdot d \cdot f_y \left(d - \frac{a_x}{2} \right) = 84.9 \text{ kNm}$$

$$m'_x = \rho_{bx} \cdot d \cdot f_y \left(d - \frac{a'_x}{2} \right) = 30.2 \text{ kNm}$$

$$m_y = \rho_{ty} \cdot d \cdot f_y \left(d - \frac{a_y}{2} \right) = 84.9 \text{ kNm}$$

$$m'_y = \rho_{by} \cdot d \cdot f_y \left(d - \frac{a'_y}{2} \right) = 30.2 \text{ kNm}$$

The coefficient of orthotropy:

$$\mu_y = \frac{m_x + m'_x}{m_y + m'_y} = 1$$

$$\mu_x = \frac{m_y + m'_y}{m_x + m'_x} = 1$$

The factor λ:

$\lambda_y = c_y/c_x = 5$

$\lambda_x = c_x/c_y = 0.2$

The factor K obtained from Fig. C.1:

$K_y = 6.9$

$K_x = 3.2$

The flexural capacity about *y*- and *x*-axis:

$$M_{yl,y} = K_y \cdot c_x \cdot \left(m_x + m'_x + m_y + m'_y\right) - \frac{V_u \cdot c_x}{2} = 275.2 \text{ kNm}$$

$$M_{yl,x} = K_x \cdot c_y \cdot \left(m_x + m'_x + m_y + m'_y\right) - \frac{V_u \cdot c_y}{2} = 609.2 \text{ kNm}$$

The ratio of unbalanced moment to the flexural capacity:

$M_{uy} / M_{yl,y} = 0.50$

$M_{ux} / M_{yl,x} = 0.22$

Specimen PI-2 (present study)

The stress in prestressing steel at the flexural strength f_{ps}:

$$f_{psx} = f_{sex} + 70 + \frac{f'_c}{300\rho_{px}} = 972 \text{ MPa}$$

$$f_{psy} = f_{sey} + 70 + \frac{f'_c}{300\rho_{py}} = 592 \text{ MPa}$$

The depth of compression block:

$$a_x = \frac{\rho_{tx} \cdot d \cdot f_y + \rho_{px} \cdot d_{px} \cdot f_{psx}}{0.85 f'_c} = 15 \text{ mm}$$

$$a'_x = \frac{\rho_{bx} \cdot d \cdot f_y}{0.85 f'_c} = 10 \text{ mm}$$

$$a_y = \frac{\rho_{ty} \cdot d \cdot f_y + \rho_{py} \cdot d_{py} \cdot f_{psy}}{0.85 f'_c} = 41 \text{ mm}$$

$$a'_y = \frac{\rho_{by} \cdot d \cdot f_y}{0.85 f'_c} = 7 \text{ mm}$$

The yield moment per unit width:

$$m_x = \rho_{tx} \cdot d \cdot f_y \left(d - \frac{a_x}{2}\right) + \rho_{px} \cdot d_{px} \cdot f_{psx} \left(d_{px} - \frac{a_x}{2}\right) = 46.2 \text{ kNm}$$

$$m'_x = \rho_{bx} \cdot d \cdot f_y \left(d - \frac{a'_x}{2}\right) = 32.1 \text{ kNm}$$

$$m_y = \rho_{ty} \cdot d \cdot f_y \left(d - \frac{a_y}{2} \right) + \rho_{py} \cdot d_{py} \cdot f_{psy} \left(d_{py} - \frac{a_y}{2} \right) = 120.2 \text{ kNm}$$

$$m'_y = \rho_{by} \cdot d \cdot f_y \left(d - \frac{a'_y}{2} \right) = 23.6 \text{ kNm}$$

The coefficient of orthotropy:

$$\mu_y = \frac{m_x + m'_x}{m_y + m'_y} = 0.54$$

$$\mu_x = \frac{m_y + m'_y}{m_x + m'_x} = 1.84$$

The factor λ:

$\lambda_y = c_y/c_x = 5$

$\lambda_x = c_x/c_y = 0.2$

The factor K obtained from Fig. C.1:

$K_y = 5.8$

$K_x = 3.3$

The flexural capacity about y- and x-axis:

$$M_{yl,y} = K_y \cdot c_x \cdot \left(m_x + m'_x + m_y + m'_y \right) - \frac{V_u \cdot c_x}{2} = 216.5 \text{ kNm}$$

$$M_{yl,x} = K_x \cdot c_y \cdot \left(m_x + m'_x + m_y + m'_y \right) - \frac{V_u \cdot c_y}{2} = 582.9 \text{ kNm}$$

The ratio of unbalanced moment to the flexural capacity:

$M_{uy} / M_{yl,y} = 0.37$

$M_{ux} / M_{yl,x} = 0.28$

APPENDIX D

DATABASE ON REINFORCED CONCRETE SLAB-COLUMN CONNECTIONS

Table D.1 Interior reinforced concrete slab-column connections having circular/square columns under symmetrical punching

Spec	h mm	CS	c_x mm	c_y mm	f'_c MPa	d mm	ρ_{tx} %	ρ_{ty} %	ρ_{bx} %	ρ_{by} %	f_y MPa	V_u kN
Elstner and Hognestad (1956)												
A-1a	152	S	254	254	14.1	118	1.15	1.15	0.56	0.56	332	302.5
A-1b	152	S	254	254	25.2	118	1.15	1.15	0.56	0.56	332	364.7
A-1c	152	S	254	254	29.0	118	1.15	1.15	0.56	0.56	332	355.8
A-1d	152	S	254	254	36.8	118	1.15	1.15	0.56	0.56	332	351.4
A-1e	152	S	254	254	20.3	118	1.15	1.15	0.56	0.56	332	355.8
A-2a	152	S	254	254	13.7	114	2.47	2.47	1.15	1.15	321	333.6
A-2b	152	S	254	254	19.5	114	2.47	2.47	1.15	1.15	321	400.3
A-2c	152	S	254	254	37.4	114	2.47	2.47	1.15	1.15	321	467.0
A-7b	152	S	254	254	27.9	114	2.47	2.47	1.15	1.15	321	511.5
A-3a	152	S	254	254	12.8	114	3.70	3.70	1.15	1.15	321	355.8
A-3b	152	S	254	254	22.6	114	3.70	3.70	1.15	1.15	321	444.8
A-3c	152	S	254	254	26.5	114	3.70	3.70	1.15	1.15	321	533.8
A-3d	152	S	254	254	34.5	114	3.70	3.70	1.15	1.15	321	547.1
A-4	152	S	356	356	26.1	118	1.15	1.15	0.56	0.56	332	400.3
A-5	152	S	356	356	27.8	114	2.47	2.47	1.15	1.15	321	533.8
A-6	152	S	356	356	25.0	114	3.70	3.70	1.15	1.15	321	498.2
A-7	152	S	254	254	28.5	114	2.47	2.47	1.15	1.15	321	400.3
A-8	152	S	356	356	21.9	114	2.47	2.47	1.15	1.15	321	435.9
A-7a	152	S	254	254	27.9	114	2.47	2.47	1.15	1.15	321	280.2
A-9	152	S	254	254	29.9	114	3.56	3.56	1.15	1.15	321	444.8
A-10	152	S	356	356	29.7	114	3.58	3.58	1.15	1.15	321	489.3
A-13	152	S	356	356	26.2	121	0.55	0.55	0.28	0.28	294	235.7
B-1	152	S	254	254	14.2	114	0.50	0.50	0.00	0.00	324	178.4
B-2	152	S	254	254	47.6	114	0.50	0.50	0.00	0.00	321	200.2
B-4	152	S	254	254	47.7	114	0.99	0.99	0.00	0.00	303	333.6
B-9	152	S	254	254	43.9	114	2.00	2.00	0.00	0.00	341	504.8
B-11	152	S	254	254	13.5	114	3.00	3.00	0.00	0.00	409	329.2
B-14	152	S	254	254	50.5	114	3.00	3.00	0.00	0.00	325	578.2

Table D.1 (Continued)

Spec	h mm	CS	c_x mm	c_y mm	f'_c MPa	d mm	ρ_{tx} %	ρ_{ty} %	ρ_{bx} %	ρ_{by} %	f_y MPa	V_u kN
Kinnunen and Nylander (1960)												
IA15a-5	149	C	150	150	27.9	117	0.80	0.80	0.00	0.00	441	255.0
IA15a-6	151	C	150	150	25.8	118	0.80	0.80	0.00	0.00	454	275.0
IA15c-11	153	C	150	150	31.4	121	1.80	1.80	0.00	0.00	436	334.0
IA15c-12	154	C	150	150	28.8	122	1.70	1.70	0.00	0.00	439	332.0
IA30a-24	158	C	300	300	25.9	128	1.00	1.00	0.00	0.00	456	430.0
IA30a-25	154	C	300	300	24.6	124	1.10	1.10	0.00	0.00	451	408.0
IA30c-30	151	C	300	300	29.5	120	2.10	2.10	0.00	0.00	436	491.0
IA30c-31	151	C	300	300	29.5	119	2.10	2.10	0.00	0.00	448	540.0
IA30d-32	155	C	300	300	25.8	123	0.50	0.50	0.00	0.00	448	258.0
IA30d-33	156	C	300	300	26.2	125	0.50	0.50	0.00	0.00	462	258.0
IA30e-34	150	C	300	300	26.9	120	1.00	1.00	0.00	0.00	461	332.0
IA30e-35	153	C	300	300	24.6	122	1.00	1.00	0.00	0.00	459	332.0
Moe (1961)												
H1	152	S	254	254	26.1	114	1.15	1.15	0.00	0.00	328	375.0
S1-60	152	S	254	254	23.3	114	1.06	1.06	0.00	0.00	399	389.2
S2-60	152	S	254	254	22.1	114	1.03	1.03	0.00	0.00	399	355.8
S3-60	152	S	254	254	22.6	114	1.02	1.02	0.00	0.00	399	363.6
S4-60	152	S	254	254	23.9	114	1.13	1.13	0.00	0.00	399	333.6
S1-70	152	S	254	254	24.5	114	1.06	1.06	0.00	0.00	482	392.3
S3-70	152	S	254	254	25.4	114	1.02	1.02	0.00	0.00	482	378.1
S4-70	152	S	254	254	35.2	114	1.13	1.13	0.00	0.00	482	373.6
S4A-70	152	S	254	254	20.5	114	1.13	1.13	0.00	0.00	482	311.4
S5-60	152	S	203	203	22.2	114	1.06	1.06	0.00	0.00	399	342.5
S5-70	152	S	203	203	24.3	114	1.06	1.06	0.00	0.00	482	378.1
R-2	152	S	152	152	26.5	114	1.38	1.38	0.00	0.00	328	311.4
M1A	152	S	305	305	23.0	114	1.50	1.50	0.00	0.00	481	432.8

Table D.1 (Continued)

Spec	h mm	CS	c_x mm	c_y mm	f'_c MPa	d mm	ρ_{tx} %	ρ_{ty} %	ρ_{bx} %	ρ_{by} %	f_y MPa	V_u kN
Taylor and Hayes (1965)												
2S2	76	S	51	51	25.9	57	1.57	1.57	0.00	0.00	376	71.7
2S3	76	S	76	76	24.5	57	1.57	1.57	0.00	0.00	376	91.1
2S4	76	S	102	102	23.2	57	1.57	1.57	0.00	0.00	376	85.8
2S5	76	S	127	127	22.1	57	1.57	1.57	0.00	0.00	376	96.5
2S6	76	S	152	152	18.4	57	1.57	1.57	0.00	0.00	376	96.5
3S2	76	S	51	51	22.8	57	3.14	3.14	0.00	0.00	376	78.4
3S4	76	S	102	102	22.6	57	3.14	3.14	0.00	0.00	376	115.2
3S6	76	S	152	152	21.6	57	3.14	3.14	0.00	0.00	376	149.9
Bernaert and Puech (1966)												
A1/M1	140	S	203	203	16.3	114	1.10	1.10	0.00	0.00	255	322.0
A1/M2	140	S	203	203	15.5	117	1.50	1.50	0.00	0.00	282	346.0
A1/M3	140	S	203	203	14.2	121	1.90	1.90	0.00	0.00	282	307.0
A1/M4	140	S	203	203	14.0	124	1.00	1.00	0.00	0.00	432	259.0
A1/M5	140	S	203	203	21.0	117	1.20	1.20	0.00	0.00	432	346.0
A2/M1	140	S	203	203	35.4	124	1.00	1.00	0.00	0.00	255	409.0
A2/M2	140	S	203	203	32.8	117	1.50	1.50	0.00	0.00	282	419.0
A2/M3	140	S	203	203	32.5	121	1.90	1.90	0.00	0.00	282	430.0
A2/T1	140	S	203	203	39.3	124	1.00	1.00	0.00	0.00	432	419.0
A2/T2	140	S	203	203	41.4	124	1.70	1.70	0.00	0.00	432	439.0
A3/M1	140	S	203	203	18.8	124	1.00	1.00	0.00	0.00	255	247.0
A3/M2	140	S	203	203	19.3	102	1.70	1.70	0.00	0.00	282	336.0
A3/M3	140	S	203	203	27.3	117	1.90	1.90	0.00	0.00	282	298.0
A3/T1	140	S	203	203	20.6	121	1.00	1.00	0.00	0.00	432	328.0
A3/T2	140	S	203	203	16.0	119	1.20	1.20	0.00	0.00	432	298.0
A4/M1	140	S	203	203	38.3	114	1.10	1.10	0.00	0.00	255	259.0
A4/M2	140	S	203	203	29.2	119	1.50	1.50	0.00	0.00	282	341.0
A4/M3	140	S	203	203	32.2	117	1.90	1.90	0.00	0.00	322	541.0
A4/T1	140	S	203	203	32.8	114	1.10	1.10	0.00	0.00	432	384.0
A4/T2	140	S	203	203	29.3	117	1.20	1.20	0.00	0.00	432	402.0

Table D.1 (Continued)

Spec	h mm	CS	c_x mm	c_y mm	f'_c MPa	d mm	ρ_{tx} %	ρ_{ty} %	ρ_{bx} %	ρ_{by} %	f_y MPa	V_u kN
Manterola (1966)												
P1-S1	125	S	100	100	25.6	107	1.10	1.10	0.00	0.00	304	216.0
P2-S1	125	S	250	250	33.8	107	1.10	1.10	0.00	0.00	304	257.0
P3-S1	125	S	450	450	29.7	107	1.10	1.10	0.00	0.00	304	301.0
P1-S2	125	S	100	100	24.2	107	1.10	1.10	0.50	0.50	324	196.0
P2-S2	125	S	250	250	33.1	107	1.10	1.10	0.50	0.50	324	283.0
P3-S2	125	S	450	450	31.9	107	1.10	1.10	0.50	0.50	324	397.0
P1-S3	125	S	100	100	39.7	107	1.10	1.10	1.10	1.10	324	184.0
P2-S3	125	S	100	100	35.8	107	1.40	1.40	1.10	1.10	324	211.0
P3-S3	125	S	100	100	39.2	107	0.50	0.50	1.10	1.10	324	165.0
P1-S4	125	S	100	100	26.4	107	0.50	0.50	0.00	0.00	451	175.0
P2-S4	125	S	250	250	31.3	107	0.50	0.50	0.00	0.00	451	246.0
P3-S4	125	S	450	450	34.2	107	0.50	0.50	0.00	0.00	451	294.0
Yitzhaki (1966)												
II-5	102	C	221	221	17.2	82	0.50	0.50	0.00	0.00	471	152.0
II-8	102	C	333	333	18.7	82	0.60	0.60	0.00	0.00	456	218.0
IIB20-1	102	S	201	201	11.0	78	0.70	0.70	0.00	0.00	403	128.0
II-1	102	C	221	221	10.5	82	1.20	1.20	0.00	0.00	457	181.0
II-4a	102	C	221	221	17.9	82	0.90	0.90	0.00	0.00	559	245.0
II-4b	102	S	201	201	9.8	82	0.90	0.90	0.00	0.00	466	162.0
II-4c	102	S	201	201	13.9	82	0.90	0.90	0.00	0.00	510	215.0
IIB20-2	102	C	201	201	15.0	83	0.90	0.90	0.00	0.00	500	307.0
IIB30-1	102	C	300	300	17.6	80	2.00	2.00	0.00	0.00	403	239.0
II-2	102	C	221	221	9.8	82	1.30	1.30	0.00	0.00	373	152.0
II-3	102	S	284	284	13.5	82	1.30	1.30	0.00	0.00	491	244.0
II-6	102	C	221	221	21.6	82	1.30	1.30	0.00	0.00	456	240.0
II-9	102	S	201	201	9.3	79	8.50	8.50	0.00	0.00	550	157.0
III-3	102	C	221	221	18.1	82	1.20	1.20	0.00	0.00	559	201.0
7	102	C	119	119	10.0	82	0.70	0.70	0.00	0.00	456	117.0
II-10	102	C	119	119	11.7	82	1.00	1.00	0.00	0.00	385	98.0

Table D.1 (Continued)

Spec	h mm	CS	c_x mm	c_y mm	f'_c MPa	d mm	ρ_{tx} %	ρ_{ty} %	ρ_{bx} %	ρ_{by} %	f_y MPa	V_u kN
Corley and Hawkins (1968)												
AN-1	146	S	254	254	18.7	111	1.54	1.54	0.00	0.00	403	334.0
BN-1	146	S	254	254	20.1	111	1.03	1.03	0.00	0.00	444	265.5
Schaeidt et al. (1970)												
P1	280	C	500	500	27.9	240	1.31	1.31	0.00	0.00	544	1662.0
Hawkins et al. (1971)												
1	152	S	305	305	30.3	117	1.12	1.12	0.00	0.00	412	383.9
Roll et al. (1971)												
A-S-000-0-0-2	61	S	102	102	35.1	46	1.15	1.15	0.00	0.00	359	65.4
A-S-000-0-0-3	61	S	102	102	28.9	46	1.15	1.15	0.00	0.00	359	63.2
A-S-000-0-0-4	61	S	102	102	28.9	46	1.15	1.15	0.00	0.00	359	61.0
A-S-000-0-0-5	61	S	102	102	29.0	46	1.15	1.15	0.00	0.00	359	63.6
B-S-000-0-0-1	61	S	102	102	31.4	46	2.53	2.53	0.00	0.00	368	88.2
B-S-000-0-0-2	61	S	102	102	29.6	46	2.53	2.53	0.00	0.00	462	87.0
H-0-a	61	S	102	102	30.3	46	1.15	1.15	0.00	0.00	374	67.1
H-0-b	61	S	102	102	29.0	46	1.15	1.15	0.00	0.00	440	81.4
Vanderbilt (1972)												
2S1-1	51	S	76	76	27.6	38	1.00	1.00	0.50	0.50	303	42.9
3S1-2	51	S	114	114	23.0	38	1.00	1.00	0.50	0.50	303	46.6
4S1-3	51	S	152	152	20.8	38	1.00	1.00	0.50	0.50	296	51.3
3C1-4	51	C	114	114	22.1	38	1.00	1.00	0.50	0.50	296	58.4
6S1-5	51	S	229	229	21.2	38	1.00	1.00	0.50	0.50	296	78.3
8S1-6	51	S	305	305	20.5	38	1.00	1.00	0.50	0.50	295	90.2
2S2-7	51	S	76	76	23.2	38	2.00	2.00	1.00	1.00	318	49.5
4S2-8	51	S	152	152	21.7	38	2.00	2.00	1.00	1.00	411	69.1
6C1-9	51	C	224	224	25.7	38	1.00	1.00	0.50	0.50	392	96.2
8S2-10	51	S	305	305	26.3	38	2.00	2.00	1.00	1.00	387	114.1
2C1-11	51	C	76	76	19.9	38	1.00	1.00	0.50	0.50	386	39.0
4C1-12	51	C	154	154	22.2	38	1.00	1.00	0.50	0.50	387	72.5
8C1-13	51	C	302	302	24.0	38	1.00	1.00	0.50	0.50	386	100.9
6S2-14	51	S	229	229	20.6	38	2.00	2.00	1.00	1.00	396	80.1
4C2-15	51	C	154	154	21.5	38	2.00	2.00	1.00	1.00	379	96.5

Table D.1 (Continued)

Spec	h mm	CS	c_x mm	c_y mm	f'_c MPa	d mm	ρ_{tx} %	ρ_{ty} %	ρ_{bx} %	ρ_{by} %	f_y MPa	V_u kN
Ladner (1973)												
M1	127	C	226	226	31.8	109	1.20	1.20	0.00	0.00	541	362.0
Stamenković and Chapman (1974)												
V/I/2	76	S	127	127	25.9	56	1.17	1.17	1.17	1.17	434	117.4
Ladner et al. (1977)												
DA6	110	S	100	100	30.0	80	1.79	1.79	1.00	1.00	550	183.0
DA7	110	S	200	200	33.5	80	1.79	1.79	1.00	1.00	550	288.0
DA10	110	S	240	240	32.0	80	1.79	1.79	1.00	1.00	550	281.0
DA11	110	S	320	320	30.4	80	1.79	1.79	1.00	1.00	550	324.0
Marti et al. (1977)												
P2	180	C	300	300	34.6	143	1.48	1.48	0.50	0.50	558	628.0
Pralong et al. (1979)												
P5	191	C	300	300	26.2	171	1.18	1.18	0.30	0.30	515	628.0
Swamy and Ali (1982)												
S1	125	S	150	150	40.1	100	0.57	0.57	0.21	0.21	462	197.7
S7	125	S	150	150	37.4	100	0.76	0.76	0.35	0.35	462	221.7
S19	125	S	150	150	37.6	100	0.38	0.38	0.21	0.21	462	130.7
Kordina and Nölting (1984, 1986)												
V5	150	C	200	200	36.8	126	0.90	0.90	0.00	0.00		349.5
Schaefers (1984)												
0	143	C	210	210	23.1	113	0.83	0.83	0.00	0.00	420	280.0
3	200	C	210	210	23.3	170	0.55	0.55	0.00	0.00	450	460.0

Table D.1 (Continued)

Spec	h mm	CS	c_x mm	c_y mm	f'_c MPa	d mm	ρ_{tx} %	ρ_{ty} %	ρ_{bx} %	ρ_{by} %	f_y MPa	V_u kN
Regan (1986)												
I/1	100	S	200	200	25.8	77	1.20	1.20	0.00	0.00	500	194.0
I/2	100	S	200	200	23.4	77	1.20	1.20	0.00	0.00	500	176.0
I/3	100	S	200	200	27.4	77	0.92	0.92	0.00	0.00	500	194.0
I/4	100	S	200	200	32.3	77	0.92	0.92	0.00	0.00	500	194.0
I/5	100	S	200	200	28.2	79	0.75	0.75	0.00	0.00	480	165.0
I/6	100	S	200	200	21.9	79	0.75	0.75	0.00	0.00	480	165.0
I/7	100	S	200	200	30.4	79	0.80	0.80	0.00	0.00	480	186.0
II/1	250	C	250	250	34.9	200	0.98	0.98	0.00	0.00	530	825.0
II/2	160	C	160	160	33.3	128	0.98	0.98	0.00	0.00	485	390.0
II/3	160	C	160	160	34.3	128	0.98	0.98	0.00	0.00	485	365.0
II/4	80	C	80	80	33.3	64	0.98	0.98	0.00	0.00	480	117.0
II/5	80	C	80	80	34.3	64	0.98	0.98	0.00	0.00	480	105.0
II/6	80	C	80	80	36.2	64	0.98	0.98	0.00	0.00	480	105.0
III/1	120	C	150	150	23.2	95	0.83	0.83	0.00	0.00	494	197.0
III/2	120	C	150	150	9.5	95	0.83	0.83	0.00	0.00	494	123.0
III/3	120	C	150	150	37.8	95	0.83	0.83	0.00	0.00	494	214.0
III/4	120	C	150	150	11.9	93	1.52	1.52	0.00	0.00	464	154.0
III/5	120	C	150	150	26.8	93	1.52	1.52	0.00	0.00	464	214.0
III/6	120	C	150	150	42.6	93	1.52	1.52	0.00	0.00	464	248.0
V/1	150	C	54	54	34.3	118	0.80	0.80	0.00	0.00	628	170.0
V/2	150	C	170	170	32.2	118	0.80	0.80	0.00	0.00	628	280.0
V/3	150	C	110	110	32.4	118	0.80	0.80	0.00	0.00	628	265.0
V/4	150	S	102	102	36.2	118	0.80	0.80	0.00	0.00	628	285.0
V/5	150	C	150	150	32.9	118	0.80	0.80	0.00	0.00	628	285.0

Table D.1 (Continued)

Spec	h mm	CS	c_x mm	c_y mm	f'_c MPa	d mm	ρ_{tx} %	ρ_{ty} %	ρ_{bx} %	ρ_{by} %	f_y MPa	V_u kN
Rankin and Long (1987a)												
1	51	S	100	100	40.0	41	0.42	0.42	0.00	0.00	530	36.4
2	51	S	100	100	40.0	41	0.56	0.56	0.00	0.00	530	49.1
3	51	S	100	100	40.0	41	0.69	0.69	0.00	0.00	530	56.6
4	51	S	100	100	40.0	41	0.82	0.82	0.00	0.00	530	56.2
5	51	S	100	100	40.0	41	0.88	0.88	0.00	0.00	530	57.3
6	51	S	100	100	40.0	41	1.03	1.03	0.00	0.00	530	65.6
7	51	S	100	100	40.0	41	1.16	1.16	0.00	0.00	530	70.9
8	51	S	100	100	40.0	41	1.29	1.29	0.00	0.00	530	71.7
9	51	S	100	100	40.0	41	1.45	1.45	0.00	0.00	530	78.6
10	51	S	100	100	40.0	41	0.52	0.52	0.00	0.00	530	43.6
11	51	S	100	100	40.0	41	0.80	0.80	0.00	0.00	530	55.0
12	51	S	100	100	40.0	41	1.11	1.11	0.00	0.00	530	67.1
13	51	S	100	100	40.0	41	0.60	0.60	0.00	0.00	530	49.4
14	51	S	100	100	40.0	41	0.69	0.69	0.00	0.00	530	52.5
15	51	S	100	100	40.0	41	1.99	1.99	0.00	0.00	530	84.8
1A	57	S	100	100	40.0	47	0.44	0.44	0.00	0.00	530	45.2
2A	57	S	100	100	40.0	47	0.69	0.69	0.00	0.00	530	66.2
3A	57	S	100	100	40.0	47	1.29	1.29	0.00	0.00	530	89.7
4A	57	S	100	100	40.0	47	1.99	1.99	0.00	0.00	530	97.4
1B	46	S	100	100	40.0	35	0.42	0.42	0.00	0.00	530	28.9
2B	46	S	100	100	40.0	35	0.69	0.69	0.00	0.00	530	37.6
3B	46	S	100	100	40.0	35	1.29	1.29	0.00	0.00	530	56.7
4B	46	S	100	100	40.0	35	1.99	1.99	0.00	0.00	530	72.5
1C	64	S	100	100	40.0	54	0.42	0.42	0.00	0.00	530	62.7
2C	64	S	100	100	40.0	54	0.69	0.69	0.00	0.00	530	87.9
3C	64	S	100	100	40.0	54	1.29	1.29	0.00	0.00	530	124.1
4C	64	S	100	100	40.0	54	1.99	1.99	0.00	0.00	530	125.9

Table D.1 (Continued)

Spec	h mm	CS	c_x mm	c_y mm	f'_c MPa	d mm	ρ_{tx} %	ρ_{ty} %	ρ_{bx} %	ρ_{by} %	f_y MPa	V_u kN
Tolf (1988)												
S2.1	240	C	250	250	24.2	200	0.80	0.80	0.00	0.00	657	603.0
S2.2	240	C	250	250	22.9	199	0.80	0.80	0.00	0.00	670	600.0
S2.3	240	C	250	250	25.4	200	0.34	0.34	0.00	0.00	668	489.0
S2.4	240	C	250	250	24.2	197	0.35	0.35	0.00	0.00	664	444.0
S1.1	120	C	125	125	28.6	100	0.80	0.80	0.00	0.00	706	216.0
S1.2	120	C	125	125	22.9	99	0.80	0.80	0.00	0.00	701	194.0
S1.3	120	C	125	125	26.6	98	0.40	0.40	0.00	0.00	720	145.0
S1.4	120	C	125	125	25.1	99	0.40	0.40	0.00	0.00	712	148.0
Lovrovich and McLean (1990)												
F3	102	C	102	102	40.0	83	1.75	1.75	1.75	1.75	531	149.0
F4	102	C	102	102	40.0	83	1.75	1.75	1.75	1.75	531	129.0
F5	102	C	102	102	40.0	83	1.75	1.75	1.75	1.75	531	138.8
Marzouk and Hussein (1991)												
HS1	120	S	150	150	67.0	95	0.49	0.49	0.10	0.10	490	178.0
HS2	120	S	150	150	70.0	95	0.84	0.84	0.10	0.10	490	249.0
HS3	120	S	150	150	69.0	95	1.47	1.47	0.10	0.10	490	356.0
HS4	120	S	150	150	66.0	90	2.37	2.37	0.44	0.44	490	418.0
HS5	150	S	150	150	68.0	125	0.64	0.64	0.08	0.08	490	365.0
HS6	150	S	150	150	70.0	120	0.94	0.94	0.08	0.08	490	489.0
HS7	120	S	150	150	74.0	95	1.19	1.19	0.10	0.10	490	356.0
HS8	150	S	150	150	69.0	120	1.11	1.11	0.33	0.33	490	436.0
HS9	150	S	150	150	74.0	120	1.61	1.61	0.33	0.33	490	543.0
HS10	150	S	150	150	80.0	120	2.33	2.33	0.33	0.33	490	645.0
HS11	90	S	150	150	70.0	70	0.95	0.95	0.14	0.14	490	196.0
HS12	90	S	150	150	75.0	70	1.52	1.52	0.14	0.14	490	258.0
HS13	90	S	150	150	68.0	70	2.00	2.00	0.14	0.14	490	267.0
HS14	120	S	220	220	72.0	95	1.47	1.47	0.10	0.10	490	498.0
HS15	120	S	300	300	71.0	95	1.47	1.47	0.10	0.10	490	560.0
NS1	120	S	150	150	42.0	95	1.47	1.47	0.10	0.10	490	320.0
NS2	150	S	150	150	30.0	120	0.94	0.94	0.08	0.08	490	396.0

Table D.1 (Continued)

Spec	h mm	CS	c_x mm	c_y mm	f'_c MPa	d mm	ρ_{tx} %	ρ_{ty} %	ρ_{bx} %	ρ_{by} %	f_y MPa	V_u kN
Chana and Desai (1992a)												
1	240	S	300	300	32.2	200	0.79	0.79	0.00	0.00	460	805.0
Chana and Desai (1992b)												
FPS1	250	S	400	400	21.4	210	0.86	0.86	0.00	0.00	460	1225.0
Tomaszewicz (1993)												
ND65-1-1	320	S	200	200	64.0	275	1.49	1.49	0.00	0.00	500	2050.0
ND65-2-1	240	S	150	150	70.0	200	1.75	1.75	0.00	0.00	500	1200.0
NG95-1-1	320	S	200	200	84.0	275	1.49	1.49	0.00	0.00	500	2250.0
ND95-1-3	320	S	200	200	90.0	275	2.55	2.55	0.00	0.00	500	2400.0
ND95-2-1	240	S	150	150	88.0	200	1.75	1.75	0.00	0.00	500	1100.0
ND95-2-1D	240	S	150	150	87.0	200	1.75	1.75	0.90	0.90	500	1300.0
ND95-2-3	240	S	150	150	90.0	200	2.62	2.62	0.00	0.00	500	1450.0
ND95-2-3D	240	S	150	150	80.0	200	2.62	2.62	0.90	0.90	500	1250.0
ND95-2-3D+	240	S	150	150	98.0	200	2.62	2.62	0.90	0.90	500	1450.0
ND95-3-1	120	S	100	100	85.0	88	1.84	1.84	0.00	0.00	500	330.0
ND115-1-1	320	S	200	200	112.0	275	1.49	1.49	0.00	0.00	500	2450.0
ND115-2-1	240	S	150	150	119.0	200	1.75	1.75	0.00	0.00	500	1400.0
ND115-2-3	240	S	150	150	108.0	200	2.62	2.62	0.00	0.00	500	1550.0
Gardner and Shao (1996)												
1	140	S	254	254	21.5	120	0.66	0.66	0.42	0.42	460	311.0
Hallgren (1996)												
HSC0	240	C	250	250	90.3	200	0.80	0.80	0.00	0.00	643	965.0
HSC1	245	C	250	250	91.3	200	0.80	0.80	0.00	0.00	627	1021.0
HSC2	240	C	250	250	85.7	194	0.82	0.82	0.00	0.00	620	889.0
HSC4	240	C	250	250	91.6	200	1.19	1.19	0.00	0.00	596	1041.0
HSC6	239	C	250	250	108.8	201	0.60	0.60	0.00	0.00	633	960.0
N/HSC8	242	C	250	250	94.9	198	0.80	0.80	0.00	0.00	631	944.0
HSC9	239	C	250	250	84.1	202	0.33	0.33	0.00	0.00	634	565.0

Table D.1 (Continued)

Spec	h mm	CS	c_x mm	c_y mm	f'_c MPa	d mm	ρ_{tx} %	ρ_{ty} %	ρ_{bx} %	ρ_{by} %	f_y MPa	V_u kN
Marzouk et al. (1996)												
N.H.Z.S.1.0	150	S	250	250	32.2	119	1.00	1.00	0.40	0.40	460	475.5
N.N.Z.S.1.0	150	S	250	250	37.2	119	1.00	1.00	0.40	0.40	460	484.8
Ramdane (1996)												
1	125	C	150	150	88.2	98	0.60	0.60	0.00	0.00	550	224.0
2	125	C	150	150	56.2	98	0.60	0.60	0.00	0.00	550	212.0
3	125	C	150	150	26.9	98	0.60	0.60	0.00	0.00	550	169.0
4	125	C	150	150	58.7	98	0.60	0.60	0.00	0.00	550	233.0
6	125	C	150	150	101.6	98	0.60	0.60	0.00	0.00	550	233.0
12	125	C	150	150	60.4	98	1.30	1.30	0.00	0.00	550	319.0
13	125	C	150	150	43.6	98	1.30	1.30	0.00	0.00	550	297.0
14	125	C	150	150	60.8	98	1.30	1.30	0.00	0.00	550	341.0
16	125	C	150	150	98.4	98	1.30	1.30	0.00	0.00	550	362.0
21	125	C	150	150	41.9	98	1.30	1.30	0.00	0.00	650	286.0
22	125	C	150	150	84.2	98	1.30	1.30	0.00	0.00	650	405.0
23	125	C	150	150	56.4	100	0.90	0.90	0.00	0.00	650	341.0
25	125	C	150	150	32.9	100	1.20	1.20	0.00	0.00	650	244.0
26	125	C	150	150	37.6	100	1.20	1.20	0.00	0.00	650	294.0
27	125	C	150	150	33.7	102	1.00	1.00	0.40	0.40	650	227.0
Hassanzadeh (1998)												
B1	220	C	250	250	41.0	190	0.29	0.29	0.00	0.00	582	439.0
Marzouk et al. (1998)												
H.H.Z.S.1.0	150	S	250	250	67.2	119	1.00	1.00	0.40	0.40	460	511.5
Broms (2000)												
9	180	S	180	180	26.9	150	0.52	0.52	0.24	0.24	500	408.0
9a	180	S	180	180	21.0	150	0.52	0.52	0.24	0.24	500	360.0
McHarg et al. (2000)												
NU	150	S	225	225	30.0	110	1.11	1.11	0.40	0.40	444	306.0
NB	150	S	225	225	30.0	110	2.15	2.15	0.40	0.40	444	349.0

Table D.1 (Continued)

Spec	h mm	CS	c_x mm	c_y mm	f'_c MPa	d mm	ρ_{tx} %	ρ_{ty} %	ρ_{bx} %	ρ_{by} %	f_y MPa	V_u kN
Melges (2000)												
M1B	160	S	180	180	26.6	127	1.58	1.58	0.00	0.00		442.0
Oliveira et al. (2000)												
1	130	S	120	120	60.9	93	1.50	1.50	0.22	0.22	695	270.0
2	130	S	120	120	62.9	97	1.40	1.40	0.21	0.21	695	335.0
Osman et al. (2000)												
NSNW0.5P	150	S	250	250	37.8	120	0.49	0.49	0.24	0.24	450	310.2
Corrêa (2001)												
LP1	130	S	150	150	50.7	105	1.17	1.17	0.00	0.00		327.0
Lee (2004)												
C11F22	200	S	250	250	34.3	160	2.08	2.08	0.88	0.88	500	627.0
1F11	125	S	180	180	82.9	87	0.98	0.98	0.98	0.98	505	370.0
1F12	125	S	180	180	82.9	85	2.12	0.98	1.01	1.01	513	410.0
1F22	125	S	180	180	83.0	84	2.12	2.12	1.02	1.02	520	420.0
2F11	200	S	290	290	80.8	159	1.01	1.01	1.20	1.20	520	800.0
2F12	200	S	290	290	83.6	156	1.93	1.01	1.23	1.23	510	1020.0
2F22	200	S	290	290	80.6	155	1.93	1.93	1.24	1.24	500	1100.0
3F11	275	S	400	400	88.1	230	1.04	1.04	0.61	0.61	500	1440.0
3F22	275	S	400	400	78.2	230	1.44	1.44	0.61	0.61	500	1640.0
Oliveira et al. (2004)												
L1a	130	S	120	120	57.0	107	1.09	1.09	0.26	0.26	749	240.0
L1b	130	S	120	120	59.0	108	1.08	1.08	0.26	0.26	749	322.4
L1c	130	S	120	120	59.0	107	1.09	1.09	0.26	0.26	749	318.0
Teng et al. (2004)												
OC11	150	S	200	200	36.0	105	1.81	1.81	1.05	1.05	461	423.0

Table D.1 (Continued)

Spec	h mm	CS	c_x mm	c_y mm	f'_c MPa	d mm	ρ_{tx} %	ρ_{ty} %	ρ_{bx} %	ρ_{by} %	f_y MPa	V_u kN
Papanikolaou et al. (2005)												
P51	100	C	150	150	33.1	80	0.54	0.54	0.00	0.00	550	210.0
P52	100	C	150	150	34.5	80	0.54	0.54	0.00	0.00	550	219.0
P53	100	C	150	150	31.1	80	0.54	0.54	0.00	0.00	550	216.0
P101	100	C	150	150	33.9	80	1.08	1.08	0.00	0.00	550	256.9
P102	100	C	150	150	31.7	80	1.08	1.08	0.00	0.00	550	244.0
P103	100	C	150	150	32.5	80	1.08	1.08	0.00	0.00	550	248.9
P10-5	100	C	150	150	29.1	80	0.54	0.54	0.00	0.00	550	164.0
P10-10	100	C	150	150	32.5	80	1.08	1.08	0.00	0.00	550	225.0
P15-5	150	C	150	150	32.1	130	0.54	0.54	0.00	0.00	550	310.4
P15-10	150	C	150	150	30.6	130	1.08	1.08	0.00	0.00	550	355.2
P20-5	200	C	150	150	30.3	180	0.54	0.54	0.00	0.00	550	459.1
P20-10	200	C	150	150	32.1	180	1.08	1.08	0.00	0.00	550	501.1
P25-5	250	C	150	150	32.5	230	0.54	0.54	0.00	0.00	550	587.5
P25-10	250	C	150	150	29.4	230	1.08	1.08	0.00	0.00	550	635.7
Birkle and Dilger (2008)												
1	160	S	250	250	36.2	124	1.54	1.54	0.40	0.40	488	483.0
7	230	S	300	300	35.0	190	1.30	1.30	0.26	0.26	531	825.0
10	300	S	350	350	31.4	260	1.00	1.00	0.19	0.19	524	1046.0
Lee et al. (2008)												
30U	150	S	225	225	30.0	110	1.11	1.11	0.27	0.27	434	306.0
30B	150	S	225	225	30.0	110	2.15	2.15	0.27	0.27	434	349.0
35U	150	S	225	225	37.2	110	1.18	1.18	0.27	0.27	445	301.0
35B	150	S	225	225	37.2	110	2.15	2.15	0.27	0.27	445	317.0
55U	150	S	225	225	57.1	110	1.18	1.18	0.27	0.27	445	363.0
55B	150	S	225	225	57.1	110	2.15	2.15	0.27	0.27	445	447.0
65U	150	S	225	225	67.1	110	1.18	1.18	0.27	0.27	445	443.0
65B	150	S	225	225	67.1	110	2.15	2.15	0.27	0.27	445	485.0

Table D.1 (Continued)

Spec	h mm	CS	c_x mm	c_y mm	f'_c MPa	d mm	ρ_{tx} %	ρ_{ty} %	ρ_{bx} %	ρ_{by} %	f_y MPa	V_u kN
Tian et al. (2008)												
LG0.5	152	S	406	406	33.2	127	0.50	0.50	0.30	0.30	455	324.0
LG1.0	152	S	406	406	27.6	127	1.00	1.00	0.30	0.30	421	400.0
G0.5	152	S	406	406	31.3	127	0.50	0.50	0.30	0.30	421	312.0
G1.0	152	S	406	406	28.0	127	1.00	1.00	0.30	0.30	421	404.0
Guandalini et al. (2009)												
PG-1	250	S	260	260	27.6	210	1.50	1.50	0.20	0.20	573	1031.0
PG-2b	250	S	260	260	40.6	210	0.25	0.25	0.20	0.20	552	440.0
PG-3	500	S	520	520	32.4	456	0.33	0.33	0.20	0.20	520	2164.0
PG-4	250	S	260	260	32.2	210	0.25	0.25	0.20	0.20	541	409.0
PG-5	250	S	260	260	29.3	210	0.33	0.33	0.20	0.20	555	563.0
PG-6	125	S	130	130	34.7	96	1.50	1.50	0.00	0.00	526	238.0
PG-7	125	S	130	130	34.7	100	0.75	0.75	0.00	0.00	550	242.0
PG-8	130	S	130	130	34.7	117	0.28	0.28	0.00	0.00	525	140.0
PG-9	130	S	130	130	34.7	117	0.22	0.22	0.00	0.00	525	116.0
PG-10	250	S	260	260	28.5	210	0.33	0.33	0.20	0.20	577	540.0
PG-11	250	S	260	260	31.5	210	0.75	0.75	0.20	0.20	570	772.0

Notes: h = slab thickness; CS = column shape (C = circular, S = square, R = rectangular); c_x, c_y = column widths in x- and y-directions, respectively; f'_c = compressive strength of concrete cylinder; d = effective depth of nonprestressed reinforcement; ρ_{tx}, ρ_{ty} = top nonprestressed reinforcement ratios within c plus 1.5h on each side of column in x- and y-directions, respectively; ρ_{bx}, ρ_{by} = bottom nonprestressed reinforcement ratios within c plus 1.5h on each side of column in x- and y-directions, respectively; f_y = yield strength of nonprestressed reinforcement; V_u = ultimate shear force; Shaded cells belong to *fib* Bulletin 12 category (1 mm = 0.0394 in, 1 MPa = 145 psi, 1 kN = 0.225 kip, 1 kN-m = 0.737 ft-kips)

Table D.2 Interior reinforced concrete slab-column connections having rectangular columns under symmetrical punching

Spec	h mm	CS	c_x mm	c_y mm	f'_c MPa	d mm	ρ_{tx} %	ρ_{ty} %	ρ_{bx} %	ρ_{by} %	f_y MPa	V_u kN
Moe (1961)												
R-1	152	R	152	457	27.6	114	1.38	1.38	0.00	0.00	328	393.6
Hawkins et al. (1971)												
2	152	R	203	406	26.3	117	1.12	1.12	0.00	0.00	412	351.4
3	152	R	152	457	32.0	117	1.12	1.12	0.00	0.00	412	333.2
4	152	R	114	495	31.0	117	1.12	1.12	0.00	0.00	412	330.5
5	152	R	152	457	26.9	117	1.44	1.44	0.00	0.00	412	355.0
6	152	R	457	152	22.7	117	1.12	1.12	0.00	0.00	412	335.8
7	152	R	152	457	25.9	117	0.87	0.87	0.00	0.00	412	319.8
8	152	R	114	495	26.1	121	0.81	0.81	0.00	0.00	414	314.5
9	152	R	152	305	29.5	121	0.77	0.77	0.00	0.00	414	315.4
Stamenković and Chapman (1974)												
V/Ir/1	76	R	152	76	25.2	56	1.17	1.17	1.17	1.17	414	108.6
Lee (2004)												
C13F22	200	R	250	750	35.4	160	1.75	1.85	0.74	0.78	500	792.0
C15F22	200	R	250	1250	35.9	160	1.91	1.85	0.81	0.78	500	1056.0
Oliveira et al. (2004)												
L2a	130	R	120	240	58.0	109	1.07	1.07	0.26	0.26	749	246.0
L2b	130	R	120	240	58.0	106	1.10	1.10	0.26	0.26	749	361.0
L2c	130	R	120	240	57.0	107	1.09	1.09	0.26	0.26	749	330.8
L3a	130	R	120	360	56.0	108	1.08	1.08	0.26	0.26	749	240.6
L3b	130	R	120	360	60.0	107	1.09	1.09	0.26	0.26	749	400.0
L3c	130	R	120	360	54.0	106	1.10	1.10	0.26	0.26	749	357.6
L4a	130	R	120	480	56.0	108	1.08	1.08	0.26	0.26	749	250.8
L4b	130	R	120	480	54.0	106	1.10	1.10	0.26	0.26	749	395.0
L4c	130	R	120	480	56.0	107	1.09	1.09	0.26	0.26	749	404.0
L5a	130	R	120	600	57.0	108	1.08	1.08	0.26	0.26	749	287.4
L5b	130	R	120	600	67.0	108	1.08	1.08	0.26	0.26	749	426.4
L5c	130	R	120	600	63.0	109	1.07	1.07	0.26	0.26	749	446.4

Table D.2 (Continued)

Spec	h mm	CS	c_x mm	c_y mm	f'_c MPa	d mm	ρ_{tx} %	ρ_{ty} %	ρ_{bx} %	ρ_{by} %	f_y MPa	V_u kN
Teng et al. (2004)												
OC13	150	R	200	600	35.8	107	1.71	1.71	1.03	1.03	461	568.0
OC13-1.6	150	R	200	600	33.0	110	1.67	1.67	1.00	1.00	461	508.0
OC13-0.63	150	R	200	600	39.7	111	1.65	1.65	1.00	1.00	461	455.0
OC15	150	R	200	1000	40.2	103	1.76	1.76	1.07	1.07	461	649.0

Notes: h = slab thickness; CS = column shape (C = circular, S = square, R = rectangular); c_x, c_y = column widths in x- and y-directions, respectively; f'_c = compressive strength of concrete cylinder; d = effective depth of nonprestressed reinforcement; ρ_{tx}, ρ_{ty} = top nonprestressed reinforcement ratios within c plus 1.5h on each side of column in x- and y-directions, respectively; ρ_{bx}, ρ_{by} = bottom nonprestressed reinforcement ratios within c plus 1.5h on each side of column in x- and y-directions, respectively; f_y = yield strength of nonprestressed reinforcement; V_u = ultimate shear force (1 mm = 0.0394 in, 1 MPa = 145 psi, 1 kN = 0.225 kip, 1 kN-m = 0.737 ft-kips)

Table D.3 Interior reinforced concrete slab-column connections having square columns with unbalanced moment transfer

Spec	h mm	CS	c_x mm	c_y mm	f'_c MPa	d mm	ρ_{tx} %	ρ_{ty} %	ρ_{bx} %	ρ_{by} %	f_y MPa	V_u kN	M_{uy} kN-m	M_{ux} kN-m
Elstner and Hognestad (1956)														
A-11	152	S	356	356	25.9	114	2.47	2.47	1.15	1.15	321	529.3	94.1	-
A-12	152	S	356	356	28.4	114	2.47	2.47	2.47	2.47	321	529.3	94.1	-
Moe (1961)														
M2A	152	S	305	305	15.5	114	1.50	1.50	0.00	0.00	481	212.6	39.4	-
M4A	152	S	305	305	17.7	114	1.50	1.50	0.00	0.00	481	143.7	62.4	-
M2	152	S	305	305	25.7	114	1.50	1.50	0.00	0.00	481	292.2	57.2	-
M3	152	S	305	305	22.7	114	1.50	1.50	0.00	0.00	481	207.3	70.0	-
M4	152	S	305	305	24.6	114	1.50	1.50	0.00	0.00	481	131.7	57.5	-
M5	152	S	305	305	27.0	114	1.50	1.50	0.00	0.00	481	101.0	62.1	-
M6	152	S	254	254	26.5	114	1.34	1.34	0.00	0.00	328	239.3	40.2	-
M7	152	S	254	254	25.0	114	1.34	1.34	0.00	0.00	328	311.4	19.0	-
M8	152	S	254	254	24.6	114	1.34	1.34	0.57	0.57	328	149.5	65.3	-
M9	152	S	254	254	23.2	114	1.34	1.34	0.00	0.00	328	266.9	33.9	-
M10	152	S	254	254	21.1	114	1.34	1.34	0.57	0.57	328	177.9	54.8	-
Hanson and Hanson (1968)														
A1	76	S	152	152	30.3	57	1.63	1.63	1.63	1.63	365	5.7	22.3	-
A9	76	S	152	152	34.8	57	1.63	1.63	1.63	1.63	369	62.9	0.7	-
A12	76	S	152	152	33.2	57	1.63	1.63	1.63	1.63	372	26.9	20.5	-
Stamenković and Chapman (1974)														
C/I/1	76	S	127	127	36.0	56	1.17	1.17	1.17	1.17	434	84.5	7.3	-
C/I/2	76	S	127	127	29.7	56	1.17	1.17	1.17	1.17	434	62.3	10.5	-
C/I/3	76	S	127	127	25.5	56	1.17	1.17	1.17	1.17	434	33.8	13.6	-
C/I/4	76	S	127	127	25.1	56	1.17	1.17	1.17	1.17	434	20.9	16.7	-
M/I/1	76	S	127	127	28.1	56	1.17	1.17	1.17	1.17	434	-	18.4	-
M/I/2	76	S	127	127	29.2	56	1.17	1.17	1.17	1.17	434	-	17.6	-
Ghali et al. (1976)														
SM0.5	152	S	305	305	36.8	120	0.50	0.50	0.17	0.17	476	129.0	100.0	-
SM1.0	152	S	305	305	33.4	120	1.00	1.00	0.33	0.33	476	129.0	128.0	-
SM1.5	152	S	305	305	40.0	120	1.50	1.50	0.50	0.50	476	129.0	133.0	-

Table D.3 (Continued)

Spec	h mm	CS	c_x mm	c_y mm	f'_c MPa	d mm	ρ_{tx} %	ρ_{ty} %	ρ_{bx} %	ρ_{by} %	f_y MPa	V_u kN	M_{uy} kN-m	M_{ux} kN-m
Islam and Park (1976)														
1	89	S	229	229	27.3	70	1.14	1.14	0.57	0.57	356	35.8	30.5	-
2	89	S	229	229	31.9	70	1.14	1.14	0.57	0.57	374	35.8	37.7	-
Elgabry and Ghali (1987)														
1	150	S	250	250	35.0	116	1.10	1.10	0.43	0.43	452	150.0	130.0	-
Hawkins et al. (1989)														
6AH	152	S	305	305	31.3	121	0.60	0.60	0.30	0.30	467	169.0	90.4	-
9.6AH	152	S	305	305	30.7	118	0.96	0.96	0.48	0.48	444	187.0	97.7	-
14AH	152	S	305	305	30.3	114	1.40	1.40	0.70	0.70	446	205.0	100.0	-
6AL	152	S	305	305	22.7	121	0.60	0.60	0.30	0.30	467	244.0	32.7	-
9.6AL	152	S	305	305	28.9	118	0.96	0.96	0.48	0.48	444	257.0	34.6	-
14AL	152	S	305	305	27.0	114	1.40	1.40	0.70	0.70	446	319.0	43.4	-
7.3BH	114	S	305	305	22.2	83	0.73	0.73	0.36	0.36	467	80.0	39.0	-
9.5BH	114	S	305	305	19.8	83	0.95	0.95	0.47	0.47	467	94.0	45.4	-
14.2BH	114	S	305	305	29.5	79	1.42	1.42	0.71	0.71	444	102.0	51.0	-
7.3BL	114	S	305	305	18.1	83	0.73	0.73	0.36	0.36	467	130.0	12.8	-
9.5BL	114	S	305	305	20.0	83	0.95	0.95	0.47	0.47	467	142.0	16.6	-
14.2BL	114	S	305	305	20.5	79	1.42	1.42	0.71	0.71	444	162.0	20.9	-
6CH	152	S	305	305	52.4	121	0.60	0.60	0.30	0.30	467	186.0	95.1	-
9.6CH	152	S	305	305	57.2	118	0.96	0.96	0.48	0.48	444	218.0	113.0	-
14CH	152	S	305	305	54.7	114	1.40	1.40	0.70	0.70	446	252.0	133.0	-
6CL	152	S	305	305	49.5	121	0.60	0.60	0.30	0.30	467	273.0	36.8	-
14CL	152	S	305	305	47.7	114	1.40	1.40	0.70	0.70	446	362.0	49.4	-
10.2FHI	152	S	305	305	25.9	114	1.02	1.02	0.52	0.52	446	153.0	74.0	-
10.2FHO	152	S	305	305	33.8	114	1.02	1.02	0.52	0.52	446	183.0	89.9	-
14FH	152	S	305	305	31.2	114	1.40	1.40	0.64	0.64	420	206.0	102.5	-
6FLI	152	S	305	305	25.9	121	0.60	0.60	0.28	0.28	472	227.0	27.1	-
10.2FLI	152	S	305	305	18.1	114	1.02	1.02	0.52	0.52	446	240.0	26.9	-
10.2FLO	152	S	305	305	26.5	114	1.02	1.02	0.52	0.52	446	290.0	35.0	-

Table D.3 (Continued)

Spec	h mm	CS	c_x mm	c_y mm	f'_c MPa	d mm	ρ_{tx} %	ρ_{ty} %	ρ_{bx} %	ρ_{by} %	f_y MPa	V_u kN	M_{uy} kN-m	M_{ux} kN-m
Luo and Durrani (1995a)														
INT1	114	S	254	254	31.0	97	0.55	0.55	0.00	0.00	418	139.7	39.2	-
INT2	114	S	254	254	30.7	97	0.55	0.55	0.00	0.00	418	152.1	31.6	-
Marzouk et al. (1996)														
N.H.L.S.0.5	150	S	250	250	43.2	119	0.50	0.50	0.40	0.40	460	266.2	44.4	-
N.H.L.S.1.0	150	S	250	250	42.7	119	1.00	1.00	0.40	0.40	460	408.2	52.7	-
N.N.H.S.1.0	150	S	250	250	36.2	119	1.00	1.00	0.40	0.40	460	163.6	117.5	-
N.H.H.S.0.5	150	S	250	250	34.0	119	0.50	0.50	0.40	0.40	460	164.3	97.8	-
N.H.H.S.1.0	150	S	250	250	35.3	119	1.00	1.00	0.40	0.40	460	250.3	116.1	-
Marzouk et al. (1998)														
H.H.H.S.0.5	150	S	250	250	74.0	119	0.50	0.50	0.40	0.40	460	200.2	118.0	-
H.H.H.S.1.0	150	S	250	250	73.8	119	1.00	1.00	0.40	0.40	460	262.4	132.6	-
Sherif and Dilger (2000a)														
S1-1	150	S	250	250	28.0	114	1.41	1.41	0.75	0.75	444	399.0	0.5	-

Notes: h = slab thickness; CS = column shape (C = circular, S = square, R = rectangular); c_x, c_y = column widths in x- and y-directions, respectively; f'_c = compressive strength of concrete cylinder; d = effective depth of nonprestressed reinforcement; ρ_{tx}, ρ_{ty} = top nonprestressed reinforcement ratios within c plus 1.5h on each side of column in x- and y-directions, respectively; ρ_{bx}, ρ_{by} = bottom nonprestressed reinforcement ratios within c plus 1.5h on each side of column in x- and y-directions, respectively; f_y = yield strength of nonprestressed reinforcement; V_u = ultimate shear force; M_{uy}, M_{ux} = ultimate unbalanced moments acting at centroid of column section about y- and x-axes, respectively (1 mm = 0.0394 in, 1 MPa = 145 psi, 1 kN = 0.225 kip, 1 kN-m = 0.737 ft-kips)

Table D.4 Interior reinforced concrete slab-column connections having rectangular columns with unbalanced moment transfer

Spec	h mm	CS	c_x mm	c_y mm	f'_c MPa	d mm	ρ_{tx} %	ρ_{ty} %	ρ_{bx} %	ρ_{by} %	f_y MPa	V_u kN	M_{uy} kN-m	M_{ux} kN-m
Hanson and Hanson (1968)														
B7	76	R	305	152	33.0	57	1.63	1.63	1.63	1.63	354	4.9	35.7	-
C8	76	R	152	305	32.8	57	1.63	1.63	1.63	1.63	411	5.6	31.4	-
B16	76	R	305	152	30.4	57	1.63	1.63	1.63	1.63	341	34.4	27.3	-
C17	76	R	152	305	36.0	57	1.63	1.63	1.63	1.63	341	31.5	24.7	-
Stamenković and Chapman (1974)														
C/Ir/1	76	R	152	76	22.6	56	1.17	1.17	1.17	1.17	414	85.7	7.3	-
C/Ir/2	76	R	152	76	29.2	56	1.17	1.17	1.17	1.17	414	67.3	10.9	-
C/Ir/3	76	R	152	76	28.6	56	1.17	1.17	1.17	1.17	414	39.9	15.7	-
C/Ir/4	76	R	152	76	26.6	56	1.17	1.17	1.17	1.17	414	21.6	16.8	-
M/Ir/1	76	R	152	76	26.0	56	1.17	1.17	1.17	1.17	414	-	18.6	-
Hawkins et al. (1989)														
9.6GH2	152	R	406	203	24.7	118	0.96	0.96	0.48	0.48	444	165.0	82.3	-
9.6GH.5	152	R	203	406	26.3	118	0.96	0.96	0.48	0.48	444	182.0	89.6	-
9.6GH3	152	R	457	152	27.0	118	0.96	0.96	0.48	0.48	444	165.0	83.4	-
Suwita et al. (2001)														
S1C1	150	R	200	600	33.0	114	1.76	1.76	0.97	0.97	515	384.0	74.2	73.0
S1C2	150	R	200	600	33.0	114	1.76	1.76	0.97	0.97	515	352.0	120.7	118.6
S1C3	150	R	200	600	33.0	114	1.76	1.76	0.97	0.97	515	316.0	40.4	80.8
S1C4	150	R	200	600	33.0	114	1.76	1.76	0.97	0.97	515	432.0	118.1	51.8

Notes: h = slab thickness; CS = column shape (C = circular, S = square, R = rectangular); c_x, c_y = column widths in x- and y-directions, respectively; f'_c = compressive strength of concrete cylinder; d = effective depth of nonprestressed reinforcement; ρ_{tx}, ρ_{ty} = top nonprestressed reinforcement ratios within c plus 1.5h on each side of column in x- and y-directions, respectively; ρ_{bx}, ρ_{by} = bottom nonprestressed reinforcement ratios within c plus 1.5h on each side of column in x- and y-directions, respectively; f_y = yield strength of nonprestressed reinforcement; V_u = ultimate shear force; M_{uy}, M_{ux} = ultimate unbalanced moments acting at centroid of column section about y- and x-axes, respectively (1 mm = 0.0394 in, 1 MPa = 145 psi, 1 kN = 0.225 kip, 1 kN-m = 0.737 ft-kips)

Table D.5 Edge reinforced concrete slab-column connections having square columns

Spec	h mm	CS	c_x mm	c_y mm	f'_c MPa	d mm	ρ_{tx} %	ρ_{ty} %	ρ_{bx} %	ρ_{by} %	f_y MPa	V_u kN	M_{uy} kN-m	M_{ux} kN-m
Hanson and Hanson (1968)														
D15	76	S	152	152	31.1	57	1.63	1.63	1.63	1.63	365	12.1	9.9	-
Zaghlool (1971)														
Z-IV(1)	152	S	178	178	27.4	121	1.49	2.41	0.00	0.00	476	122.3	45.0	-
Z-V(1)	152	S	267	267	34.3	121	1.31	1.60	0.00	0.00	474	215.3	84.6	-
Z-V(2)	152	S	267	267	40.5	121	1.58	2.00	0.00	0.00	474	246.9	93.5	-
Z-V(3)	152	S	267	267	38.7	118	1.82	1.65	0.00	0.00	475	268.2	103.6	-
Z-V(4)	152	S	267	267	35.0	121	1.31	1.60	0.00	0.00	437	-	81.4	-
Z-V(5)	152	S	267	267	35.2	121	1.31	1.60	0.00	0.00	476	279.3	0.0	-
Z-V(6)	152	S	267	267	31.3	121	1.31	1.60	0.00	0.00	476	117.0	88.1	-
Z-VI(1)	152	S	356	356	26.0	121	1.16	2.41	0.00	0.00	476	265.1	106.9	-
Stamenković and Chapman (1974)														
Ct/E/1	76	S	127	127	27.9	56	1.17	1.17	1.17	1.17	448	45.8	-	4.9
Ct/E/2	76	S	127	127	28.4	56	1.17	1.17	1.17	1.17	448	34.9	-	5.7
Ct/E/3	76	S	127	127	27.9	56	1.17	1.17	1.17	1.17	414	23.5	-	9.4
Ct/E/4	76	S	127	127	29.2	56	1.17	1.17	1.17	1.17	448	12.9	-	10.1
Mt/E/1	76	S	127	127	29.0	56	1.17	1.17	1.17	1.17	448	-	-	12.1
V/E/1	76	S	127	127	28.7	56	1.17	1.17	1.17	1.17	496	74.7	0.0	-
Cn/E/1	76	S	127	127	30.8	56	1.17	1.17	1.17	1.17	448	73.2	5.6	-
Cn/E/2	76	S	127	127	25.9	56	1.17	1.17	1.17	1.17	496	54.7	9.2	-
Cn/E/3	76	S	127	127	27.2	56	1.17	1.17	1.17	1.17	496	24.9	10.1	-
Cn/E/4	76	S	127	127	27.5	56	1.17	1.17	1.17	1.17	496	10.9	8.8	-
Mn/E/1	76	S	127	127	24.3	56	1.17	1.17	1.17	1.17	496	-	8.5	-
Mn/E/2	76	S	127	127	26.5	56	1.17	1.17	1.17	1.17	496	-	8.4	-
Hawkins et al. (1978)														
E1	165	S	305	305	22.5	130	0.76	0.76	0.00	0.00	463	63.6	67.7	-
E2	178	S	406	406	29.5	140	1.07	1.07	0.00	0.00	425	83.2	151.0	-

Table D.5 (Continued)

Spec	h mm	CS	c_x mm	c_y mm	f'_c MPa	d mm	ρ_{tx} %	ρ_{ty} %	ρ_{bx} %	ρ_{by} %	f_y MPa	V_u kN	M_{uy} kN-m	M_{ux} kN-m
Regan (1981)														
SE9	125	S	250	250	41.9	98	0.54	0.92	0.00	0.00	480	123.0	35.7	-
SE10	125	S	250	250	41.1	98	0.54	0.92	0.00	0.00	480	114.0	36.0	-
SE11	125	S	250	250	51.5	98	0.54	0.92	0.00	0.00	480	138.0	39.5	-
Gilbert and Glass (1987)														
1	70	S	100	100	35.1	52	0.71	0.71	0.00	0.00	377	35.0	4.6	-
5	70	S	200	200	30.8	52	0.71	0.71	0.00	0.00	377	48.8	8.4	-
Rangan (1990)														
C	80	S	170	170	28.4	60	0.41	0.41	0.33	0.33	480	21.9	9.4	-
Mortin and Ghali (1991)														
JS1	152	S	254	254	43.2	122	0.60	0.95	0.40	0.40	420	105.0	60.5	-
JS4	152	S	254	254	32.2	122	0.80	1.28	0.40	0.40	420	141.0	60.3	-
Falamaki and Loo (1992)														
W5-B	100	S	200	200	26.8	83	0.19	0.59	0.00	0.00	535	71.2	16.6	0.0
Lim and Rangan (1995)														
Slab 1	110	S	250	250	25.0	87	0.41	0.46	0.33	0.26	516	105.8	16.2	-
Luo and Durrani (1995b)														
EXT1	114	S	254	254	31.2	97	0.55	0.55	0.00	0.00	418	22.7	23.0	-
EXT2	114	S	254	254	32.1	97	0.55	0.55	0.00	0.00	418	32.9	26.9	-
Gardner and Shao (1996)														
3	140	S	254	254	21.5	120	0.66	0.66	0.42	0.42	460	144.0	14.6	-
5	140	S	254	254	21.5	120	0.66	0.66	0.42	0.42	460	144.0	14.6	-
Megally (1998)														
E-1	150	S	178	178	33.5	117	0.91	0.91	0.46	0.46	408	110.0	46.4	-
E-2	150	S	203	203	33.4	117	1.38	1.38	0.70	0.70	408	130.0	63.1	-
El-Salakawy et al. (1999)														
XXX	120	S	250	250	33.0	90	0.75	0.75	0.45	0.45	545	125.0	37.5	-

Table D.5 (Continued)

Spec	h mm	CS	c_x mm	c_y mm	f'_c MPa	d mm	ρ_{tx} %	ρ_{ty} %	ρ_{bx} %	ρ_{by} %	f_y MPa	V_u kN	M_{uy} kN-m	M_{ux} kN-m
Sherif and Dilger (2000a)														
S1-2	150	S	250	250	29.0	114	1.41	1.41	1.00	1.11	523	185.0	43.9	-
Khwaounjoo (2001)														
S1	100	S	200	200	24.1	80	1.01	1.15	1.81	0.58	675	96.5	29.2	-

Notes: h = slab thickness; CS = column shape (C = circular, S = square, R = rectangular); c_x, c_y = column widths in x- and y-directions, respectively; f'_c = compressive strength of concrete cylinder; d = effective depth of nonprestressed reinforcement; ρ_{tx}, ρ_{ty} = top nonprestressed reinforcement ratios within c plus 1.5h on each side of column in x- and y-directions, respectively; ρ_{bx}, ρ_{by} = bottom nonprestressed reinforcement ratios within c plus 1.5h on each side of column in x- and y-directions, respectively; f_y = yield strength of nonprestressed reinforcement; V_u = ultimate shear force; M_{uy}, M_{ux} = ultimate unbalanced moments acting at centroid of column section about y- and x-axes, respectively (1 mm = 0.0394 in, 1 MPa = 145 psi, 1 kN = 0.225 kip, 1 kN-m = 0.737 ft-kips)

Table D.6 Edge reinforced concrete slab-column connections having rectangular columns

Spec	h mm	CS	c_x mm	c_y mm	f'_c MPa	d mm	ρ_{tx} %	ρ_{ty} %	ρ_{bx} %	ρ_{by} %	f_y MPa	V_u kN	M_{uy} kN-m	M_{ux} kN-m
Hawkins et al. (1978)														
E3	178	R	495	203	22.6	140	1.42	1.54	0.00	0.00	447	82.3	127.0	-
Kane (1978)														
K-1	51	R	100	68	30.2	41	0.99	1.38	0.00	0.00	480	24.0	2.4	-
K-3	48	R	114	75	41.2	38	1.12	1.32	0.00	0.00	480	25.1	2.5	-
Scavuzzo (1978)														
S1	64	R	152	102	38.1	50	0.73	1.03	0.00	0.00	379	32.1	4.7	-
Regan (1981)														
SE1	125	R	300	200	35.5	98	1.08	1.15	0.00	0.00	480	198.0	39.5	-
SE4	125	R	200	300	26.6	98	1.08	1.15	0.00	0.00	480	152.0	30.5	-
SE7	125	R	200	300	39.8	98	0.77	1.15	0.00	0.00	490	129.0	31.7	-
Hall and Rangan (1983)														
3A	100	R	250	200	44.0	79	1.99	1.99	0.33	0.33	426	84.5	30.3	-
4A	100	R	250	200	28.0	79	1.09	1.09	0.35	0.35	426	83.0	26.0	-
5A	100	R	250	450	31.0	79	0.85	0.85	0.33	0.33	426	94.0	34.2	-
Gilbert and Glass (1987)														
2	70	R	100	150	30.1	52	0.71	0.71	0.00	0.00	377	37.0	4.7	-
3	70	R	100	200	33.9	52	0.71	0.71	0.00	0.00	377	39.0	5.3	-
4	70	R	200	100	30.2	52	0.71	0.71	0.00	0.00	377	40.0	7.7	-
6	70	R	150	100	33.9	52	0.68	0.68	0.00	0.00	377	40.8	5.3	-
Rangan (1990)														
B	100	R	250	200	48.3	82	0.75	0.75	0.34	0.34	462	108.2	27.9	-

Table D.6 (Continued)

Spec	h mm	CS	c_x mm	c_y mm	f'_c MPa	d mm	ρ_{tx} %	ρ_{ty} %	ρ_{bx} %	ρ_{by} %	f_y MPa	V_u kN	M_{uy} kN-m	M_{ux} kN-m
Falamaki and Loo (1992)														
M5-B	100	R	300	400	34.0	84	0.18	2.15	0.00	0.00	643	87.8	41.1	1.6
Anggadjaja and Teng (2008)														
E0U	135	R	900	180	33.3	107	1.10	1.10	0.33	0.33	529	245.0	81.0	-

Notes: h = slab thickness; CS = column shape (C = circular, S = square, R = rectangular); c_x, c_y = column widths in x- and y-directions, respectively; f'_c = compressive strength of concrete cylinder; d = effective depth of nonprestressed reinforcement; ρ_{tx}, ρ_{ty} = top nonprestressed reinforcement ratios within c plus 1.5h on each side of column in x- and y-directions, respectively; ρ_{bx}, ρ_{by} = bottom nonprestressed reinforcement ratios within c plus 1.5h on each side of column in x- and y-directions, respectively; f_y = yield strength of nonprestressed reinforcement; V_u = ultimate shear force; M_{uy}, M_{ux} = ultimate unbalanced moments acting at centroid of column section about y- and x-axes, respectively (1 mm = 0.0394 in, 1 MPa = 145 psi, 1 kN = 0.225 kip, 1 kN-m = 0.737 ft-kips)

Table D.7 Corner reinforced concrete slab-column connections having square columns

Spec	h mm	CS	c_x mm	c_y mm	f'_c MPa	d mm	ρ_{tx} %	ρ_{ty} %	ρ_{bx} %	ρ_{by} %	f_y MPa	V_u kN	M_{uy} kN-m	M_{ux} kN-m
Zaghlool et al. (1970)														
I-1	140	S	140	140	24.1	114	1.47	1.47	0.63	0.63	379	107.6	10.4	8.8
I-2	140	S	140	140	24.1	114	1.47	1.47	0.63	0.63	379	107.1	7.4	10.4
I-3	140	S	140	140	24.1	114	1.47	1.47	0.63	0.63	379	106.1	10.4	7.4
I-4	140	S	140	140	24.1	114	1.47	1.47	0.63	0.63	379	104.8	8.8	6.7
II-1	140	S	165	165	30.2	114	1.47	1.47	0.59	0.59	379	108.6	18.7	15.4
II-2	140	S	165	165	30.2	114	1.47	1.47	0.59	0.59	379	104.1	16.0	17.5
II-3	140	S	165	165	30.2	114	1.47	1.47	0.59	0.59	379	108.9	19.1	15.4
II-4	140	S	165	165	30.2	114	1.47	1.47	0.59	0.59	379	107.4	16.0	17.5
III-1	140	S	165	165	20.7	114	1.47	1.47	0.59	0.59	379	101.5	16.0	16.0
III-2	140	S	165	165	20.7	114	1.47	1.47	0.59	0.59	379	100.5	16.1	16.0
III-3	140	S	165	165	20.7	114	1.47	1.47	0.59	0.59	379	101.3	16.0	16.0
III-4	140	S	165	165	20.7	114	1.47	1.47	0.59	0.59	379	99.0	16.1	16.0
IV-1	140	S	165	165	35.8	114	1.47	1.47	0.59	0.59	379	122.5	15.7	22.0
IV-2	140	S	165	165	35.8	114	1.47	1.47	0.59	0.59	379	124.3	15.8	22.0
IV-3	140	S	165	165	35.8	114	1.47	1.47	0.59	0.59	379	121.2	15.8	22.0
IV-4	140	S	165	165	35.8	114	1.47	1.47	0.59	0.59	379	117.9	15.8	22.0
Zaghlool and Rawdon de Paiva (1973)														
Z-I(1)	152	S	178	178	32.7	121	1.23	1.23	1.23	1.23	379	74.3	19.2	19.2
Z-II(1)	152	S	267	267	33.0	121	1.23	1.23	1.23	1.23	389	137.9	38.5	38.5
Z-II(2)	152	S	267	267	33.4	121	1.65	1.65	1.65	1.65	405	177.2	53.4	53.4
Z-II(3)	152	S	267	267	27.7	118	2.23	2.23	2.23	2.23	451	177.9	58.0	58.0
Z-II(4)	152	S	267	267	30.8	121	1.23	1.23	1.23	1.23	389	-	28.3	28.3
Z-II(5)	152	S	267	267	34.7	121	1.23	1.23	1.23	1.23	381	148.6	0.0	0.0
Z-II(5)d	152	S	267	267	34.3	121	1.23	1.23	1.23	1.23	381	137.9	0.0	0.0
Z-II(6)	152	S	267	267	33.6	121	1.23	1.23	1.23	1.23	381	82.3	38.9	38.9
Z-III(1)	152	S	356	356	33.6	121	1.23	1.23	1.23	1.23	379	179.7	52.7	52.7

Table D.7 (Continued)

Spec	h mm	CS	c_x mm	c_y mm	f'_c MPa	d mm	ρ_{tx} %	ρ_{ty} %	ρ_{bx} %	ρ_{by} %	f_y MPa	V_u kN	M_{uy} kN-m	M_{ux} kN-m
Ingvarsson (1974)														
1	120	S	180	180	25.8	95	1.89	1.89	0.00	0.00	454	108.0	20.9	20.9
2	120	S	180	180	33.3	95	0.96	0.96	0.00	0.00	454	76.0	16.7	16.7
4	120	S	180	180	32.0	95	0.96	0.96	0.00	0.00	452	101.0	18.1	18.1
5	120	S	180	180	29.2	95	1.45	1.45	0.00	0.00	452	110.0	22.1	22.1
Stamenković and Chapman (1974)														
V/C/1	76	S	127	127	32.2	56	1.17	1.17	1.17	1.17	448	27.2	0.0	-
C/C/1	76	S	127	127	30.4	56	1.17	1.17	1.17	1.17	448	24.9	6.2	-
C/C/2	76	S	127	127	28.3	56	1.17	1.17	1.17	1.17	448	15.9	6.4	-
C/C/3	76	S	127	127	25.8	56	1.17	1.17	1.17	1.17	448	8.0	6.2	-
C/C/4	76	S	127	127	30.6	56	1.17	1.17	1.17	1.17	448	3.6	5.6	-
M/C/1	76	S	127	127	28.2	56	1.17	1.17	1.17	1.17	448	-	4.6	-
Walker and Regan (1987)														
SC1	125	S	300	300	43.3	100	1.29	1.29	0.26	0.26	450	81.5	25.2	25.2
SC2	125	S	300	300	47.9	100	0.83	0.83	0.36	0.36	450	74.8	24.0	24.0
SC3	125	S	300	300	37.4	100	1.67	1.67	0.16	0.16	450	74.2	31.6	31.6
SC4	125	S	220	220	40.8	100	1.29	1.29	0.26	0.26	450	63.8	16.7	16.7
SC5	125	S	220	220	46.5	100	1.86	1.86	0.41	0.41	450	82.2	18.8	18.8
SC7	125	S	220	220	43.8	100	1.86	1.86	0.41	0.41	450	82.2	27.6	27.6
SC8	85	S	160	160	37.4	64	0.55	0.55	0.51	0.51	595	33.0	4.7	4.7
SC9	85	S	160	160	34.3	64	1.13	1.13	0.31	0.31	595	33.0	5.9	5.9
SC11	81	S	160	160	27.2	60	3.69	1.98	0.64	0.45	595	33.0	4.6	2.2
SC12	81	S	300	300	40.7	60	2.41	1.08	0.64	0.35	595	36.8	12.7	8.9
Hammill and Ghali (1994)														
NH1	150	S	250	250	41.5	114	1.85	1.85	0.92	0.92	440	146.9	43.0	43.0
NH2	150	S	250	250	42.2	114	1.85	1.85	0.92	0.92	440	139.1	40.2	40.2
NH4	150	S	250	250	36.9	114	1.86	1.86	0.92	0.92	440	-	46.6	46.6
Gardner and Shao (1996)														
8	140	S	254	254	21.5	120	0.66	0.66	0.42	0.42	460	81.0	10.5	10.5

Table D.7 (Continued)

Spec	h mm	CS	c_x mm	c_y mm	f'_c MPa	d mm	ρ_{tx} %	ρ_{ty} %	ρ_{bx} %	ρ_{by} %	f_y MPa	V_u kN	M_{uy} kN-m	M_{ux} kN-m
Desayi and Seshadri (1997)														
S101	100	S	100	100	36.0	80	0.53	0.53	0.50	0.50	720	32.6	6.2	6.2
S201	100	S	100	100	36.0	80	0.80	0.80	0.67	0.67	720	47.0	9.0	9.0
S301	100	S	100	100	20.0	80	1.07	1.07	0.93	0.93	720	55.1	10.5	10.5
S102	100	S	100	100	24.8	80	0.53	0.53	0.50	0.50	720	52.2	7.6	7.6
S202	100	S	100	100	27.2	80	0.80	0.80	0.67	0.67	720	40.7	5.9	5.9
S302	100	S	100	100	22.4	80	1.07	1.07	0.93	0.93	720	42.8	6.2	6.2

Notes: h = slab thickness; CS = column shape (C = circular, S = square, R = rectangular); c_x, c_y = column widths in x- and y-directions, respectively; f'_c = compressive strength of concrete cylinder; d = effective depth of nonprestressed reinforcement; ρ_{tx}, ρ_{ty} = top nonprestressed reinforcement ratios within c plus 1.5h on each side of column in x- and y-directions, respectively; ρ_{bx}, ρ_{by} = bottom nonprestressed reinforcement ratios within c plus 1.5h on each side of column in x- and y-directions, respectively; f_y = yield strength of nonprestressed reinforcement; V_u = ultimate shear force; M_{uy}, M_{ux} = ultimate unbalanced moments acting at centroid of column section about y- and x-axes, respectively (1 mm = 0.0394 in, 1 MPa = 145 psi, 1 kN = 0.225 kip, 1 kN-m = 0.737 ft-kips)

Table D.8 Corner reinforced concrete slab-column connections having rectangular columns

Spec	h mm	CS	c_x mm	c_y mm	f'_c MPa	d mm	ρ_{tx} %	ρ_{ty} %	ρ_{bx} %	ρ_{by} %	f_y MPa	V_u kN	M_{uy} kN-m	M_{ux} kN-m
Falamaki and Loo (1992)														
M5-A	100	R	200	300	34.0	82	0.39	0.18	0.00	0.00	589	34.4	9.4	14.0
W5-C	100	R	200	400	26.8	85	0.18	0.18	0.00	0.00	530	37.3	12.0	8.3
M5-C	100	R	300	400	34.0	81	0.18	0.50	0.00	0.00	589	38.4	17.2	12.4
Widjaja and Teng (2006)														
SC-H	150	R	180	900	38.7	122	1.09	1.09	0.43	0.52	524	115.7	116.4	96.5

Notes: h = slab thickness; CS = column shape (C = circular, S = square, R = rectangular); c_x, c_y = column widths in x- and y-directions, respectively; f'_c = compressive strength of concrete cylinder; d = effective depth of nonprestressed reinforcement; ρ_{tx}, ρ_{ty} = top nonprestressed reinforcement ratios within c plus 1.5h on each side of column in x- and y-directions, respectively; ρ_{bx}, ρ_{by} = bottom nonprestressed reinforcement ratios within c plus 1.5h on each side of column in x- and y-directions, respectively; f_y = yield strength of nonprestressed reinforcement; V_u = ultimate shear force; M_{uy}, M_{ux} = ultimate unbalanced moments acting at centroid of column section about y- and x-axes, respectively (1 mm = 0.0394 in, 1 MPa = 145 psi, 1 kN = 0.225 kip, 1 kN-m = 0.737 ft-kips)

APPENDIX E
DATABASE ON POST-TENSIONED SLAB-COLUMN CONNECTIONS

Table E.1 Post-tensioned slab-column connections under symmetrical punching

Spec	h mm	CS	c_x mm	c_y mm	f'_c MPa	d mm	ρ_{tx} %	ρ_{ty} %	d_{px} mm	d_{py} mm	f_{pcx} MPa	f_{pcy} MPa	V_p kN	V_{pd} kN	V_u kN
Gerber and Burns (1971)															
C-2	178	S	305	305	31.7	142	0.67	0.67	133	121	1.72	1.72	8.8	8.8	856.7
C-3	178	S	305	305	33.9	142	0.67	0.67	133	121	1.72	1.72	8.8	8.8	901.2
Smith and Burns (1974)															
S-2	70	S	203	203	28.9	55	0.71	0.71	50	59	2.24	2.24	3.1	6.2	121.4
S-3	70	S	203	203	31.9	55	0.85	0.85	50	59	2.24	2.24	3.1	6.2	134.8
Burns and Hemakom (1977)															
SI-5	74	S	203	203	33.8	60	0.63	0.63	44	59	2.24	2.24	4.0	7.9	117.4
SI-6	74	S	203	203	33.8	60	0.63	0.63	59	59	2.24	2.24	4.9	9.9	161.9
SI-7	74	S	203	203	33.8	60	0.63	0.63	59	59	2.24	2.24	5.1	10.2	150.3
SI-9	74	S	203	203	33.8	60	0.63	0.63	44	59	2.24	2.24	3.8	7.6	112.5
SI-10	74	S	203	203	33.8	60	0.63	0.63	59	59	2.24	2.24	4.8	9.6	164.6
SI-11	74	S	203	203	33.8	60	0.63	0.63	59	59	2.24	2.24	4.9	9.9	125.0
SI-15	74	S	203	203	33.8	60	0.63	0.63	44	59	2.24	2.24	4.0	7.9	115.2
Franklin and Long (1982)															
7B	58	S	169	169	38.0	45	0.55	0.55	41	48	2.43	2.43	6.5	10.1	127.9
Shehata (1982)															
SP1	175	S	150	150	36.5	157	0.27	0.27	135	135	3.94	3.94	18.5	103.3	988.0
SP4	175	S	150	150	41.7	157	0.27	0.27	135	135	4.81	4.81	21.0	100.5	884.0
SP5	175	S	150	150	40.9	157	0.27	0.27	135	135	3.28	3.28	0.0	16.5	780.0
SP6	175	S	150	150	42.5	157	0.27	0.27	135	135	3.50	3.50	0.0	35.3	728.0
Kordina and Nölting (1984, 1986)															
V1	150	C	200	200	33.6	128	0.62	0.62	114	114	1.70	1.70	65.7	113.9	450.0
V2	150	C	200	200	36.0	126	0.90	0.90	114	114	1.66	1.66	60.6	105.9	525.0
V3	150	C	200	200	36.0	128	0.62	0.62	114	114	3.09	3.09	115.6	200.6	570.0
V6	150	C	200	200	30.4	128	0.62	0.62	75	75	1.77	1.77	0.0	0.0	375.0
V7	150	C	200	200	31.2	128	0.62	0.62	114	114	1.77	1.77	67.5	117.1	475.0
V8	150	C	200	200	35.2	128	0.62	0.62	114	114	1.77	1.77	70.3	121.9	518.0

Table E.1 (Continued)

Spec	h mm	CS	c_x mm	c_y mm	f'_c MPa	d mm	ρ_{tx} %	ρ_{ty} %	d_{px} mm	d_{py} mm	f_{pcx} MPa	f_{pcy} MPa	V_p kN	V_{pd} kN	V_u kN
Burns and Hemakom (1985)															
SII-10	73	S	203	203	32.8	60	0.76	0.76	64	56	0.93	0.93	6.1	9.1	99.2
Hassanzadeh (1998)															
A1	180	C	250	250	31.0	150	0.18	0.18	151	151	2.79	2.79	151.6	227.4	668.0
A2	180	C	250	250	28.7	150	0.18	0.18	144	144	2.74	2.74	0.0	131.8	564.0
B2	220	C	250	250	39.0	190	0.29	0.29	110	110	2.12	2.12	0.0	0.0	827.0
B3	220	C	250	250	38.6	190	0.29	0.29	191	191	2.21	2.21	194.8	292.2	1113.0
B4	220	C	250	250	40.5	190	0.29	0.29	190	190	1.99	1.99	0.0	173.2	952.0
Melges (2000)															
M4	160	S	180	180	51.9	134	0.92	0.92	120	120	1.95	1.95	26.8	61.2	773.0
Corrêa (2001)															
LP2	130	S	150	150	52.4	105	1.17	1.17	65	65	2.19	2.19	0.0	0.0	355.0
LP3	130	S	150	150	52.4	105	1.17	1.17	65	65	4.28	4.28	0.0	0.0	415.0
LP4	130	S	150	150	50.7	105	1.17	1.17	81	81	0.80	0.80	7.6	17.0	390.0
LP5	130	S	150	150	50.7	105	1.17	1.17	81	81	1.33	1.33	13.0	29.1	475.0
LP6	130	S	150	150	52.4	105	1.17	1.17	81	81	1.76	1.76	11.0	35.5	437.0
Silva (2004)															
A1	125	S	100	100	37.8	109	0.62	0.62	91	91	3.31	3.31	31.3	94.0	380.0
A2	127	S	100	100	37.8	113	0.47	0.47	97	97	2.14	2.14	36.3	72.6	315.0
A3	128	S	100	100	37.8	109	0.62	0.62	86	86	3.16	3.16	0.0	23.5	352.7
A4	129	S	100	100	37.8	104	0.51	0.51	86	86	1.98	1.98	0.0	22.4	321.0
B1	124	S	200	200	40.1	114	0.60	0.60	98	98	3.39	3.39	79.7	119.5	582.5
B2	124	S	200	200	40.1	110	0.48	0.48	94	94	2.23	2.23	70.4	70.4	488.0
B3	124	S	200	200	40.1	108	0.63	0.63	90	90	3.12	3.12	29.3	58.6	519.8
B4	124	S	200	200	40.1	106	0.50	0.50	89	89	2.16	2.16	29.0	58.1	458.8
C1	126	S	300	300	41.6	111	0.61	0.61	94	94	3.33	3.33	68.5	102.7	720.0
C2	122	S	300	300	41.6	105	0.50	0.50	89	89	2.26	2.26	62.0	62.0	556.7
C3	124	S	300	300	41.6	106	0.64	0.64	90	90	3.48	3.48	32.3	64.7	636.6
C4	123	S	300	300	41.6	102	0.52	0.52	85	85	2.31	2.31	26.5	53.1	497.1
D1	124	S	200	200	44.1	100	0.68	0.68	83	83	3.34	3.34	23.5	70.4	497.1
D2	123	S	200	200	44.1	106	0.50	0.50	90	90	2.23	2.23	31.1	62.2	385.2
D3	125	S	200	200	44.1	103	0.51	0.51	90	90	2.27	2.27	0.0	62.2	395.2
D4	125	S	300	300	44.1	111	0.48	0.48	95	95	2.22	2.22	72.0	72.0	531.5

Table E.1 (Continued)

Spec	h mm	CS	c_x mm	c_y mm	f'_c MPa	d mm	ρ_{tx} %	ρ_{ty} %	d_{px} mm	d_{py} mm	f_{pcx} MPa	f_{pcy} MPa	V_p kN	V_{pd} kN	V_u kN
Present study															
PI-0	150	R	180	900	33.0	118	0.47	1.01	108	126	0.95	1.87	21.1	40.7	511.8

Notes: h = slab thickness; CS = column shape (S = square, R = rectangular); c_x, c_y = column widths in x- and y-directions, respectively; f'_c = compressive strength of concrete cylinder; d = effective depth of nonprestressed reinforcement; ρ_{tx}, ρ_{ty} = top nonprestressed reinforcement ratios within c plus 1.5h on each side of column in x- and y-directions, respectively; d_{px}, d_{py} = effective depths of tendons at column centerlines in x- and y-directions, respectively; f_{pcx}, f_{pcy} = compressive stresses in concrete due to all effective prestress forces at centroid of section in x- and y-directions, respectively; V_p = vertical component of all effective prestress forces crossing critical section; V_{pd} = vertical component of all effective prestress forces crossing critical section (Eurocode 2); V_u = ultimate shear force (1 mm = 0.0394 in, 1 MPa = 145 psi, 1 kN = 0.225 kip)

Table E.2 Post-tensioned slab-column connections with unbalanced moment transfer

Spec	CT	h	c_x	c_y	f'_c	d	ρ_{tx}	ρ_{ty}	ρ_{bx}	ρ_{by}	f_y	d_{px}	d_{py}	ρ_{px}	ρ_{py}	f_{py}	f_{sex}	f_{sey}	f_{pcx}	f_{pcy}	V_p	V_{pd}	V_u	M_{uy}	M_{ux}
		mm	mm	mm	MPa	mm	%	%	%	%	MPa	mm	mm	%	%	MPa	MPa	MPa	MPa	MPa	kN	kN	kN	kN-m	kN-m
Franklin and Long (1982)																									
1B	I	58	169	169	38.2	48	0.51	0.51	0.00	0.00	517	45	51	1.24	0.43	1400	1045	1043	2.97	2.29	11.7	20.7	100.1	11.9	-
2M	I	58	169	169	37.8	48	0.51	0.51	0.00	0.00	517	45	51	1.24	0.22	1400	1140	1134	3.09	2.29	9.1	13.4	102.6	8.1	-
3M	I	58	169	169	37.0	45	0.55	0.55	0.00	0.00	517	41	48	1.08	0.23	1400	1185	1205	2.53	2.43	5.9	9.9	74.5	6.5	-
4M	I	58	169	169	40.4	45	0.55	0.55	0.00	0.00	517	41	48	1.08	0.23	1400	1185	1205	2.53	2.43	5.9	9.9	79.4	13.5	-
5B	I	58	169	169	41.2	45	0.55	0.55	0.00	0.00	517	41	48	1.08	0.23	1400	1045	1045	2.43	2.43	6.5	10.1	57.6	13.2	-
6B	I	58	169	169	37.2	45	0.55	0.55	0.00	0.00	517	41	48	1.08	0.23	1400	1045	1045	2.43	2.43	6.5	10.1	55.2	17.1	-
Burns and Hemakom (1985)																									
SII-1	E	73	203	203	32.8	60	1.39	0.51	0.00	0.00	379	37	64	0.15	0.23	1670	1139	1085	0.93	0.93	1.9	3.4	32.0	4.9	1.6
SII-2	E	73	203	203	32.8	60	1.39	0.51	0.00	0.00	379	37	64	0.15	0.23	1670	1139	1085	0.93	0.93	1.9	3.4	30.7	4.9	-
SII-9	I	73	203	203	32.8	60	0.63	0.76	0.00	0.00	379	64	56	0.34	0.10	1670	1085	1139	0.93	0.93	6.1	9.1	77.8	3.1	-
SII-15	I	73	203	203	32.8	60	0.63	0.88	0.00	0.00	379	56	64	0.10	0.34	1670	1139	1085	0.93	0.93	6.1	9.1	70.3	3.1	-
Kosut et al. (1985)																									
SIII-2	E	71	203	203	27.2	58	1.33	0.71	0.40	0.36	421	36	62	0.46	0.48	1470	986	986	1.17	1.24	4.9	6.2	72.9	8.3	-
SIII-6	E	71	178	178	27.2	58	0.85	0.78	0.42	0.39	421	36	62	1.14	0.26	1470	986	986	1.32	1.24	4.3	4.9	49.8	10.6	-
SIII-7	C	71	203	203	27.2	58	1.43	1.43	0.36	0.36	421	40	32	0.74	0.46	1470	986	986	1.24	1.24	1.6	2.0	42.7	6.3	6.3
Foutch et al. (1990)																									
S1	E	102	305	305	50.3	81	0.86	0.57	0.29	0.38	501	51	76	1.24	0.32	1670	1147	955	4.48	1.70	5.7	8.0	57.7	67.3	-
S2	E	102	305	305	42.7	81	0.86	0.57	0.29	0.38	501	51	76	1.24	0.32	1670	1219	1262	4.76	2.24	6.1	8.6	83.2	62.7	-
S3	E	102	305	305	42.1	81	0.86	0.57	0.29	0.38	501	51	76	0.35	0.79	1670	1262	1245	1.79	2.65	2.5	2.5	67.2	50.5	-
S4	E	102	305	305	48.3	81	0.86	0.57	0.29	0.38	501	51	76	0.35	0.79	1670	1281	1190	1.82	2.54	2.6	2.6	113.8	53.0	-
Long and Cleland (1993)																									
E1	E	56	163	163	35.8	44	1.29	0.87	0.00	0.00	517	28	48	0.82	0.48	1400	890	890	2.35	2.44	2.8	4.5	46.7	13.0	-
E2	E	56	163	163	37.9	44	0.86	0.87	0.00	0.00	517	28	48	1.64	0.32	1400	1001	1001	2.35	2.47	4.4	5.1	49.8	13.4	-
E3	E	56	163	163	40.8	44	0.86	0.87	0.00	0.00	517	28	41	1.64	0.56	1400	1001	1001	3.81	3.57	2.9	4.1	56.0	15.6	-
E4	E	56	163	163	38.2	44	0.86	0.87	0.00	0.00	517	28	48	0.82	0.16	1400	1001	1001	1.17	0.96	2.2	2.5	40.9	10.0	-
E5	E	56	163	163	36.2	44	0.86	0.87	0.00	0.00	517	36	48	1.12	0.32	1400	1001	1001	2.20	2.47	4.7	5.6	52.9	15.1	-

Table E.2 (Continued)

Spec	CT	h	c_x	c_y	f'_c	d	ρ_{tx}	ρ_{ty}	ρ_{bx}	ρ_{by}	f_y	d_{px}	d_{py}	ρ_{px}	ρ_{py}	f_{py}	f_{sex}	f_{sey}	f_{pcx}	f_{pcy}	V_p	V_{pd}	V_u	M_{uy}	M_{ux}
		mm	mm	mm	MPa	mm	%	%	%	%	MPa	mm	mm	%	%	MPa	MPa	MPa	MPa	MPa	kN	kN	kN	kN-m	kN-m
Khwaounjoo (2001)																									
S2	E	100	200	200	24.9	80	1.01	1.15	0.93	0.58	675	50	59	0.20	0.25	1030	860	990	0.80	0.70	2.2	2.2	108.0	29.7	-
S3	E	100	200	200	26.3	80	1.01	1.15	0.93	0.58	675	50	59	0.82	0.49	1030	990	1050	2.27	2.25	2.8	5.7	136.0	32.5	-
S4	C	100	200	200	37.5	80	0.86	0.86	1.44	1.15	675	50	50	0.58	0.58	1030	1000	1000	2.20	2.15	1.1	2.1	87.8	22.2	14.0

Notes: CT = connection type (I = interior, E = edge, C = corner); h = slab thickness; c_x, c_y = column widths in x- and y-directions, respectively; f'_c = compressive strength of concrete cylinder; d = effective depth of nonprestressed reinforcement; ρ_{tx}, ρ_{ty} = top nonprestressed reinforcement ratios within c plus 1.5h on each side of column in x- and y-directions, respectively; ρ_{bx}, ρ_{by} = bottom nonprestressed reinforcement ratios within c plus 1.5h on each side of column in x- and y-directions, respectively; f_y = yield strength of nonprestressed reinforcement; d_{px}, d_{py} = effective depths of tendons at column centerlines in x- and y-directions, respectively; ρ_{px}, ρ_{py} = prestressed reinforcement ratios within c plus 1.5h on each side of column in x- and y-directions, respectively; f_{py} = yield strength of prestressing steel; f_{sex}, f_{sey} = effective stresses in prestressing steel in x- and y-directions, respectively; f_{pcx}, f_{pcy} = compressive stresses in concrete due to all effective prestress forces at centroid of section in x- and y-directions, respectively; V_p = vertical component of all effective prestress forces crossing critical section; V_{pd} = vertical component of all effective prestress forces crossing critical section (Eurocode 2); V_u = ultimate shear force; M_{uy}, M_{ux} = ultimate unbalanced moment acting at centroid of column section about y- and x-axes, respectively (1 mm = 0.0394 in, 1 MPa = 145 psi, 1 kN = 0.225 kip, 1 kN-m = 0.737 ft-kips)

APPENDIX F

SYMMETRICAL PUNCHING BASED ON YIELD-LINE THEORY

The slab is assumed isotropic with negative ultimate moment of resistance per unit width m. Applying vertical displacement δ at the column, the V/m ratio of the yield line pattern shown in Figure 7.1 can be worked out as:

(a) Interior slab-column connections having circular columns:

External work = Internal work

$$V \cdot \delta = m \cdot 2\pi \cdot a_v \cdot \frac{\delta}{a_v} + m \cdot \pi \cdot c \cdot \frac{\delta}{a_v}$$

$$\frac{V}{m} = 2\pi + \frac{\pi \cdot c}{a_v} \tag{7.3}$$

(b) Interior slab-column connections having rectangular columns:

External work = Internal work

$$V \cdot \delta = m \cdot 2\pi \cdot \frac{(a_{vx} + a_{vy})}{2} \cdot \frac{2 \cdot \delta}{(a_{vx} + a_{vy})} + m \cdot 2c_x \cdot \frac{\delta}{a_{vy}} + m \cdot 2c_y \cdot \frac{\delta}{a_{vx}}$$

$$\frac{V}{m} = 2\pi + \frac{2c_x}{a_{vy}} + \frac{2c_y}{a_{vx}} \tag{7.4}$$

(c) Edge slab-column connections having rectangular columns:

External work = Internal work

$$V \cdot \delta = m \cdot \frac{2\pi}{2} \cdot \frac{(a_{vx} + a_{vy})}{2} \cdot \frac{2 \cdot \delta}{(a_{vx} + a_{vy})} + m \cdot 2c_x \cdot \frac{\delta}{a_{vy}} + m \cdot c_y \cdot \frac{\delta}{a_{vx}}$$

$$\frac{V}{m} = \pi + \frac{2c_x}{a_{vy}} + \frac{c_y}{a_{vx}} \tag{7.5}$$

(d) Corner slab-column connections having rectangular columns:

External work = Internal work

$$V \cdot \delta = m \cdot \frac{2\pi}{4} \cdot \frac{(a_{vx} + a_{vy})}{2} \cdot \frac{2 \cdot \delta}{(a_{vx} + a_{vy})} + m \cdot c_x \cdot \frac{\delta}{a_{vy}} + m \cdot c_y \cdot \frac{\delta}{a_{vx}}$$

$$\frac{V}{m} = \frac{\pi}{2} + \frac{c_x}{a_{vy}} + \frac{c_y}{a_{vx}} \tag{7.6}$$

APPENDIX G

DATABASE ON SLAB-COLUMN CONNECTIONS UNDER CYCLIC LOADING

Table G.1 Reinforced concrete slab-column connections under cyclic loading

Spec	CT	h mm	CS	c_x mm	c_y mm	f'_c MPa	d mm	ρ_{tx} %	ρ_{ty} %	ρ_{bx} %	ρ_{by} %	f_y MPa	V_u kN	M_{uy} kN-m	M_{ux} kN-m	DR_{ux} %	DR_{uy} %
Hanson and Hanson (1968)																	
A2	I	76	S	152	152	31.3	57	1.63	1.63	1.63	1.63	376	4.8	24.3	-	3.30	-
Hawkins et. al. (1974b)																	
S1	I	150	S	300	300	34.8	117	1.20	1.20	0.59	0.59	459	128.1	145.0	-	3.75	-
S2	I	150	S	300	300	23.4	117	0.84	0.84	0.49	0.49	463	142.3	88.0	-	2.00	-
S3	I	150	S	300	300	22.1	117	0.55	0.55	0.40	0.40	455	138.8	53.7	-	2.00	-
S4	I	150	S	300	300	32.3	117	1.20	1.20	0.59	0.59	459	149.9	125.0	-	2.60	-
Islam and Park (1976)																	
3C	I	89	S	229	229	29.7	70	1.14	1.14	0.57	0.57	316	35.8	35.8	-	3.30	-
Symmonds et. al. (1976)																	
S6	I	150	S	300	300	23.2	114	1.81	1.81	0.91	0.91	459	268.0	72.8	-	1.10	-
S7	I	150	S	300	300	26.5	114	0.84	0.84	0.49	0.49	459	270.0	42.5	-	1.00	-
Morrison et al. (1983)																	
S1	I	76	S	305	305	45.8	61	0.65	0.65	0.65	0.65	323	5.8	34.2	-	4.70	-
S2	I	76	S	305	305	35.1	61	0.98	0.98	0.98	0.98	330	5.8	38.8	-	2.80	-
S3	I	76	S	305	305	33.9	61	1.31	1.31	1.31	1.31	335	5.8	41.1	-	4.20	-
S4	I	76	S	305	305	34.9	61	0.98	0.98	0.98	0.98	320	11.8	35.5	-	4.50	-
S5	I	76	S	305	305	35.0	61	0.98	0.98	0.98	0.98	340	26.0	37.5	-	4.80	-
Zee and Moehle (1984)																	
INT	I	60	S	140	140	26.2	52	0.65	0.65	0.52	0.52	435	16.0	10.3	-	3.30	-
Pan and Moehle (1989)																	
AP1	I	123	S	274	274	29.3	103	0.86	0.86	0.29	0.29	484	103.7	52.9	-	1.60	-
AP2	I	123	S	274	274	30.3	103	0.86	0.86	0.29	0.29	484	103.7	41.5	32.6	1.70	0.90
AP3	I	123	S	274	274	31.7	103	0.86	0.86	0.29	0.29	484	53.4	81.4	-	3.70	-
AP4	I	123	S	274	274	31.0	103	0.86	0.86	0.29	0.29	484	53.4	74.9	62.6	3.50	1.80
Robertson and Durrani (1990)																	
1	I	114	S	254	254	38.0	97	0.83	0.83	0.83	0.83	501	45.4	64.7	-	2.75	-
2C	I	114	S	254	254	33.0	97	0.83	0.83	0.83	0.83	501	44.5	66.2	-	3.50	-
3SE	I	114	S	254	254	44.0	97	0.83	0.83	0.83	0.83	501	42.3	72.3	-	3.50	-
4S	I	114	S	254	254	43.9	97	0.83	0.83	0.83	0.83	501	44.0	74.0	-	3.50	-
5SO	I	114	S	254	254	38.0	97	0.83	0.83	0.83	0.83	501	44.9	66.8	-	3.50	-
6LL	I	114	S	254	254	32.2	97	0.83	0.83	0.83	0.83	525	125.0	25.6	-	0.85	-
7L	I	114	S	254	254	30.8	97	0.83	0.83	0.83	0.83	525	85.4	39.9	-	1.45	-
8I	I	114	S	254	254	39.3	92	0.83	0.83	0.83	0.83	525	47.1	66.7	-	3.50	-

Table G.1 (Continued)

Spec	CT	h mm	CS	c_x mm	c_y mm	f'_c MPa	d mm	ρ_{tx} %	ρ_{ty} %	ρ_{bx} %	ρ_{by} %	f_y MPa	V_u kN	M_{uy} kN-m	M_{ux} kN-m	DR_{ux} %	DR_{uy} %
Robertson and Durrani (1990)																	
2C	E	114	S	254	254	33.0	92	0.83	0.83	0.83	0.83	501	54.3	40.3	-	3.50	-
7L	E	114	S	254	254	30.8	92	0.83	0.83	0.83	0.83	525	67.2	34.7	-	1.45	-
6LL	E	114	S	254	254	32.2	92	0.83	0.83	0.83	0.83	525	82.3	38.4	-	0.85	-
Dilger and Cao (1991)																	
CD1	I	150	S	250	250	40.4	117	1.50	1.50	0.50	0.50	395	299.8	49.9	-	0.90	-
CD2	I	150	S	250	250	31.2	117	1.50	1.50	0.50	0.50	395	200.2	68.0	-	1.20	-
CD8	I	150	S	250	250	27.0	117	1.50	1.50	0.50	0.50	395	149.9	85.0	-	1.40	-
Robertson and Durrani (1991)																	
A-w	E	115	S	254	254	33.0	91	0.83	0.83	0.56	0.56	525	54.7	39.8	-	3.50	-
A-e	E	115	S	254	254	33.0	91	0.83	0.83	0.56	0.56	525	53.4	40.8	-	3.50	-
B-w	E	115	S	254	254	30.8	91	0.83	0.83	0.56	0.56	525	66.7	35.0	-	1.50	-
B-e	E	115	S	254	254	30.8	91	0.83	0.83	0.56	0.56	525	67.6	34.2	-	1.50	-
C-w	E	115	S	254	254	32.2	91	0.83	0.83	0.56	0.56	525	79.2	38.9	-	1.00	-
C-e	E	115	S	254	254	32.2	91	0.83	0.83	0.56	0.56	525	85.0	38.0	-	1.00	-
Pan and Moehle (1992)																	
1	I	122	S	274	274	33.3	103	0.76	0.76	0.25	0.25	472	111.2	74.8	-	1.50	-
2	I	122	S	274	274	33.3	103	0.76	0.76	0.25	0.25	472	111.2	55.8	40.7	1.50	0.79
3	I	122	S	274	274	31.4	103	0.76	0.76	0.25	0.25	472	48.9	105.5	-	3.10	-
4	I	122	S	274	274	31.4	103	0.76	0.76	0.25	0.25	472	48.9	102.0	70.0	3.20	1.75
Robertson and Durrani (1992)																	
A	I	114	S	254	254	33.0	92	0.83	0.83	0.31	0.31	501	44.5	70.4	-	3.50	-
B	I	114	S	254	254	30.8	92	0.83	0.83	0.31	0.31	525	85.8	41.4	-	1.40	-
C	I	114	S	254	254	32.2	92	0.83	0.83	0.31	0.31	525	121.0	27.1	-	1.00	-
Wey and Durrani (1992)																	
SC0	I	114	S	254	254	39.3	97	0.82	0.82	0.12	0.12	525	66.3	62.0	-	3.50	-
Farhey et al. (1993)																	
1	I	80	R	300	200	35.1	60	1.00	1.00	0.67	0.67	370	-	33.0	-	4.81	-
2	I	80	R	300	200	35.1	60	1.00	1.00	0.67	0.67	370	-	33.0	-	4.04	-
3	I	80	R	300	200	15.0	60	1.00	1.00	0.67	0.67	370	25.0	19.0	-	3.56	-
4	I	80	R	300	120	15.0	60	1.00	1.00	0.67	0.67	370	25.0	15.0	-	2.40	-

Table G.1 (Continued)

Spec	CT	h mm	CS	c_x mm	c_y mm	f'_c MPa	d mm	ρ_{tx} %	ρ_{ty} %	ρ_{bx} %	ρ_{by} %	f_y MPa	V_u kN	M_{uy} kN-m	M_{ux} kN-m	DR_{ux} %	DR_{uy} %
Dilger and Brown (1994)																	
SJB7	I	150	S	250	250	29.0	117	1.30	1.30	0.40	0.40	400	149.9	84.0	-	2.40	-
Durrani et. al. (1995)																	
DNY-1	I	114	S	254	254	35.3	97	0.59	0.59	0.00	0.00	372	68.5	47.2	-	3.00	-
DNY-2	I	114	S	254	254	25.7	97	0.59	0.59	0.00	0.00	372	85.4	33.4	-	2.00	-
DNY-3	I	114	S	254	254	24.6	97	0.59	0.59	0.00	0.00	372	50.7	48.4	-	2.00	-
DNY-4	I	114	S	254	254	19.1	97	0.59	0.59	0.00	0.00	372	52.9	44.1	-	2.60	-
Durrani et. al. (1995)																	
DNY-1	E	114	S	254	254	35.3	97	0.49	0.49	0.00	0.00	372	39.1	24.0	-	3.00	-
DNY-2	E	114	S	254	254	25.7	97	0.49	0.49	0.00	0.00	372	46.3	18.6	-	2.00	-
DNY-3	E	114	S	254	254	24.6	97	0.49	0.49	0.00	0.00	372	39.1	22.9	-	2.00	-
Luo and Durrani (1995a)																	
I.I	I	114	S	254	254	20.7	97	0.59	0.59	0.00	0.00	381	17.6	39.3	-	5.00	-
Luo and Durrani (1995b)																	
IE	E	114	S	254	254	20.7	97	0.49	0.49	0.00	0.00	381	16.5	20.1	-	5.00	-
Emam et. al. (1997)																	
HHHC0.5	I	150	S	250	250	75.8	119	0.50	0.50	0.40	0.40	460	125.0	134.5	-	5.20	-
HHHC1.0	I	150	S	250	250	72.3	119	1.00	1.00	0.40	0.40	460	125.0	163.0	-	5.20	-
NHHC0.5	I	150	S	250	250	36.8	119	0.50	0.50	0.40	0.40	460	125.0	100.5	-	3.80	-
NHHC1.0	I	150	S	250	250	35.4	119	1.00	1.00	0.40	0.40	460	125.0	127.2	-	3.80	-
Megally (1998)																	
MG-1	E	150	S	250	250	34.2	117	0.92	1.72	0.52	0.80	526	120.0	60.7	-	1.57	-
MG-2A	E	150	S	250	250	31.6	117	1.82	1.72	1.07	0.80	475	120.0	65.1	-	0.63	-
MG-7	E	150	S	250	250	31.2	117	1.82	1.72	1.07	0.80	429	60.0	72.4	-	1.89	-
MG-8	E	150	S	250	250	34.3	117	1.82	1.72	1.07	0.80	408	90.0	76.7	-	1.70	-
MG-9	E	150	S	250	250	84.2	117	1.82	1.72	1.07	0.80	457	120.0	95.9	-	1.78	-
Robertson et al. (2002)																	
1C	I	115	S	250	250	35.4	95	0.70	0.70	0.42	0.42	420	37.9	58.3	-	3.50	-
Tan and Teng (2005)																	
YL-L1	I	150	R	180	900	40.0	122	1.20	1.20	0.40	0.40	525	81.0	187.3	-	5.57	-
YL-H2	I	150	R	180	900	40.0	122	1.20	1.20	0.40	0.40	525	133.5	137.3	136.0	1.96	1.45
YL-L2	I	150	R	180	900	40.0	122	1.20	1.20	0.40	0.40	525	81.0	141.2	184.6	2.08	2.02

Table G.1 (Continued)

Spec	CT	h mm	CS	c_x mm	c_y mm	f'_c MPa	d mm	ρ_{tx} %	ρ_{ty} %	ρ_{bx} %	ρ_{by} %	f_y MPa	V_u kN	M_{uy} kN-m	M_{ux} kN-m	DR_{ux} %	DR_{uy} %
Han et al. (2006b)																	
RE-50	E	130	S	300	300	32.3	110	1.45	0.87	0.41	0.43	466	86.8	73.1	-	2.50	-
Ritchie et al. (2006)																	
1	E	150	S	250	250	26.2	122	1.17	1.04	0.94	0.52	432	142.0	13.6	-	0.28	-
Robertson and Johnson (2006)																	
ND1C	I	114	S	254	254	29.6	100	0.53	0.53	0.09	0.09	400	52.0	42.3	-	3.00	-
ND4LL	I	114	S	254	254	32.3	100	0.53	0.53	0.09	0.09	400	76.3	44.4	-	3.00	-
ND5XL	I	114	S	254	254	24.1	100	0.53	0.53	0.09	0.09	400	95.6	32.5	-	1.50	-
ND6HR	I	114	S	254	254	26.3	100	0.93	0.93	0.23	0.23	400	65.9	58.5	-	3.00	-
ND7LR	I	114	S	254	254	18.8	100	0.39	0.39	0.10	0.10	400	52.0	30.0	-	3.00	-
Widjaja and Teng (2006)																	
SC-LD	C	150	R	180	900	38.7	122	1.09	1.09	0.43	0.52	524	44.8	88.5	116.7	2.52	2.52
SC-HD	C	150	R	180	900	47.0	122	1.09	1.09	0.43	0.52	524	61.8	92.7	158.2	1.48	1.49
Anggadjaja and Teng (2008)																	
E1H	E	135	R	900	180	33.0	107	1.10	1.10	0.33	0.33	532	100.0	146.1	-	3.02	-
E2H	E	135	R	900	180	32.5	107	1.10	1.10	0.33	0.33	528	100.0	50.1	101.5	-	4.29
E12L	E	135	R	900	180	34.4	107	1.10	1.10	0.33	0.33	530	50.0	104.3	74.0	2.02	2.51
E12H	E	135	R	900	180	35.4	107	1.10	1.10	0.33	0.33	531	100.0	93.7	60.0	1.60	2.10
Kang and Wallace (2008)																	
C0	I	150	S	250	250	38.6	130	0.52	0.52	0.20	0.20	452	125.0	103.0	-	1.85	-
Tian et al. (2008)																	
L0.5	I	152	S	406	406	25.6	127	0.50	0.50	0.30	0.30	469	105.0	128.0	-	1.50	-

Notes: CT = connection type (I = interior, E = edge, C = corner); h = slab thickness; CS = column shape (S = square, R = rectangular); c_x, c_y = column widths in x- and y-directions, respectively; f'_c = compressive strength of concrete cylinder; d = effective depth of nonprestressed reinforcement; ρ_{tx}, ρ_{ty} = top nonprestressed reinforcement ratios within c plus 1.5h on each side of column in x- and y-directions, respectively; ρ_{bx}, ρ_{by} = bottom nonprestressed reinforcement ratios within c plus 1.5h on each side of column in x- and y-directions, respectively; f_y = yield strength of nonprestressed reinforcement; V_u = ultimate shear force; M_{uy}, M_{ux} = ultimate unbalanced moments acting at centroid of column section about y- and x-axes, respectively; DR_{ux}, DR_{uy} = ultimate drift ratios in x- and y-directions, respectively (1 mm = 0.0394 in, 1 MPa = 145 psi, 1 kN = 0.225 kip, 1 kN-m = 0.737 ft-kips)

Table G.2 Post-tensioned slab-column connections under cyclic loading

Spec	CT	h	CS	c_x	c_y	f'_c	d	ρ_{tx}	ρ_{ty}	ρ_{bx}	ρ_{by}	f_y	d_{px}	d_{py}	ρ_{px}	ρ_{py}	f_{py}	f_{sex}	f_{sey}	f_{pcx}	f_{pcy}	V_p	V_u	M_{uy}	M_{ux}	DR_{ux}	DR_{uy}
		mm		mm	mm	MPa	mm	%	%	%	%	MPa	mm	mm	%	%	MPa	MPa	MPa	MPa	MPa	kN	kN	kN-m	kN-m	%	%
Trongtham and Hawkins (1977)																											
S1	I	140	S	356	356	26.5	108	0.62	0.62	0.62	0.62	455	102	114	0.25	0.90	1689	842	719	1.12	1.03	56.2	296.0	69.9	-	2.39	-
S2	E	140	S	356	356	29.0	108	0.31	0.63	0.31	0.63	455	70	114	0.36	0.31	1689	786	786	1.04	1.03	16.1	137.0	50.2	-	3.94	-
S3	I	140	S	356	356	25.2	108	0.62	0.62	0.62	0.62	455	114	102	0.90	0.25	1689	719	944	1.91	1.01	36.5	301.0	85.0	-	3.30	-
S4	I	140	S	356	356	26.2	108	0.62	0.62	0.62	0.62	455	102	114	0.25	0.22	1689	842	944	1.12	1.01	24.7	310.0	40.6	-	2.77	-
S5	I	140	S	356	356	24.8	108	0.62	0.62	0.62	0.62	455	102	114	0.25	0.22	1689	842	944	1.12	1.01	24.7	112.0	134.3	-	4.20	-
Dilger and Shatila (!989)																											
S1	E	150	S	250	250	35.8	120	0.42	0.37	0.00	0.00	375	75	122	1.51	0.34	1667	345	836	1.20	1.20	19.2	180.0	94.0	-	5.78	-
S5	I	150	S	250	250	41.3	120	0.42	0.34	0.00	0.00	375	75	122	1.51	0.23	1667	345	1200	1.20	1.20	24.2	180.0	139.0	-	5.78	-
Martinez-Cruzado et al. (1994)																											
I1	I	89	S	203	203	28.1	71	0.85	0.85	0.00	0.00	545	76	66	0.31	1.06	1670	1147	1147	1.40	1.40	43.8	111.2	8.9	9.7	0.82	1.60
I2	I	89	S	203	203	28.1	71	0.85	0.85	0.00	0.00	545	76	66	0.31	1.06	1670	1147	1147	1.40	1.40	43.8	104.5	15.6	13.4	1.60	1.60
I3	I	89	S	203	203	27.6	71	0.85	0.85	0.00	0.00	545	76	66	0.31	1.06	1670	1147	1147	1.40	1.40	43.8	82.3	32.2	33.5	1.60	1.60
E1	E	92	S	195	195	33.1	73	0.83	1.90	0.00	0.00	545	46	76	1.52	0.43	1670	1022	1022	1.19	1.55	21.6	40.0	21.1	17.7	1.95	3.38
E2	E	92	S	195	195	31.9	73	0.83	1.90	0.00	0.00	545	46	76	0.51	0.87	1670	1022	1022	1.21	1.63	25.2	38.1	15.3	24.6	1.89	3.26
C1	C	92	S	195	195	40.6	75	0.86	0.86	0.00	0.00	545	46	46	0.72	1.44	1670	1022	1022	1.61	1.49	9.0	32.2	10.1	12.7	1.53	3.08
C2	C	92	S	195	195	42.3	75	0.86	0.86	0.00	0.00	545	46	46	0.72	1.44	1670	1022	1022	1.45	1.41	9.0	22.2	11.9	13.9	1.74	2.81
Han et al. (2006a)																											
PI-B50	I	130	S	300	300	32.3	108	0.84	0.84	0.53	0.53	466	104	104	0.83	0.28	1555	715	914	1.21	1.21	23.2	132.0	91.6	-	3.30	-
PI-B30	I	130	S	300	300	32.3	108	0.84	0.84	0.53	0.53	466	104	104	0.83	0.28	1555	715	914	1.21	1.21	23.2	82.0	100.4	-	5.90	-
PI-D50	I	130	S	300	300	32.3	108	0.84	0.84	0.53	0.53	466	104	104	0.28	0.83	1555	953	914	1.21	1.21	27.5	132.0	99.3	-	4.00	-
PI-D30	I	130	S	300	300	32.3	108	0.84	0.84	0.53	0.53	466	104	104	0.28	0.83	1555	953	914	1.21	1.21	27.5	82.0	109.6	-	5.40	-
Han et al. (2006b)																											
PE-B50	E	130	S	300	300	32.3	110	0.83	0.87	0.31	0.43	466	65	110	1.32	0.36	1555	715	779	1.21	1.21	14.8	84.2	66.7	-	3.30	-
PE-D50	E	130	S	300	300	32.3	110	0.83	0.87	0.31	0.43	466	65	110	0.44	0.73	1555	953	779	1.21	1.21	16.3	80.2	66.9	-	4.30	-
Present study																											
PI-1	I	150	R	180	900	36.1	118	0.47	1.01	0.47	0.34	513	108	126	0.14	0.77	1779	782	533	0.91	1.70	19.7	164.0	-	185.5	-	2.50
PI-2	I	150	R	180	900	34.0	118	0.47	1.01	0.47	0.34	513	108	126	0.14	0.77	1779	821	507	0.95	1.62	19.8	170.6	79.8	162.1	1.49	1.52

Notes: CT = connection type (I = interior, E = edge, C = corner); h = slab thickness; CS = column shape (S = square, R = Rectangular); c_x, c_y = column widths in x- and y-directions, respectively; f'_c = compressive strength of concrete cylinder; d = effective depth of nonprestressed reinforcement; ρ_{tx}, ρ_{ty} = top nonprestressed reinforcement ratios within c plus 1.5h on each side of column in x- and y-directions, respectively; ρ_{bx}, ρ_{by} = bottom nonprestressed reinforcement ratios within c plus 1.5h on each side of column in x- and y-directions, respectively; f_y = yield strength of nonprestressed reinforcement; d_{px}, d_{py} = effective depths of tendons at column centerlines in x- and y-directions, respectively; ρ_{px}, ρ_{py} = prestressed reinforcement ratios within c plus 1.5h on each side of column in x- and y-directions, respectively; f_{py} = yield strength of prestressing steel; f_{sex}, f_{sey} = effective stresses in prestressing steel in x- and y-directions, respectively; f_{pcx}, f_{pcy} = compressive stresses in concrete due to all effective prestress forces at centroid of section in x- and y-directions, respectively; V_p = vertical component of all effective prestress forces crossing critical section; V_u = ultimate shear force; M_{uy}, M_{ux} = ultimate unbalanced moments acting at centroid of column section about y- and x-axes, respectively; DR_{ux}, DR_{uy} = ultimate drift ratios in x- and y-directions, respectively (1 mm = 0.0394 in, 1 MPa = 145 psi, 1 kN = 0.225 kip, 1 kN-m = 0.737 ft-kips)

APPENDIX H

VBA PROGRAMMING

Subroutine for ACI 318-11 method

```
Sub ACI()
    ReadData First, Last
    For i = First To Last
        ReadInput i, ST, CT, l1, l2, h, Col, c1, c2, fc, d, rhot1,
rhot2, rhob1, rhob2, fy, dp1, dp2, rhop1, rhop2, fpy, fpu, fse1,
fse2, fpc1, fpc2, Vp, Vpd, V, M1, M2, DR1, DR2
        'calculation
        Select Case ST
            Case "RC"
                fps1 = fps2 = 0
            Case "PCU"
                fps1 = Application.WorksheetFunction.Min(fse1 + 70
+ fc / 300 / (rhop1 / 100), fpy, fse1 + 210)
                fps2 = Application.WorksheetFunction.Min(fse2 + 70
+ fc / 300 / (rhop2 / 100), fpy, fse2 + 210)
            Case "PCB"
                Select Case fpy / fpu
                    Case Is >= 0.8
                        gammap = 0.55
                    Case Is >= 0.85
                        gammap = 0.4
                    Case Is >= 0.9
                        gammap = 0.28
                End Select
                Select Case fc
                    Case Is <= 28
                        beta1 = 0.85
                    Case Is >= 28
                        beta1 =
Application.WorksheetFunction.Max(1.05 - 0.007 * fc, 0.65)
                    Case Is >= 55
                        beta1 = 0.65
                End Select
                omegat1 = (rhot1 / 100) * fy / fc
                omegat2 = (rhot2 / 100) * fy / fc
                fps1 = fpu * (1 - (gammap / beta1) * ((rhop1 / 100)
* fpu / fc + (d / dp1) * omegat1))
                fps2 = fpu * (1 - (gammap / beta1) * ((rhop2 / 100)
* fpu / fc + (d / dp2) * omegat2))
        End Select
        Select Case CT
            Case "I"
                alphas = 40
                b1 = c1 + d
                b2 = c2 + d
                If Col = "C" Then
                    bo = 3.14 * b1
                Else
                    bo = 2 * (b1 + b2)
                End If
                bt1 = c2 + 3 * h
                bt2 = c1 + 3 * h
                a1 = ((rhop1 / 100) * bt1 * dp1 * fps1 + (rhot1 /
100) * bt1 * d * fy) / (0.85 * fc * bt1)
                a2 = ((rhop2 / 100) * bt2 * dp2 * fps2 + (rhot2 /
100) * bt2 * d * fy) / (0.85 * fc * bt2)
                Mft1 = ((rhop1 / 100) * bt1 * dp1 * fps1 * (dp1 -
a1 / 2) + (rhot1 / 100) * bt1 * d * fy * (d - a1 / 2)) / 10 ^ 6
```

```
                Mft2 = ((rhop2 / 100) * bt2 * dp2 * fps2 * (dp2 -
a2 / 2) + (rhot2 / 100) * bt2 * d * fy * (d - a2 / 2)) / 10 ^ 6
                Mfb1 = (rhob1 / 100) * bt1 * fy * d ^ 2 * (1 -
(rhob1 / 100) * fy / 1.7 / fc) / 10 ^ 6
                Mfb2 = (rhob2 / 100) * bt1 * fy * d ^ 2 * (1 -
(rhob2 / 100) * fy / 1.7 / fc) / 10 ^ 6
                Mf1 = Mft1 + Mfb1
                Mf2 = Mft2 + Mfb2
                gammaf1 = 1 / (1 + (2 / 3) * (b1 / b2) ^ 0.5)
                gammaf2 = 1 / (1 + (2 / 3) * (b2 / b1) ^ 0.5)
                gammav1 = 1 - gammaf1
                gammav2 = 1 - gammaf2
                cE = b1 / 2
                cW = b1 / 2
                cN = b2 / 2
                CS = b2 / 2
                g1 = 0
                g2 = 0
                Jc1 = 2 * b1 * d ^ 3 / 12 + 2 * d * b1 ^ 3 / 12 + 2
* b2 * d * (b1 / 2) ^ 2
                Jc2 = 2 * b2 * d ^ 3 / 12 + 2 * d * b2 ^ 3 / 12 + 2
* b1 * d * (b2 / 2) ^ 2
                Ms1 = M1 - V * g1 / 1000
                Ms2 = M2 - V * g2 / 1000
                vuNE = V * 10 ^ 3 / bo / d + gammav1 * Ms1 * 10 ^ 6
* cE / Jc1 + gammav2 * Ms2 * 10 ^ 6 * cN / Jc2
                vuNW = V * 10 ^ 3 / bo / d - gammav1 * Ms1 * 10 ^ 6
* cW / Jc1 + gammav2 * Ms2 * 10 ^ 6 * cN / Jc2
                vuSW = V * 10 ^ 3 / bo / d - gammav1 * Ms1 * 10 ^ 6
* cW / Jc1 - gammav2 * Ms2 * 10 ^ 6 * CS / Jc2
                vuSE = V * 10 ^ 3 / bo / d + gammav1 * Ms1 * 10 ^ 6
* cE / Jc1 - gammav2 * Ms2 * 10 ^ 6 * CS / Jc2
                vu = Application.WorksheetFunction.Max(Abs(vuNE),
Abs(vuNW), Abs(vuSW), Abs(vuSE))
            Case "E"
                alphas = 30
                b1 = c1 + d / 2
                b2 = c2 + d
                bo = 2 * b1 + b2
                bt1 = c2 + 3 * h
                bt2 = c1 + 1.5 * h
                a1 = ((rhop1 / 100) * bt1 * dp1 * fps1 + (rhot1 /
100) * bt1 * d * fy) / (0.85 * fc * bt1)
                a2 = ((rhop2 / 100) * bt2 * dp2 * fps2 + (rhot2 /
100) * bt2 * d * fy) / (0.85 * fc * bt2)
                Mft1 = ((rhop1 / 100) * bt1 * dp1 * fps1 * (dp1 -
a1 / 2) + (rhot1 / 100) * bt1 * d * fy * (d - a1 / 2)) / 10 ^ 6
                Mft2 = ((rhop2 / 100) * bt2 * dp2 * fps2 * (dp2 -
a2 / 2) + (rhot2 / 100) * bt2 * d * fy * (d - a2 / 2)) / 10 ^ 6
                Mfb1 = (rhob1 / 100) * bt1 * fy * d ^ 2 * (1 -
(rhob1 / 100) * fy / 1.7 / fc) / 10 ^ 6
                Mfb2 = (rhob2 / 100) * bt1 * fy * d ^ 2 * (1 -
(rhob2 / 100) * fy / 1.7 / fc) / 10 ^ 6
                Mf1 = Mft1
                Mf2 = Mft2 + Mfb2
                gammaf1 = 1 / (1 + (2 / 3) * (b1 / b2) ^ 0.5)
                gammaf2 = 1 / (1 + (2 / 3) * (b2 / b1) ^ 0.5)
                gammav1 = 1 - gammaf1
                gammav2 = 1 - gammaf2
```

```
                cE = 2 * b1 * d * (b1 / 2) / (2 * b1 * d + b2 * d)
                cW = b1 - cE
                cN = b2 / 2
                CS = b2 / 2
                g1 = b1 - c1 / 2 - cE
                g2 = 0
                Jc1 = 2 * b1 * d ^ 3 / 12 + 2 * d * b1 ^ 3 / 12 + 2
* b1 * d * (b1 / 2 - cE) ^ 2 + b2 * d * cE ^ 2
                Jc2 = 2 * b1 * d * cN ^ 2 + b2 * d ^ 3 / 12 + b2 ^
3 * d / 12
                Ms1 = M1 - V * g1 / 1000
                Ms2 = M2 - V * g2 / 1000
                vuNE = V * 10 ^ 3 / bo / d + gammav1 * Ms1 * 10 ^ 6
* cE / Jc1 + gammav2 * Ms2 * 10 ^ 6 * cN / Jc2
                vuNW = V * 10 ^ 3 / bo / d - gammav1 * Ms1 * 10 ^ 6
* cW / Jc1 + gammav2 * Ms2 * 10 ^ 6 * cN / Jc2
                vuSW = V * 10 ^ 3 / bo / d - gammav1 * Ms1 * 10 ^ 6
* cW / Jc1 - gammav2 * Ms2 * 10 ^ 6 * CS / Jc2
                vuSE = V * 10 ^ 3 / bo / d + gammav1 * Ms1 * 10 ^ 6
* cE / Jc1 - gammav2 * Ms2 * 10 ^ 6 * CS / Jc2
                vu = Application.WorksheetFunction.Max(Abs(vuNE),
Abs(vuNW), Abs(vuSW), Abs(vuSE))
            Case "C"
                alphas = 20
                b1 = c1 + d / 2
                b2 = c2 + d / 2
                bo = b1 + b2
                bt1 = c2 + 1.5 * h
                bt2 = c1 + 1.5 * h
                a1 = ((rhop1 / 100) * bt1 * dp1 * fps1 + (rhot1 /
100) * bt1 * d * fy) / (0.85 * fc * bt1)
                a2 = ((rhop2 / 100) * bt2 * dp2 * fps2 + (rhot2 /
100) * bt2 * d * fy) / (0.85 * fc * bt2)
                Mft1 = ((rhop1 / 100) * bt1 * dp1 * fps1 * (dp1 -
a1 / 2) + (rhot1 / 100) * bt1 * d * fy * (d - a1 / 2)) / 10 ^ 6
                Mft2 = ((rhop2 / 100) * bt2 * dp2 * fps2 * (dp2 -
a2 / 2) + (rhot2 / 100) * bt2 * d * fy * (d - a2 / 2)) / 10 ^ 6
                Mfb1 = (rhob1 / 100) * bt1 * fy * d ^ 2 * (1 -
(rhob1 / 100) * fy / 1.7 / fc) / 10 ^ 6
                Mfb2 = (rhob2 / 100) * bt1 * fy * d ^ 2 * (1 -
(rhob2 / 100) * fy / 1.7 / fc) / 10 ^ 6
                Mf1 = Mft1
                Mf2 = Mft2
                gammaf1 = 1 / (1 + (2 / 3) * (b1 / b2) ^ 0.5)
                gammaf2 = 1 / (1 + (2 / 3) * (b2 / b1) ^ 0.5)
                gammav1 = 1 - gammaf1
                gammav2 = 1 - gammaf2
                cE = b1 * d * (b1 / 2) / (b1 * d + b2 * d)
                cW = b1 - cE
                cN = b2 * d * (b2 / 2) / (b1 * d + b2 * d)
                CS = b2 - cN
                g1 = b1 - c1 / 2 - cE
                g2 = b2 - c2 / 2 - cN
                Jc1 = b1 * d ^ 3 / 12 + b1 ^ 3 * d / 12 + b1 * d *
(b1 / 2 - cE) ^ 2 + b2 * d * cE ^ 2
                Jc2 = b2 * d ^ 3 / 12 + b2 ^ 3 * d / 12 + b2 * d *
(b2 / 2 - cN) ^ 2 + b1 * d * cE ^ 2
                Ms1 = M1 - V * g1 / 1000
                Ms2 = M2 - V * g2 / 1000
```

```
                vuNE = V * 10 ^ 3 / bo / d + gammav1 * Ms1 * 10 ^ 6
* cE / Jc1 + gammav2 * Ms2 * 10 ^ 6 * cN / Jc2
                vuNW = V * 10 ^ 3 / bo / d - gammav1 * Ms1 * 10 ^ 6
* cW / Jc1 + gammav2 * Ms2 * 10 ^ 6 * cN / Jc2
                vuSW = 0
                vuSE = V * 10 ^ 3 / bo / d + gammav1 * Ms1 * 10 ^ 6
* cE / Jc1 - gammav2 * Ms2 * 10 ^ 6 * CS / Jc2
                vu = Application.WorksheetFunction.Max(Abs(vuNE),
Abs(vuNW), Abs(vuSE))
        End Select
        beta = Application.WorksheetFunction.Max(c1, c2) /
Application.WorksheetFunction.Min(c1, c2)
        If ST = "RC" Then
            vc1 = (1 + 2 / beta) * fc ^ 0.5 / 6
            vc2 = (2 + alphas * d / bo) * fc ^ 0.5 / 12
            vc3 = fc ^ 0.5 / 3
            vc = Application.WorksheetFunction.Min(vc1, vc2, vc3)
        Else
            betap = Application.WorksheetFunction.Min(0.29, 0.083 *
(alphas * d / bo + 1.5))
            betapm = Application.WorksheetFunction.Min(0.29, 0.083
* (alphas * d / bo + 1.5), 0.083 * (1.5 + 4 / beta))
            fpc = (fpc1 + fpc2) / 2
            vc = betap * fc ^ 0.5 + 0.3 * fpc + Vp * 10 ^ 3 / bo /
d
            vcm = betapm * fc ^ 0.5 + 0.3 * fpc + Vp * 10 ^ 3 / bo
/ d
        End If
        Vo = vc * bo * d / 10 ^ 3
        Vom = vcm * bo * d / 10 ^ 3
        If M1 = 0 Then
            MR1 = 0
        Else
            MR1 = gammaf1 * Ms1 / Mf1
        End If
        If M2 = 0 Then
            MR2 = 0
        Else
            MR2 = gammaf2 * Ms2 / Mf2
        End If
        Select Case vu
            Case vuNE
                Mv1 = vc * Jc1 / gammav1 / cE / 10 ^ 6
                Mv2 = vc * Jc2 / gammav2 / cN / 10 ^ 6
            Case vuNW
                Mv1 = vc * Jc1 / gammav1 / cW / 10 ^ 6
                Mv2 = vc * Jc2 / gammav2 / cN / 10 ^ 6
            Case vuSW
                Mv1 = vc * Jc1 / gammav1 / cW / 10 ^ 6
                Mv2 = vc * Jc2 / gammav2 / CS / 10 ^ 6
            Case vuSE
                Mv1 = vc * Jc1 / gammav1 / cE / 10 ^ 6
                Mv2 = vc * Jc2 / gammav2 / CS / 10 ^ 6
        End Select
        Mo1 = Application.WorksheetFunction.Min(Mf1, Mv1)
        Mo2 = Application.WorksheetFunction.Min(Mf2, Mv2)
        'output
        Cells(i, "BM").Value = vc
        Cells(i, "BN").Value = vu
```

```
        Cells(i, "BO").Value = vu / vc
        Cells(i, "BP").Value = V / Vo
        Cells(i, "BZ").Value = Mf1
        Cells(i, "CA").Value = gammaf1 * Ms1
        Cells(i, "CB").Value = MR1
        Cells(i, "CC").Value = Mf2
        Cells(i, "CD").Value = gammaf2 * Ms2
        Cells(i, "CE").Value = MR2
        Cells(i, "CF").Value = Application.WorksheetFunction.Max(vu
/ vc, MR1, MR2)
        Cells(i, "CG").Value = vcm
        Cells(i, "CH").Value = vu / vcm
        Cells(i, "CI").Value = V / Vom
    Next i
MsgBox "Calculation complete!", vbOKOnly, "ACI Method"
End Sub
```

Subroutine for proposed method

```
Sub Proposed()
    ReadData First, Last
    For i = First To Last
        ReadInput i, ST, CT, l1, l2, h, Col, c1, c2, fc, d, rhot1,
rhot2, rhob1, rhob2, fy, dp1, dp2, rhop1, rhop2, fpy, fpu, fse1,
fse2, fpc1, fpc2, Vp, Vpd, V, M1, M2, DR1, DR2
        'calculation
        Select Case ST
            Case "RC"
                rho = (rhot1 + rhot2) / 2
                fps1 = fps2 = 0
            Case "PCU"
                rho = (rhot1 + rhot2) / 2
                fps1 = Application.WorksheetFunction.Min(fse1 + 70
+ fc / 300 / (rhop1 / 100), fpy, fse1 + 210)
                fps2 = Application.WorksheetFunction.Min(fse2 + 70
+ fc / 300 / (rhop2 / 100), fpy, fse2 + 210)
            Case "PCB"
                rho = (rhot1 + rhot2 + rhop1 + rhop2) / 4
                Select Case fpy / fpu
                    Case Is >= 0.8
                        gammap = 0.55
                    Case Is >= 0.85
                        gammap = 0.4
                    Case Is >= 0.9
                        gammap = 0.28
                End Select
                Select Case fc
                    Case Is <= 28
                        beta1 = 0.85
                    Case Is >= 28
                        beta1 =
Application.WorksheetFunction.Max(1.05 - 0.007 * fc, 0.65)
                    Case Is >= 55
                        beta1 = 0.65
                End Select
                omegat1 = (rhot1 / 100) * fy / fc
                omegat2 = (rhot2 / 100) * fy / fc
                fps1 = fpu * (1 - (gammap / beta1) * ((rhop1 / 100)
* fpu / fc + (d / dp1) * omegat1))
                fps2 = fpu * (1 - (gammap / beta1) * ((rhop2 / 100)
* fpu / fc + (d / dp2) * omegat2))
        End Select
        fpc = (fpc1 + fpc2) / 2
        dp = (dp1 + dp2) / 2
        Select Case CT
            Case "I"
                b1 = c1 + d
                b2 = c2 + d
                bo = 2 * (b1 + b2)
                bt1 = c2 + 3 * h
                bt2 = c1 + 3 * h
                a1 = ((rhop1 / 100) * bt1 * dp1 * fps1 + (rhot1 /
100) * bt1 * d * fy) / (0.85 * fc * bt1)
                a2 = ((rhop2 / 100) * bt2 * dp2 * fps2 + (rhot2 /
100) * bt2 * d * fy) / (0.85 * fc * bt2)
                Mft1 = ((rhop1 / 100) * bt1 * dp1 * fps1 * (dp1 -
a1 / 2) + (rhot1 / 100) * bt1 * d * fy * (d - a1 / 2)) / 10 ^ 6
```

```
                Mft2 = ((rhop2 / 100) * bt2 * dp2 * fps2 * (dp2 -
a2 / 2) + (rhot2 / 100) * bt2 * d * fy * (d - a2 / 2)) / 10 ^ 6
                Mfb1 = (rhob1 / 100) * bt1 * fy * d ^ 2 * (1 -
(rhob1 / 100) * fy / 1.7 / fc) / 10 ^ 6
                Mfb2 = (rhob2 / 100) * bt1 * fy * d ^ 2 * (1 -
(rhob2 / 100) * fy / 1.7 / fc) / 10 ^ 6
                Mf1 = Mft1 + Mfb1
                Mf2 = Mft2 + Mfb2
                Vd = 7.5 * h ^ 2 * fpc * (1 + 6 * (dp - h / 2) / h)
/ 6 / 1000
            Case "E"
                b1 = c1 + d / 2
                b2 = c2 + d
                bo = 2 * b1 + b2
                bt1 = c2 + 3 * h
                bt2 = c1 + 1.5 * h
                a1 = ((rhop1 / 100) * bt1 * dp1 * fps1 + (rhot1 /
100) * bt1 * d * fy) / (0.85 * fc * bt1)
                a2 = ((rhop2 / 100) * bt2 * dp2 * fps2 + (rhot2 /
100) * bt2 * d * fy) / (0.85 * fc * bt2)
                Mft1 = ((rhop1 / 100) * bt1 * dp1 * fps1 * (dp1 -
a1 / 2) + (rhot1 / 100) * bt1 * d * fy * (d - a1 / 2)) / 10 ^ 6
                Mft2 = ((rhop2 / 100) * bt2 * dp2 * fps2 * (dp2 -
a2 / 2) + (rhot2 / 100) * bt2 * d * fy * (d - a2 / 2)) / 10 ^ 6
                Mfb1 = (rhob1 / 100) * bt1 * fy * d ^ 2 * (1 -
(rhob1 / 100) * fy / 1.7 / fc) / 10 ^ 6
                Mfb2 = (rhob2 / 100) * bt1 * fy * d ^ 2 * (1 -
(rhob2 / 100) * fy / 1.7 / fc) / 10 ^ 6
                Mf1 = Mft1
                Mf2 = Mft2 + Mfb2
                Vd = 4 * h ^ 2 * fpc * (1 + 6 * (dp - h / 2) / h) /
6 / 1000
            Case "C"
                b1 = c1 + d / 2
                b2 = c2 + d / 2
                bo = b1 + b2
                bt1 = c2 + 1.5 * h
                bt2 = c1 + 1.5 * h
                a1 = ((rhop1 / 100) * bt1 * dp1 * fps1 + (rhot1 /
100) * bt1 * d * fy) / (0.85 * fc * bt1)
                a2 = ((rhop2 / 100) * bt2 * dp2 * fps2 + (rhot2 /
100) * bt2 * d * fy) / (0.85 * fc * bt2)
                Mft1 = ((rhop1 / 100) * bt1 * dp1 * fps1 * (dp1 -
a1 / 2) + (rhot1 / 100) * bt1 * d * fy * (d - a1 / 2)) / 10 ^ 6
                Mft2 = ((rhop2 / 100) * bt2 * dp2 * fps2 * (dp2 -
a2 / 2) + (rhot2 / 100) * bt2 * d * fy * (d - a2 / 2)) / 10 ^ 6
                Mfb1 = (rhob1 / 100) * bt1 * fy * d ^ 2 * (1 -
(rhob1 / 100) * fy / 1.7 / fc) / 10 ^ 6
                Mfb2 = (rhob2 / 100) * bt1 * fy * d ^ 2 * (1 -
(rhob2 / 100) * fy / 1.7 / fc) / 10 ^ 6
                Mf1 = Mft1
                Mf2 = Mft2
                Vd = 2 * h ^ 2 * fpc * (1 + 6 * (dp - h / 2) / h) /
6 / 1000
        End Select
        betar = (Application.WorksheetFunction.Max(b1, b2) /
Application.WorksheetFunction.Min(b1, b2)) ^ -0.25
        DRu = Application.WorksheetFunction.Max(DR1, DR2)
        If rho = 0 Then
```

```
            vc = 0.33 * Sqr(fc)
        Else
            vc = 0.55 * betar * rho ^ (1 / 3) * fc ^ (1 / 3) * (1 +
d / 1000) ^ -0.5 + (Vd + Vp) * 10 ^ 3 / bo / d
        End If
        Vo = vc * bo * d / 10 ^ 3
        If M1 = 0 Then
            MR1 = 0
        Else
            MR1 = M1 / Mf1
        End If
        If M2 = 0 Then
            MR2 = 0
        Else
            MR2 = M2 / Mf2
        End If
        MR = Application.WorksheetFunction.Max(MR1, MR2)
        K = Application.WorksheetFunction.Max(1 - V / Vo, 0)
        vu = V * 1000 / bo / d + K * MR ^ (1 / 4) * vc
        'output
        Cells(i, "BU").Value = vc
        Cells(i, "BV").Value = vu
        Cells(i, "BW").Value = vu / vc
        Cells(i, "BX").Value = V / Vo
        Cells(i, "BY").Value = DRu
    Next i
MsgBox "Calculation complete!", vbOKOnly, "Proposed Method"
End Sub
```

Subroutine for reading number of data

```
Sub ReadData(First, Last)
    First = 6                           'First row of data
    Number = Cells(3, "A").Value        'Number of data
    Last = First + Number - 1           'Last row of data
End Sub
```

Subroutine for reading input data

```
Sub ReadInput(i, ST, CT, l1, l2, h, Col, c1, c2, fc, d, rhot1,
rhot2, rhob1, rhob2, fy, dp1, dp2, rhop1, rhop2, fpy, fpu, fse1,
fse2, fpc1, fpc2, Vp, Vpd, V, M1, M2, DR1, DR2)
    ST = Cells(i, "D").Value            'Structural type
    CT = Cells(i, "E").Value            'Connection type
    l1 = Cells(i, "G").Value            'Loading span dir-1 (mm)
    l2 = Cells(i, "H").Value            'Loading span dir-2 (mm)
    h = Cells(i, "I").Value             'Thickness of slab (mm)
    Col = Cells(i, "J").Value           'Column shape
    c1 = Cells(i, "K").Value            'Column width dir-1 (mm)
    c2 = Cells(i, "L").Value            'Column width dir-2 (mm)
    fc = Cells(i, "M").Value            'Compressive strength of
concrete cylinder(MPa)
    d = Cells(i, "O").Value             'Distance from extreme
compression fiber to centroid of tension reinforcement (mm)
    rhot1 = Cells(i, "T").Value         'Top bonded reinforcement
ratio within c + 1.5h on each side of the column dir-1 (%)
    rhot2 = Cells(i, "U").Value         'Top bonded reinforcement
ratio within c + 1.5h on each side of the column dir-2 (%)
    rhob1 = Cells(i, "X").Value         'Bot bonded reinforcement
within c + 1.5h on each side of the column ratio dir-1 (%)
    rhob2 = Cells(i, "Y").Value         'Bot bonded reinforcement
within c + 1.5h on each side of the column ratio dir-2 (%)
    fy = Cells(i, "AJ").Value           'Yield strength of bonded
reinforcement (MPa)
    dp1 = Cells(i, "AK").Value          'Distance from extreme
compression fiber to centroid of prestressing steel dir-1 (mm)
    dp2 = Cells(i, "AL").Value          'Distance from extreme
compression fiber to centroid of prestressing steel dir-2 (mm)
    rhop1 = Cells(i, "AS").Value        'Ratio of prestressing steel
within c + 1.5h on each side of the column dir-1 (%)
    rhop2 = Cells(i, "AT").Value        'Ratio of prestressing steel
within c + 1.5h on each side of the column dir-2 (%)
    fpy = Cells(i, "AW").Value          'Yield strength of
prestressing steel (MPa)
    fpu = Cells(i, "AX").Value          'Ult strength of
prestressing steel (MPa)
    fse1 = Cells(i, "AY").Value         'Effective stress of
prestressing steel dir-1 (MPa)
    fse2 = Cells(i, "AZ").Value         'Effective stress of
prestressing steel dir-2 (MPa)
    fpc1 = Cells(i, "BA").Value         'Compressive stress in
concrete dir-1 (MPa)
    fpc2 = Cells(i, "BB").Value         'Compressive stress in
concrete dir-2 (MPa)
    Vp = Cells(i, "BC").Value           'Vertical component of
effective prestress force within c + d/2 on each side of the column
(kN)
```

```
    Vpd = Cells(i, "BD").Value          'Vertical component of
effective prestress force within c + 2d on each side of the column
(kN)
    V = Cells(i, "BE").Value            'Ult shear force (kN)
    M1 = Cells(i, "BF").Value           'Ult unbalanced moment dir-1
(kNm)
    M2 = Cells(i, "BG").Value           'Ult unbalanced moment dir-2
(kNm)
    DR1 = Cells(i, "BH").Value          'Ult drift ratio dir-1 (%)
    DR2 = Cells(i, "BI").Value          'Ult drift ratio dir-2 (%)
End Sub
```